High Capacity Short Range Transport Aircraft

Final Report - Fall DSE 2019

Group 4

Delft University of Technology

TU Delft Delft University of Technology

Challenge the future

HIGH CAPACITY SHORT RANGE TRANSPORT AIRCRAFT

FINAL REPORT - FALL DSE 2019

by

Anas Adnani (1379526)
Jonas Holtermann (4299329)
Jose Akbar Juoro (4534735)
Kim Bloemendaal (4552113)
Ruben Meester (4453964)
Sander Hazelaar (4552784)
Saru Shrestha (4570847)
Viktoriya Markileva (4533828)
Wessel de Waart (4438434)
Yolande Muris (4143000)

January 28, 2020

Principal Tutor: Roelof Vos
Coaches: Salil Luesutthiviboon, Yasir Zahoor

Version Control

Date	Version
20.01.2020	Draft, Initial Release
28.01.2020	Final Release

TU Delft Delft University of Technology

NOMENCLATURE

Acronyms

ALP	aircraft list price	$
BPR	bypass ratio	–
c.g.	centre of gravity	–
EPS	electrical power system	–
MTOW	maximum take off weight	N
MTTF	mean time to failure	h
MTTR	mean time to repair	h
OEW	operating empty weight	N
SAR	specific air range	kg/km
TAW	tube- and wing	–

Greek Symbols

α	0.8	–
α_{approach}	approach angle	deg
Γ	dihedral angle	deg
γ_{approach}	approach angle	deg
λ	hazard rate	–
λ	taper ratio	–
Λ_{LE}	leading edge sweep angle	deg
Λ_{vt}	25% mac tail sweep	rad
μ	ground friction coefficient	–
ν	poisson ratio	–
ϕ	ground clearance angle	deg
ρ	air density	kg/m^3
σ	density ratio	–
σ_{bend}	stress due to bending	Pa
σ_{cc}	crippling stress	Pa
σ_{fatigue}	fatigue stress	Pa
σ_{yield}	yeild stress	Pa
σ_{cr}	critical buckling stress	Pa
σ_h	stress in ceiling	Pa
τ	aileron effectiveness	–
τ_{shear}	shear stress from transverse shear	Pa
τ_{torsion}	shear stress from torsion	Pa
θ_{overnose}	pilot overnose angle	deg

Roman Symbols

$\frac{t}{c}$	thickness to chord ratio	–
$\overline{D_g}$	take off ground drag	N
$\overline{D}$	take off drag	N
$\overline{T}$	take off thrust	N
S_{winglet}	winglet area	m^2
W_{engine}	engine weight	N
$(\text{L/D})_{\text{cr}}$	cruise lift over drag	–
(t/c)	thickness to chord ratio	–
$(\text{t/c})_{\text{max}}$	maximum thickness to chord ratio	–
A	aspect ratio	–
$\text{A}_{\text{airfoil}}$	airfoil area	m^2
A_i	ares of ith element	m^2
A_m	enclosed area	m^2
$\text{A}_{OS_{\text{ce}}}$	cross-sectional area of central overhead bin	m^2
$\text{A}_{OS_{\text{lat}}}$	cross-sectional area of lateral overhead bin	m^2
A_v	aspect ratio vertical tail	–
b	span	m
b	wing span	m
b_1	aileron start span location	m
b_2	aileron end span location	m

C	buckling coefficient	–
c	chord	m
C_d	airfoil drag coefficient	–
c_j	specific fuel consumption	kg/Ns
C_{d_0}	airfoil's 2d drag coefficient	–
C_{D_0}	zero-lift drag	–
C_{l_α}	airfoil's 2d lift curve slope	1/rad
$C_{l_{\delta a}}$	aileron control derivative	–
$C_{L_{cr}}$	cruise lift coefficient	–
$C_{L_{max}}$	maximum lift coefficient	–
$C_{l_{max}}$	maximum airfoil lift coefficient	–
C_{l_p}	roll damping coefficient	–
C_D	aircraft drag coefficient	–
C_{f_e}	friction coefficient	–
C_l/C_d	airfoil lift to drag coefficient ratio	–
c_r	root chord	m
c_t	tip chord	m
c(y)	chord at particular lateral location	m
d	distance between engines	m
D_g	gas generator gondle diameter	m
D_n	nacelle diameter	m
D_{ef}	exit fan diameter	m
D_{eg}	gas generator exit diameter	m
d_{fus}	diameter of fuselage	m
$D_{logistic}$	logistic delay	h
D_{mw}	outer diameter main wheel	m
d_{mw}	inner diameter main wheel	m
D_{nw}	outer diameter nose wheel	m
d_{nw}	inner diameter nose wheel	m
d_{spars}	distance between spars	m
D_{ef}	gas generator gondle diameter	m
D_e	engine diameter	m
E	modulus of elasticity	Pa
E	young's modulus	Pa
e	oswald efficiency factor	–
E_{ltr}	loiter time	s
F_{crit}	critical buckling force	N
F_{mw}	main gear reaction force	N
F_{nw}	nose gear reaction force	N
F_f	friction force	N
F_h	horizontal force component	N
F_i	force at section i	N
F_v	vertical force component	N
g	gravitational acceleration	m/s^2
h_{aisle}	aisle height	m
$h_{exits_{emergency}}$	height of emergency exits	m
$h_{headroom}$	headroom height below overhead storage	m
h_{seat}	seat height	m
H_t	horizontal tail height above fuselage	ft
H_v	vertical tail height above fuselage	ft
I	moment of inertia	m^4
I_{xx}	moment of inertia	m^4
j	safety factor	–
K_{mp}	landing gear type factor	–
K_{np}	engine mounting type factor	–
K_z	aircraft yawing radius of gyration	ft
l_c	engine exit cone length	m
l_g	gas generator gondle length	m
l_n	nacelle length	m
$l_{cockpit}$	longitudinal length of cockpit	m
L_{ec}	length from engine front to cockpit	ft
l_{engine}	engine length	m
l_{fan}	fan length	m
l_{fus}	fuselage length	m
l_{fus}	length of fuselage	m

l_{lower}	length from hinge below	m	P	roll rate	rad/s
l_{mw}	distance from main gear to c.g.	m	p	pressure	Pa
l_{nw}	distance from nose gear to c.g.	m	P_f	probability of failure	–
$l_{pitch_{business}}$	seat pitch in business class	m	Q	first moment of area	m^3
$l_{pitch_{economy}}$	seat pitch in economy class	m	R_{cr}	cruise range	m
$l_{section}$	length of seat section considered for overhead bins	m	R_{system}	system reliability	–
l_{spare}	spare length for landing gear mechanism	m	R_i	radius at section i	m
l_{strut}	strut length	m	S	total wing area	m^2
l_{upper}	length from hinge above	m	S	wing area	m^2
L_m	length of main landing gear	in ·	S_1	wing area	m^2
L_n	nose gear length	ft	S_2	total wing area	m^2
L_t	tail length	ft	S_2	wing area	m^2
M	moment	Nm	$s_{clearance}$	lateral cabin clearance distance	m
M_{cr}	cruise mach number	–	S_{ref}	wing surface area	ft^2
MAC	mean aerodynamic chord	m	S_{vt}	vertical tail surface area	ft^2
MTOW	maximum take-off weight	N	S_{wet}	wetted area	m^2
n	0.6	–	SF	engine scaling factor	–
N_{en}	number of engines	–	T	thrust	N
$n_{exits_{emergency}}$	number of emergency exits	–	t	thickness	m
n_{max}	maximum load factor	–	t_{floor}	vertical floor thickness	m
N_{mss}	number of main gear shock struts	–	t_{spar}	spar thickness	m
N_{mw}	number of main wheels	–	T_{TO}	take-off thrust	N
N_{nw}	number of nose wheels	–	t_c	honeycomb thickness	m
$n_{pax_{business}}$	number of passengers in business class	–	t_f	sheet thickness	m
$n_{pax_{economy}}$	number of passengers in economy class	–	T/W	thrust loading	–
$n_{seats\ crew_{cabin}}$	number of cabin crew seats	–	V	speed	m/s
N_{seats}	number of seats	–	$V_{approach}$	approach speed	deg
N_l	ultimate landing load factor	–	V_{cr}	cruise speed	m/s
N_t	number of fuel tanks	–	$V_{luggage}$	luggage volume	deg
N_z	ultimate load factor	–	$V_{luggage}$	total luggage volume required	m^3
			V_{stall}	stall speed	kts
			V_i	integral tanks volume	gal
			V_{LOF}	lift off speed	m/s
			V_p	protected tanks volume	gal
			V_t	total fuel volume	gal

W_F	fuel weight	N	W_{TO}	take-off weight	N
W_{actual}	actual wing mass	kg	W_l	landing design gross weight	lb
w_{aisle}	aisle width	m	W/S	wing loading	N/m^2
$w_{armrest_{business}}$	arm rest width in business class	m	x_{brake}	brake distance	m
$w_{armrest_{economy}}$	arm rest width in economy class	m	x_{climb}	climb horizontal distance distance	m
$W_{baggage}$	baggage weight	N	$x_{descent}$	descent distance	m
W_{calc}	calculated wingbox mass	kg	x_{flare}	flare distance	m
W_{crew}	crew weight	N	x_{ground}	ground run horizontal distance	m
W_{dg}	design gross weight	lb	$x_{landing}$	landing distance	m
W_{engine}	engine width	m	X_{LEMAC}	longitudinal position of the leading edge of the mac	m
$w_{exits_{emergency}}$	width of emergency exits	m	$x_{take\text{-}off}$	take off distance	m
W_{mw}	width main wheel	m	$x_{transition}$	transition horizontal distance	m
W_{nw}	width nose wheel	m	y	distance from neutral line	–
W_{OE}	operational empty weight	N	y_{mlg}	lateral distance from main landing gear to cg	m
$w_{passageway}$	passageway width	m	z_{mlg}	vertical distance from main landing gear to cg	m
W_{pax}	passenger weight	N	z_e	vertical distance from engine centre line to cg	m
W_{PL}	payload weight	N			
$w_{seat_{business}}$	seat width in business class	m			
$w_{seat_{economy}}$	seat width in economy class	m			

ACKNOWLEDGEMENTS

We would like to express our deep gratitude to our supervisor Dr.ir. Roelof Vos for making this entire project possible and for his patient guidance and dedication. We also wish to thank Salil Luesutthiviboon and Yasir Zahoor for their advice and supervision. We would like to extend our thanks to Dr. Calvin Rans for helping us with the structural analysis and integration, to Dr.ir. Otto Bergsma for providing us with information and data for composite material properties, to ir. Joris Melkert for helping us with the integration of sustainability in our design, to Eddy van den Bos and Daniel Atherstone for their valuable CAD guidance and making the iteration process faster, to Malcom Brown for showing us that a blended wing body design is not impossible.

Executive Summary

Major airports around the world are experiencing congestion due to the increase in air travel demand. Flying to smaller satellite airports or using larger long-haul wide-body aircraft has proven to be a solution, however, the problem arises due to the increasingly negative impact from a higher frequency of flight. This project aims to solve this problem, as a response to a request for proposal by the American Institute for Aeronautics and Astronautics (AIAA), by designing a high capacity short-range transport aircraft with a capacity of 400 passengers and range of 3,500 nautical miles. Three design concepts have been considered for the high capacity short range aircraft design as presented in the Baseline Report [1] and after a trade off process, one of them has been chosen for a final design [2]. The main focus of this report is to develop this concept further, to create a conceptual design for it and to analyse its characteristics.

Market Analysis

The concept of having a large aircraft on short flights is still not applied widely, which opens up possibilities. This short-range market is mainly dominated by single-aisle aircraft. Over the next 10 years, the global fleet is forecast to grow at a rate of 3.6 % per year and the single-aisle aircraft at a rate of 4.9 % to meet the demand. By 2029, the share of single-aisle aircraft will increase from 58 % to 66 %. Furthermore, the larger type of narrow-body aircraft is expected to make up a larger percentage of the total narrow-body fleet by 2029. This illustrates the demand for aircraft with higher passenger capacity over a short-range. Most of the narrow-body fleet is divided over West Europe, North America and Asia.

In the coming 15 years, the global air passenger demand will be doubled to 7.2 billion. To meet this growing demand, the single-aisle aircraft fleet size is expected to grow with an annual rate of 4.9 % to 26,000 aircraft. Part of these single-aisle aircraft fly on high demand routes and can be replaced by the high capacity short range aircraft.

An analysis has been done to find strengths, weaknesses, opportunities and threats for the high capacity short range aircraft. One of the main strengths is that the project is supervised by an experienced aircraft designer. A weakness is that there are limited resources and time for the project. The main opportunity is there is a global rise in demand of commercial air travel and a threat is that it is difficult to reach a position in the current market which is being dominated by two large aircraft manufacturers; Boeing and Airbus.

Looking at similar aircraft, a production time of 15 years is estimated. With an expected global fleet size of 25,777 single-aisle aircraft in 2029 and an annual growth of 4.9 %, the global fleet size in 2044 is expected to be 52,828. Comparing to other new aircraft manufacturers, a market share of the short-range high capacity aircraft of 5 % is projected. With an estimated price of 320 million USD, this results in prediction of 1,353 sold aircraft and a revenue of 433 billion USD in the period 2029-2044.

Objectives and Requirements

Requirements are needed in order to steer the design to the desired result. They can be set by stakeholders which for this project are the airlines, authorities, passengers, airports and manufacturers. Stakeholder requirements and objectives are then derived to get a detailed requirement or constraint for the design to function properly. In the end, the design has to meet all the requirements to be considered successful.

First, design objectives are mentioned to list out the main goal of the design to ensure it is aligned with the stakeholder's demand and interest. Table 1 shows the derived design objectives for the high capacity short range aircraft design.

Table 1: Design Objectives

Objective	Type
Aircraft recurrence cost shall be minimised.	Cost
Non-recurrence cost shall be minimised.	Cost
The aircraft's carbon footprint over the entire life cycle shall be minimised.	Sustainability
The aircraft's NO_x emissions shall be minimised.	Sustainability
Minimise noise inside the cabin.	Sustainability
Increase passenger comfort by lowering cabin altitude from 8,000 ft.	Passenger comfort
Increase passenger boarding efficiency and decrease turn around time compared to competing aircraft.	Passenger comfort

The design requirements are then summarised into 5 different categories; structures, performance, operations, stability & control, and sustainability. The list of requirements is derived from the American Institute of Aeronautics and Astronautics (AIAA), the Federal Aviation Administration (FAA), International Civil Aviation Organisation (ICAO) and the market analysis. The checkpoints to comply the requirements are during the Mid-term report and Final report. Eventually, a requirement compliance matrix is made to analyse whether the design has met the requirements.

Sustainable Development Strategy

Aside from the design, it is also important for the project to prioritise sustainability. Therefore, three different aspects are considered for the sustainability development strategy.

First, the technical approach to the design. As part of the design objectives, the design of high capacity short range aircraft needs to minimise the negative impact on the environment. The key parameters for this to be achieved are fuel consumption, global warming impact and the noise. All three of these parameters need to be minimised to ensure the sustainability goal is achieved.

Next, the manufacturing process. Aside from the design, the manufacturing process of such design needs to be sustainable as well. Thus, the lean manufacturing methodology was implemented in the manufacturing process to ensure that the waste is minimum. The transport of material and the production line both need to be minimal, since they contribute to the amount of emissions. This would be beneficial regarding time, money and the emissions.

Finally, the end of life of the design is taken into account. After the aircraft retires, it needs to be recycled. The materials, chemicals and assembly need to take into account the recycling process. Possibilities of spare parts to be reused is considered.

Design phases

There are three phases for the design of the high capacity short range aircraft. A brief summary of the phases is as follows:

- **Design phase I**: Market and requirement analysis to produce three initial design concepts.
- **Design phase II**: Refining of the concepts using class I sizing to obtain preliminary specifications and performance characteristics for the concepts trade-off.
- **Design phase III**: Iterating the chosen concept to further details, using class II sizing to further analyse the performance and design the system interfaces.

Initially, in phase I, three concepts are selected from the analysis of the market and requirements. These three designs are the Conventional aircraft, Double Decker aircraft and the Blended Wing Body as shown in Figure 1, 2 and 3 respectively. Then, in phase II, the designs are developed to the detail of class I sizing to obtain a preliminary analysis in regards to their main characteristics. By having the preliminary analysis, a trade-off is done in order to choose the most suitable concept out of the three options to proceed with the design process.

Figure 1: Conventional aircraft

Figure 2: Double Deck aircraft

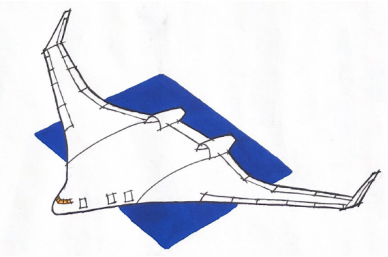

Figure 3: Blended Wing Body aircraft

The main trade-off criteria that has been assessed for the three concepts are the cost, risk, sustainability, turnaround time, passenger comfort, flexibility and originality. Each of these criteria is given a weight factor in terms of the design priority such that cost is considered the highest priority and passenger comfort is the lowest. The result of the trade-off indicates that the Blended Wing Body concept outperforms the other two concepts. Therefore, the Blended Wing Body concept is chosen to continue with the design process.

With phase III, the design started to come into shape. With the implementation of class II sizing, almost all of the systems are re-designed and other specifications are defined. The main focus of phase III is the design of the following:

- Cabin Design
- Wing Planform Design
- Engine Design
- Landing Gear Design
- Vertical Tail Design
- Control Surfaces Design
- High Lift Devices Design
- Structural Design
- Aircraft Weight
- Centre of Gravity

Each of these parameters is implemented to the iteration loop to size the entire design accordingly. Especially as a small change in one parameter influenced the others in varying magnitude. With the iteration loop, the final concept design of the high capacity short range aircraft based on the Blended Wing Body concept is obtained. In which it is now named as the Flying B or for short the FB400.

Design Analysis

During the design process, each system is designed and analysed according to the requirements. The analysis includes the performance, stability & control, operations & logistics and sustainability.

In terms of performance, the FB400 is designed for a range of 3,500 nmi. However the efficiency needs to be optimised for the 700 nmi range. In comparison to the Boeing 777, the FB400 flies 0.5 km higher at an altitude of 11.5 km. The L/D ratio of FB400 is higher from having more wetted area. It flies slower at Mach 0.75 compared to Mach 0.84 of the Boeing 777. However, it is beneficial for the reduction of the radiative forcing impact to fly slower.

The stability and control analysis of the FB400 involves locating the aerodynamic centre of the wing-fuselage combination behind the most aft centre of gravity. The aerodynamic centre of the wing and fuselage is the neutral point of the aircraft as there are no horizontal tails. Longitudinal stability is obtained by changing wing position and sweep angle. To change the centre of gravity, the position of the engines is changed slightly as well. For trimming the aircraft, the forward centre of gravity is important. Limiting the centre of gravity range allows the trim deflection of the elevators to be minimised. With a centre of gravity range of about 0.8 meters, the trim deflection in cruise can be kept below 5 degrees. For the dynamic stability, it is required to obtain level 1 handling qualities. Required stability and damping for the symmetric motions is obtained by introducing a PI controller. The dutch roll damping requirement can be met by a simple proportional gain with a washout filter to not over-stabilise the spiral mode.

For the operations, FB400 suits the condition to operate at congested major hubs such as Kuala Lumpur

and Singapore. It is expected to compete with the narrow-body in terms of ground operation at 45 minutes turnaround time with full airport compatibility. In terms of the design logistics, it is estimated for the design to experience a lengthy process of testing and certification as currently there is no similar aircraft flying. On the bright side, the estimated time for testing and certification is estimated to be 58 months, which is still faster than the A380.

In regards to the emission produced, the global warming impact and the radiative forcing is analysed based on the altitude and the fuel consumption. Even though the global warming impact is 10% worse than the A320, it is still considered to be comparable to the emission produced by a narrow-body aircraft. Therefore, FB400 is estimated to have the emission level of a narrowbody aircraft with the capacity of a wide-body aircraft. In terms of noise, it is analysed that FB400 complies with the noise limit set by ICAO and is comparable to Boeing 787-8. However, this is only an initial estimate and the noise needs to be tested from the prototype.

The unit cost of the FB400 is 283 Million dollar. The direct operating cost 89.6 dollars per nautical mile. The price per aircraft seat-mile for a mission of 600 nmi is 0.0392 dollar cents. This is lower than the 737-7MAX and A319NEO, which have a value of 0.0430 and 0.0425 respectively. The recurring cost is 334 billion dollars. These costs have been minimised by minimising the fuel weight for the design.

Future Planning

As the concept design is finalised, the next stages need to be planned. The two main points are the production plan and project design & development logic. The production plan priority is to be able to produce the design on time while also minimising the waste byproduct. An example is to minimise milling and drilling and considering the possibility of 3D printing. For the project design & development, the next stage are the detailed design, manufacturing, prototypes & testing and finally mass production. It is estimated for the first delivery to take place in the fourth quarter of 2029.

Final Concept Design

Finally, after the iteration loop and analysis from the perspective of different performances parameters, the final concept design of the FB400 is produced. The main specification is compiled in Table 2 and the final isometric view is shown in Subsection 18.2.2.

Table 2: Design summary table

Parameter	Result
Altitude	11.5 km for design mission of 3,500 nmi and 10.9 km for reference mission of 700 nmi
Cruise speed	222 m/s for design mission of 3,500 nmi and 220 m/s for reference mission of 700 nmi
Cruise Mach number	0.75 for both missions
MTOW	151 MT
OEW	67.4 MT
Fuel Weight	42 MT for design mission of 3,500 nmi and 19 MT for reference mission of 700 nmi
L/D_{cruise}	20.3
L/D_{max}	23.3
C_L	0.19
$C_{L_{max}}$	1.05
Total wing area	797 m^2
Aspect ratio	5.4
Wing span	64.8 m
Fuselage length	40 m
Fuselage width	15 m
Engines	Two GEnx - 1B70 engines placed on top of the fuselage
Vertical tail	Two tails with area of 22 m^2 and height of 6 m
Winglets	Area of each winglet is 4 m^2 with a length of 3 m and inclined at 70 deg wrt to the wing
Seats	350 economy class, 50 business class
Nose landing gear	1 strut, 2 wheels, 9.2 m from nose, 4.8 m high
Main landing gear	2 struts, 4 wheels on each strut, 26.4 m from nose, 8.8 m apart, 4.8 m high
SAR	1.05 kg/100km/passenger for design mission range of 3,500 nmi and 1.07 kg/100km/passenger for reference mission of 700 nmi

CONTENTS

1

INTRODUCTION

The demand for air travel increases all around the world resulting in many major airports operating at or beyond full capacity. Flying to smaller satellite airports or using larger long-haul wide-body aircraft on short routes are some measures used to meet the demand. Aside from the risk of airport congestion, the increasing flight frequency may result in a negative impact on the environment, passenger comfort, and costs. In response to a request for proposal by the American Institute for Aeronautics and Astronautics (AIAA), the aim of this project is to create an aircraft design with an Entry Into Service (EIS) by 2029, a passenger capacity of 400 and 3,500 nautical miles of range to address this problem.

The mission need statement of this project is:
To reduce the total number of short-range flights while keeping competitive ticket prices and minimum environmental impact.

The project objective statement of this project is:
To design a competitive aircraft capable of carrying 400 passengers over a distance of 3,500 nmi with 10 students in 10 weeks.

The purpose of this report is to present the final design concept of the high capacity short range aircraft. The entire design process is summarised in this report to elaborate the design philosophy behind the decision made. Together with the preliminary analysis of the performance and properties, it is justified how the concept is able to fit in the targeted market and outperform its competitors. So to convince the stakeholders in the advancement of this design operations.

The structure of the report is as follows. First, the market and functionality are analysed respectively in Chapter 2 and Chapter 3. Then, the objectives and requirements are defined in Chapter 4. Sustainability development is analysed in Chapter 5. Before the design is presented, the methodology is presented in Chapter 6. Design phases I and II are summarised in Chapter 7. As the main focus of this report, design phase III is elaborated in Chapter 8. Afterwards, the analysis begins with performance analysis in Chapter 9. In Chapter 10 the stability and control is analysed, and in Chapter 11 the operations and logistics. Sustainability is analysed in Chapter 12. The aircraft (sub)systems are defined in Chapter 13 and the future planning follows in Chapter 14. The financial and technical risk aspect of the design are discussed in Chapter 15 and Chapter 16. The RAMS analysis is explored in Chapter 17, before the final concept design is presented in Chapter 18. Finally, the final report is concluded in Chapter 19.

Cover image credit.[1]

[1] Airbus. Final Assembly and Tests. Accessed November 2019. https://www.airbus.com/aircraft/how-is-an-aircraft-built/final-assembly-and-tests.html

2

Market Analysis

Although the aircraft market for both short range flights and long range flights has matured over the past decades, the concept of having a large aircraft on short flights is still not applied widely. With the fast expanding market for air travel, this could be a useful solution. First, the current market is analysed in Section 2.1. Then, the high demand route is explored in Section 2.2. SWOT analysis of the market follows in Section 2.3. Afterwards, the interests of the potential customer and a first prediction of the price are described in Section 2.4. Lastly, the section is concluded with a calculation of the market potential in Section 2.5.

2.1. Current Market Analysis

Before initiating the design of high capacity short range aircraft, it is important to identify, define and analyse the market (size) that this aircraft can provide services to. The aircraft to be designed is to transport 400 passengers over a short range which could be an alternative to current commercial single aisle aircraft. Hence, the target market for the aircraft would be the current single aisle aircraft market for short-medium range.

By 2018, all airlines globally had a combined fleet size of 24,492 commercial aircraft. Since a larger portion of the population can afford air travel globally due to reasons like rising incomes, consumer spending and government funding, the commercial aircraft industry is ever expanding. Over the next 10 years, the global fleet is forecast to grow at a rate of 3.6 % per year to meet the rising air travel demand. Within the commercial aircraft class, the single aisle or narrow-body aircraft fleet size is expected to grow from 15,900 in 2019 to 25,700 by 2029 at an annual rate of 4.9 %. By 2029, the share of single aisle aircraft will increase from 58 % to 66 %. The increase in fleet size represents mainly the additions to the fleet or replacements with more efficient alternatives. Furthermore, the larger type of narrow-body aircraft is expected to make up a larger percentage of the total narrow-body fleet by 2029. This further illustrates the demand by operators for aircraft with higher passenger capacity over short range [1].

The existing narrow-body aircraft market is mainly dominated by Boeing and Airbus with a total market share of about 93 % [2] as observed in Figure 2.1. The deliveries of single aisle aircraft through 2028 is expected to be fulfilled by Boeing and Airbus alone. Hence, they are the key players and competition for the aircraft to be designed.

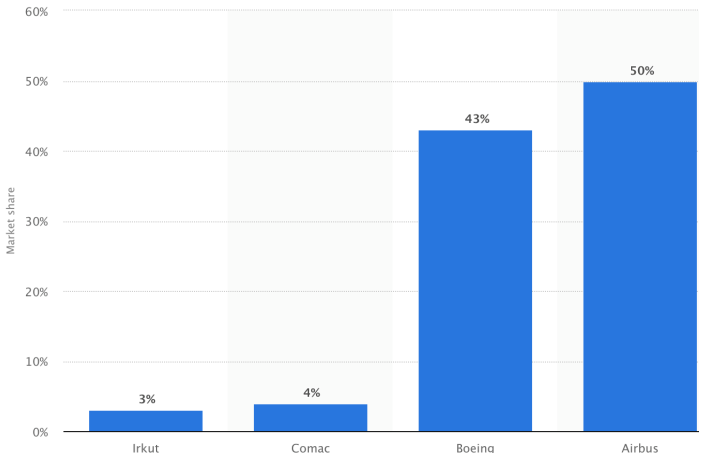

Figure 2.1: Projected market share of narrow-body aircraft deliveries between 2018 and 2037, by manufacturer

[1] Global Fleet & MRO Market Forecast Commentary 2019-2029. Accessed November 2019. https://www.oliverwyman.com/content/dam/oliver-wyman/v2/publications/2019/January/global-fleet-mro-market-forecast-commentary-2019-2029.pdf

[2] Projected market share of narrowbody aircraft deliveries between 2018 and 2037, by manufacturer. Accessed November 2019. https://www.statista.com/statistics/601831/single-aisle-deliveries-by-jet-manufacturers-worldwide/

To further define the market, a global geographical segmentation in 2019 is visualised in Figure 2.2 based on the 2019-2029 global fleet forecast [3]. It shows that North America, Western Europe and China have the largest narrow-body fleet, making them a well suited market for a larger short range aircraft.

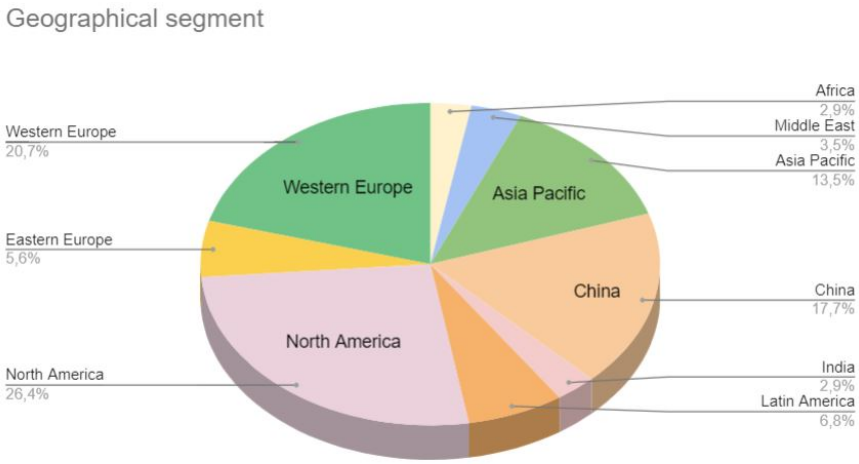

Figure 2.2: Global geographical segmentation of narrow-body aircraft in 2019

When analysing the relevant reference aircraft considered in the market analysis, it becomes evident that most aircraft can be classified either as long range high capacity or short range low capacity. This becomes clear when the reference aircraft payload is plotted against range as shown in Figure 2.3. In this figure, the target gap of the aircraft is plotted as well. Note that the goal is to design a new aircraft to fit in the graph that is not yet occupied by existing aircraft.

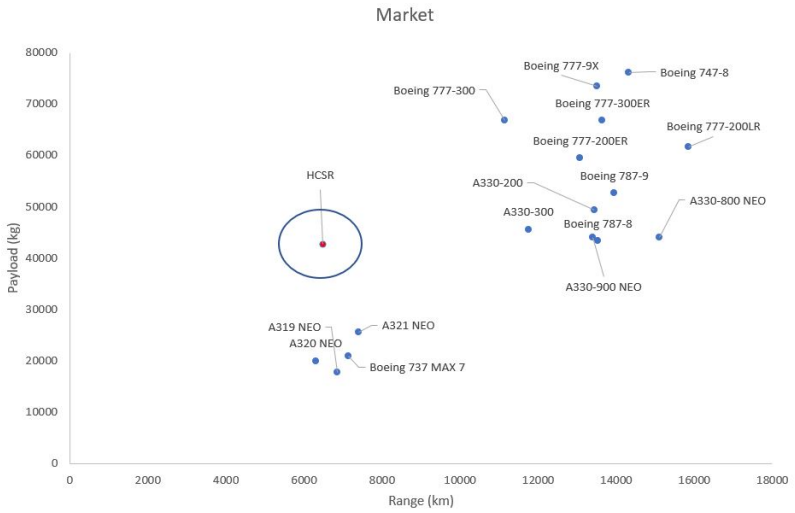

Figure 2.3: Market gap

As the global passenger demand is predicted to double to 7.2 billion in 2035, it is useful to analyse the future of both existing and upcoming markets to determine if a high capacity short range aircraft meets future needs[4]. Experience has shown that airlines operating from congested airports are inclined to reduce the number of short range flights to this destination. Once an airport is at full capacity, the only way to grow in terms of passenger count and finance is to attract bigger aircraft.

[3] Global Fleet & MRO Market Forecast Commentary 2019-2029. Accessed November 2019. https://www.oliverwyman.com/content/dam/oliver-wyman/v2/publications/2019/January/global-fleet-mro-market-forecast-commentary-2019-2029.pdf

[4] New IATA Passenger Forecast Reveals Fast-Growing Markets of the Future. Accessed November 2019. https://www.iata.org/pressroom/pr/Pages/2014-10-16-01.aspx

2.2. High demand routes

The idea of bringing a new short haul high capacity aircraft on the market initially arose from the problem of airport congestion. When analysing the amount of seats on high demand routes, it becomes clear that increasing the amount of seats per flight will lower congestion.

Existing wide-body aircraft typically have a larger range compared to narrow-body aircraft. Apart from being more efficient on short haul routes, narrow-body aircraft have the advantage of faster turnaround times and have lower risk in terms of empty seats. Another reason for the current preference of narrow-body aircraft is that in a competitive market, airlines prefer frequency of flights. Other then offering passengers freedom of choice between departures, one of the main reasons of increasing frequency in a highly competitive market is schedule delay[3], which is defined as 'the passenger's preferred time of departure and the nearest available service'. However, the expected increase in demand is limited by the capacity of the aircraft. This means that in next 10 years, wide-body aircraft will increase in popularity on short to medium routes.

The relation of high demand and the use of larger aircraft can already be seen around the hubs, Kuala Lumpur (KUL), Singapore (SIN) and also Bangkok (BKK) and Hong Kong (HKG). The Asia Pacific market is by far the busiest and the extensive use of wide-body aircraft on short routes around Asian hub airports confirms this. In Japan and China, an impressive 4,700 and 4,400 respectively, aircraft depart every week to fly routes less than 4,500km. Every week, 1,900 of such flights depart from Tokyo Haneda(HND), evidently making a high capacity short range aircraft fit the current market without any change on the flight schedule. Already 8 out of 10 flights of the route Hong Kong(HKG) - Taipei(TPE) are operated by wide-body aircraft, underlining the massive demand for air travel in the Asia-Pacific region. All of the top 10 short distances flown with wide-body aircraft routes are intra-Asia Pacific flights. After the Asia-Pacific region, Dubai International Airport (DXB) follows up with almost 1,000 departures per week.

2.3. Market SWOT Analysis

This section shows analysis of the Strengths, Weaknesses, Opportunities and Threats (SWOT) of design - market research conducted for the high capacity short range transport aircraft. They can originate both internally and externally. In Table 2.1 a detailed SWOT analysis can be found.

Table 2.1: SWOT Analysis

	Helpful	Harmful
Internal	- Team under the supervision of Roelof Vos (project leader at flying-v, similar concept). - Less contribution to environmental impact by the design. - Team guided by coaches with specialisation related to the project. - More comfortable flying experience. - Readily available professional help from within the university.	- Less frequent flight. - Limited accessibility to the global market forecasts. - Limited time and resources for the project.
External	- Increment in demand of larger narrow-body aircraft in market. - Trend in more green/sustainable air travel. - Global rise in demand of commercial air travel. - Availability of new technology.	- Market mainly dominated by two large manufacturers so difficult to make a position in the current market. - Existence of better alternative design concepts. - Technology demanded by the design might be non-existent, not matured yet or entering to service with outdated technology. - Sudden fluctuations in market dynamics forecast (for example due to unforeseen accidents like that of Boeing 737 max). - Aspects of design might not comply with governmental laws and rules leading to termination of the project.

2.4. Customer Interests and Aircraft Pricing

As the customer will have a large influence on the design of the aircraft, it is important to know what the customer is looking for in an early stage of the design. A way to analyse the customer is by looking at the aircraft's costs and revenues. This can be summarised in the return on investment (ROI) shown in Equation 2.1. The definition of the ROI is taken from Roskam [4].

$$ROI = \frac{(REV - DOC - IOC)V_{bl}}{AEP(1 - tx_{inv})}(1 - tx_{rev})U_{ann} \tag{2.1}$$

As the manufacturer has very little influence on indirect operating cost (IOC), investment tax credit (tx_{inv}) and income tax rate (tx_{rev}), these can be neglected. For the direct operating cost (DOC) the take-off weight, aerodynamic efficiency and fuel efficiency are the driving factors. Block speed is mostly influenced by the cruise speed of the aircraft. Revenue per km (REV) is influenced by the seating capacity and payload capacity. The annual utilisation of the aircraft (U_{ann}) is

influenced by the maintainability and the flexibility of the payload and fuel arrangement. Lastly, the estimated aircraft price (AEP) can already be computed from reference aircraft, which can be found in Section A.1. To do this, the average list price is equated to the maximum take-off weight in Figure 2.4. As the mission objective is a short range aircraft with a high capacity, a wide variety of aircraft were chosen as a reference with the only requirement being that they are still in production. The 777-300 is taken as a direct reference for the maximum take-off weight, as it is relatively similar in terms of capacity and range. Then, a first target for the price of the aircraft is computed as shown in Figure 2.4 and is approximately 180 million USD.

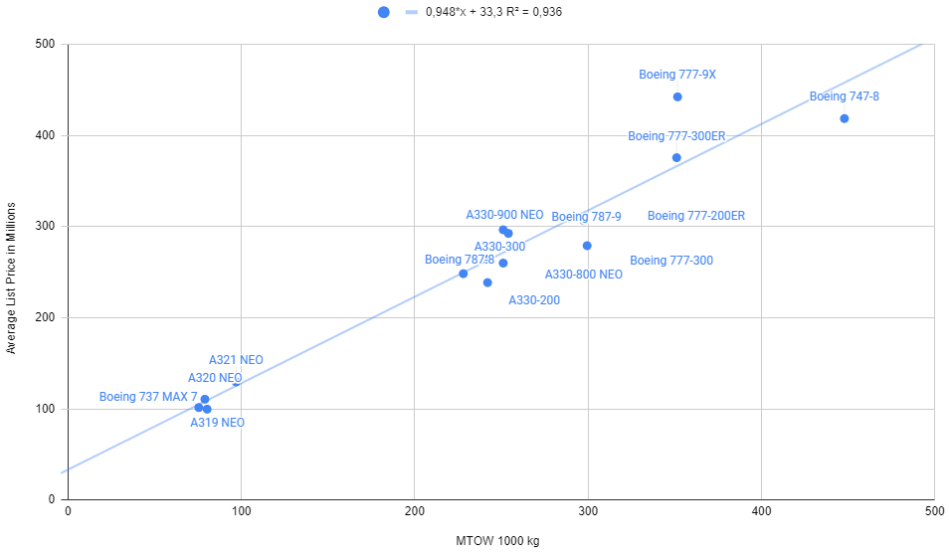

Figure 2.4: Aircraft price target

2.5. Market Potential

With the global market trend, it is possible to compute a first estimate of the total amount of aircraft that can be sold throughout the expected production time. Looking at similar aircraft a production time of 15 years is a reasonable first estimate, which means a production period from 2029 to 2044. With a global fleet size of 25,777 in 2029 and extrapolating with 4.9 %, the global fleet size by 2044 is estimated to be 52,828. This means that a total of 27,051 aircraft will be sold in this period. Furthermore, the projected market share of a relatively new manufacturer like Comac is 4%, as shown in Figure 2.1. Although Comac is a Chinese state-owned manufacturer, this number can still be useful to estimate a rate of growth in the aircraft market. Then also taking into account that a large 400 passenger aircraft will only be used on the most populated routes, a projected market share of the short range high capacity aircraft of 5% is taken as a first estimate for the period: 2029-2044. This means that a total of 1,353 will be sold. At a price of 320 million USD, this results in a revenue of 433 billion USD in the period: 2029-2044.

3

FUNCTIONAL ANALYSIS

In this chapter, the operation of an aircraft is analysed to create a functional breakdown structure and a functional flow diagram. These can be found in Section 3.1 and Section 3.2 respectively and are used to determine the functions that the aircraft to be designed has to accomplish.

The aircraft operation is split into six parts; pre-flight, take off, flight, landing, post-flight and maintenance. The pre-flight operations are defined to begin the moment a new crew enters the aircraft and end right before push back. Then, the take-off operations run from push back until the aircraft finishes the climb to cruise level. The cruise part of the mission profile is included in the flight operations and lasts until right before the approach procedure. Landing operations begin with the approach check up to when the aircraft parks at the gate. After the aircraft is parked, the post-flight operations start until when the auxiliary power supply is shut down. Finally, the aircraft can go into a maintenance phase. Of course, aircraft maintenance is not always necessary after a flight, which is why the functional flow diagram in Section 3.1 shows it as an optional phase. If the aircraft is not put through the maintenance phase, it will return to the pre-flight operations.

The phases, as discussed above, are defined to be the first level in the functional breakdown structure and are coloured in yellow. The second level is coloured in blue, the third in green and the fourth in red. The same colouring structure is used in the functional flow diagram.

3.1. FUNCTIONAL FLOW DIAGRAM

The functions defined in the functional breakdown in Section 3.2, are organised in chronological order in the functional flow diagram. The purpose of this visualisation is to see the interdependence between each function. Moreover, it shows the optional routes as sometimes more than one options are available to attain the success of the main function. Each function in the functional flow diagram contains a number that corresponds to the same function in the functional breakdown structure.

3.2. FUNCTIONAL BREAKDOWN

A functional breakdown is a logical grouping of functions according to a predetermined set of criteria [5]. As mentioned beforehand, the main criteria to be developed are functions belonging to the six parts of the aircraft operation. Each criterion is developed further down, to a maximum of 3 levels deeper, into more detailed functions. However, for the aid of the design of purpose, only the functions that have a significant impact on the concept design are further developed.

Function flow diagram

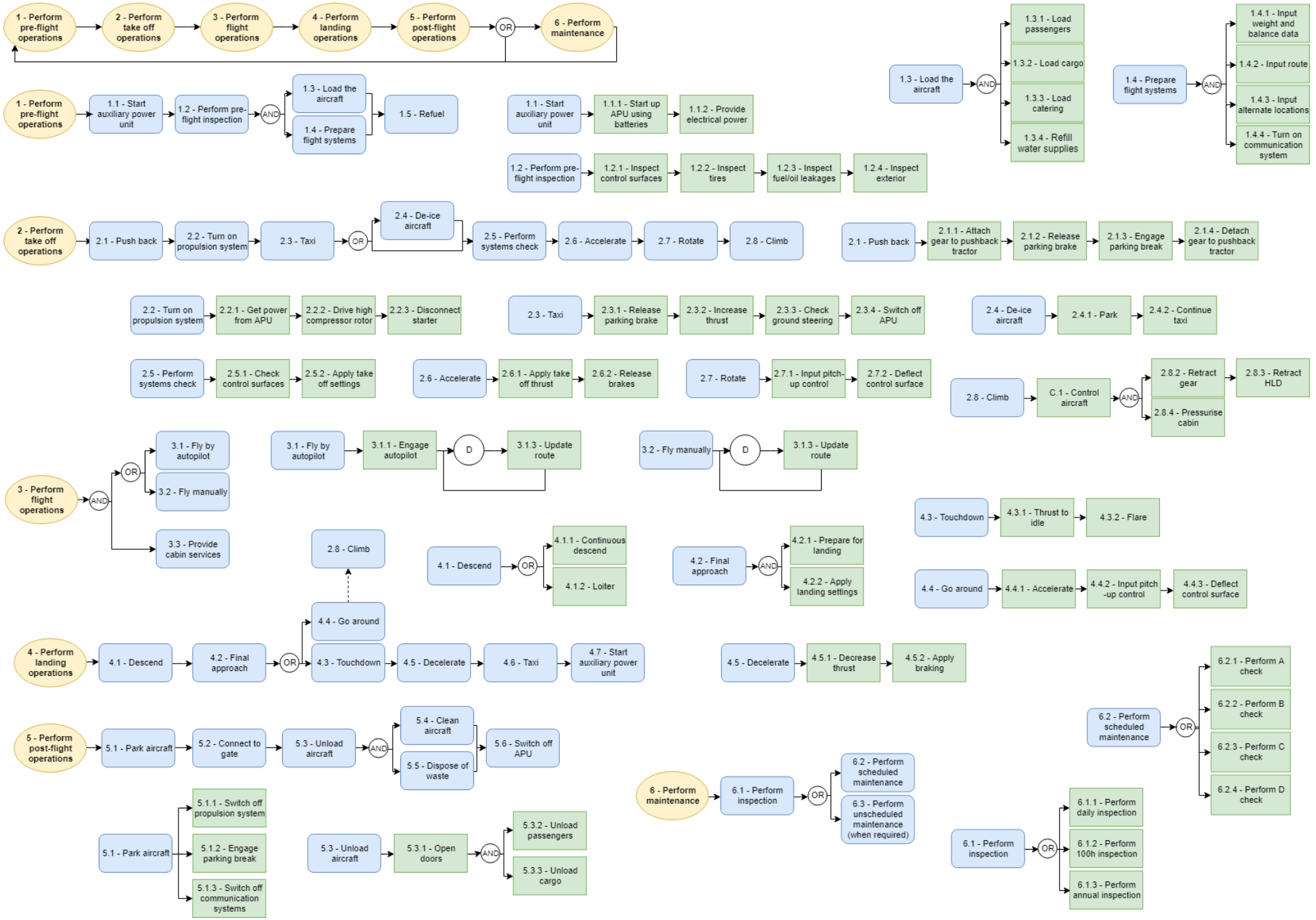

Function breakdown structure

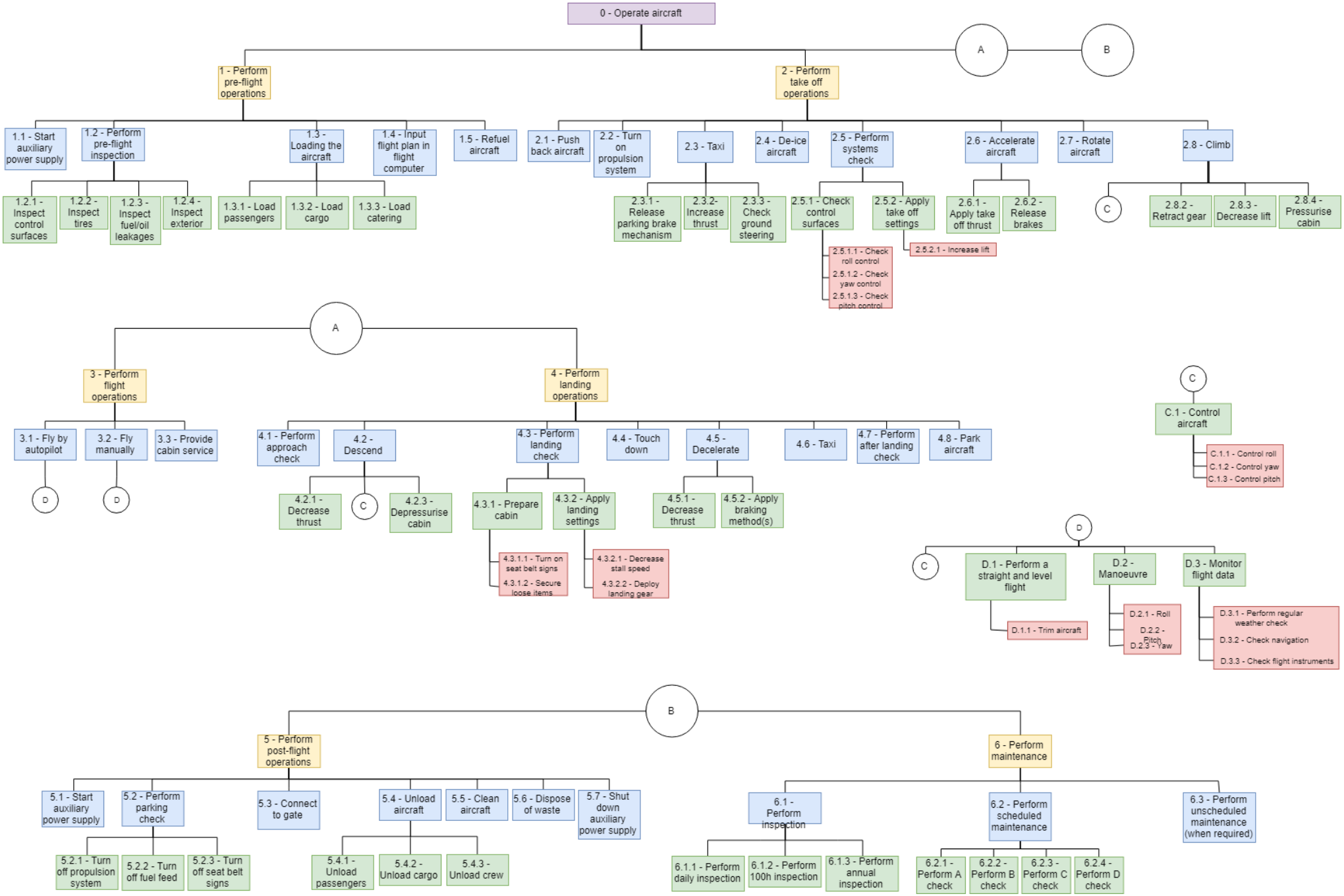

4

OBJECTIVES AND REQUIREMENTS

In this chapter, the objectives and requirements that drive the design are explained. The design objectives are shown in Section 4.1 and the requirements list is shown in Section 4.2.

4.1. DESIGN OBJECTIVES

In order to design a competitive aircraft that can compete on the global market and contribute to a future of sustainable aviation, a set of design objectives have been defined. The design objectives are listed in Table 4.1

Table 4.1: Design Objectives

Objective	**Type**
Aircraft recurrence cost shall be minimised.	Cost
Non-recurrence cost shall be minimised.	Cost
The aircraft's carbon footprint over the entire life cycle shall be minimised.	Sustainability
The aircraft's NO_x emissions shall be minimised.	Sustainability
Minimise noise inside the cabin.	Sustainability
Increase passenger comfort by lowering cabin altitude from 8000 ft.	Passenger comfort
Increase passenger boarding efficiency and decrease turn around time compared to competing aircraft.	Passenger comfort

The design objectives originate from the market analysis and the project objectives of the team. Minimising non-recurring costs will allow for competitive aircraft pricing and higher returns. Recurring cost, and direct operating cost, in particular, are key parameters to airlines and therefore a strong indication of market competitiveness. Measures of reducing direct operating cost include, for example, reducing operating empty weight and reducing engine specific fuel consumption.

As environmental considerations become more important around the world, special emphasis is put on reducing the aircraft's emissions and reducing noise both inside the cabin and outside of the aircraft. Sustainable design includes, amongst others, reducing CO_2 and NO_x emissions.

4.2. REQUIREMENTS

The requirements are shown in Table 4.2 and are presented in five different categories: structural, performance, operations, stability & control and sustainability. Alongside the requirements, the means of compliance is specified to indicate how compliance with requirements can be proven. The timeline and origin of the requirement are specified to trace the timeline and source respectively. The timeline is defined to be the checkpoint when the requirement can already be checked and two of them are established; mid-term report (MTR) and final report (FR). Regarding the sources, there are four main origins of the requirements; the American Institute of Aeronautics and Astronautics (AIAA), the Federal Aviation Administration (FAA)[1], International Civil Aviation Organization (ICAO) and the market analysis. All requirements specified have been cross-referenced with the authority regulations to meet the current aviation standards.

[1] FAA Regulations. Accessed November 2019. https://www.faa.gov/regulations_policies/faa_regulations/

Table 4.2: Requirements list

Identifier	Requirement	Means of compliances	When	Origin
Structural				
HCSR-STR-001	The cabin shall be pressurised to 8,000 ft pressure altitude at maximum flight altitude	Hoop stress, circumferential stress analysis	MTR	AIAA
HCSR-STR-002	Wing span shall be smaller than 65 m to conform to type V gate dimensions	Class I configuration design	MTR	AIAA
HCSR-STR-003	Tail height shall be smaller than 20.1 m to conform to type V gate dimensions.	Class I configuration design	MTR	AIAA
HCSR-STR-004	Business class seats shall have a 36" pitch	Cabin layout Class I	MTR	AIAA
HCSR-STR-005	Business class seats shall have a 21" width	Cabin layout Class I	MTR	AIAA
HCSR-STR-006	Economy class seats shall have a 32" pitch	Cabin layout Class I	MTR	AIAA
HCSR-STR-007	Economy class seats shall have a 18" width	Cabin layout Class I	MTR	AIAA
HCSR-STR-008	The aircraft shall fit in a A380 hangar of 180m x 140m x 27.5 m	Aircraft layout Class I	MTR	Market Analysis
HCSR-STR-009	Aircraft cargo compartments shall allow storage of at least 5 cubic feet of luggage per passenger	Cabin layout class I	MTR	AIAA
HCSR-STR-010	The pilot overnose angle shall be atleast 11 degrees	Class I cockpit/fuselage design	MTR	Market Analysis
HCSR-STR-011	The pilot overside angle shall be atleast 35 degrees	Class I cockpit/fuselage design	MTR	Market Analysis
HCSR-STR-012	The aircraft systems shall fit into the aircraft	Class I cockpit/fuselage design	MTR	Market Analysis
HCSR-STR-013	All passengers and crew shall fit and be seated in the aircraft	Class I cockpit/fuselage design	MTR	Market Analysis
HCSR-STR-014	The required volume of fuel shall fit inside the tanks	Class I cockpit/fuselage design	MTR	Market Analysis
HCSR-STR-015	The passenger cargo shall fit inside the cargo hold	Class I cockpit/fuselage design	MTR	Market Analysis
Performance				
HCSR-PER-001	The aircraft shall be able to take-off from a runway with dry pavement (sea level ISA+15 degrees C) with a balanced field length of 9000 feet at maximum take-off weight according to FAA 14 CFR part 25	Class I sizing thrust loading/wing loading diagrams	MTR	AIAA
HCSR-PER-002	The aircraft shall be able to land on a runway with dry pavement (sea level ISA +15 degrees C) at the end of the design range mission	Class I sizing thrust loading/wing loading diagrams	MTR	AIAA
HCSR-PER-003	The maximum approach speed shall be 145 kts at the end of the design range mission	Class I sizing thrust loading/wing loading diagrams	MTR	AIAA
HCSR-PER-004	The aircraft shall have a parking brake	Aircraft system feature	FR	Market Analysis
HCSR-PER-006	For a mission range of 700 nmi the aircraft shall have a flight time of under 2 hours 15 minutes under no wind conditions	Aircraft design cruise speed	MTR	Market Analysis
HCSR-PER-007	The engines shall have a specific fuel consumption (SFC) lower than 0.6	Engine specification	MTR	Market Analysis
HCSR-PER-008	In the landing configuration, the steady gradient of climb may not be less than 3.2 percent	Class I climb performance	MTR	FAA
HCSR-PER-009	With one engine inoperative take off and landing gear retracted, The steady gradient of climb may not be less than 2.4 percent for two-engine aircraft	Class I climb performance	MTR	FAA
HCSR-PER-010	Take-off distance shall be the distance greater between the OEI take off length, the accelerate-stop distance and 115 % of the take off distance when all engines operatives	Class I sizing thrust loading/wing loading	MTR	FAA
HCSR-PER-011	The positive limit manoeuvring load factor n for any speed up to Vn shall not be less than 2.1 + 24,000/ (W + 10,000) except that n may not be less than 2.5 and need not be greater than 3.8 - where W is the design maximum takeoff weight	Class I V-n diagram	MTR	FAA
HCSR-PER-012	The negative limit manoeuvring load factor shall not be less than -1.0 at speeds up to VC	Class I V-n diagram	MTR	FAA
HCSR-PER-013	If wing flaps are to be used during takeoff, approach, or landing the resulting limit load factor shall not exceed +2.0	Class I V-n diagram	MTR	FAA
Operational				
HCSR-OPR-001	The aircraft shall fit 400 passengers	Cabin layout	MTR	AIAA
HCSR-OPR-002	Business class shall fit 50 passengers	Cabin layout	MTR	AIAA
HCSR-OPR-003	Economy 350 passengers	Cabin layout	MTR	AIAA
HCSR-OPR-004	The aircraft's Entry into Service shall be 2029	Confirm availability of each subsystem	FR	AIAA
HCSR-OPR-005	The aircraft shall have a turnaround time of less than 1h45m	Statistical estimation with reference cabin layout	FR	Market Analysis
HCSR-OPR-006	The aircraft crew shall consist of 2 pilots and 8 cabin attendants	Cabin layout	MTR	AIAA
HCSR-OPR-007	Aircraft fuselage shall have at least two type A doors available for standard boarding operations.	Cabin layout class II	FR	FAA
HCSR-OPR-008	If a Type A, Type B, or Type C exit is installed, there shall be at least two Type C or larger exits in each side of the fuselage.	Exterior specification, door and fuselage sizing, and cabin layout	FR	FAA
HCSR-OPR-009	Emergency exits at each side of the aircraft shall include at least two Type I exits or larger	Exterior specification, door and fuselage sizing, and cabin layout	FR	FAA
HCSR-OPR-010	For the maximum number of passengers in the aircraft, the amount and type of emergency exits shall be installed complying with part 25.807 of 14 CFR part 25	Exterior specification, door and fuselage sizing, and cabin layout	FR	FAA
HCSR-OPR-011	At any point between seats, the passenger aisle width more than 63.5 cm above floor shall be at least 50.8 cm and the passenger aisle with less than 63.5 cm above floor shall be at least 38.1 cm	Cabin layout and fuselage sizing	MTR	FAA
HCSR-OPR-012	For any passenger seat in the cabin, their shall be no more than two adjacent seats between seat and a cabin aisle	cabin layout and fuselage sizing	MTR	FAA
HCSR-OPR-013	In case of emergency, all passengers (in full capacity) and number crew members shall be evacuated from the aircraft to the ground within 90 seconds	cabin layout with statistical comparison	FR	FAA
HCSR-OPR-014	Aircraft's dimension and layout shall be compatible with the gate V ground servicing equipment with sufficient clearance and distance for ground operation	Class I sizing, design comparison with reference aircraft ground handling manual	MTR	Market Analysis
HCSR-OPR-015	The aircraft shall have atleast one accessible lavatory	Cabin layout and fuselage sizing	FR	FAA
Stability and Control				
HCSR-SCR-001	The aircraft shall have level 1 handling qualities when all systems are in their normal operating state; level 2 flying qualities after failures occuring approximatly once during the aircrafts lifetime; level 3 flying qualities after rare failures	Control and stability diagrams (Flight dynamics)	FR	FAA
HCSR-SCR-002	The time to achieve 30 deg bank angle shall be less than 1.5 sec	Sizing ailerons and compute control derivative	FR	FAA
HCSR-SCR-003	Longitudinal control force for prolonged application shall be less than 10 lbs	Designing trim tab and calculate control force	FR	FAA
HCSR-SCR-004	The aircraft shall have stable longitudinal eigenmotions	Real part Longitudinal eigenvalues <0	FR	FAA
HCSR-SCR-005	The aircraft shall have stable dutch roll mode characteristics	Real part lateral eigenvalue <0	FR	FAA
Sustainability				
HCSR-NF-SUS-001	The aircraft shall allow for segregated waste stowage on board	Aircraft subsystem feature	FR	FAA
HCSR-NF-SUS-002	Noise level shall comply with the ICAO chapter 4 standards	Engine specification, MTOW-Noise statiscal comparison	FR	ICAO

5

SUSTAINABILITY DEVELOPMENT STRATEGY

One of the important parts of project is the development of sustainable aircraft. So first, the main criteria of sustainability in this particular context are defined. After doing an in-depth analysis of the main criteria, it was decided to put the main focus on the following pivotal aspects:

- Determine the optimum fuel consumption.
- Reducing the emissions of NO_x
- Reducing the emissions of CO_2.
- Reducing the cumulative noise levels as a result of airframe and propulsive noise.

To assess the performance of the FB400 aircraft from a sustainable point of view, it is necessary to meet the preset requirements. From this perspective, it is important to have a proper look at an appropriate reference aircraft that has implemented the current state-of-art technology and try to achieve better results. Simultaneously, it is required to make the output values of the fuel consumption analysis a valuable part of the continuous iteration process. In Section 5.1, more details will be provided regarding the technical aspects under the auspices of sustainability. Moreover, the manufacturing process of the FB400 aircraft will be discussed in Section 5.2. And last but not least, some relevant end of life solutions will be analysed and discussed in Section 5.3.

5.1. THE TECHNICAL APPROACH

As can be deduced from Chapter 12, it is necessery to achieve an optimum fuel consumption at the first place. In order to conduct a comprehensive analysis, the 'SAR-methodology ' has been carried out and implemented in a very detailed way. To be able to calculate the specific air range that is denoted by the term 'SAR ', it is scientifically and mathematically Equation 12.2 required to have detailed information (SAR) on the following three main input parameters:

$$SAR = \frac{V_{cr}}{c_T \cdot 0.5 \cdot \rho V_{cr}^2 S \left(C_{D_0} + \left(\frac{W_{cr}}{0.5 \cdot \rho V_{cr}^2 S} \right)^2 \cdot \frac{1}{\pi A e} \right)} \tag{5.1}$$

- Altitude
- Weight
- Velocity

To dive a bit deeper into this method, but at the same time keeping a clear overview, the specific air range is the direct derivative of the distance (which is covered by the aircraft throughout the entire flight or a specific stage) relative to the continuous change in total weight of the aircraft. As the FB400 aircraft should be able to cover a total distance of 3,500 nm, the conclusion was drawn that the cruise stage is by far the most dominant stage throughout the entire flight; not only in terms of flown distance, but especially the amount of fuel weight that needs to be consumed. As the SAR can be regarded as the instantaneous ratio between the total distance flown through the air and the amount of fuel that is burned in order to cover that particular distance, by making use of the steady level flight conditions (throughout the cruise stage) and thus the arrangement and substitution of terms, it becomes clear that the SAR is directly dependent on the following aircraft design parameters:

- Zero lift drag coefficient
- Lift over drag ratio
- Total wing area

By implementing the analysed and calculated aircraft design characteristics (mainly obtained from implementing the Class I method), the SAR at different altitudes for different velocities can be obtained. However, the purpose of this analysis is to feed the overall ongoing iteration process on a consistent basis. So a detailed sensitivity analysis of the SAR vs the main parameters as the wing area, lift over drag ratio, velocity at varying altitudes had to be conducted.

The obtained results in terms of optimum fuel consumption at a specific altitude and for a particular velocity are incorporated in the iterative process in order to enhance the contribution of sustainability to the overall design.

At a certain stage during this project, it is obligatory to assess the different conceptual designs based on different main criteria. Regarding the decisive trade-off that needs to take place between the different conceptual designs, sustainability is one of the absolute heavyweight factors. The fuel consumption analysis is carried out for each individual design and the subsequent impact on global warming at each altitude is analysed by looking at one common point in terms of velocity and altitude. As far as noise is concerned, the propulsive noise due to the chosen engines for each concept is assessed and taken into consideration in the trade-off.

As far as the FB400 design is concerned, which comes as the absolute winner out of the trade-off, it is already mentioned how the fuel consumption detailed analysis is incorporated in the process of continuous iteration. Secondly, the global warming impact of the greenhouse emissions needs to be analysed in depth. However, it is known from constructive literature studies that the lower an aircraft flies the beneficial it becomes from the perspective of global warming impact. The main and only output of the global warming analysis is altitude. From this perspective, recommendations can be made regarding the altitude that the FB400 preferably can fly at. The main metrics that are used in order to carry out this analysis are the global warming potential (GWP) and the radiative forcing (RF). These analyses are mainly based on the fact that the emissions of CO_2 and NO_x should be reduced as much as possible.

The third pillar, regarding sustainability, that needs to be taken into consideration is the emission of noise. Noise can be subdivided into two subcategories:

- Propulsive noise
- Airframe noise

The decision is taken to come up with a noise analysis, rather than a complicated analysis that should be part of the continuous iteration process. The noise analysis will be based on the final aircraft lay-out and configuration. As the impact on the interation process is so huge in the case that the engines and landing gear should be shifted up- or downstream the trailing edges of the FB400, it is chosen to come up with recommendations regarding favourable engine- and airframe positions.Furthermore, by analysing ways to apply shielding and acoustic liners (at the fan inlet location) an overall reduced cumulative noise level can be achieved.

5.2. The Manufacturing Process

In the manufacturing process, all the parts are created with the final goal of completing the assembly and rolling the aircraft out of the production line. Making a sustainable design already starts at the manufacturing process. Lean manufacturing plays an important role here. The motivation behind this specific type of manufacturing is that the amount of waste should be minimised. In this context, the meaning of the word waste in lean manufacturing is any costs or effort that have been spent regarding the transformation of raw materials into an item the customer is actually not willing to pay for. The easy conclusion to draw is that waste in any form or shape should be prevented. It looks at the different type of actions taken during the process and rates them as valuable or waste. They are defined as follows [6]:

- Actions that lead to something in which the buyer sees value.
- Actions that do not have a direct value for the potential customer, but in every way it is inevitable to undertake these. For example, the transportation of parts to warehouses.
- Actions which have absolutely no additional value (waste) and should be avoided as much as possible.

Out of the three aforementioned categories, only the first one can not be regarded as waste. The preset goal is to reduce waste wherever possible in order to enhance the positive implementation of sustainability. From this perspective, it is essential to cut down the waste from categories two and three. As one can imagine there are different sorts of waste, such as processing, transportation and economical waste. All these forms of waste are directly or indirectly related to sustainability. It can be of pragmatic importance to make use of manufacturing inventory software in order to speed up the manufacturing process and to save time by eliminating unnecessary steps. Furthermore, it is important to minimise the usage of water. One of the pioneering techniques that definitely can be used is 3D printing, as this particular technique does not generate any waste.

Reducing waste as a result of processing is of large importance as well. For composite materials a lay-up processes are preferred since they limit the waste material. For metals like aluminum, casting is a good solution. It will limit the waste which would otherwise be cause by milling or drilling for example.

One of the actions that is interesting to have a deeper look at is the transportation of parts and assemblies to certain

locations. It would be an ideal situation to have all the components coming from the same area, however this is not realistic. The parts of a transport aircraft nowadays come from countries throughout the whole world. Nevertheless, it is still interesting to research the possibilities.

For the final assembly line, it might be interesting to discuss the possibility of having it near an airport. Once it rolls off the band and is ready to fly, it can easily transport itself to the location the buyer would like to have it. For the production of the smaller components, like high lift devices, doors and windows, the location does not have many restrictions. An idea would be to place it close to a railway station as these components can be easily transported by train.

5.3. End of Life Solutions

Until this very day, the vast majority of the aircraft that are no longer operative can be labelled as inefficient. Logical sense dictates that it should be possible to come up with creative ways to find sustainable solutions for an aircraft that has exceeded its lifetime cycle. The idea that immediately could pop up is that such an aircraft should be recycled by disintegrating the parts that it is composed of. The process of recycling can definitely contribute to minimise the environmental impacts. There are various different customers, which can be potentially interested in specific parts that are still functioning well and/or materials. From this perspective, it is highly recommended to unfold a strategy to recycle as many parts of the aircraft as possible after the expiration of the lifetime cycle [7].

The plan of approach is to remove numerous components and materials including short and long glass and carbon fibre composites, aluminium, wires, textiles and carpet, landing gears, electronic devices, foam, fluids, galley carts, trays, and overhead bins and engines [8]. By far,the parts that represent the most valuable value are the engines and parts which can be reused or renovated and resold. From the perspective of retrieving parts, which still represent considerable financial value, it is essential to keep a detailed maintenance log [8].In order to avoid unnecessary waste of time, money, transport and energy, it is important to re-use functioning parts or to sell them to interested customers. Parts that still represent value but are not immediately ready for reuse should be considered whether they can be subjected to renovation or not. After this, these parts can also be reused or resold.

After all the aforementioned procedures has taken place, the airframe of the original aircraft is left over. The airframe structure can be composed of different metal sorts, alloys and (thermoset and thermoplastic) composite parts. In regard to the FB400, the airframe structure is in its entirety composed of quasi-isotropic carbon fibre composite and aluminum alloy. Composite materials are widely used in the aerospace industry, as these materials have a higher strength, lower weight and less maintenance compared to conventional materials, as well as a long lifespan [9]. Being aware of all the aforementioned benefits, the conclusion can be drawn that the use of composite materials is justified from a sustainable point of view.

The following step, which is necessary before the recycling process can begin, that needs to be performed is separating quasi-isotropic carbon fibre composite from aluminum alloys. One of the most jaw dropping current state of the art techniques, which can be applied to recycle composite materials, is thermal co-processing [9]. The benefits can be summarized as follows [9]:

- Suitable for post-consumer waste.
- Lower carbon emissions (compared to conventional techniques) of cement processings.
- Decreases costs of waste management.
- Saves on virgin materials.
- No residues left behind.
- Energy from resin matrix.
- Solid residue (fibre ashes,mineral fillers).
- Actual system “mission proven” through successful ground or space mission operations (TRL 9).

With the increase in prices of virgin raw material and the high standard environmental norms set by the government, it has become compulsory to recycle metal waste [10]. Some innovative techniques had to be developed in order to attain a higher yield than the conventional recycling processes [10]. High-pressure torsion (HPT) is applied as a new technique for the recycling of aluminum. The main objective of this specific technique is to convert nonferrous waste directly into the end product by making use of shear for effective consolidation. The re-melting procedure is abandoned with this new technique.

6

DESIGN METHODOLOGY

In this chapter, the overview of the design process is presented. First, the three design phases are presented in Section 6.1. Then, the trade-off method is given in Section 6.2. Finally, the verification and validation procedure is explained in Section 6.3.

6.1. DESIGN PHASES

The design process of the High Capacity Short Range aircraft is divided into 3 different phases.

To begin with, in design phase I the requirements are defined and the concepts are explored with the aid of a design option tree. The combination of the two creates a starting point to generate three conceptual designs. These three designs are the outcome of design phase I as a contender for the design of the High Capacity Short Range aircraft. The results of design phase I is summed up in the baseline report [1].

In Design phase II the three design concepts are developed with class I sizing method. In this phase, the main aircraft system (such as pressurisation, hydraulics, and control systems) are defined with an additional brief insight on the operation of the three designs. Each of these designs' properties are analysed to be traded off and give out an output of only one final design. The results of design phase II is summed up in the midterm report [2].

Finally, In Design phase III the chosen design is improved using class II sizing methods and this is iterated with parts of the class I sizing. This is combined with more detailed analysis of the various disciplines, namely aerodynamics, structures and control and stability. Taking the outcomes of these into account the performance of the aircraft is optimised to be compatible and competitive in the targeted market. Furthermore, a financial analysis of the aircraft design is performed and a production and project plan are composed to complete the design process. The results of design phase III is summed up in this report.

6.2. TRADE-OFF METHOD

The trade-off methodology is taken based on the method explained in the Systems Engineering & Technical Management Techniques lecture notes [5]. It is chosen to go for a trade-off method using weight factors. The criteria get a weight factor from one to five, with one being the least important and five the most important. Furthermore, each concept or design option can get one of the following ranks: poor - mediocre - sufficient - good - excellent. For calculation purposes, these ranks are given a score one to five respectively. Furthermore, the weights are normalised to enable a standardised comparison between the criteria.

6.3. VERIFICATION AND VALIDATION METHOD

During the whole design process, the design has to be verified and validated. The procedures are defined in the following sections, starting with the verification and the validation follows after. It is important to define the procedures in an early stage, so that they can be maintained throughout the development of the design.

6.3.1. VERIFICATION

Multiple models are created during the design. It is necessary to verify the models from the start of the project in order to minimise wrong inputs to further design phases.

In the design process, different programs such as spreadsheets, Python and MATLAB are used. The spreadsheets are mainly used for calculating the take-off weight, the c.g. position and other aircraft parameters important for sizing in design phase I, II and III. Python is used in design phase II to analyse the environmental impact and operational analysis. MATLAB is used in design phase III to calculate the fuselage weight and the stability and controllability of

the aircraft. These models are verified using unit tests and system tests, as described below.

In design phase I, II and III there are multiple spreadsheets for each conceptual design and topics. These spreadsheets include multiple tabs and hundreds of references between them. Each of these topics are verified using unit tests. Firstly, all the equations and values are checked whether they are correct and entered correctly. Also the units are checked, because there is a large combination of SI and imperial units. Secondly, all parameters are checked if they are linked to a central tab, meaning that if the user changes the value here, it changes everywhere it needs to change in the calculation sheets automatically. Thirdly, different inputs are given to the model and the expected results should follow. For example, if the equation is a long multiplication of values, this would mean that increasing a value by a factor two will also increase the outcome by a factor two and setting it equal to zero should lead to an outcome of zero.

After checking all tabs on their individual functionality, a system test is needed to check if the different tabs also work well together. Firstly, it is checked whether all the values are linked well together. Secondly, an input is changed and the expected outcome is compared to the calculated one. This can be either a realistic input or a singular input. If they are in a range of 5% of each other, the test is considered successful.

In design phase II and III Python and MATLAB are used. Verifying the code is done in multiple ways. Firstly, running the code through the compiler will bring up syntax errors which are then fixed by the user. Secondly, unit tests are needed to verify the individual units of the code. These tests can for example check the system's response on a singularity input. Also for the stability and control analysis, the conversion to state space can be verified by checking whether the state-, feed-forward-, input- and control matrix dimensions are correct. Furthermore, the resulting system responses of the aircraft dynamics can be plotted to verify if the responses match the expected results from theory. The root locus graph can be plotted to compare eigenvalues, damping ratios and natural frequencies of the resulting system with reference aircraft. After tuning the controller gains, the gain values can be compared to other aircraft controllers to verify if the gain is reasonable.

The accuracy of the used tools also has to be taken into account. It is known that the spreadsheets only have an accuracy of 14 decimal digits. However, when multiplying this with aircraft weight in the order of 10^6 this is still acceptable. The accuracy of python and MATLAB can be increased far beyond 14 decimal digits and is thus considered not to be limiting.

6.3.2. VALIDATION

During validation, it is checked whether the results of the models represent the physical problem accurately. This is done with the use of reference aircraft.

In order to validate the spreadsheets, the aircraft parameters from a reference aircraft are entered and the result is checked. Furthermore, parameters from examples in the book of Roskam [4] can be entered to validate the spreadsheets. Since class I weight estimations belong to the start of conceptual design, a margin of 10% is used when comparing the spreadsheets to the reference aircraft.

The stability derivatives and corresponding system eigenvalues can be validated using reference aircraft. For Blended Wing Body aircraft, this means comparing obtained derivatives to values supplied by other papers. If it is not possible to find certain values of reference aircraft, it is possible to take data from other aircraft. NASA provides data from state space matrices from the X-29A and X-31A [1] [2] . As a last resort, a lot of quantitative data is available for the Cessna Citation II from the flight test performed in the third year of the Bachelors of Science. Validation using this data should be performed keeping in mind that the Blended Wing Body will have different flight behaviour. The eigenvalues give information about different motions. These motions can for example be short period, spiral, phugoid and dutch roll. The aircraft responses during these motions is compared to the responses of the reference aircraft.

The validation is different for every type of model. This is why most of the validation techniques are described at the end of each chapter, if used. Also the results will be presented.

[1] Linearized Aerodynamic and Control Law Models of the X-29A Airplane and Comparison With Flight Data. Accessed December 2019. http://jsbsim.sourceforge.net/NASA_TM-4356.pdf

[2] Linearized Poststall Aerodynamic and Control Law Models of the X-31A Aircraft and Comparison With Flight Data. Accessed December 2019. https://ntrs.nasa.gov/archive/nasa/casi.ntrs.nasa.gov/19980004669.pdf

7

DESIGN PHASE I AND II

In this chapter the first two phases of the design is summarised. Starting off with the recap of Phase I, the concept selection is summarised in Section 7.1. Then, phase II starts with the refining of the concept in Section 7.2. The trade-off of the concepts starts with the definition of the criteria in Section 7.3, then the trade-off is done in Section 7.4. Sensitivity analysis is conducted in Section 7.5 and finally the outcome of phase I and II is concluded in Section 7.6.

7.1. CONCEPT SELECTION

After analysing the requirements list in Section 4.2, multiple options are considered. Three of these concepts are taken into the next phase, which is class I sizing, and will go through a secondary trade-off later. Here are the multiple options considered that are not chosen to go through the next phase.

Redesign existing aircraft: Since long-range aircraft with the same amount of passengers exist, its wings and engines could be redesigned for short-range. This option is a very feasible one as all technology already exists. Sustainability can be taken into account by selection of sustainable materials, engines and manufacturing techniques.

Delta wing: This concept is mostly related to wing planform design for efficiency. Such aircraft already exist but the delta wing is most efficient for supersonic flights. However, FAA Regulations state that supersonic flight over land is not allowed [1]. As the aircraft is going to be designed for short to medium range, most flights will take place over land and the delta wing is not fuel-efficient at subsonic speeds so this is not a preferred concept

Flying wing: This concept suggests that no fuselage and tail exist but only a wing. This wing is made thicker so that it can accommodate passengers in it. With this design, the aerodynamic performance is improved. An example of a flying wing design for commercial aviation is the Flying V. It is more fuel-efficient than conventional designs. However, the technology readiness level is still low and certification processes, in general, take a long time. Initial certifications can take up to five years as well as amended certifications [11]. Thus, getting such an aircraft into service before 2029 is unrealistic.

Double bubble flat fuselage: This idea suggests expanding the fuselage horizontally. This will improve the aerodynamic properties of the aircraft and allows for more cabin space. It should, however, be considered that oval cross-sectional shapes are worse in dealing with the pressurisation of the cabin than circular cross-sections. The concept of the double bubble flat fuselage is relatively new and its technology readiness level is low. According to NASA, it is predicted that this type of aircraft can have an entry into service by 2030-2035 [2]. This is at least one year too late for this project and is thus not a preferred concept.

All the concepts have their advantages and disadvantages but taking into account requirements and design objectives, three concepts are chosen to continue to the next design stage. The chosen concepts are Conventional aircraft (Figure 7.1) because it is feasible and reliable, Double Deck aircraft (Figure 7.2) in order to investigate if an implementation of the high fuselage and small wings and engines is possible and Blended Wing Body (Figure 7.3) because of aerodynamic performance.

Conventional aircraft: Instead of redesigning an existing aircraft, as stated as one of the options above, it might be more efficient to start the design of a conventional aircraft from scratch. The aim is to come up with a conventional aircraft design for short-range flights with 400 passengers by also implementing sustainability in all steps of the design. This concept is feasible since similar aircraft have already been developed. A sketch of this concept can be found in Figure 7.1.

Double Deck aircraft: Double Deck aircraft combines the idea of having two decks in order to accommodate passengers more efficiently and at the same time have a conventional small wing and short fuselage to fulfil the requirements

[1] FAA Regulations. Accessed November 2019. https://www.faa.gov/regulations_policies/faa_regulations/
[2] Double Bubble D8. Accessed November 2019. https://www.nasa.gov/content/the-double-bubble-d8-0

for short-range. This concept is feasible because double-deck aircraft are already in service.

Blended Wing Body: The idea behind this concept is to improve the aerodynamic properties of Conventional aircraft by blending the wing and the fuselage. This will make the passenger deck wide enough to accommodate 400 passengers while increasing the fuel efficiency. A lot of research, wind tunnel tests and some scale model test flights have already been done for this concept so it is a feasible option [12].

Figure 7.1: Conventional aircraft

Figure 7.2: Double Deck aircraft

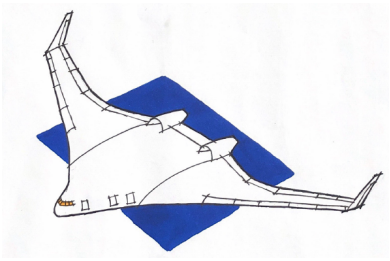

Figure 7.3: Blended Wing Body aircraft

7.2. Preliminary Sizing of Concept

Three concepts are selected to enter the preliminary design and consequently the trade off process. This design stage consists of initial system sizing. Firstly, the payload weight is calculated based on requirements, after which the maximum take off weight and operating empty weight are calculated with the help of the mission definition and fuel fractions. The weights are then iterated with respect to empirical relations. Afterwards, design constraints are defined and matching diagrams are constructed based on those requirements. Moreover, the drag polar is estimated based on wetted area vs wing area ratio, friction coefficient and optimum lift coefficient. From the take off weight and the wing loading computed in the matching diagrams, the wing area is calculated. After that, the main wing parameters such as span, aspect ratio, sweep angle, MAC and thickness to chord ratio are calculated. This is followed by airfoil selection and engine sizing. The engines of the aircraft are sized with the rubber sizing method using the GE9X for a reference engine [13]. Furthermore, a trade off is performed in order to select the type of engine that is going to be used in the design. The fuselage sizing is performed based on requirements and the concept layout chosen earlier. A circular cross section is chosen for both the Conventional and Double Deck aircraft, whereas the fuselage of the Blended Wing Body is sized according to the triple arc principle. The cabin arrangement for each concept is also designed at this stage. Afterwards, a preliminary estimation of the centre of gravity is done, which is then used to determine the position and size of the landing gear and the tails of all the concepts. The most important parameters from the design process are shown in Table 7.1.

Table 7.1: Concept design parameter summary

	Blended Wing Body	**Conventional Aircraft**	**Double Deck Aircraft**
Altitude [km]	13	11.6	11
M_{cr} [ ]	0.81	0.81	0.81
W_{to} [kN]	1589	1754	1719
W_{oe} [kN]	848	917	900
$(L/D)_{cr}$	23.3	18.6	19.2
Wing	Mid	Low	
Engine	n = 2, fuselage-mounted	n = 2, wing-mounted	
Tail	2 vertical on fuselage	1 conventional on fuselage	
Landing Gear	Tricycle, nose wheel = 2, main wheel = 8		
S [m^2]	591	327	321
A [ ]	5.4	10.8	10.9
b [m]	56.7	59.7	59.5
l_{fus} [m]	Outboard = 22.3 Center = 42.5	72.0	60.8
d_{fus} [m]	Rear bulkhead = 10 x 3.3 Mid bulkhead = 13.7 x 4.9	6.3	6.3
S_{wet}/S [ ]	2.5	6.3	5.8

7.3. Trade-off Criteria

For the design trade-off, the criteria needs to be defined. Among the various properties of the designs, only the most significant ones are chosen. Each criteria is assigned a weight factor as an indication of the level of importance decided by the group.

The chosen trade-off criteria are the followings:

- **Cost:** Cost dictates the features of the design, as a more advanced design may be more profitable and more efficient, but comes with a higher cost. Two sub-categories of cost are analysed: recurring and direct operating cost. Recurring cost is paid only once while direct operating cost is a repetitive cost. From the perspective of the customer, the recurring cost is given a weight of 2 and the more significant direct operating cost is given a weight of 5.
- **Risk:** This category consists of technology readiness level, reliability and external threats. Since TRL and reliability are very important for a new design, especially having in mind the time constrain for the product, they are given a weight of 2, whereas the external threats have a weight of 1.
- **Sustainability:** Another main objective of the design is to minimise the environmental impact and create a sustainable design. Two parameters are taken into account: fuel consumption and global warming impact, both with a weight of 3.
- **Turnaround Time:** In terms of profitability of an aircraft, to have a shorter turnaround time is favourable. It is an important trade-off criteria but at this point of the design phase, it is not as significant as the others. Therefore, it is given a weight factor of 2.
- **Passenger Comfort:** Even though passenger comfort is an important factor, it is not the top priority for the design. So the given weight factor is 1.
- **Originality:** To have an advantage in the market, the design needs a unique selling point. For this reason a weight factor of 3 is given to originality.
- **Flexibility:** To be able to expand the market share, it is favourable to have a design that is flexible enough in terms of its payload-range properties and the possibility of it having a family design. However, it is not the priority of this design phase, so both of its categories, being design flexibility and mission flexibility, are given a weight factor of 2.

7.4. Concept Trade-Off

In the following, the criteria are analysed and the final trade-off is summarised in Table 7.2. Each main category is in different colour and has multiple subcategories, as described in Section 7.3. Moreover, the most favourable design for each category is coloured in green and the least favourable in red, the one in between is coloured in yellow.

Table 7.2: Trade-off Summary Table

	Criteria	Weight factor	Blended Wing Body	Conventional Aircraft	Double Deck Aircraft
Cost	Recurring cost	2	2 Mediocre *92.8 M$/unit*	4 Good *87.1 M$/unit*	4 Good *87.2 M$/unit*
	Direct operating cost	5	5 Excellent *219 $/nmi*	2 Mediocre *232 $/nmi*	4 Good *223 $/nmi*
Risk	Reliability	2	3 Sufficient	4 Good	4 Good
	TRL	2	2 Mediocre	4 Good	3 Sufficient
	External threats	1	3 Sufficient	4 Good	3 Sufficient
Sustainability	Fuel consumption	3	5 Excellent *0.00774 kg/km/pax*	3 Sufficient *0.0116 kg/km/pax*	4 Good *0.0106 kg/km/pax*
	Global warming impact	3	5 Excellent	3 Sufficient	4 Good
turnaround time		2	5 Excellent *boarding = 17.2 mins* *Fuel for 700 nmi = 23.000 L*	3 Sufficient *boarding = 21.1 mins* *Fuel for 700 nmi = 28.000 L*	3 Sufficient *boarding = 28.1 mins* *Fuel for 700 nmi = 27.000 L*
Passenger comfort		1	3 Sufficient	4 Good	4 Good
Flexibility	Design flexibility	2	2 Mediocre	4 Good	4 Good
	Mission flexibility	2	2 Mediocre	5 Excellent	4 Good
Originality		3	5 Excellent	1 Poor	3 Sufficient
Total Score			**4.1**	**3.1**	**3.7**

7.4.1. Cost

The cost is important for two of the project objectives: Minimise the operating cost of the aircraft for the reference mission and minimise recurring cost. For the operating cost only the direct operating cost will be taken into account for the trade-off, since the indirect operating cost is only given as a fraction of the direct operating cost in this stage. A higher direct operating cost will thus result in a higher operating cost.

Table 7.3: Direct operating cost and recurring cost

	Blended Wing Body	Conventional Aircraft	Double Deck Aircraft
C_{doc} [$/nmi]	219	232	223
Recurring cost [M$/unit]	92.8	87.1	87.2

The table shows that the Blended Wing Body has a lower direct operating cost than the other concepts, but a higher recurring cost. For the Conventional Aircraft this is the other way around and the Double Deck Aircraft scores average for both criteria. Different weights are given to both criteria.

7.4.2. RISK ANALYSIS

The risk trade off is based on the technical risk analysis. The most dangerous risks and the potential threats are analysed for each concept individually. Afterwards, weight is assigned based on the severity of the risks for each concept. Based on these factors the total risk score is determined and filled in Table 7.2. It is expected that the more original and innovative a concept is, the larger risk it has. This is because of TRL, uncertainty in the design parameters, certification issues or client and user uncertainty.

The most severe risks for the blended wing body are infeasible design, high cost due to low TRL, difficulties in certification, clients and users not trusting in the aircraft and low maintenance flexibility. These risks are related to all three parameters, which is why this concept has lowest score. The risks that are most severe for the conventional design are lack of flexibility in terms of sensitivity and structural failure due to impact with foreign objects. However, these are only two of the 28 severe risks that are analysed for each concept, which is why the risk score of the conventional aircraft is overall high. The Double Deck aircraft has four severe risks, including infeasible design, high cost due to low TRL, low maintenance and low design flexibility. This is what categorises this concept between the other two in terms of risk.

7.4.3. SUSTAINABILITY

To trade off the concepts regarding sustainability, actual values were needed to compare the concepts. The specific air range (SAR) has been used to compare the concepts when it comes to radiative forcing. The SAR was used to compute the amount of kilograms of fuel needed per kilometre per passenger. Table 7.4 shows this fuel consumption. The last column shows the fuel consumption of the three designs when flying on the same altitude. This is because the radiative forcing is not just dependent on the fuel consumption, but also on the height. In order to create a valid comparison between the concepts, they are considered to fly at the same altitude for this calculation.

Table 7.4: Fuel consumption rate per passenger corresponding to the design criteria and common criteria

Aircraft	h_{cr} **[km]**	V_{cr} **[m/s]**	**Fuel consumption per pax [kg/km/pax]**	**Fuel consumption per pax for common cruise speed and altitude [kg/km/pax]**
Conventional Aircraft	11.6	240	0.011	0.0116
Double Deck Aircraft	11.0	240	0.011	0.011
Blended Wing Body	13.0	240	0.008	0.008
Airbus A300-600	10.7	235	0.011	0.011

It can be concluded that the Blended Wing Body scores the best since it has the lowest fuel consumption. A reference aircraft, the Airbus A300-600, has been included to validate the data. Fuel consumption is one of the criteria which goes into the trade-off, which is the amount of fuel consumption at the concept's altitude. The global warming criteria includes flying at the same height and then comparing the different fuel consumption. Both criteria are dominated by the Blended Wing Body concept.

7.4.4. ORIGINALITY

The current commercial aircraft market consists of aircraft that have very similar characteristics. If a new aircraft is brought to the market, it would be advantageous to have a distinguishable design. By bringing originality to the design, the aircraft can have a unique selling point in the market. In order to design a unique aircraft, the originality of the three concepts is taken into account in the concept trade-off. The originality of the concepts is analysed individually after which a score is assigned by means of a trade-off weight. The weight is assigned based on the originality of the aircraft layout and how similar it is to existing aircraft already on the market. The conventional design uses a classic tube and wing configuration. The design is comparable to aircraft that are currently operating on the market like, for example, the Boeing 777. The aircraft has a configuration that has been proven to be effective in the past and therefore has high reliability. However, since it is seen in the current aircraft market in comparable form, it is assigned a poor originality score. The double deck design also has a classic tube and wing configuration like the conventional design. However, the design has two decks of passenger seating. Currently, the Airbus A380 is one of the few operating aircraft that operates with two passenger decks. Unlike the A380, however, the double deck design operates with just two engines making this design more distinguishable from aircraft on the current market. For this reason, the double deck design is assigned a 'sufficient' originality score. Out of the three concepts, the Blended Wing Body is the most original design. Currently there is no aircraft like the Blended Wing Body that is regularly seen in the commercial

aviation market. Therefore, the Blended Wing Body receives a 'excellent' originality score.

7.4.5. Turnaround Time

The turnaround time is traded-off based on the boarding and fuelling time. The boarding time simulation result is shown in Table 7.5 and the fuel volume is estimated for each design concept according to the mission objective of optimising the performance for a 700 nmi range. By assuming that every aircraft is being filled under the same fuel flow (litre/minutes), the fuel volume required is compared.

- Blended Wing Body: 23,270 L
- Conventional Aircraft: 28,500 L
- Double Deck Aircraft: 26,800 L

It can be seen that the Blended Wing Body requires less fuel to fly the same distance. So, the fuelling time for the Blended Wing Body is predicted to be the shortest compared to the other designs. The result of the boarding time from the fastest to slowest is Blended Wing Body - Conventional Aircraft - Double Deck Aircraft. The result for the fuelling time from the fastest to slowest is Blended Wing Body - Double Deck Aircraft - Conventional Aircraft. Therefore, it can be seen that Blended Wing Body has the fastest turnaround time according to the measured parameters. The Conventional and Double Deck Aircraft has the same score for the turnaround time category as they are both better at one of each parameters, but still not as good as the Blended Wing Body.

Table 7.5: Design concepts boarding simulation time.

Aircraft	Entry point	Boarding cycle [ ]	Boarding time [min]
KLM 777-300	One door	1471	20.5
	Two door	1285	17.9
Blended Wing Body	One door	1233	17.2
	Two door	938	13.1
Conventional Aircraft	One door	1512	21.1
	Two door	1239	17.3
Double Deck Aircraft	Single door	2010	28.1
	Two door (top, bottom)	1268	17.7
	Three door (2 top, 1 bottom)	927	12.9

7.4.6. Mission Flexibility

The mission flexibility is visualised in the payload-range diagrams, which can be found in Figure 7.4. The maximum payload and maximum fuel capacity are constrained by the volume of the cargo holds and fuel tanks respectively. It can be seen that the Conventional aircraft has the greatest flexibility in possible flight missions, as it can fly furthest with a range of 13,100 km and it can carry 58.3 tons of payload. The Double Deck Aircraft and the Blended Wing Body have no extra cargo volume and therefore the maximum payload is equal to the design payload, which is 42.8 tons. As the Blended wing body has a large part of the wing occupied by passengers, there is only a small part of the wing available to store fuel. This makes the maximum operating range only marginally larger than the design mission range. This means that the Blended wing body has the smallest flexibility in the missions it can perform. Therefore Blended Wing Body scores a 2 in the trade-off. The Conventional aircraft scores best with a 5. Lastly, the Double Deck aircraft scores a 4.

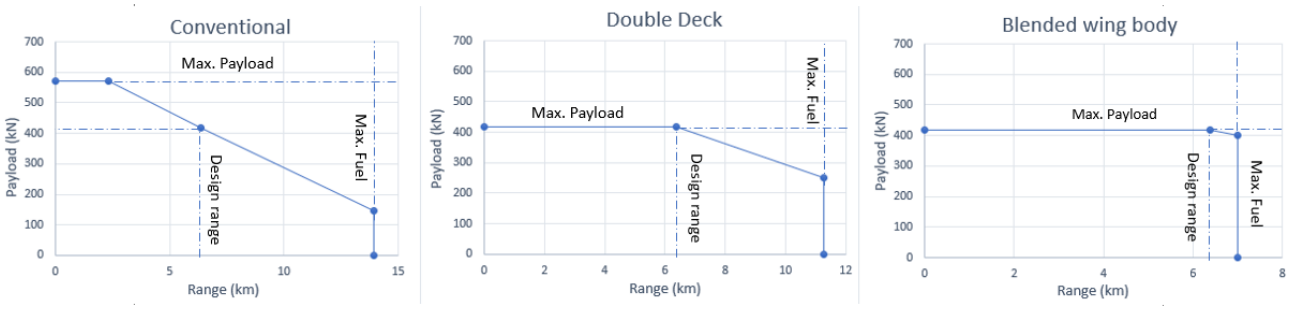

Figure 7.4: Payload-Range Diagram

7.4.7. Design Flexibility

As the cost of designing and certifying an aircraft can be very high, aircraft manufacturers usually design multiple variations of an aircraft. This results in relatively small adjustments to change the mission objective to a longer range or a higher payload. For the three concepts the conventional aircraft and the Double Deck aircraft are the easiest to

make variations on, therefore scoring a 4 in the trade-off. As the Blended wing body has a more complex integration of the wing with the fuselage, designing a variation of it with other missions capabilities would likely require a complete redesign of the aircraft. Therefore it scores a 2 in the trade-off.

7.4.8. Passenger Comfort

Regarding passenger comfort in aircraft, a qualitative analysis can be done of each of the concepts. In order to compare the concepts, only parameters that are different for each concept are taken into account. They include cabin noise, vibrations in the cabin, light, seat abreast, cabin luggage space, in-flight entertainment system, boarding time and window view.

The Blended Wing Body has an advantage in terms of vibrations due to shorter fuselage length. It also has better in-flight entertainment system because it will have more screens instead of windows. Furthermore, the boarding time of the Blended Wing Body is shorter which improves the passenger comfort. However, it has a disadvantage in terms of noise because the fuselage-mounted engines could increase the cabin noise. Moreover, this concept also has disadvantages in terms of natural light due to the limited amount of windows. The Blended Wing Body has a seat abreast of 3-5-5-5-3 in its widest section. This is a disadvantage in terms of visual, sound comfort and personal space. Furthermore, the luggage space is small compared to the other two aircraft because the height of the cabin is less.

The advantages of the conventional aircraft compared to the other two concepts are in terms of cabin noise due to its seats abreast and the wing-mounted engines. However, the passengers of the conventional aircraft could experience more vibrations than in the other two designs because of the length of the fuselage.

The Double Deck aircraft is best in terms of seat abreast. It has 2-3-2 in the economy class section, which is good in terms of visual, sound and personal space. Thus, more people will be able to see the light from the windows, which is part of the passenger comfort during flight. Moreover, this concept is designed with a possibility for more luggage space next to the window seats, which will be easier to reach by the passengers and will allow for more cabin luggage. The main disadvantage of the Double Deck aircraft is the longer boarding time.

7.5. Sensitivity Analysis

To check the validity of the trade-off, a sensitivity analysis is performed on the weights of the criteria. Per concept it is analysed how much the weights have to change in order for that concept to have the highest overall score. To do this the weights for the criteria that the concept scores better at than the other concepts are increased uniformly until it has the highest overall score. This is shown in Table 7.6. It can be seen that for the Double Deck aircraft the weights have to be increased by 40%. For the Conventional aircraft these weights and the weight of the external threats need to be increased by 96%. This means that the trade-off is not sensitive to a change in the weight factors.

Table 7.6: Trade-off Sensitivity Analysis of the Double Deck Aircraft

Criteria	Old Weight factor	New Weight factor	Blended Wing Body	Conventional Aircraft	Double Deck Aircraft
Recurring cost	2	2.8	3	4	4
Direct operating cost	5	5	5	2	4
Reliability	2	2.8	3	4	4
TRL	2	2.8	2	4	3
External threats	1	1	3	4	3
Fuel consumption /passenger/km	3	3	5	3	4
Global warming impact	3	3	5	3	4
turnaround time	2	2	5	3	3
Passenger comfort	1	1.4	3	4	4
Design flexibility	2	2.8	2	4	4
Payload-range flexibility	2	2.8	2	5	4
Originality	3	3	5	1	3
Total score			**3.7**	**3.3**	**3.7**

7.6. Trade-off Conclusion

From both a cost and sustainability perspective, the Blended Wing Body has an advantage over the Double Deck aircraft which in turn performs better than the Conventional aircraft. However, in terms of flexibility and risk, the Conventional aircraft performs better than the Double Deck aircraft which in turn is better than the Blended Wing Body. The turnaround time of the Blended Wing Body is slightly better than the turnaround time of the two other concepts. Regarding originality, the Blended Wing Body is much better. Considering all the factors described above, the trade-off indicates that the Blended Wing Body is the best concept among the three design concepts.

8

Design Phase III

In this chapter the methodology of Design Phase III is explained and the outcomes are summarised. In Section 8.1 an overview of the process can be found. In the subsequent sections the different models are further explained. First the design of the cabin is described in Section 8.2 and wing planform in Section 8.3. It continues with the engine design in Section 8.4 and landing gear design in Section 8.5. Afterwards, the vertical tail, control surface and high lift devices are designed in Section 8.6, 8.7 and 8.8 respectively. The structure is designed in Section 8.9 and aircraft weight is estimated in Section 8.10 with the centre of gravity estimated in Section 8.11.

8.1. Phase III Methodology

After the Blended Wing Body concept has been chosen for a final design, its design has to be developed into more detail and optimised. This process consists of updating the previous design with more advanced calculation methods, new tools for further analysis and iterations between the different design modules. This is represented with an N-2 chart, shown in Figure 8.1, and a flow diagram of the iteration cycle is shown in Figure 8.2. Each design module, coloured yellow in the N2-chart, is a main design step in the entire design process. On the rows are the outputs of the design steps and on the columns are the inputs for them. Each design step uses different tools and methods which will be elaborated upon in this chapter. The iteration flow diagram starts at the the top level requirements and ends at the conceptual design.

The sizing and design of the main parameters, as well as the weight estimations and structural model are made in Google Spreadsheets. For the aerodynamic and control and stability analysis, AVL is used together with some empirical methods. The geometry of the design is modelled in CATIA V5 and is updated with every design iteration. MATLAB is used for the estimation of the fuselage weight and control gain tuning. Finally, Python is used to calculate the SAR and thus optimal cruise altitude and mach number.

8.2. Fuselage Design

Aside from its interaction with other functions described in subsequent chapters, the driving factors behind sizing the fuselage of a Blended Wing Body are the cabin, cockpit and cargo hold. This section addresses these assemblies and how they are designed to meet the requirements HCSR-STR-004 to 007, HCSR-STR-009 to 011, HCSR-STR-013, HCSR-STR-015, HCSR-OPR-001 to 003, HCSR-OPR-006 to 013 and HCSR-OPR-015 from Table 4.2.

8.2.1. Cabin Planform

In the fuselage shaping process, the planform of the cabin is sized first. This is done using the method described in [14], where a rectangular centre section joined to a tapered front- and aft section define the cabin outline. An advantage of this method is that the two tapered sections allow for more efficient packaging of cabin equipment of different dimensions compared to more traditional Blended Wing Body cabin concepts which only have one tapered section in the front. The method also allows for the application of a structural concept that is addressed in Subsection 8.2.6.

With a total floor area target of $300\,m^2$, resulting in a fair $0.75\,m^2$ per passenger [15], the packaging was iterated such that all emergency exits are positioned in the front tapered section, the planform follows the shape of the distributed seats as tightly as possible and galleys are accessible with the wider cross-aisles. Other dimensions used are listed in Table 8.1, most of which are driven by requirements from Table 4.2. Seats are distributed in cross-section view based on their dimensions, as shown in Figure 8.3, and rearranged in top view until a tight fit into the planform is achieved. This results in the cabin planform shown in Figure 8.4.

Class I Weight Estimation	MTOW	MTOW	Payload Weight	MTOW	MTOW		MTOW	MTOW Gross Weight OEW n_max		Cruise Weight			Cruise Weight	Cruise Weight
Cruise Speed	T/W - S/W Diagrams	Wing loading(W/S)		Thrust Loading (T/W)				Cruise Speed						
Aspect Ratio Cruise Altitude Wing Area Wing Swet L/D	Aspect Ratio L/D Wing Swet Cruise Altitude	Wing Sizing			Wing Position	Wing Area Span MAC	Dihedral angle Wing Span Vertical Wing Position	Wing Geometry	Wing configutation	L/D C_L C_D Swet/S	Wing Area Wing Span Tip Chord	Wing Area Wing Span Root chord Tip chord Sweep Angle Dihedral	Wing Area Wing Span Root chord Tip chord	Wing Area Wing Span Root chord Tip chord Sweep Angle
Fuselage S_wet	Fuselage S_wet		Fuselage Sizing		Fuselage Dimensions		Fuselage Dimensions	Fuselage Dimensions	Fuselage Configuration and Dimensions	Swet/S			Cabin Design Fuselage Dimensions	
SFC				Engine Sizing	Engine Longitudinal Position	Engine Lateral Position	Engine DImensions	Engine Weight	Engine Dimensions	Engine Vertical Position		Engine Lateral Position Engine Vertical Position	Engine Dimensions	SFC
		Wing Position			CG Position	Longitudinal CG Position	Longitudinal CG Position Vertical CG Position					Most aft CG CG Travel	Lateral weight distribution	
Tail S_wet	Tail S_wet				Tail Arm	Vertical Tail Sizing		Tail Geometry	Vertical Tail Dimensions			Rudder size	Rudder size Vertical Tail Dimensions	
		Required Main Gear Storage	Scrape Angle Required Nose Gear Storage		Landing Gear Disposition		Landing gear Sizing and Position	Landing Gear Design and Disposition	Landing Gear Design and Disposition					
OEW MTOW					Component weight			Class II Weight Estimation					Wing Weight	
		S_wet/S					Scrape angle Tip back angle Tip over angle Take off wing tip clearance		CAD Design	Wing Area Wing Span Root chord Tip chord Sweep Angle		Aircraft Layout and Design	Wing Planform	Wing Area Wing Span Root chord Tip chord Sweep Angle
L/D M_cr		L/D C_L C_D					C_L_TO C_L_landing CL/Alpha Curve			Aerodynamic Performance	C_L_cruise C_L_max			M_cr ALtitude
L/D	C_L_max	L/D						HLD Weight	HLD Dimensions	C_L_max	HLD Design		Spar position	
		Sweep angle Dihedral Wing position			Wing position Vertical tail position Engine position	Vertical tail size Vertical tail position Rudder size		Control Surfaces Dimensions	Wing position Vertical tail position Engine position Sweep Angle Dihedral		Elevon Size Elevator Size	Stability and Control		
			Thickness	Pylon Design	Fuel Tank Location	Spar Position of Vertical Tail	Spar Position	Wing weight Fuselage Weight	Fuel tank volume Wing Spars Vertical Tail Spars		Spar Position		Structural Analysis & Design	
		M_cr ALtitude								M_cr Cruise Altitude				Sustainability Analysis

Figure 8.1: N2 Chart FB400 Design

Table 8.1: Cabin interior sizing parameters

Parameter	Value	Origin	Parameter	Value	Origin
$n_{\text{pax}_{\text{business}}}$ [−]	50	from [17]	$w_{\text{aisle}}[m]$	0.51	from FAA § 25.815
$n_{\text{pax}_{\text{economy}}}$ [−]	350	from [17]	$h_{\text{aisle}}[m]$	2.2	from [18]
$w_{\text{seat}_{\text{business}}}[m]$	0.53	from [17]	$h_{\text{headroom}}[m]$	1.7	from [19]
$w_{\text{seat}_{\text{economy}}}[m]$	0.46	from [17]	$h_{\text{seat}}[m]$	1.3	from [16]
$w_{\text{armrest}_{\text{business}}}[m]$	0.076	from [19]	$t_{\text{floor}}[m]$	0.3	from [16]
$w_{\text{armrest}_{\text{economy}}}[m]$	0.051	from [19]	$l_{\text{pitch}_{\text{business}}}[m]$	0.91	from [17]
$s_{\text{clearance}}[m]$	0.03	from [19]	$l_{\text{pitch}_{\text{economy}}}[m]$	0.81	from [17]
$n_{\text{seat}_{\text{econ-foldable}}}$ [-]	145	from Subsection 8.2.3			

8.2.2. Galleys and Lavatories

The required lavatory- and galley spaces are based on initial sizing methods [4],[19]. In Figure 8.4, these are labelled with numbers 1 & 3 and 2 & 4 respectively. Additional considerations for their positioning were the option to remove a dividing wall between two adjacent stalls (marked with 1) or extend the dimensions of a single lavatory (marked with 3) to create a more accessible arrangements for passengers with disabilities. Both options are possible with the lavatories shown, but not fully reflected in the actual dimensions in this case. The final monument dimensions are shown in Table 8.2.

Additionally, crew seats are located within the cabin. They are assumed to include their own support structure to not rely on monument placement nearby and thus have a planform dimensions of 0.88 m wide and 0.8 m deep for

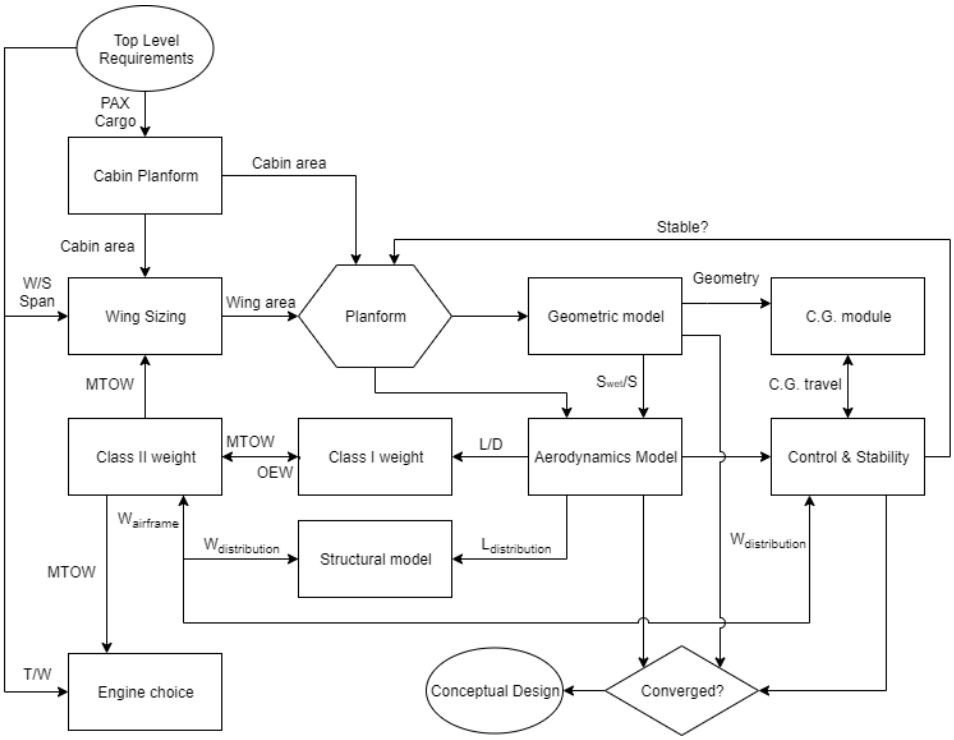

Figure 8.2: Iteration Flow Diagram

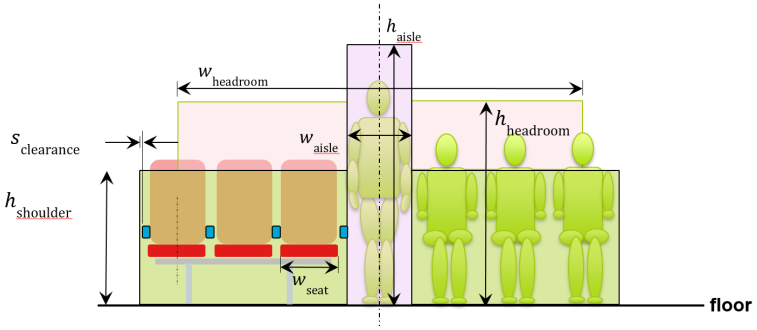

Figure 8.3: Cross-sectional distribution of cabin seats [16]

Table 8.2: Galley and lavatory dimensions

Parameter	Value	Notes
Total Galley Area [m^2]	14	Based on 0.09 m^2/business-pax and 0.027m^2/economy-pax
Centre Galley Dimensions XxY [m]	2x3.1	X-Direction is longitudinal, Y-Direction is lateral
Outer Galley Dimensions XxY [m]	2x1.95	see Centre Galley Dimensions
Total Lavatories [-]	12	Based on 17 business-pax/lavatory and 45 economy-pax/lavatory
Lavatory Dimensions XxY [m]	1x1	see Centre Galley Dimensions, based on [16]

double-seats and 0.44 m wide and 0.8 m deep for single seats, as suggested by [1]. For the event of an evacuation, requirement HCSR-OPR-006 prescribes a seat per emergency exit, while up to 9 attendants may be required. This is further addressed in Subsection 8.2.4. Thus the seats marked with 5 in Figure 8.4 are reserved for this purpose. The seats marked with 6 are optional, should customers wish to include extra cabin crew.

The final cabin packaging result is shown in Figure 8.5 and Figure 8.6, where business class seats are shown in blue, economy class seats in red. Purple seats are folding, which are elaborated in Subsection 8.2.3. Crew seats are represented in green. OVerhead bins are included in translucent white above the passenger seats where applicable.

[1] Cabin Crew Seats. Accessed January 2020. https://aeromockups.com/seats/crew-seats/cabin/

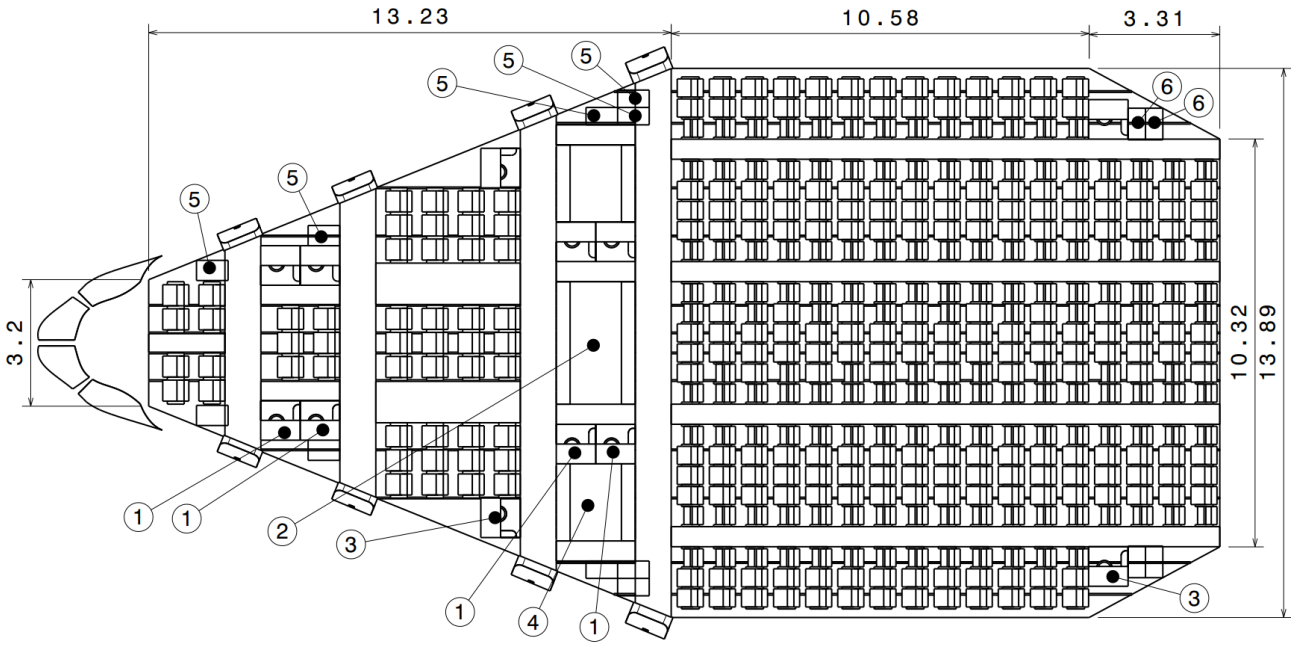

Figure 8.4: Cabin Design Outline, all dimensions are in metres unless otherwise stated

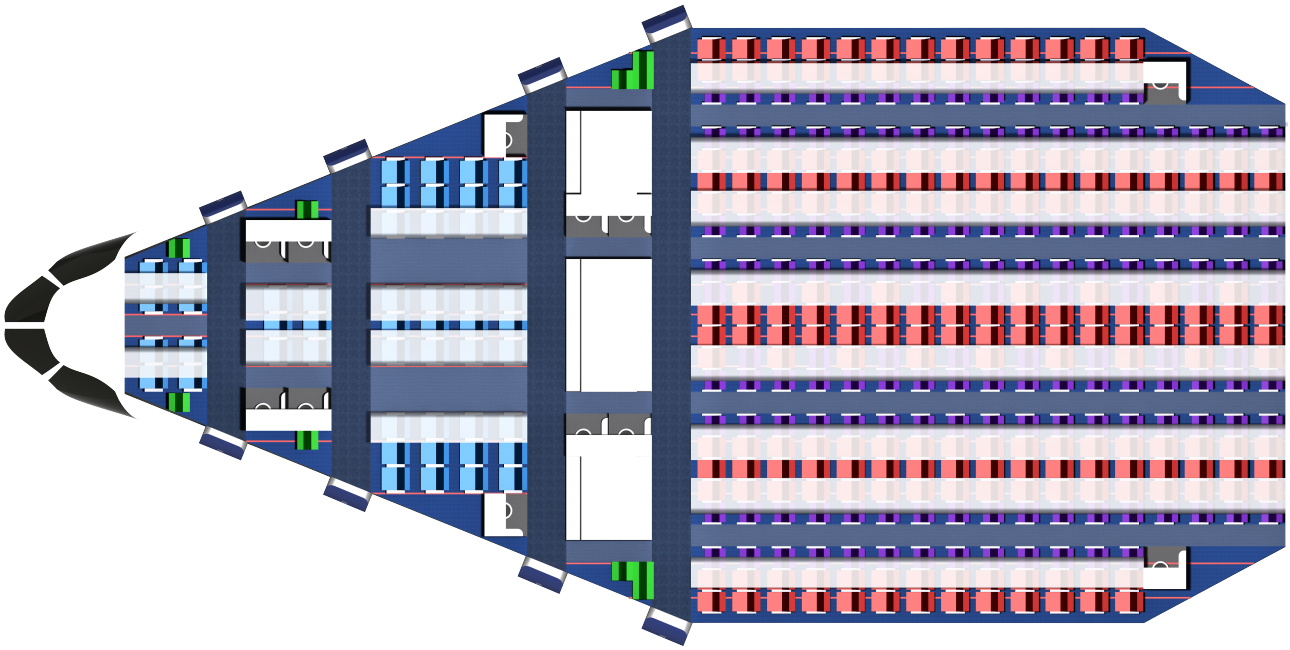

Figure 8.5: Cabin with passenger seats, galleys and lavatories

8.2.3. FOLDABLE PASSENGER SEATS

As described in Chapter 2, the significance of a fast turnaround time is growing. In modern cabin design, lowering the turnaround time is one of the guiding themes. The concept of foldable passenger seats is aimed at creating more moving space for passengers upon embarking and disembarking. The feasibility of this was demonstrated in the ALOHA Project [20]. In this project, turnaround times and resulting operational cost changes are studied. Simulation results estimated a reduction of 44.9% and 16.6% in de-boarding and boarding time respectively. Additionally, a reduction of 33% was found for cleaning time. This simulation was based on a conventional tube cabin in which all aisle seats automatically fold. For the FB400, the foldable seat concept will only be applied to the economy section of the cabin. 50 Business seats have conventional seating, meaning that this needs to be taking into account in the turn around time reduction of the FB400.

A three-seat block containing one folding chair adds a weight of 10.1 kg to the seat weight. With the configuration shown in Figure 8.7, a weight increase of 1.157 kg is estimated. The drawbacks of the foldable seat are possible higher maintenance cost due to the folding mechanism. Additionally, the use of hand luggage under the aisle seats is not

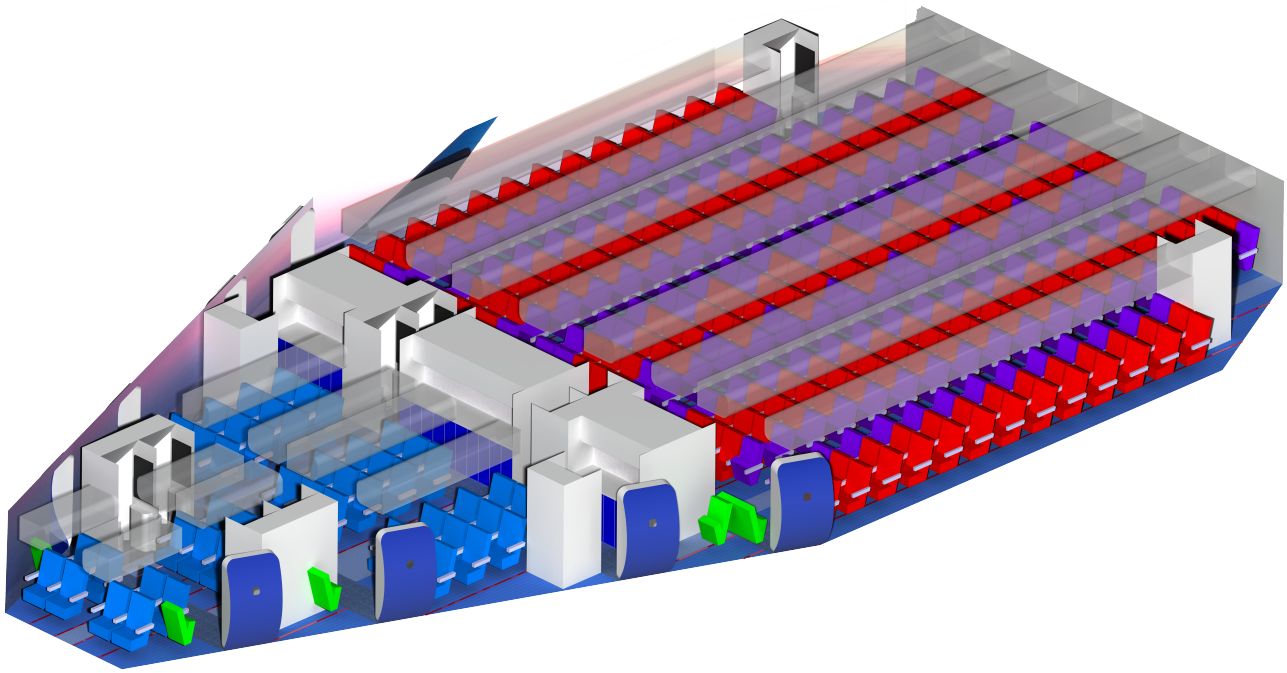

Figure 8.6: Cabin isometric view

convenient as it counteracts the effect of more moving space. Additionally, there is no seat pedestal under the aisle seats, allowing potential luggage to move freely and therefore interfering with safety measures. This might reduce the available luggage space in the cabin, which is a drawback especially on short haul flights.

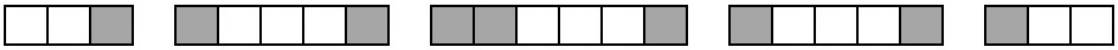

Figure 8.7: Locations of foldable seats

8.2.4. EMERGENCY EXITS AND CABIN CREW

The emergency exit arrangement included considerations about the visibility of a second exit in case the first exit route chosen by a passenger, the feasibility of exit doors that are compliant to existing regulations and the vicinity to galleys. While a full evacuation simulation was not possible within the scope of this project, the overall larger number of longitudinal aisles and better accessibility of multiple exits from the same seat compared to tube-and-wing fuselages in general are great advantages. It is thus not expected that the time taken to evacuate will be lower than conventional aircraft of the same passenger capacity. Table 8.3 outlines the dimensions used in the final design. Aisles and passageways are shown in light and dark blue in Figure 8.9 respectively.

Table 8.3: Emergency exit parameters according to FAA § 25.807

$n_{\text{exits}_{\text{emergency}}}$	8
$w_{\text{exits}_{\text{emergency}}}[m]$	1.07
$h_{\text{exits}_{\text{emergency}}}[m]$	1.83
$w_{\text{passageway}}[m]$	0.91
$w_{\text{aisle}}[m]$	0.51

Regulations require the FB400 to have four pairs of Type-A emergency exits. This number of exits allows for a maximum of 440 passengers by FAA § 121.391. For 400 passengers, regulations require 8 cabin crew members. However, for the number of emergency exits, 9 cabin crew members are more suitable to comply with both requirement HCSR-STR-013 and HCSR-OPR-006. Thus the cabin seating should allow for at least 9 crew members near the emergency exits. This is shown in Figure 8.4, with an explanation of the numbering provided in Subsection 8.2.1.

8.2.5. Passenger Comfort

In order to ensure the passenger comfort during flight, initial estimations of the passenger comfort index are performed. They are based on aircraft geometry, specifications and estimations of the environment inside the cabin. The comfort index is measured on a scale from 1 to 7, where 1 is the most comfortable and 7 is the least comfortable. Methods from D. William Conner and Ira D. Jacobson [21] are used to assess the passenger comfort. Note that the accuracy of the results is not very reliable because some of the parameters cannot be measured at this stage of the design. This includes cabin temperature, cabin noise and turbulence attitude. The temperature is estimated to be 20°C, the noise level is based on the noise level of a Boeing 787 [2] (65 dB) and the turbulence attitude is estimated based on methods from Roskam [4]. The results are shown in Table 8.4.

Table 8.4: Passenger comfort index

Comfort index	Value	Comfortability level
Environmental	6.4	Uncomfortable
Seating space economy class	2.5	Somewhat comfortable
Seating space business class	<1	Very comfortable
Noise	1.0	Very comfortable
Altitude change	<1	Very comfortable
Temperature	<1	Very comfortable
Motion	3.4	Somewhat comfortable
Turning maneuver	4.7	Somewhat uncomfortable
Pitchover maneuver	4.4	Neutral
Descend or climb maneuver	5.1	Somewhat uncomfortable
Compound maneuver	4.7	Somewhat uncomfortable
Average economy	**3.2**	**Somewhat comfortable**
Average business	**2.9**	**Somewhat comfortable**

There are multiple doubts that a blended wing body is comfortable due to the accelerations that passengers might experience during flight. As can be seen from the preliminary calculations, the most uncomfortable events during flight are the turning, compound and descend/climb manoeuvres which classify as somewhat uncomfortable. Moreover, the environmental comfort index can be decreased by adding entertainment systems. The fact that there are no windows next to the passengers' seats is dealt with by using cameras outside and a cabin screen wall inside, showing the outside view, as presented in Figure 8.6. This means that the FB 400 is no worse in terms of comfort than other commercial transport aircraft nowadays.

8.2.6. Open Planform

Since the pressure vessel packaged around the cabin does not require any structural members to intrude the cabin volume, the cabin presented offers the opportunity for different configurations if desired by customers. This is because of the triple-arc pressure hull, which is further outlined in Subsection 8.9.4. This is highlighted by Figure 8.8, where only the dark blue cross aisles defined by the emergency exits pose the same limits to the arrangements as with conventional aircraft. The seating areas shown in medium blue and light blue longitudinal aisles can be redistributed. Additionally, the seat rails required for the presented layout offer freedom for wider or narrower seat arrangements.

8.2.7. Cockpit

In order to create the cockpit, the internal layout is determined in plan views first. For this purpose, a pilot puppet with dimensions suggested by [4] is placed in a simple chair in front of an instrument panel according to [22]. This, together with the necessity to place a weather radar in the nose, drives the dimensions for the spline that deviates from the shape of the central fuselage airfoil. It also highlights the necessity to shift the cockpit floor upwards to achieve a grazing angle with respect to the lower forward visibility limit of above 30°, as [16] suggests. The resulting side view is shown in Figure 8.9.

Next, the top view of the internal layout is created around the pilot seat drawn in side view earlier. The Airbus A320 cockpit is used as a reference due to the similar range requirements. Additionally, because of its popularity among flight simulator enthusiasts, detailed dimensions of the interior are available. With this, the pedal box location, distance to instrument panels, lateral spacing between the pilots, longitudinal position and the overall cockpit floor dimensions are refined and also updated in the side view. The resulting top view is shown in Figure 8.10.

[2] How noisy is your airplane cabin?, Accessed in January 2020, https://www.uscreditcardguide.com/how-noisy-is-you-airplane-cabin/

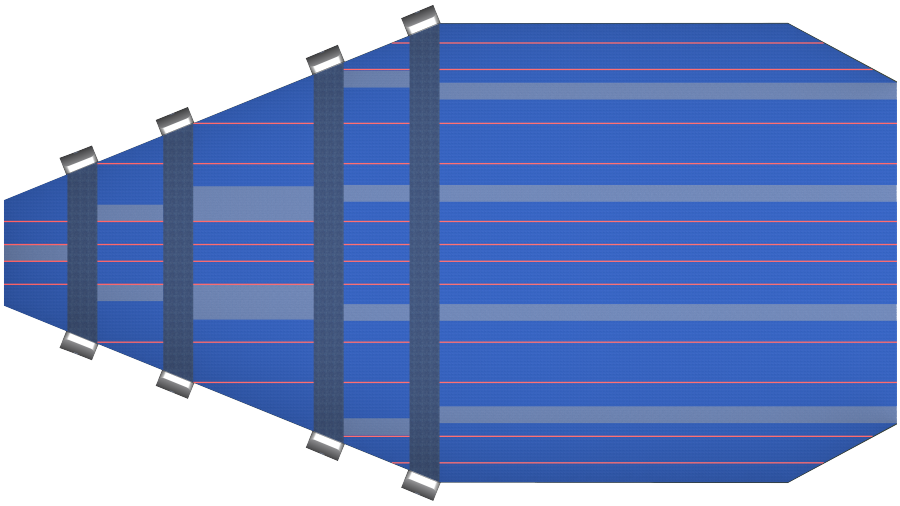

Figure 8.8: Empty cabin planform

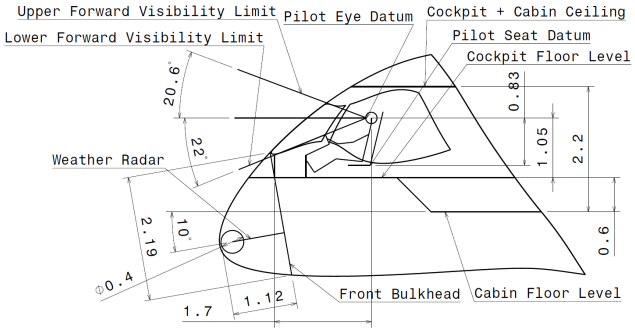

Figure 8.9: Cockpit in side view, dimensions are in metres unless otherwise stated

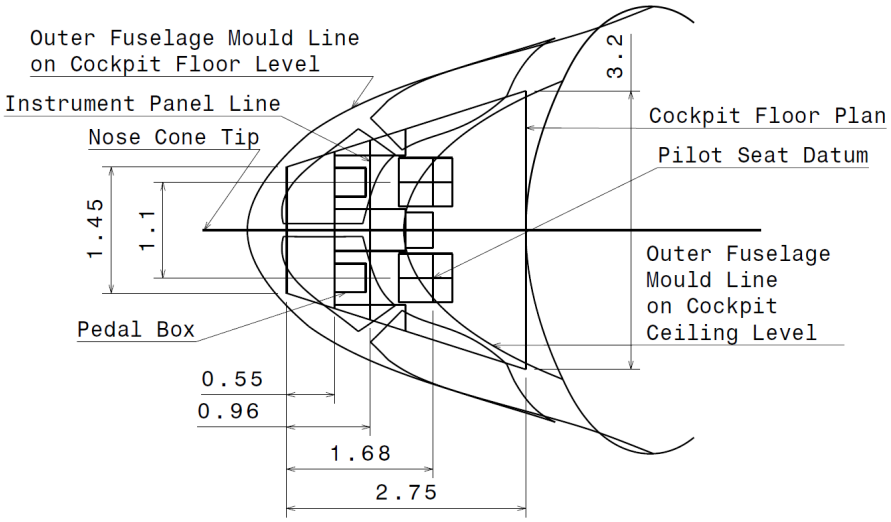

Figure 8.10: Cockpit in top view, dimensions are in metres

With the pilot positioned, the visibility requirements can be addressed. The upper and lower limits of the field of view of the port side pilot seat are determined from 30 degree to the right to 130° to the left, as shown in Figure 8.11. Most limits are driven by the ideal field of view suggested in [4]. Notable exceptions are the lower limits towards the front and side as well as the leftmost limit.

The lower limits are instead driven by the sideways overside visibility requirement (HCSR-STR-011) of 35° and a higher approach angle than conventional aircraft of approximately 10°. Together with a more conventional approach speed of 268 km/h, Equation 8.1 provided by [19] defines the new lower visibility limit and also satisfies HCSR-STR-010. The leftmost visibility limit is lowered compared to the suggested ideals, since regulations only require a limit of 130° [22]

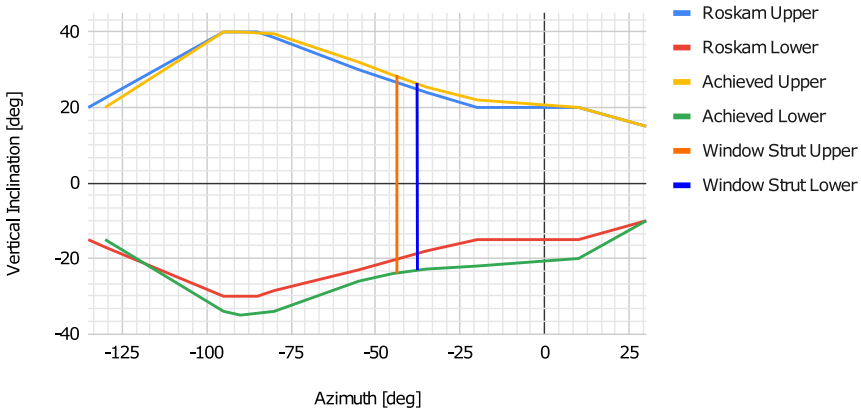

Figure 8.11: Recommended and actual field of view from port side pilot seat

and a higher value intersects the visibility limits with the internal cabin structure.

$$\theta_{\text{overnose}} = \alpha_{\text{approach}} + 0.04 \cdot V_{\text{approach}} \tag{8.1}$$

Subsequently, the visibility limit lines are intersected with the fuselage surface to define the contour of the cockpit windows. Minor adjustments are made to achieve a smoother window outline, leading to some more minor deviations outside of the ideal field. Splines are then used to create the outline of two windows, leaving only one strut on the centre-line and one at approximately 45° azimuth to the left (Figure 8.11). While traditionally three or more windows per side are used, the increased field of view due to missing struts of modern cockpit designs (e.g. Boeing 787) is preferred by pilots [3].

8.2.8. CARGO

In order to satisfy HCSR-STR-009, the available overhead storage space was analysed first. Overhead bins are positioned in the cross-section view as shown in Figure 8.12. Lateral bins over seat sections with access to only one aisle are smaller than their central counterparts, as suggested by [16]. Another constraint are the dimensions of an ordinary boarding trolley to fit in a way similar to modern overhead bin concepts [4]. Next, with a knockdown factor of 0.83 to account for the bin structure, the available surface area of the bins is multiplied with the length that each bin can extend over, not accounting for sectioning between individual bins. Of note is, that the business class analysis is based on clustering all seats into one rectangular block due to the way the seats abreast are split up. The results of this are presented in the first column of Table 8.5.

While a traditional overhead storage concept with longitudinal bins is used, its influence on boarding operations was not considered. Factors such as the poor accessibility of the bins for passengers in the centre economy rows and the resulting delay could still be improved. For example, lateral bins could be implemented, especially because of the rectangular cabin space not found in conventional aircraft. However, other factors such as the required space for air-conditioning vents, oxygen masks and other passenger amenities should be considered before implementing such a concept.

From this it is apparent, that nearly all of the cargo volume required could fit into the cabin, with only a small number of containers required in the cargo hold. However, as outlined in the second column of Table 8.5, another constraint was imposed based on the number of bags that can fit into a single LD3-45 unit [5]. LD3-45 units are chosen since their reduced height is beneficial for the packaging within the triple-arc pressure vessel and they are widely used in other popular aircraft types. The result shows that a much higher number of containers is required to be fitted to provide adequate flexibility to operating customers regarding their baggage policies. The final number of containers is rounded down from the number required to fit a bag per passenger since the requirement for total storage volume is already met. The locations of the containers are then driven by the locations of spars and the available space be-

[3] Wired Test-Drives Boeing's New 787 Dreamliner. Accessed January 2020. https://www.wired.com/2012/07/boeing-787-dreamliner-flight/

[4] Onboard Innovation: Viva La Evolucion!. Accessed January 2020. https://www.futuretravelexperience.com/2014/03/onboard-innovation-viva-la-evolucion/

[5] Aircraft Loading 101. Accessed January 2020. http://fly-sea.com/forum/viewtopic.php?f=14&t=804

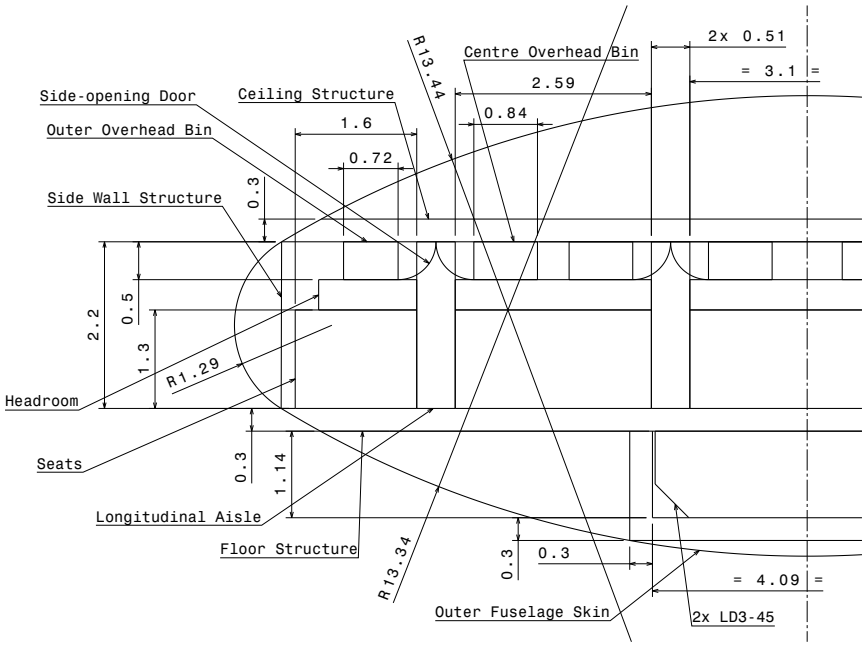

Figure 8.12: Cabin cross section view at maximum width, all dimensions are in metres

Table 8.5: Cargo volume calculations

Cabin Section	Parameter	Unit	Value	Parameter	Unit	Value
General	$A_{OS_{lat}}$	[m^2]	0.3	Total cargo volume required	[m^3]	56.63
	$A_{OS_{ce}}$	[m^2]	0.35	Volume per LD3-45	[m^3]	4.3
Centre Economy	l_{section}	[m]	10.6	Total LD3-45 required for volume	[-]	3.2
	$n_{OS_{lat}}$	[-]	2	Bags per LD3-45	[-]	35
	$n_{OS_{ce}}$	[-]	6	Total LD3-45 required for bags	[-]	11.5
Rear Economy	l_{section}	[m]	3.3	Total LD3-45 used	[-]	11
	$n_{OS_{lat}}$	[-]	0			
	$n_{OS_{ce}}$	[-]	6			
Business	l_{section}	[m]	5.66			
	$n_{OS_{lat}}$	[-]	2			
	$n_{OS_{ce}}$	[-]	2			
Total available overhead volume	[m^3]	42.91				

tween the cabin floor and the centre fuselage airfoil. Additionally the longitudinal position is chosen as close to the operating-empty-weight centre of gravity to minimise the excursion of the latter. This resulted in the need for two compartments due to the spar locations. The final configuration is outlined in Figure 8.13.

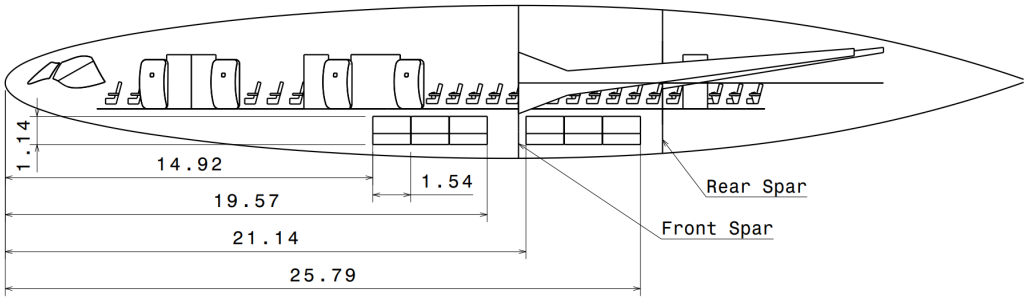

Figure 8.13: Longitudinal cargo position in approximated airframe, all dimensions are in metres

In order to load and unload the containers, a cargo door per compartment is required. The local curvature of the fuselage and the local distance to ground do not allow for the conventional approach of an upward opening door with ground equipment driving up directly to the cargo floor. Therefore the cargo door doubles as a loading ramp similar to large military transport aircraft to roll the containers along its flat surface further outboard, such that ground equipment does not interfere with the airframe. This is shown in Figure 8.14. Further details regarding ground operations are discussed in Chapter 11.

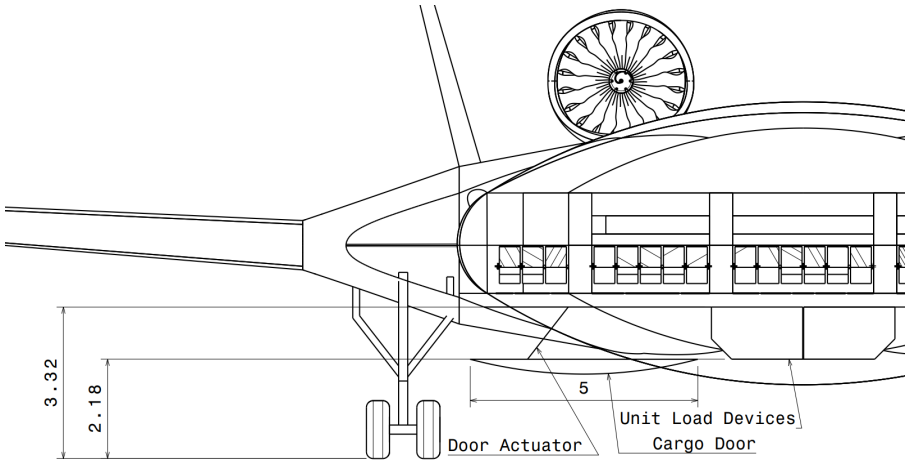

Figure 8.14: Cargo Door Integration for operations with Unit Load Devices, all dimensions are in metres

8.2.9. Shaping of remaining fuselage

The remaining fuselage shaping continues with defining a central fuselage airfoil to fit the cabin and cargo holds into in side view. A symmetric NACA 16-015 was chosen due to its far aft maximum thickness location. Additional considerations are that subsequently the maximum radii of the pressure vessel arcs enclosing the cabin (further discussed in Section 8.9) should not exceed ≈ 15 m. This drives the location of the cabin and cargo holds within the airfoil to a large extent. The airfoil is also rotated nose down by 0.2° to reduce the overall length, but larger values may be possible. Afterwards, the wing planform is created based on the leading- and trailing edge points of the centre fuselage airfoil and the area occupied by it. For this purpose, another NACA 16-015 airfoil is positioned on the outer boundary of the pressure vessel to ensure a smooth surface of the centre fuselage section. This then transitions into the wing section with its supercritical NASA SC(2)-0414 airfoils at the "wing" root and tip. This process is illustrated in Figure 8.15, with further explanation of the planform in Section 8.3. Considerations for the chord of the second symmetric airfoil and the outer dimensions of the wing planform revolve around the total reference area, total wetted area, centre of gravity position and stability and control characteristics.

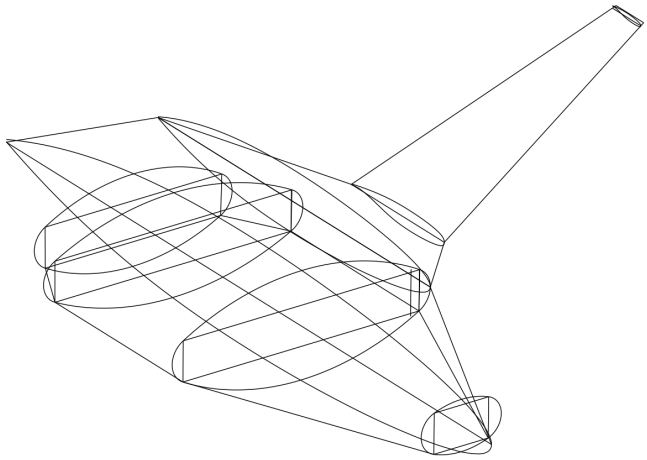

Figure 8.15: Shape-defining features of the fuselage

8.3. Wing Planform Design

The wing of the aircraft is designed according to requirements HCSR-STR-002, HCSR-STR-008 and HCSR-STR-014 from Table 4.2. The wing also has to provide lift during the flight, aiming at optimal performance parameters.

8.3.1. Wing Planform Method

The method for wing design uses aerodynamic, stability and sustainability analysis in order to improve the design, according to the objectives of the project. First, the geometry is simulated in AVL and the drag polar, lift and drag coefficients and span efficiency factor are used as an input to the wing planform design. Secondly, the sustainability analysis is used to recommend a cruise altitude and mach number for which the SAR is minimum and lastly, the stability analysis in AVL exports the required longitudinal position of the wing. These parameters are iterated multiple

times until convergence is achieved.

In order to estimate the wing area, a matching diagram is created to define the design space for the aircraft, as shown in Figure 8.16. The same top level requirements hold as in design phase II (HCSR-PER-008, HCSR-PER-009, HCSR-PER-010), therefore only minor changes can be seen in the diagram. This is mostly due to a lower $C_{L_{\max}}$. Moreover, the climb rate requirement is lowered to 1,500 ft/min, as this is enough to guarantee if the turn-around time requirement is met. According to Figure 8.16, the design space is restricted by take off and stall conditions. In order to reach an optimal design, the aircraft should have wing loading as high as possible and thrust loading as low as possible. The point of the design space at which this is achieved, is the design point of the aircraft. In this case, the wing loading is 2,237.5 and the thrust loading is 0.28.

With the wing loading and the take off weight, the minimal lifting area can be calculated. Afterwards, the span of the aircraft is kept at the maximum span allowable for a type V airport gate, i.e. 65 meters, and a margin of 0.25 m is left for additional attachments such as lights and electrostatic devices, such that the total span becomes 64.75 m. Winglets are added in order to reduce wing tip vortices, increase the lateral stability and increase the effective span to 65.6 m.

The fuselage planform is used to update and minimise the ratio of wetted area to reference area $S_{\text{wet}}/S_{\text{ref}}$ and the friction drag. The vertical tails, engines and winglets are also added to the wetted area. The planform is divided into three sections - fuselage (section 1), blending section (section 2) and wing section (section 3), as can be seen in Figure 8.25. The area of the fuselage section comes from cabin sizing and the area of the blended and wing sections are varied in order to reach the desired mach number and lift. Sweep angles are then selected for each section according to the drag divergence mach number and stability requirements. Afterwards, the wing taper ratio is defined based on statistical relations with the sweep angle from Torenbeek [22] and the root, tip and mean aerodynamic chords are calculated. This leads to calculation of the thickness to chord ratio of the airfoil and airfoil selection, which is based on airfoil characteristics and performance such as moment coefficient, design lift coefficient, lift curve slope, zero lift angle of attack and stall angle of attack. Finally, the dihedral angle is estimated according to ground clearance and lateral stability constraints.

8.3.2. Wing Planform Results

The matching diagram is shown in Figure 8.16, Table 8.6 provides the main parameters obtained from the wing design, whereas Figure 8.17 shows a top view of the wing planform with relevant dimensions.

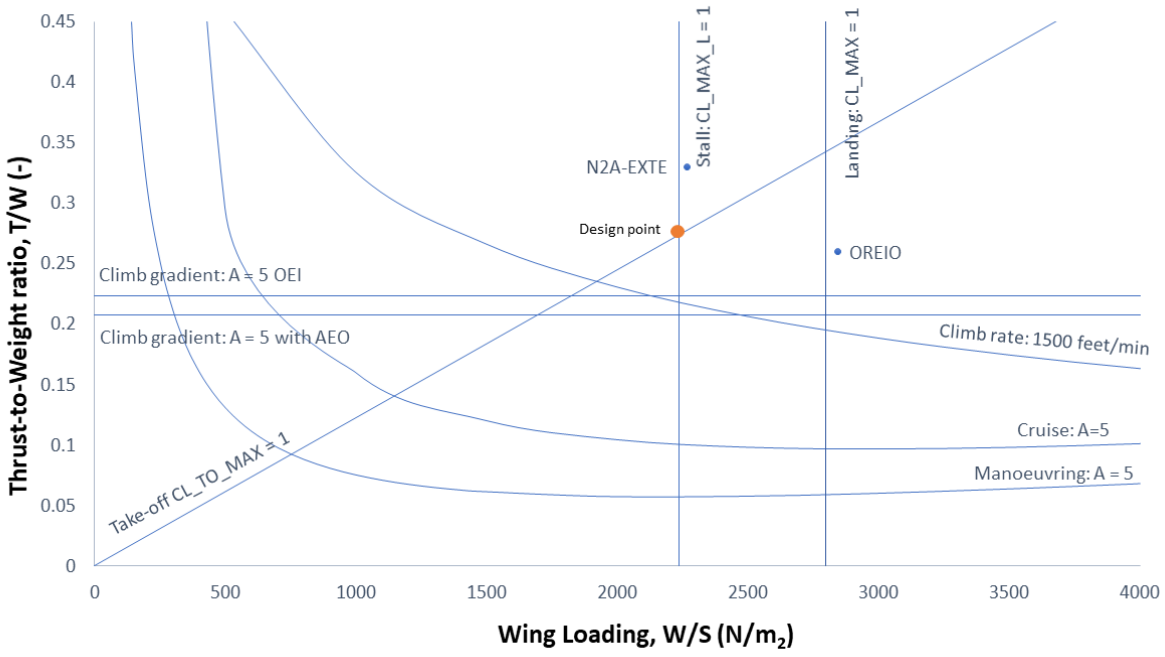

Figure 8.16: Matching Diagram

The method is verified as described in Section 6.3 and validated by plotting reference points on the matching diagram. Reference points show similar results for wing and thrust loading.

Table 8.6: Main wing parameters

Parameter	Value	Unit
S	797	$[m^2]$
S_1	486	$[m^2]$
S_2	106	$[m^2]$
S_3	205	$[m^2]$
S_{winglets}	7.9	$[m^2]$
b	64.8	[m]
A	5.4	[-]
λ	0.296	[-]
c_r	7.7	[-]
c_t	2.3	[-]
$\Lambda_{1_{\text{LE}}}$	66	[deg]
$\Lambda_{2_{\text{LE}}}$	52	[deg]
$\Lambda_{3_{\text{LE}}}$	32	[deg]
MAC	23.8	[m]
Γ	3.5	[deg]
Wing twist angle	3	[deg]
t/c_1	0.15	[-]
t/c_3	0.12	[-]
Airfoil type Section 1 Root	NACA 16-015	[-]
Airfoil type Section 2 Root	NACA 16-015	[-]
Airfoil type Section 3 Root	NASA SC(2)-0414	[-]

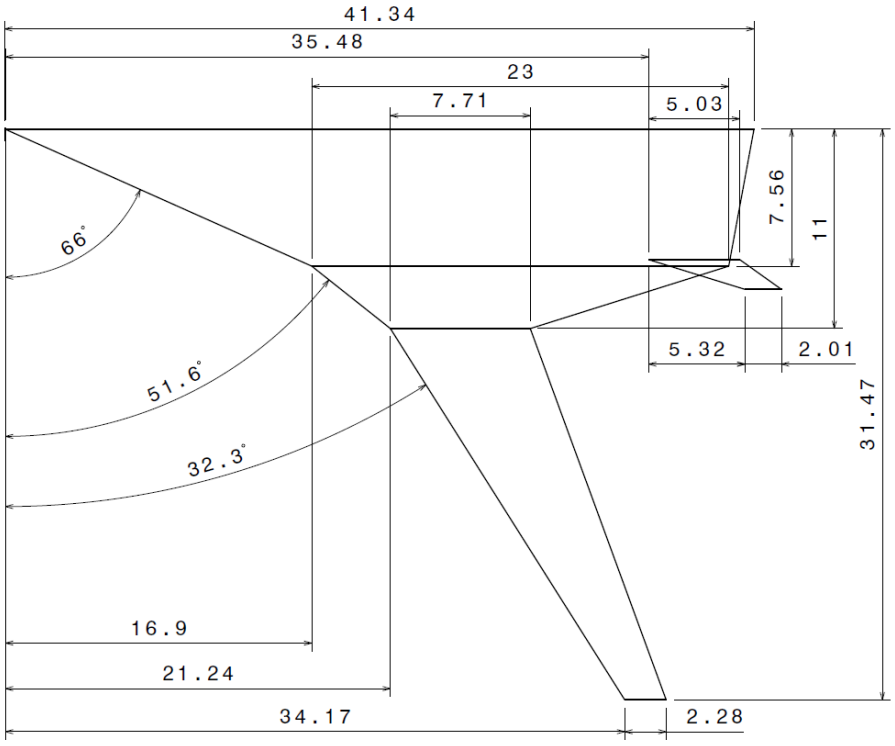

Figure 8.17: Wing parameters, dimensions are given in metres unless otherwise stated

8.4. Engine Design

The aircraft has two engines which are designed according to requirements HCSR-PER-007, HCSR-PER-006 and NCSR-NF-SUS-003. The engine has to provide enough thrust during each flight phase but it also has to be sustainable and with low noise emissions.

8.4.1. Engine Design Method

The initial sizing of the engines used in Design Phase II is applied in the same manner, i.e. rubber engine sizing with GE-9X as a reference engine. Based on the parameters the sizing factor between the engine needed for the aircraft and the GE-9X is 0.5 which means that the GE-9X is too large and would lead to over-design, which is why a smaller engine is chosen, namely the GEnx-1B70. Furthermore, the value for the specific fuel consumption, weight and thrust are updated with the specification of the GEnx-1B70 [6], which also affects the mission fuel mass fractions and eventually fuel weight, as discussed later in Chapter 9.

The engine nacelle is designed using method described in Aircraft Design and System Engineering Elements [13]. This method calculates the length of main nacelle components such as exposed gas generator length and nacelle length and also diameters of the nacelle, inlet, gas generator cowling and exit fan. Moreover, chevrons are added on the fan gondel and gas generator gondel for drag and noise reduction.

The pylon attaching the engine to the fuselage is also designed based on bending and shear conditions and transfer of the loads from the engine to the fuselage. This is done by adding thicker diagonal spars on the leading and trailing edge of the pylon, such that they provide a load path for the shear flow. They are also supported by ribs between them, which will also account for buckling and bending moment resistance.

Additionally, the engines are placed laterally and vertically such that the total shrapnel probability is smaller than 5 %, in case of a compressor or turbine blade failure. The total probability is calculated using Equation 8.2 [23].

$$p_{total} = \frac{atan\left(\frac{D_e}{d}\right)}{\pi} \cdot \left(min\left(\frac{1}{2}, \frac{2}{\psi} \cdot atan\left(\frac{l_{\text{nac}_1}}{d}\right)\right) + min\left(\frac{1}{2}, \frac{2}{\psi} \cdot atan\left(\frac{l_{\text{nac}_2}}{d}\right)\right)\right) \tag{8.2}$$

where ψ is the maximum angle of azimuth interference, l_{nac_1} is the length from the start of the nacelle to the most aft turbine disc position and l_{nac_2} is the total nacelle length minus l_{nac_1}. All other engine dimensions can be taken from Table 8.7. This results in a relation between engine diameter and interference of failed engine fragments with crucial aircraft elements such as the other engine, fuel tanks and vertical tails. The resulting probabilities are listed below:

- Probability of fracturing the other engine: 0.0494
- Probability of fracturing the vertical tail: 0.0375
- Probability of fracturing the fuel tank: 0.0000

The probabilities are lower than 5 % which results in engine centre lines being 8 m apart and changes in the longitudinal separation between engines and vertical tails. A protective layer of Kevlar inside the engine cowl is added in order to catch the failed blades and prevent them from damaging critical structural components.

The vertical placement of the engines also depends on the interference of the flow going over the fuselage. The engines are initially placed 0.78 m above the fuselage but it has been found that they create too large pitch down moment, which affects the stability of the aircraft. This is why the decision has been made to lower the engines to 0.18 m above the fuselage and change the shape of the nacelle to a D-shaped instead of circle shaped, with the flat part towards the fuselage (see Figure 8.18).

8.4.2. Engine Design Results

The results from engine design as well as the side view of the engine are shown in Table 8.7 and Figure 8.18 respectively.

After the engines are selected, their weight is added to the component weight, described in Section 8.10. It should be noted that the engine weight and thus the aircraft weight could be decreased by choice of smaller engines. However, the GEnx-1B70 is chosen because it is 20 % more efficient compared to other engines of this type and because it is one of the few bleedless engines on the market, which would make the aircraft more electric, thus more efficient in terms of power.

8.5. Landing Gear Design

The landing gear design is crucial for the feasibility of the aircraft design. It has to perform different functions during different phases of the flight envelope. Some of these functions are to withstand the weight of the aircraft and steer

[6] GENX™ high bypass turbofan engines. Accessed January 2020. https://www.geaviation.com/sites/default/files/datasheet-genx.pdf

Table 8.7: Main engine and nacelle parameters

Parameter	Value	Unit
T_{TO}	310.5	[kN]
D_{engine}	2.82	[m]
l_{engine}	4.69	[m]
W_{engine}	18000	[kg]
BPR	9	[-]
l_f	4.47	[m]
D_n	3.12	[m]
l_n	5.95	[m]
D_g	1.85	[m]
l_g	1.49	[m]
l_c	0.46	[m]
D_{ef}	2.53	[m]
D_{eg}	1.02	[m]

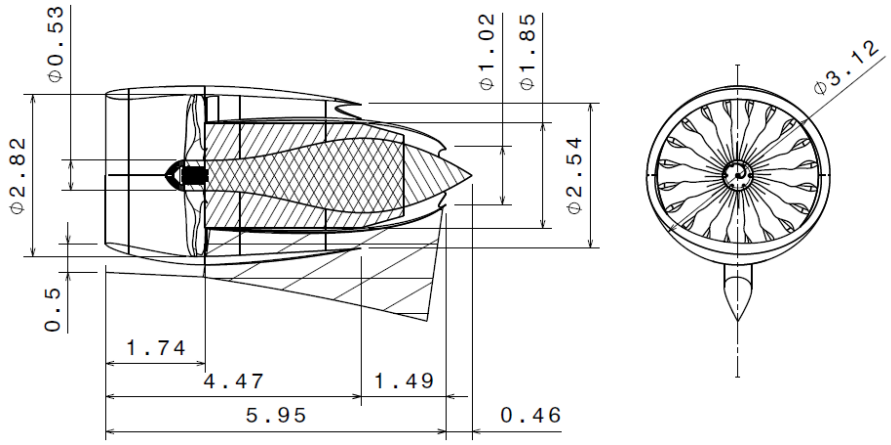

Figure 8.18: Engine and nacelle parameters, dimensions are given in metres

during ground operations, to allow for wing tip clearance, avoid tail strike and be able to provide enough space for rotation during landing and take off. It should also be stowed in the airframe during flight. This is why the landing gear is designed according to requirements HCSR-STR-012, HCSR-PER-001, HCSR-PER-002 and HCSR-PER-004.

8.5.1. Landing Gear Design Method

Multiple constraints are used to design the landing gear of the aircraft, especially considering the low aspect ratio and larger angle of attack which it has to reach during take off as well as the approach angle during landing.

Firstly, the number of tires per strut is determined based on the aircraft weight. Afterwards, the tire pressure and the maximum static load for each gear is determined which provides tire dimensions obtained by methods from Torenbeek [22]. The next step is to determine how many percent of the weight does each gear have to carry. This is restricted by the ground steering requirements, i.e. the nose gear can only carry from 8 to 15 % of the MTOW of the aircraft in order to be able to steer. Since the aircraft is short, the nose gear has to carry more load compared to conventional aircraft. This load distribution also affects the longitudinal position of both landing gears. The percentage of the nose gear loading is also computed after landing with the usage of thrust reversers to ensure that the nose gear will still be able to withstand the loads and steer shortly after landing. This is done by summing the moments around the centre of gravity of the aircraft, as shown in Figure 8.19 and described in Equation 8.3. Thrust reversers are assumed to reverse 25 % of the thrust.

$$\sum^{\text{CCW}+} M_{CG} = 0 : F_m \cdot l_{nw} - F_{nw} \cdot l_{nw} - 0.25 \cdot T_L \cdot z_e + F_f \cdot z_{mlg} = 0 \tag{8.3}$$

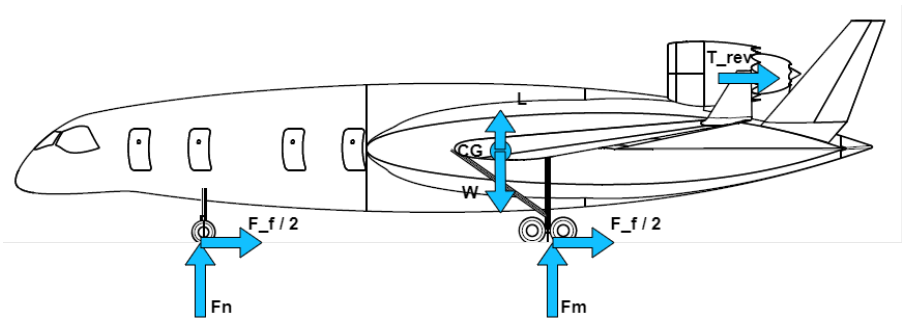

Figure 8.19: Free Body Diagram Landing

The symbols are described in the nomenclature. Note that the friction force F_f is calculated via Equation 8.4, where μ is the ground friction coefficient.

$$F_f = \mu \cdot (W - L) \tag{8.4}$$

Rewriting Equation 8.3 leads to Equation 8.5 which is the nose gear load after landing.

$$F_n = \frac{(W - L) \cdot l_{mw} - 0.25 \cdot T_L \cdot z_e + F_f \cdot z_{mlg}}{l_{mw} + l_{nw}} \tag{8.5}$$

With the current design this load is 12 % of the landing weight. Note that two scenarios are considered - with the largest landing weight (after a nominal mission (Figure 9.2 and Figure 9.3)) and with the smallest landing weight (after the whole mission profile (Figure 9.1)). It turns out that the lowest weight is more critical for the nose gear, since it results in smaller loads and it is thus a driving factor for the design.

In order to ensure that the tail does not strike the ground during take off, the tip back angle has to be larger than the scrape angle, as shown in Figure 8.20. This fulfils the longitudinal tip over requirement. For the lateral tip over requirement, the overturn angle should be no more than 55° (see Figure 8.21) and Equation 8.6 should be fulfilled.

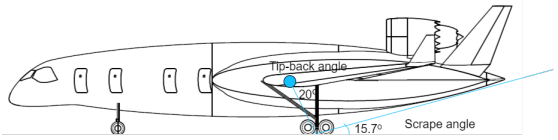

Figure 8.20: Landing gear longitudinal tip over criterion

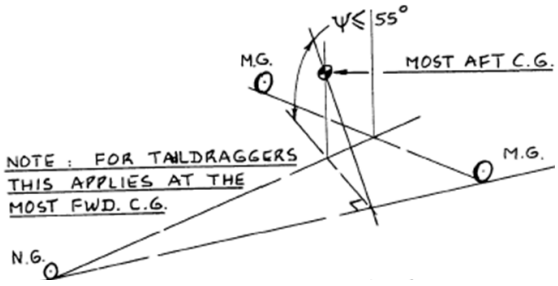

Figure 8.21: Landing gear lateral tip over criterion [24]

$$y_{mlg} > \frac{l_{nw} + l_{mw}}{\sqrt{\frac{l_{nw}^2 \cdot (\tan\psi)^2}{z^2} - 1}} \tag{8.6}$$

Here ψ is the overturn angle, z is the vertical distance from the centre of gravity to the landing gear and l_{mw} and l_n are the distances from the main and nose landing gear to the centre of gravity. Due to the specific geometry of the design, these two conditions are not limiting the design of the landing gear. What could be a design constrain is the large angle of attack (14.6°) combined with a bank angle of 8° and the swept wing which could cause the wing tip to touch the ground during take off and landing. This is taken into account by increasing the height of the struts and the dihedral angle of the wing, as well as making the gear track wider, i.e. increasing y_{mlg}. Since there is a limited space to store the landing gear during flight, a double hinge linkage mechanism is designed such that it pulls the bogey up with reduced rearward travel compared to a single hinge mechanism, see Figure 8.23. This mechanism is very similar to the one of the B58-Hustler and it is more convenient to stow them in a forwards motion as the flow will help to lower the gear in case the mechanism fails. The lengths of the individual links are sized using Equation 8.7, where the spar spacing and the strut length are known from the wing and landing gear design calculations respectively. This is done

to provide a short load path to the primary structure. However it also requires the vertical limitation of tank volume available in this section to make room for the struts, as shown in Figure 8.24. Furthermore, the main landing gear will be provided with an electronically driven parking brake to comply with HCSR-PER-004. The nose landing gear retracts to the back with a single hinge mechanism used in most conventional transport aircraft. While a forward retraction would be beneficial for assisting a manual lowering, it would require further reshaping iterations which could not be implemented in time.

$$\begin{bmatrix} -1 & 1 & 0 \\ 1 & 1 & 0 \\ -1 & 0 & 1 \end{bmatrix} \cdot \begin{bmatrix} l_{\text{upper}} \\ l_{\text{lower}} \\ l_{\text{attach}} \end{bmatrix} = \begin{bmatrix} 0 & 0 & 1 \\ 0 & 1 & 0 \\ -1 & 1 & 0 \end{bmatrix} \cdot \begin{bmatrix} d_{\text{spars}} \\ l_{\text{strut}} \\ l_{\text{spare}} \end{bmatrix} \tag{8.7}$$

8.5.2. Landing Gear Design Results

Table 8.8 represents all the relevant landing gear parameters including tyre sizes, important angles and longitudinal, lateral and vertical distance from the centre of gravity. It can be seen that compared to the previous design stage, the nose landing gear is carrying more load than before, namely 15 % compared to 10 %, which is why its longitudinal position has moved further from the nose. Moreover, the struts are now 30 cm higher and the gear track is increased due to take off constraints.

Table 8.8: Landing gear parameters

Parameter	Value	Unit
D_{mw}	1.27	[m]
W_{mw}	0.51	[m]
d_{mw}	0.56	[m]
D_{nw}	1.18	[m]
W_{nw}	0.41	[m]
d_{nw}	0.51	[m]
l_{mw}	2.62	[m]
l_{nw}	14.85	[m]
y_{mlg}	8.79	[m]
z_{mlg}	4.80	[m]
Tip back angle	20.0	[deg]
Scrape angle	15.7	[deg]
Overturn angle	35.7	[deg]
Wing tip ground clearance during take off	0.14	[m]

Table 8.9 and Figure 8.22 show the dimensions of the main gear mechanism after applying Equation 8.7. Figure 8.23 outlines the retraction sequence of the double hinged mechanism in the context of the aircraft. Figure 8.24 presents the longitudinal position of both landing gears in deployed position.

Table 8.9: Main landing gear mechanism dimensions

Parameter	Value	Unit
d_{spars}	5.08	[m]
l_{strut}	5.54	[m]
l_{spare}	1.59	[m]
l_{lower}	2.47	[m]
l_{upper}	0.88	[m]
l_{attach}	1.34	[m]

8.6. Vertical Tail Design

After the wing planform design and the centre of gravity is known, the vertical and horizontal tail surfaces can be designed. The vertical tail should provide lateral control of the aircraft in flight and allow the aircraft to maintain stable in case of one engine inoperative condition. The horizontal tail should provide longitudinal stability and control.

A twin vertical tail configuration is applied. Since the aircraft is a Blended Wing Body, it does not have a fuselage and a

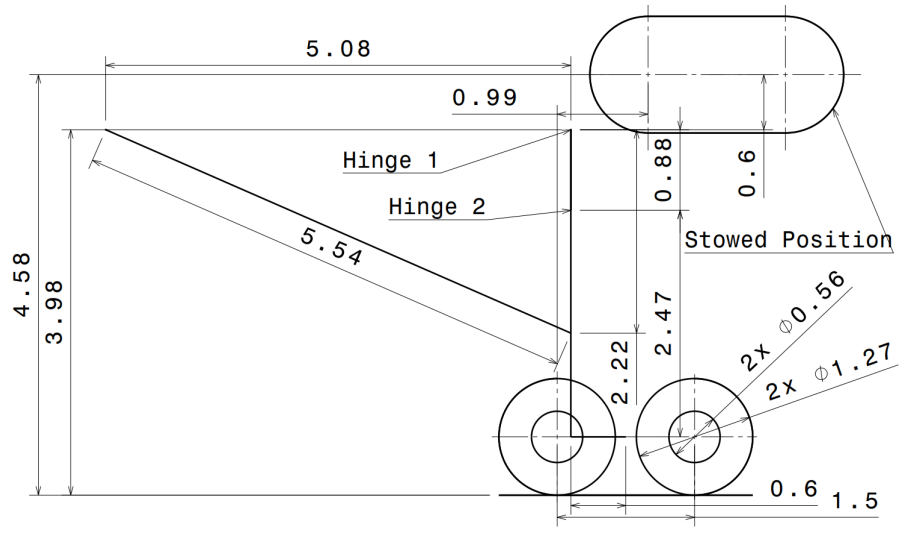

Figure 8.22: Main gear mechanism dimensions in deployed position, all dimensions are in metres

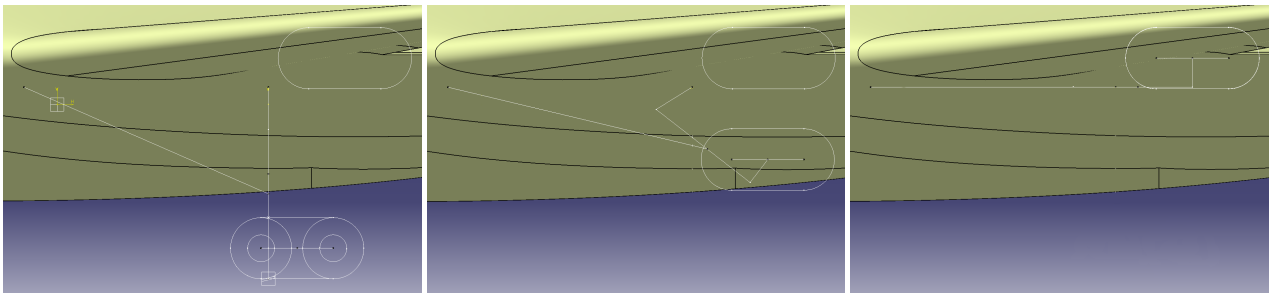

(a) Fully deployed position (b) Intermediate position (c) Fully stowed position

Figure 8.23: Double-hinge landing gear mechanism retraction sequence

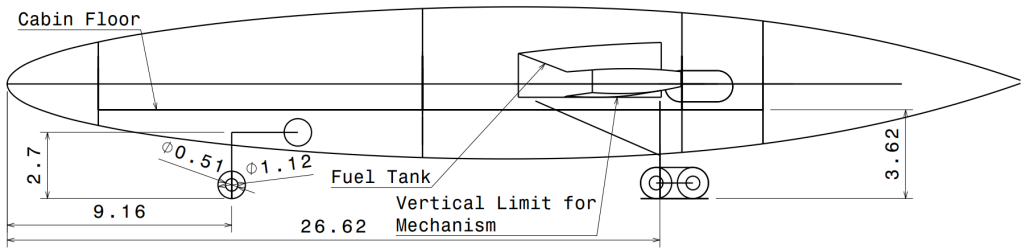

Figure 8.24: Nose- and Main gear positions with respect to the nose in deployed position, all dimensions are in metres

different positioning of the engines, the tail volumes found from reference aircraft can not be applied. Instead, the tail areas are calculated by summing moments about the centre of gravity in case of a one engine inoperative condition. The aircraft does not have horizontal tail surfaces as the longitudinal control is obtained by means of control surfaces on the trailing edge of the wings.

The dimensions of the tail surfaces are presented in Table 8.10. Tail parameters like sweep angles and aspect ratio have been chosen such that tail surfaces stall at higher angles of attack than the aircraft wings and near sonic flow phenomenon occur at the wings before they occur on the tail surfaces.

Table 8.10: Dimension of vertical tail surface

Parameter	**Value**	**Unit**
Tail area	22.3	m^2
Span/height	6.3	m
Quarter chord sweep	35.8	deg
Aspect ratio	1.8	-
Taper ratio	0.4	-

8.7. Control Surfaces Design

In this section, the method to design the ailerons and elevators is described. On the wing, the functions of these control surfaces are combined, resulting in elevons.

8.7.1. Aileron Design

Requirement HCSR-SCR-002 states that the time to achieve a 30 degrees bank angle shall be less than 1.5 seconds. The ailerons are designed based on this requirement. The design is based on Oliviero's method [25]. The first step was to determine a certain aileron geometry, which was an estimation of the final result. The use is made of an inboard and outboard aileron. During low speeds both are used to get the bank angle and at high speeds it is assumed that only the inboard aileron is enough to bank the aircraft. The second step was to calculate the aileron control derivative using Equation 8.8 and the roll damping coefficient using Equation 8.9. The aileron control derivative depends on the airfoil lift curve slope c_{l_α}, the aileron effectiveness τ, the wing area S_{ref}, the span b, the location of the aileron b_1 and b_2, the chord at a particular lateral distance $c(y)$ and the lateral distance y. The aileron effectiveness τ is a function of the chord ratio. Most of the inputs are the same for the roll damping coefficient, except for the zero lift drag coefficient C_{d_0} and the half span $b/2$.

$$C_{l_{\delta a}} = \frac{2c_{l_\alpha}\tau}{S_{\text{ref}}b}\int_{b1}^{b2} c(y)y\,dy \tag{8.8}$$

$$C_{l_p} = -\frac{4(c_{l_\alpha}+c_{d_0})\tau}{S_{\text{ref}}b^2}\int_{0}^{b/2} c(y)y^2\,dy \tag{8.9}$$

After, in the third step, the aircraft roll rate is calculated using Equation 8.10. δa represents the average deflection angle of the aileron and V the speed at which the time of 1.5 seconds must hold. This is the approach speed when using both ailerons and when using only the inboard the cruise speed is used.

$$P = -\frac{C_{l_{\delta a}}}{C_{l_p}}\delta a\left(\frac{2V}{b}\right) \tag{8.10}$$

The fourth step is to calculate the time needed to bank the aircraft using Equation 8.11. $\Delta\phi$ represents the required bank angle.

$$\Delta t = \frac{\Delta\phi}{P} \tag{8.11}$$

The final step is to change the airfoil geometry in such a way that the time requirement is reached. The results are shown in Table 8.11.

Table 8.11: Aileron design

	Inboard	**Outboard**	**Total**
Aileron start [%]	10	67.2	-
Aileron end [%]	33.4	90	-
Chord ratio	0.25	0.25	-
$C_{l_{\delta a}}$	0.0165	0.0324	0.0488
C_{l_p}	-0.126	-0.126	-0.126
P_{slow} [rad/s]	0.118	0.232	0.350
t_{slow} [s]	4.831	2.259	1.496
P_{fast} [rad/s]	0.351	-	-
t_{fast} [s]	1.491	-	-

The aileron start and end percentages are from the outer wing section, which is section 3 in Figure 8.25. The subscripts slow and fast refer to the speed it is flying at. So at slow speed both ailerons are required to bank within 1.5 seconds and at high speeds only the inboard aileron is enough.

8.7.2. Elevator Design

The elevator design can be a crucial aspect in the design of a tailless aircraft. Since the aircraft does not have horizontal stabilisers, trimming can only be done by using wing (or fuselage) mounted control surfaces. Since the ailerons

are also located on the wings, the two control surfaces are combined as elevon surfaces. A design challenge arises in designing the elevons since the moment arm of the elevons to the centre of gravity is very small, requiring large deflections. The most constraining requirement on the elevon design, is the take-off rotation. During rotation, the elevons must produce a pitch up moment around the main landing gear that is greater than the moment generated by the aircraft weight and engine thrust about the main landing gear. Since the aspect ratio of the Blended Wing Body is relatively small compared to conventional aircraft, the angle of attack and thus the rotation has to be relatively high. This imposes high demands on the elevon design.
To make sure that the pitching moment for rotation is large enough, several different sizes of the elevon have been tested in the Athena Vortex Lattice software (AVL). In the end, the elevon surfaces have been located on the entire width of the outboard wing section starting behind the rear spar. Furthermore, at the rear of the centre fuselage, an elevator surface is applied. For take-off conditions at maximum take-off weight and 145 kts at ISA+15C conditions, this results in an elevator deflection of $-16°$ (negative indicating upwards deflection) and an angle of attack of 14.6° in order to rotate the aircraft and lift off. Elevator trim deflections in cruise flight have been analysed as well, the results are presented in Chapter 10. The large deflections particularly at high angles of attack may cause the elevon hinge moments to become significant. However, the aircraft uses a fly by light system allowing the hydraulics to provide the required moments instead of the pilots. In order to allow the pilots to feel the amount of hinge moment in the control surfaces, a 10 pound spring force can be applied on the control sticks.

8.7.3. Rudder Design

Now that the design of the control surfaces for roll and pitch have been discussed, the design of the rudder for yaw control is explained in this subsection. As there are two vertical tails, there will also be two rudders.

The rudder design is based on maintaining course without slipping with one engine inoperative. With one engine inoperative, the thrust is asymmetric and therefore causes a moment which the rudders should counteract. The deflection necessary is analysed for the most critical flight conditions, which is at sea level when flying at stall speed at take-off thrust. The required deflection can be calculated by using the following formula:

$$\delta_R = \frac{T_{\text{OEI}} \cdot y_T}{-0.5 \cdot \rho \cdot V_{\text{stall}}^2 \cdot S \cdot b \cdot C_{\text{n}_{\delta_R}}} \tag{8.12}$$

Here, T_{OEI} is the take off thrust of one engine, which is equal to 310.5 kN and y_T is the 4 meters lateral distance between the engines and the aircraft centre line, as mentioned in Section 8.4. The density taken in this equation is the density at sea level, which is equal to $1.225\,\text{kg/m}^3$ and the stall speed is equal to 60.6 m/s. The surface area and span are stated in Section 8.3 and the rudder control derivative is obtained using AVL. It has been chosen to not allow the rudder to deflect more than 30°. This results in a required rudder control derivative of at least 0.000356/°. This can be accomplished by two rudders that have their hinge lines at 45% of the chord of the vertical tails, which gives a $C_{n\delta_R}$ of 0.000357/° and an accompanying rudder deflection of 29.9 degrees. The dimensions of the vertical tails can be found in Section 8.6.

8.8. High Lift Devices Design

In this section, the design of the high lift devices is described. The purpose of high lift devices is to increase the aerodynamic performance of the aircraft. As the trailing edge of the wing is already filled with elevons and elevators, as mentioned in Section 8.7, the only HLD that can be added are leading edge HLD.

First, it was determined whether HLD were necessary. From an analysis using the program Athena Vortex Lattice, it was found that the maximum lift coefficient in the clean configuration is equal to 0.90. However, according to the design point from the matching diagrams, the $C_{L_{max}}$ for take-off, landing and stall speed is required to be higher. The most critical situation is the stall speed, which is equal to 60.6 m/s or 118 knts, for which a $C_{L_{max}}$ of 1.025 is necessary. Thus, there is indeed a need for some form of HLD. The most effective leading edge HLD are slats as they both extend the lift-curve and increase its slope [26]. The consequences of adding slats can be analysed by first calculating the extension of the lift-curve and then the change in slope.

Starting with the extension of the lift-curve, the following formula can be used [26]:

$$\Delta C_{L_{max}} = 0.9 \cdot \Delta C_{l_{max}} \cdot \frac{S_{wf}}{S} \cdot cos(\Lambda_{\text{hinge-line}}) \tag{8.13}$$

For slats, the value of $\Delta C_{l_{max}}$ is equal to 0.4 times c'/c. The ratio c'/c is the extended chord length as a result of the slats over the original chord length. It is chosen that the slats will increase the chord by 20% and thus the ratio c'/c will be

equal to 1.2. Furthermore, the slats are placed on the entire wing section so the reference wing flapped surface area is equal to the total area of the wing section. The total reference area is a summation of the first, second and third section. Furthermore, the hinge-line is located at 15% of the chord so they do not interfere with the wing box spars. The sweep angle at the hinge-line is determined by the wing planform geometry and is equal to 22.3 degrees. Filling in the formula results in an extension of the $C_{L_{max}}$ of 0.098 and thus a total new $C_{L_{max}}$ of 0.998. Now, the increase in lift-curve slope is calculated. The lift-curve slope in clean configuration is equal to 3.937 1/rad and the angle of attack for which C_L is equal to 0 is -0.13 rad. The latter will remain the same even when extending the slats. The change in slope can be calculated by using the following formula [26]:

$$C_{L_\alpha \text{slats}} = \frac{S'}{S} \cdot C_{L_\alpha \text{clean}} \tag{8.14}$$

$$C_L = C_{L_{0-\alpha}} + C_{L_\alpha} \cdot \alpha \tag{8.15}$$

Here, the ratio S' over S means the ratio between the surface area of the wings with the slats extended over the original surface area, which is equal to 1.05. This gives a new lift curve slope of 4.14 1/rad. Furthermore, Equation 8.15 shows the actual formula of the linear part of the lift-curve. By setting up this equation and assuming that the angle of attack at which the maximum lift coefficient is located is the same for the extended lift-curve, the new and final value for $C_{L_{max}}$ can be obtained. This is equal to 1.05 and meets the required $C_{L_{max}}$ for stall speed.

8.9. Structural Design

The structural design of the Blended Wing Body mainly focuses on the wing box structure and the interfaces of wing with the fuselage. So this section analyses the loads on wing and fuselage which also acts like a wing for a Blended Wing Body aircraft.

8.9.1. Wing Structure Design Method

The wing structure of the FB400 is designed to be able to withstand the loads experienced during its operation. The wing has to carry the external loads like lift, structural weight and fuel weight since the engines and landing gear are situated on the fuselage of the aircraft. In order to design the wing for these loads, the internal loads created are analysed. Hence the main purpose of this design is to re-iterate the structural weight, for the external and hence internal loads experienced.

Load Distribution

To determine the internal loads experienced by the wing, the external loads, lift and weight needs to be calculated. Regarding the FB400, the whole aircraft is considered as a continuation of the wing. So the aircraft is cut in half longitudinally and the half part is further divided into 30 sections along the span. For each section the lift and weight distribution is computed and the internal loads for each section is calculated. The main 3 segmentation is shown in Figure 8.25.

Due to the FB400 design, the fuselage also act as a wing to generate lift. Therefore, the total lift generated by the aircraft is distributed along the entire surface area of the aircraft. Therefore, the relation of lift distribution is simplified by looking at the proportionality of the total lift to the surface area. It is assumed for the other parameter to be constant along the span. Thus, a discretisation of the lift distribution can be obtained for the 30 sections along the span.

Initially, the wing weight is estimated based on statistical relation of the wing weight to the maximum take off weight. Referring to the thesis of Malcolm Brown [27], it is found that the wing weight of a Blended Wing Body ranges from 7 to 13% of the maximum take off weight. Therefore, an initial estimation of the wing weight is taken as the middle value, which is 10% of the maximum take off weight, and to be distributed along the span of the wing.

The total fuel volume required is estimated to be 57.3 m^3 and using the fuel density of 800 kg/m^3, the total weight is calculated to be 45,812.4 kg. The fuel volume is distributed equally in the half wing (part 2 and 3 in Figure 8.25). So the fuel volume starts at (0.25) 7.9 m and ends at (0.418)13.2 m along span from the root of part 1 in Figure 8.25.

Assuming a constant density of wing, the section weight is estimated from the wing weight as follows:

$$\text{Section weight} = \frac{\text{Wing weight}}{\text{Wing volume}} \text{Section volume} \tag{8.16}$$

where, section volume is the area of airfoil times the span wise section length. The airfoil area is estimated as:

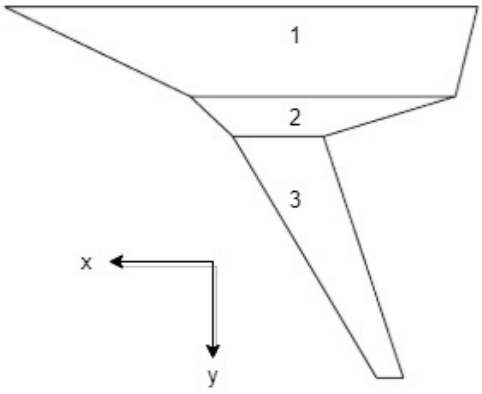

Figure 8.25: Three main sections

$$A_{\text{airfoil}} = \frac{k+3}{6}\left(\frac{t}{c}\right)c^2 \tag{8.17}$$

[26]

where k is the location of airfoil maximum thickness and c is the average of root chord and tip chord in the section. Assuming a trapezoidal wing, the chord length for each section as a function of span is :

$$c = c_{\text{r}} - \frac{c_{\text{r}} - c_{\text{t}}}{b/2}y \tag{8.18}$$

where, y is the chord distance along the span of the wing starting at the root.

The internal forces and moments follow the axis system as shown in Figure 8.26. But to be consistent with the convention of positive upwards, the shear load is considered positive upwards. Bending is positive such that the upper wing panel is in compression and the lower wing panel is in tension. Similarly, torque would be positive in counter-clockwise direction according to the right hand convention, but to be consistent with the convention of pitching up as positive for wing, clockwise direction is taken as positive torque. Also the wing loads and moments are analysed based on assumption as shown Figure 8.26, where the beam is fixed to the wall and free at the tip.

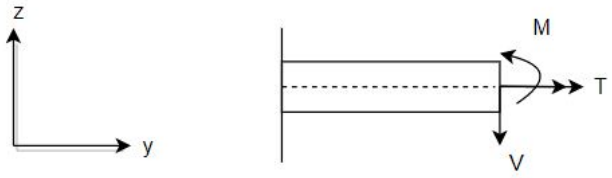

Figure 8.26: Right hand convention for shear, moment and torque

- **Shear Load**: Starting at the tip of the wing, the shear load is superposition of the net load on a section with that of previous section. Net load being the summation of section weight, lift and fuel weight taking into account its direction of action. Thus it has a linear distribution along the span.
- **Bending Moment**: It is the area under shear load graph. So the moment will follow a quadratic distribution.
- **Torsion**: The torque distribution is calculated from the relation between pitching moment and moment due to lift that is assumed to act on the quarter chord with the moment arm taken as the distance to the shear centre. In which shear centre is assumed to be located in the middle of the wingbox, so at 45 % of the chord.

The wing is designed for the maximum internal loads which occur at the most extreme condition. The extreme condition is obtained through the gust and manoeuvre V-n diagrams, which can be found in Figure 8.27 and Figure 8.28.

These diagrams are constructed with the method required from 14 CFR 25.335. In this case manoeuvre load is more limiting than gust load. Hence the most critical point at the limit load factor of 2.5 with no fuel to provide the bending moment relief is chosen to design the wing box structure which is shown in Figure 8.27. Also, a safety factor of 1.5 is implemented in the load distribution resulting into following distributions as observed in Figure 8.30, Figure 8.31 and Figure 8.32.

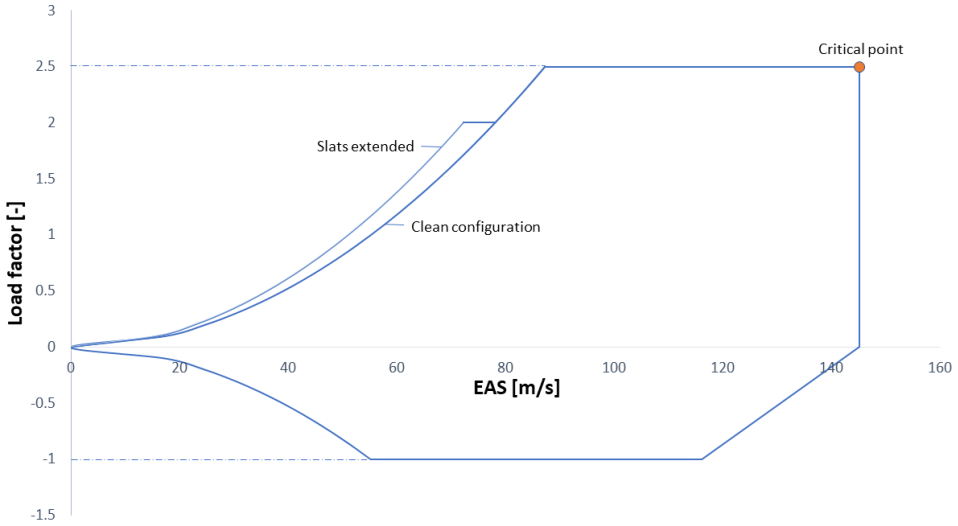

Figure 8.27: Manoeuvre V-n Diagram

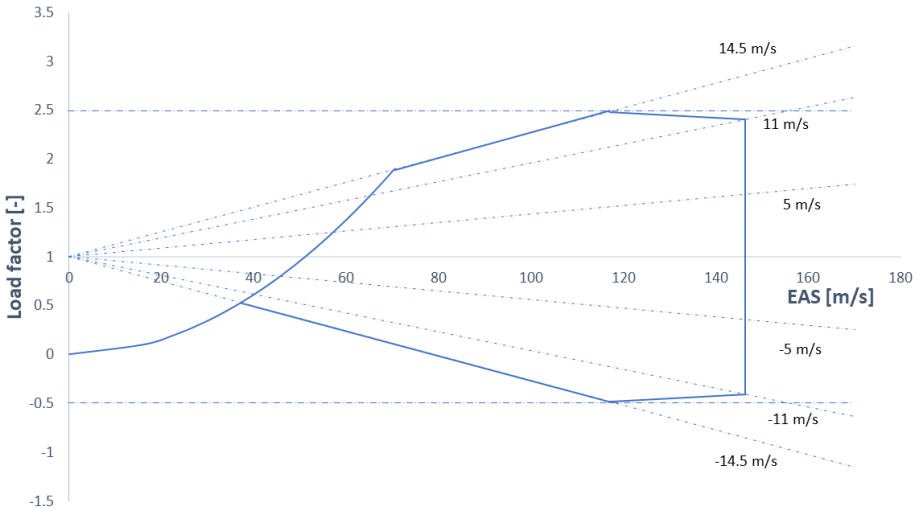

Figure 8.28: Gust load V-n Diagram

Wing Box Weight

The design of the wingbox starts with the definition of the front and rear spars which are located in 0.20 and 0.70 of the chord length respectively. This is done to take into account the space for high lift devices and other subsystem that may be implemented in the wing. Since it is a Blended Wing Body, the wingbox structure spans along the fuselage as well. However, the dimension and orientation differs in the fuselage section compared to the wing, as it has to take into account the cabin and fuselage shape while still maintaining the load distribution from the wing.

As seen in Figure 8.33, the length of top/bottom panel (a) of wingbox is assumed to be 50 % of the average chord length of the corresponding sections. The spar height (b) is taken as the average of the airfoil thickness which is 10.6 % of the average chord. And the wingbox structure is also assumed to be a thin walled structure.

After having defined the wingbox, it is sized to carry the critical forces and moments as mentioned above in load

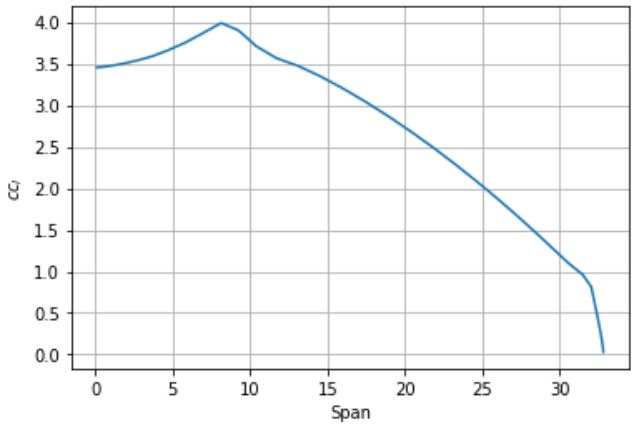

Figure 8.29: Lift distribution along the span of Figure 8.25

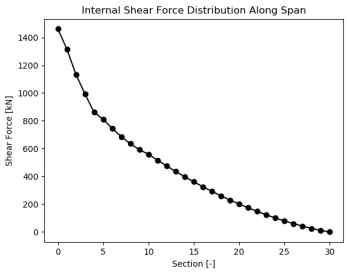

Figure 8.30: Shear force distribution

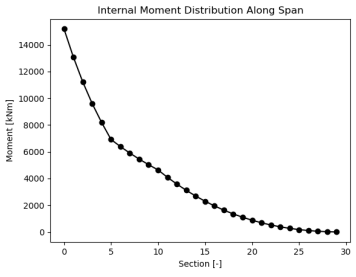

Figure 8.31: Moment distribution

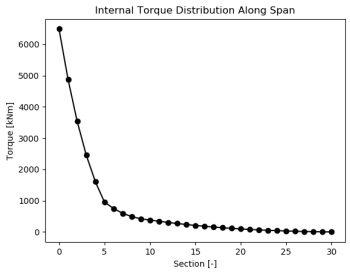

Figure 8.32: Torsion distribution

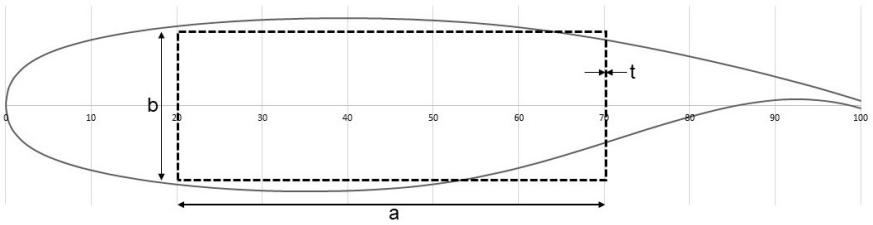

Figure 8.33: Wing box definition

distribution. The flow of the wingbox structural analysis can be seen from Figure 8.34.

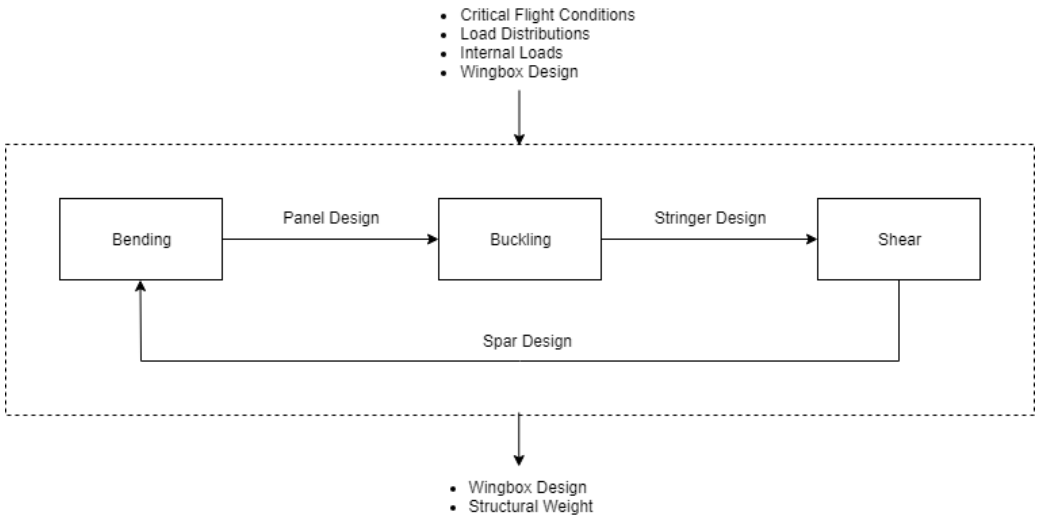

Figure 8.34: Wingbox structural design flow

First the top and bottom panel, responsible to carry compressive and tensile stresses respectively, due to bending moment experienced by the wing are sized. The panel thicknesses for each section along the span are designed so as to withstand the fatigue stress of the material using Equation 8.19. At this point, Aluminium and Composite are considered for the wingbox structure, which will result in different thicknesses and total weight for the different material. In the end, comparison can be done to pick which material suits best by comparing the weight and the cost inflicted to the design.

$$\sigma_{\text{bend}} = \frac{My}{I_{\text{xx}}} \tag{8.19}$$

where, I_{xx} is calculated using Equation 8.20 following the dimension of wingbox in Figure 8.33.

$$I_{\text{xx}} = t\left(\frac{ab^2}{2} + \frac{b^3}{6}\right) \tag{8.20}$$

Thereafter, using the minimum skin thickness, the additional required thickness is transferred to the reinforcements. So stringers are added to the skin and buckling analysis is done to ensure that the stiffened panel fails with buckling stress higher than the actual bending stress in the panels. At the same time the bending stresses in the wingbox should be lower than the fatigue stress. A hat stringer is chosen which provides the largest moment of inertia and is found to be the most used stringer shape in aircraft wing. Buckling stress of the stiffened panel is calculated using Equation 8.21, Equation 8.22 and Equation 8.23 where, b is the distance between stringers, as obtained from the structural analysis course [28].

$$\sigma_{cr} = C\frac{\pi^2 E}{12(1-\nu^2)}\left(\frac{t}{b}\right)^2 \tag{8.21}$$

$$\frac{\sigma_{\text{cc}}^{(i)}}{\sigma_{\text{y}}} = \alpha\left[\frac{C}{\sigma_{\text{y}}}\frac{\pi^2 E}{12(1-\nu^2)}\left(\frac{t}{b}\right)^2\right]^{1-n} \tag{8.22}$$

$$(\sigma_{\text{cc}})_{\text{panel}} = \frac{\Sigma\sigma_{\text{cc}}^{(i)} A_{\text{i}}}{\Sigma A_{\text{i}}} \tag{8.23}$$

In this way the top and bottom panels are designed to have less compressive and tensile stresses respectively than fatigue as well as buckling stresses.

Furthermore, the spar is assumed to carry the shear stresses from transverse shear loads and torsion experienced by the wingbox. A c-sectioned spar shape is chosen assuming it provides more enclosed area(A_m) and hence introduces less shear stresses as suggested by Equation 8.25. The spar cap is assumed to occupy 10 % of wingbox length (a in Figure 8.33) and its height is assumed to be equal to height of wingbox (b in Figure 8.33). The spar thickness is then estimated by analysing the shear stresses in the spar which should be less than the yield shear stress of material used. The shear stresses in spar is calculated as Equation 8.24 and Equation 8.25.

$$\tau_{\text{shear}} = \frac{VQ}{I_{\text{xx}}\, t_{\text{spar}}} \tag{8.24}$$

$$\tau_{\text{torsion}} = \frac{T}{2\, t_{\text{spar}} A_{\text{m}}} \tag{8.25}$$

$$\tau_{\text{total}} = \tau_{\text{shear}} + \tau_{\text{torsion}} \tag{8.26}$$

Due to the time constraint, the design of the rib is excluded from the structural analysis. However, since ribs play an integral role to the wing structure, the placement is assumed to be 0.4 meter apart from each other. This spacing is taken from a journal about the "Effect of Ribs and Stringer Spacing on the Weight of Aircraft Structure for Aluminium Material" [29]. It has to be taken into account that the current analysis, without ribs, already taken into account the buckling constraint in regards to the stringers placement. So the ribs weight is takes into account for the wing weight estimation, but it is not yet iterated to the design.

Hence, the total wingbox weight including skin, spars and ribs is obtained at the end. The total wing weight is then estimated using Equation 8.27, which shows the relation of total wing weight and the wingbox weight from [30].

$$W_{\text{actual}} = 9.1669 W_{\text{calc}}^{0.8248} \tag{8.27}$$

To summarise, with the inputs that are mentioned in Figure 8.34, the structural analysis and iteration can proceed along the flow. The goal of this iteration is to iterate the wingbox design to be strong enough to withstand the most critical loads while keeping the weight as low as possible. First, the stress due to the bending moment along the span is analysed to iterate the thickness of the wingbox panels. Then, critical stress due to buckling is assessed to iterate the amount of stringers in the panel. Afterwards, shear stresses due to transverse shear and torsion is assessed to iterate the spar design. The loop then repeats until the wing weight converges with a margin of 5%.

8.9.2. Wing Structure Design Results

The purpose of the structural design as restated is to estimate the wing box weight and hence the wing weight, re-iterating it to the loads experienced by the FB400 aircraft. With the method explained in Subsection 8.9.1, the final wingbox design is presented. The design is able to withstand the maximum bending moment, shear force and torque experienced at the root of the wing (root of part 2 in Figure 8.25) which is mentioned in Table 8.12.

Table 8.12: Maximum values at the wing root

Fuel fraction	Load factor	Shear force [kN]	Moment [kNm]	Torque [kNm]
0	2.5	653.7	5575.2	386.7

Using Carbon as the material for all the components of wingbox including, skin, stringers, spars and ribs, the total wingbox weight is calculated to be 2,684.7 kg and the total wing weight obtained from Equation 8.27 is 10,931.1 kg. For an aluminium wingbox with a density of 2,770 kg/m^3, the wingbox sizing changes resulting in weight of 4,729.6 kg with total wing weight of 17,438.5 kg. It is estimated a range of 100-1000 Euro of weight penalty for every kilogram added to the operational cost of the aircraft[31]. With the estimated cost of 6 USD (5.44 EUR) per kg for aluminium and 80 USD (72.56 EUR) per kg [32] for composite, a comparison between weight and cost is done.

Table 8.13: Composite vs aluminium with 400 EUR per kg weight penalty

Material	Wingbox Mass [kg]	Material Cost [EUR/kg]	Wingbox Cost [EUR]	Weight Penalty [EUR]	Total Cost [EUR]
Carbon-fibre-composite	10,931.1	72.56	793,160.30	0.00	793,160.30
Aluminium (2024 T6)	17,424.5	5.44	94,789.22	2,597,357.36	2,692,146.58

With the result of the trade off shown in Table 8.13, composite is justified to be the preferred material for the design for a 400 EUR penalty per kg. Even though the material price is significantly more expensive than aluminium, the weight penalty estimation is able to counteract the difference. Aluminium is only profitable when the penalty is 100 EUR. Since the range varies from 100 up to 1000 EUR it is more profitable in the long run to cut the operating cost.

Table 8.14: Properties of material used

Material	Density [kg/m^3]	E [GPa]	Poisson ratio	Fatigue stress [Mpa]	Fatigue shear stress [Mpa]
M21E IMA	1,582	68.7	0.295	206	118.9

Using quasi-isotropic carbon fibre composite with properties as shown in Table 8.14, the design resulted in varying thicknesses along the span for 20 different section for wing excluding the fuselage part (part 1 in Figure 8.25), calculated with method mentioned above using excel. The material mentioned is also used in parts of A350.The top and bottom panel thicknesses are found to vary from minimum thickness of 1.472 mm at the tip to 4.416 mm towards the root, with increasing thickness towards the root since the root has to be strong enough to withstand the maximum bending stresses there. Similarly, the C-spar thickness also increases towards the root from 1.472 mm to 4.416 mm. Again this is expected as the shear stresses are maximum at the root since the shear force and torque is maximum there. The hat shaped stringer with dimension, 50 mm height and 4.416 thick is used. A maximum of 21 stringers are at the root while there is a minimum of 4 stringers at the tip section of wingbox. Lastly total of 20 ribs of 3 mm thickness are in the wingbox.

Since the fuselage part (part 1 in Figure 8.25) also generates lift as shown in Figure 8.29, that part also experiences internal shear forces and torque as seen in Figure 8.30 and Figure 8.32. The shear stresses in the structure from the shear forces and torque is thus carried by the spars. The front and rear spars of thickness 5.888 mm continues through the fuselage top and bottom skin as shown in Figure 8.35.

Next to shear and torque, also bending is introduced in the fuselage. Since the wing is deflected upwards, the spars going through the top of the cabin are compressed, while the spars going through the bottom of the cabin will be in tension. Instead of designing the spars for buckling, an analysis is done on the ceiling thickness in Subsection 8.9.4 and it is assumed that the ceiling will take most of the compressive loads caused by bending.

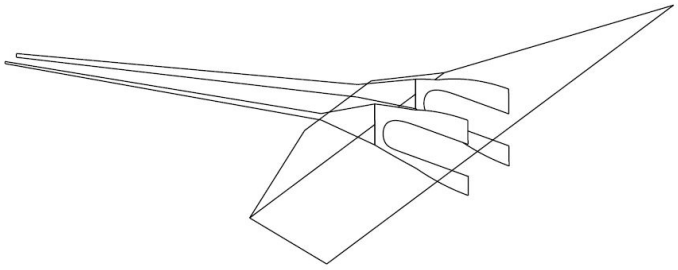

Figure 8.35: Spar continuation along the fuselage

8.9.3. Verification and Validation for Wing Structure

The structural analysis tool is verified by first making sure the equation implemented in the excel sheet matches with the actual equation being used. So the reference cells have to match correctly. Then, by visualising the load distributions, it can be verified to the trend based on the lecture of structural analysis [28]. With the stress analysis, the verification is done by testing how the input affects the output, i.e. by setting the moment to be zero, the tool should output a panel thickness of zero. The validation is done by comparing the output to the range of values found on the references. For example, the skin thickness is found to be about 7 mm, spar thickness about 15mm and rib thickness of 3 mm from [33].

8.9.4. Fuselage Structure Design Method

Multiple fuselage designs have been created for blended wing bodies. Most of them are using the multi-shell method, where the fuselage consists of several smaller circular cross sections aligned next to each other. However, vertical walls between the sections are required when this fuselage design is pressurised. Hoogreef's method proposes a design where no vertical walls between the section are needed, which allows for one large open section [34]. This is in favour for the flexibility of the cabin configuration and the passengers, since the spacious layout will give a more comfortable feeling than a narrow circular section. His method is used for the fuselage design.

Figure 8.36 shows the design of the fuselage. The structure is designed to withstand the forces created by the pressurisation of the aircraft. Figure 8.37 shows a schematic drawing of the left side of the fuselage. Throughout the length of the aircraft, the cabin height will remain constant. However, the radii R1, R2 and R3 are not constant between the longitudinal sections. Figure 8.38 shows how the forces in the outside skin are transferred into the fuselage structure.

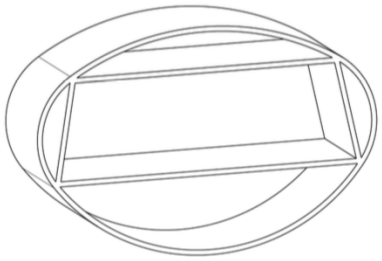

Figure 8.36: Oval fuselage concept [34]

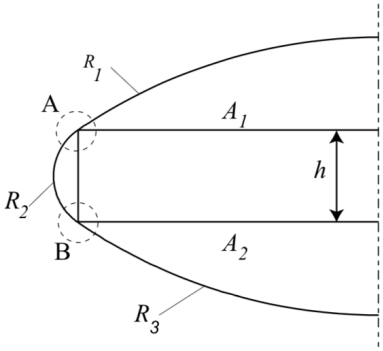

Figure 8.37: Semi cross section [34]

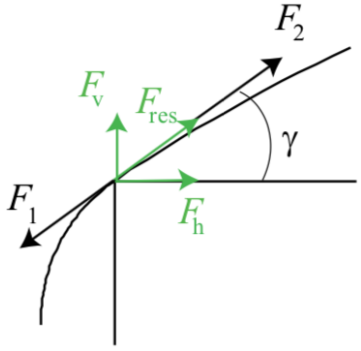

Figure 8.38: Force equilibrium at A [34]

The structure is divided into 16 longitudinal sections, and the forces and resulting thicknesses are calculated at every section. The front part of the cabin is divided into 5 sections, the middle part into 6 sections and the last part into 5 sections, as shown in Figure 8.39.

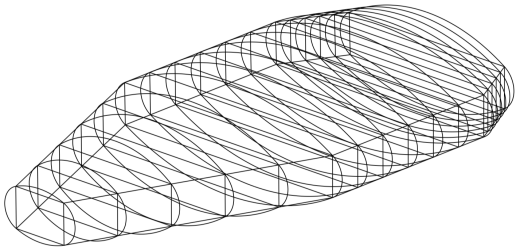

Figure 8.39: Fuselage sections

The forces in the skins are calculated using Equation 8.28, where $\frac{F_i}{\Delta l}$ is the force in the skin per unit length, j is a safety factor, Δp is the pressure difference in flight and R_i is the radius of the skin geometry. Since the radii of the top and bottom skin are larger, the resulting forces at sections A and B will cause a tensile stress in the vertical walls and a compressive stress in the floor and ceiling. Forces in horizontal and vertical direction are calculated using simple trigonometry. The angle under which the resultant force acts is a function of the angle of the tilted wall and the radius of the skin and will thus be different for all the sections. The required pressure difference is the difference between the pressure at cruise altitude and a pressurised cabin according to requirement HCSR-STR-001: The cabin shall be pressurised to 8,000 ft pressure altitude at maximum flight altitude.

$$\frac{F_i}{\Delta l} = j \Delta p R_i \tag{8.28}$$

In order to calculate the skin thicknesses needed, Equation 8.29 is used. Comparing it to Equation 8.28, it basically divides the force in the skin per unit length over the fatigue stress, resulting in a value for the thickness.

$$t_{\text{skin}} = \frac{j \Delta p R}{\sigma_{\text{fatigue}}} \tag{8.29}$$

The wall thickness is depended on the fatigue stress of the material and the vertical force applied, as shown in Equation 8.30. Since this is different for every section, 16 different wall thickness will be calculated.

$$t_{\text{wall}} = \frac{F_{\text{v}}}{\sigma_{\text{fatigue}} \Delta l} \tag{8.30}$$

The compressive stress in the floor and ceiling is compared to the maximum allowable stress due to buckling. The critical buckling force is given by Equation 8.31, where E is the Young's modulus, I the moment of inertia and b the span at that section.

$$F_{\text{crit}} = \frac{\pi^2 E I}{b^2} \tag{8.31}$$

Since the critical buckling force increases when the moment of inertia increases, use is made of a sandwich panel in the ceiling and floor. At first, the thickness combination between the panels and the honeycomb of the sandwich structure was optimised for having the lowest weight possible. However, it soon turned out that the resulting sandwich structure thickness of $0.5m$ did not fit inside the fuselage and use had to be made of a maximum honeycomb thickness of $0.28m$, so that the complete sandwich structure thickness would not exceed far beyond $0.30m$.

One important assumption made by Hoogreef is that the loads caused by pressurisation are driving the required fuselage skin thickness [34]. The major concern for this assumption was that the bending loads during extreme load cases had not been taken into account. These loads will introduce a bigger compressive stress in the ceiling of the cabin. To be sure about the assumption, analysis has been done on the stresses. Equation 8.32 gives the stress in the ceiling at locations in the middle section of the fuselage.

$$\sigma_{\mathrm{h}} = \frac{F_{\mathrm{h}}}{(2 \cdot t_{\mathrm{f}} + t_{\mathrm{c}}) \cdot \Delta l_1} \tag{8.32}$$

The highest compressive stress found is in the back of the middle section and is equal to $176.2 MPa$. The fuselage thickness has been designed to withstand this with a safety factor of 1.5. The compressive stress due to bending is found using Equation 8.33. The moment is maximum near the centre line of the aircraft and is equal to $15.2 MNm$. The ceiling's y-location is $1.2m$. The moment of inertia of the ceiling in the section between the two spars is equal to $1.59 m^4$.

$$\sigma_{\mathrm{bend}} = \frac{M \cdot y}{I_{\mathrm{xx}}} \tag{8.33}$$

The resulting extra compressive stress equals $11.5 MPa$. This means that the assumption made by Hoogreef was correct in the sense that the pressurisation loads are the driving factor for the thickness of the skin. However, the loads caused by the loading cases should not be neglected, since the safety factor of the whole structure drops below 1.5 if the ceiling thickness is not increased.

The application of composites has also been discussed in the fuselage section. For the outer skin this seems like a reasonable option since the material has high fatigue stresses. However, for the floor, wall and ceiling structure this becomes rather impossible, since the forces at the corners will cause interply bending and the different layers will come loose. In the end the decision was made to manufacture only the outer skin out of composites.

8.9.5. Fuselage Structure Design Results

In this section, the required thicknesses for the floor, ceiling, walls and the three outside skins are presented. The inputs for the program, along the dimensions of each section, are shown in Table 8.15.

Table 8.15: Input parameters for fuselage weight

Parameter	Value	Unit	Description
E_{al}	73.8	GPa	Young's modulus aluminium
E_{comp}	68.7	GPa	Young's modulus composite
ρ_{al}	2,770	kg/m^3	Density aluminium
ρ_{comp}	1,852	kg/m^3	Density composite
ρ_{c}	50	kg/m^3	Density aluminium honeycomb
j	1.5	-	Safety factor
σ_{fat}	135	MPa	Fatigue strength aluminium (100,000 cycles)
$\sigma_{\mathrm{fat_{comp}}}$	206	MPa	Fatigue strength composite (at 0.3% strain)
Δp	54,346	Pa	Pressure difference in cabin
t_{c}	0.28	m	Thickness of the aluminium honeycomb

The resulting thicknesses are shown in Figure 8.40. The largest thickness is found in the top and bottom skins of the fuselage. The lowest thickness is found in the floor and ceiling skin, which is logical since it is made of aluminium and is part of a sandwich structure. Furthermore, the thicknesses in the middle section of the fuselage are the largest. This is expected, since the largest span is at this section, which decreases the critical buckling stress and thus a bigger moment of inertia is needed to compensate for that. The thicknesses of the bottom, top and side skin are changing step wise. This is due to the fact that one layer of the chosen composite equals $1.472 mm$. This includes 8 layers in 4 different directions: 0, 45, 90, -45, -45, 90, 45 and 0 degrees. If the required thickness would exceed $1.472 mm$, another layer of the same thickness is added.

8.9.6. Fuselage Structure Design Verification and Validation

The code has been verified using the procedures described in Subsection 6.3.1. The validation of the code using Hoogreef's data is not completely certain, since the values for the skin radii are not presented in his paper. When estimating the radii from the drawings and entering this into the code, it gave an error on the final weight of less than 2%. However, estimation certain radii will give insufficient certainty of the validation, so another method is required. In the validation of Section 8.10 the fuselage weight will also be addressed, together with the wing weight.

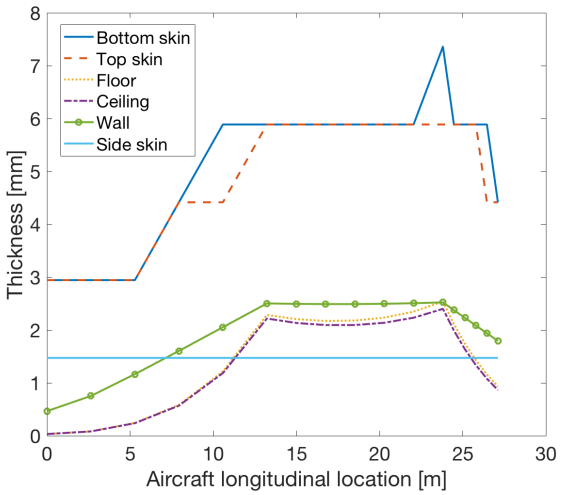

Figure 8.40: Thickness along fuselage length

8.9.7. Aircraft Structure Integration

The structure shown in Figure 8.41 is intended to provide a load path for the loads introduced by the vertical tail, engine and fuselage elevator from their location to the rear fuselage spar and subsequently the rest of the structure. For simplicity, only one engine and one tail is drawn. 4 beams are attached using stiffeners and rivets to the rear spar of the wingbox, both at the top and at the bottom. The outer beams are required for the tails and the inner beams for the engines. In case that the rear spar is unable to withstand the forces caused by thrust, it would be possible to create cutouts in the spars and continue the beams to the nose of the aircraft and back along the bottom. The spars in the tail are continued as lateral spars. Also, between the engines an extra spar is created to increase the maximum load. In the most aft spar, holes will have to be created in order to allow for the elevator systems. The tail is made out of 12 ribs, since the tail height is over 6 meters and in his third book, Roskam proposes a rib spacing of around $60cm$ [4]. In the middle section of the fuselage, multiple spars are positioned above and below the fuselage to connect the cabin to the outer skin. Cutouts will be made in these spars to allow for longitudinal stringers. These have not been drawn but are assumed to be needed. The cabin itself is visible as the large horizontal cylinder. This cylinder will decrease its span until it hits the rib between the two engines, where it will end.

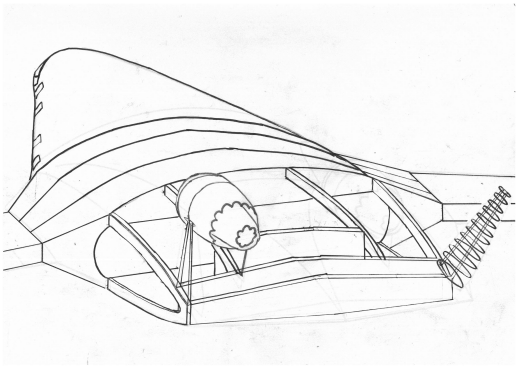

Figure 8.41: Tail and engine support structure

Figure 8.42 shows the structure of the front of the aircraft. Large beams run from the front spar to the nose of the cockpit. Additionally, extra stringers are placed in between these beams, which have not been drawn. Furthermore, hoops are connected via the beams to allow for pressurisation of the cabin.

Figure 8.43 shows the integration between wing and fuselage. The front and back spar are continued from out the wing and two extra spars are created through the fuselage. They will account for the bending moment, where the top spar will be in compression and the bottom spar will be in tension. The stringers in the wing will be continued in between the spars around the fuselage. However, when entering the fuselage, they will be more spar shaped, meaning straight and higher, to allow for cutouts for the longitudinal stringers. The spars going through the fuselage will be continuously riveted to the ceiling and the outer skin on the top, and the floor and the outer skin on the bottom. This can be done using either stringers or a C-shaped spar. The spars in section 2 of the wing, as described in Figure 8.25, will also have cutouts to allow for systems to pass through. Additionally, Figure 8.44 shows the positioning of the fuel

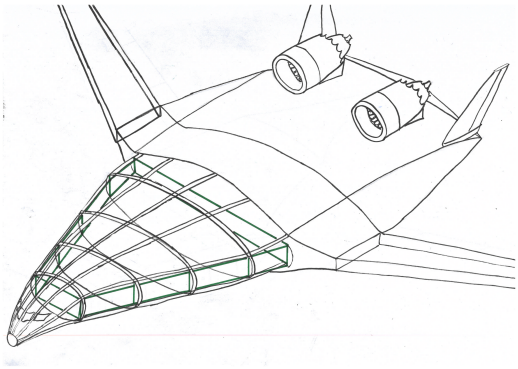

Figure 8.42: Structure front of the aircraft

tank between the front and rear wing spar and its integration with the landing gear for the shortest possible load path.

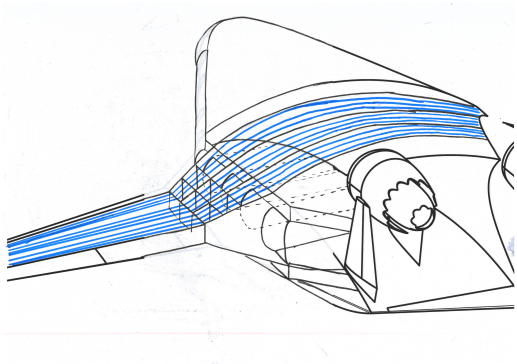

Figure 8.43: Wing fuselage interaction with stringers in blue

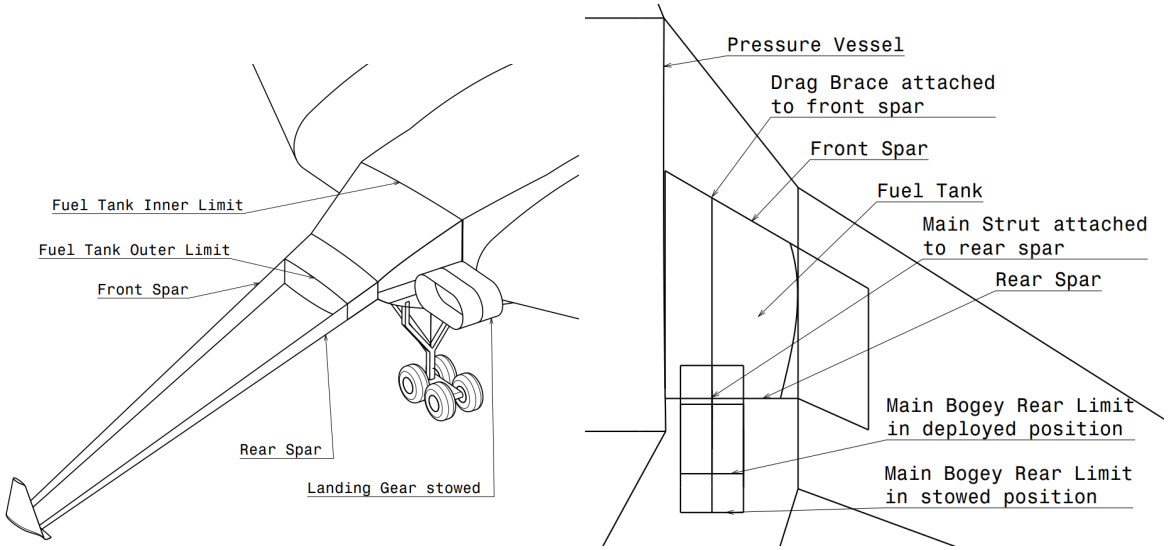

(a) Fuel tank integration in isometric view

(b) Fuel tank integration from below

Figure 8.44: Fuel tank and landing gear integration in the spar structure

8.10. Aircraft Weight

The weight of the aircraft is an important sizing factor because it affects the dimensions of the structural components as well as the planform dimensions and thus stability characteristics and flight performance. Therefore, the weight estimation performed during the previous design stage is improved by calculation of the weights of the aircraft systems and combined in order to provide a more accurate prediction of the total aircraft weight.

8.10.1. Aircraft Weight Method

The aircraft weight is calculated using two methods - an initial estimation based on mission fuel weight fractions, using Roskam's book [4] and component weight estimations, using Raymer's book [19], Desktop Aeronautics [35] and Hoogreef's method [34]. The component weight estimation is used to provide an OEW which is then used as a fraction of the MTOW as an input to the first method and iterated until a difference below 1 % is achieved compared to the first method.

The initial weight prediction from the previous design stage, as shown in Table 7.1 has changed compared to the previous design stage. This is because the values for specific fuel consumption during the cruise and reserve cruise phase were updated. Additionally, the values for L/D and cruise speed changed due to optimisation of performance in terms of both aerodynamics and sustainability. This is explained in more details in Chapter 9.

A more detailed weight estimation method is performed in this design stage which is calculating the weight of each aircraft component or system separately.

Hoogreef's method [34] showed a good estimation for the fuselage weight. The wing weight results from creating a structural design and calculating the wing weight using a penalty factor. Extra weight has been added for the spars which continue from the wing into the fuselage, which have not been taken into account by the method from Hoogreef. The weight estimations from Desktop Aeronautics [35] and Raymer [19] are applicable for the other components of the aircraft. A look has also been taken at Torenbeek, however all the weights that resulted from his method seemed low compared to the other methods [22]. His results will be discussed in Subsection 8.10.2. Table 8.16 shows the component weights calculated using Desktop Aeronautics' method. S_v is the vertical tail surface area, S_{ref} is the wing reference area and N_{seats} is the number of seats in the aircraft.

Table 8.16: Imperial component weights Desktop Aeronautics [lbs] [35]

Component	**Equation**
Flight controls & hydraulics	$3.5 \cdot S_{vt} + 0.65 \cdot S_{ref}$
APU	$7 \cdot N_{seats}$
Instrument	1,200 for long range
Electrical	$13 \cdot N_{seats}$
Avionics	between 900 and 1,500 for big aircraft
Furnishing	$78.6 \cdot N_{seats}$
Air conditioning	$15 \cdot N_{seats}$

Table 8.17 shows the components weights calculated using Raymer's method. Explanation for the symbols can be found in the nomenclature.

Table 8.17: Imperial component weights Raymer [lbs] [19]

Component	**Equation**
Vertical tail	$0.0026 \cdot (1 + \frac{H_t}{H_v})^{0.225} \cdot W_{dg}^{0.556} \cdot N_z^{0.536} \cdot L_t^{-0.5} \cdot S_{vt}^{0.5} \cdot K_z^{0.875} \cdot \cos(\Lambda_{vt})^{-1} \cdot A_v^{0.35} \cdot (\frac{t}{c})^{-0.5}$
Main landing gear	$0.0106 \cdot K_{mp} \cdot W_l^{0.888} \cdot N_l^{0.4} \cdot N_{mn}^{0.321} \cdot N_{mss}^{-0.5} \cdot V_{stall}^{0.1}$
Nose landing gear	$0.032 \cdot K_{np} \cdot W_l^{0.646} \cdot N_l^{0.2} \cdot L_n^{0.5} \cdot N_{nw}^{0.45}$
Engine controls	$5.0 \cdot N_{en} + 0.80 \cdot L_{ec}$
Fuel system	$2.405 \cdot V_t^{0.606} \cdot (1 + \frac{V_i}{V_t})^{-1.0} \cdot (1 + \frac{V_p}{V_t}) \cdot N_t^{0.5}$
Handling gear	$3.0 \cdot 10^{-4} \cdot W_{dg}$

The aircraft's empty weight is calculated by adding all the components weight to the fuselage and wing weight. For the operating empty weight, the weight of the crew, the engine and the trapped oil and fuel is added.

8.10.2. Aircraft Weight Results

After converging all the inputs and outputs of the design, the weights followed and are presented in Table 8.18. In order to extract the weight of the fuselage, the values of the sheet are multiplied with the density of aluminium and the density of an aluminium honeycomb is applied where necessary. However, this will not give the total weight of the fuselage yet. Behind the cabin, where the engine and tails are positioned, there is also a large amount of skin which has not been accounted for yet. Also, the bulkheads at the front and back of the cabin are not taken into account yet. For the first, the area of the skin is calculated and an average thickness 1 mm is chosen, which resulted in a weight of $6.8kN$. For the latter, the thickness required for the bulkheads due to the pressurisation is calculated, together with the shape, and the weight follows from there. The front bulkhead has a weight of $0.2kN$ and the rear bulkhead has a weight of $2.5kN$, due to the larger diameter.

Table 8.18: Operating empty weight components

Component	Weight [kN]	Component	Weight [kN]
Flight controls & hydraulics	30.0	Vertical tail	12.7
APU	12.5	Main landing gear	66.5
Instruments	5.3	Nose landing gear	8.3
Electrical systems	23.1	Engine controls	0.8
Avionics	5.8	Fuel system	2.5
Furnishing	151.2	Handling gear	0.5
Air conditioning	26.7	Trapped fuel and oil	8.8
Engine	36.0	Crew	10.2
Wing	121.0	Fuselage	368.3
Total operation empty weight		**890.1 kN**	

The MTOW is calculated by adding the weight of the payload and the fuel to the operating empty weight and results in $1750kN$.

The choice for Raymer and Desktop Aeronautics weight estimations is because Torenbeek gave values that were expected to be too low. The weight estimations for the hydraulics and the landing gear were comparable with the used methods and the weight for instruments and avionics was even estimated 4.5 kN higher than the current value. However, for flight controls, APU, electrical systems, furnishing and air conditioning the values were low. If Torenbeeks method would have been applied, the operating empty weight would have been around 100 kN lower. This was thought to be unreasonable and that is why the decision was to implement Raymer's and Desktop Aeronautics' weight estimations instead.

8.10.3. Aircraft Weight Verification and Validation

The calculations for the component weights are verified as described in Subsection 6.3.1. For validation data from reference aircraft is taken from Brown's thesis [14]. The reference aircraft consist of OREIO, N2A-EXTE, SAX-40, BWB150, BWB250 and BWB400. The component's percentage of MTOW is presented in the second and fifth column in Table 8.19. The third and sixth column show the reference aircraft data.

Table 8.19: Component weight fractions [14]

Component	%MTOW	Ref.	Component	%MTOW	Ref.
Flight controls & hydraulics	1.7	0.8-2.9	Vertical tail	0.7	0.5-0.8
APU	0.7	0.2-0.8	Landing gear	4.3	2.7-4.6
Instruments & avionics	0.6	0.9-1.9	Engine controls	0.1	0.1-0.9
Electrical systems	1.3	0.3-0.8	Fuel system	0.1	0.1-0.2
Furnishing	8.6	5.9-6.4	Air conditioning & anti-ice	1.5	0.1-1.7
Wing	6.9	7.1-12.9	Fuselage	21.1	12.0-18.5

There are some noticeable differences in the table. The first one that can be seen is the 8.4% furnishing weight fraction. This weight is slightly higher than normal because the design allows for foldable chairs in multiple locations. Furthermore, interesting in particular are the wing weight and the fuselage weight. The wing weight fraction is lighter than the reference aircraft, but the fuselage weight fraction appears to be larger. This is caused by the definition of wing and fuselage. It is assumed that all the mass in the area surrounding the cabin is called the fuselage. However, multiple methods also call this a part of the wing. This is why a part of the fuselage weight is considered to be wing weight for some methods. An extra verification is done using Howe's method [36]. In his paper, Howe presents a prediction for wing and fuselage weight, again with different definitions for the two. However, now the weights for wing and fuselage have been added and are compared to the total weight of the wing and fuselage in the results. The resulting difference in total weight of wing and fuselage is only 2.8%. Since his method is mainly based on statistics, it is preferred to stick to the calculated weights for fuselage and wing based on the structural needs.

8.11. Centre of Gravity

During ground operations and during flight the centre of gravity of the aircraft will shift. This has consequences for the stability and control of the aircraft, which will be analysed later in this report. An overview of the c.g. excursion is shown in Figure 8.45. For stability and control of the aircraft it is important that the c.g. stays in front of the neutral point, but not to far in front because that will require a high elevator deflection for trimming the aircraft in flight. Therefore the most aft c.g. location should be close to the neutral point and the c.g. travel should be small. To obtain the c.g. travel, first a starting point is set as the OEW c.g.. This is computed from the individual component c.g.

locations, which can be found in Table 8.20. The total OEW c.g. is then 24.0 m, measured from the nose of the aircraft. During ground operations the aircraft is loaded with passengers, cargo and fuel. To keep the c.g. travel small, the full fuel tank is designed to have its c.g. close to the OEW c.g.. In that way the c.g. shifts forward when loading passengers and backwards when loading fuel. The most forward c.g. is computed from the situation with full payload and no fuel, which results in a c.g. location of 23.2 m, measured from the nose of the aircraft. The most aft c.g. happens when only fuel is loaded and this is at the same location as the OEW c.g..

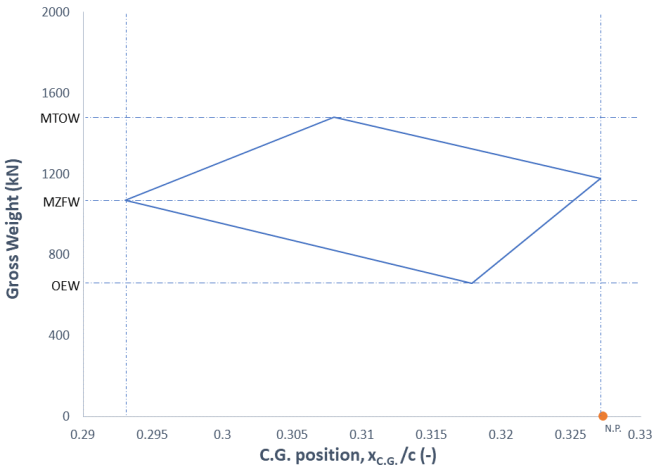

Figure 8.45: Loading Diagram

Table 8.20: C.G. location of the components

Component	**C.G. location from nose [m]**	**% MAC**	**Method**
Flight controls	15.7	-0.023	Middle between cockpit and middle of rear spar
Hydraulics	33.3	0.72	Middle of the spars where control surfaces are located
APU	21.2	0.21	At landing gear longitudinal position
Instruments	2.00	-0.60	2 m from aircraft nose
Electrical systems	22.4	0.26	Middle of cabin area
Avionics	2.00	-0.60	2 m from aircraft nose
Furnishing	22.2	0.25	Middle of cabin
Air conditioning	22.2	0.25	Middle of cabin
Engine	34.5	0.77	At engine C.G.
Wing	27.7	0.48	40 percent of MAC of wing section 2 and 3
Vertical tail	38.7	0.95	40 percent of MAC of the tail
Main landing gear	20.2	0.21	At longitudinal strut position
Nose landing gear	9.30	-0.30	At longitudinal strut position
Engine controls	18.3	0.086	Halfway between cockpit and engine
Fuel system	24.5	0.35	Center of fuel tank
Handling gear	11.6	-0.20	Between gear and cockpit
Trapped fuel and oil	24.5	0.35	Center of fuel tank
Crew	22.2	0.25	Middle of cabin
Fuselage	22.4	0.26	Middle of cabin area
OEW	**23.7**		

9

PERFORMANCE ANALYSIS

This chapter describes the mission profile for the reference mission of 700 nmi and the design mission of 3500 nmi. It also provides aerodynamic performance parameters. Fuel weight and main performance parameters are presented in Section 9.1, aerodynamic performance is analysed in Section 9.2, Section 9.3 shows how the FB400 performs during take off, cruise and landing and finally, the FB400 is compared with aircraft on the current market in Section 9.5.

9.1. MISSION PROFILE

The aircraft is designed to fly for short and medium range missions. The reference mission, i.e. the mission which it is going to perform most often has a range of 700 nmi. However, the design mission range is 3500 nmi, therefore the aircraft should be able to perform both missions with optimal parameters and minimal global warming impact.

In order to achieve this, the aircraft is designed for the medium range of 3500 nmi and its performance parameters are computed based on planform parameters, stability requirements and OEW prediction. The mission is assumed to consist of 11 phases, as shown in Figure 9.1. The phases are as follows: phase 1 - start of the engines, phase 2 - taxi, phase 3 - take-off, phase 4 - climb 1, phase 5 - cruise, phase 6 - descent 1, phase 7 - climb 2, phase 8 - cruise 2, phase 9 - loiter, phase 10 - descent 2 and phase 11 - landing. Note that the mission profile includes reserve fuel in case cruise to alternate destination and loiter are required. This is where the second part of the mission profile is included.

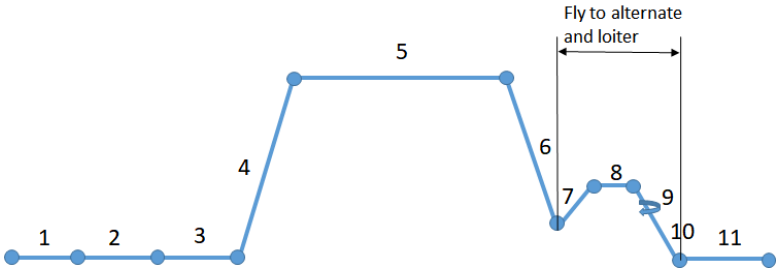

Figure 9.1: Aircraft mission profile [37]

The ratio between the weight at the beginning and at the end of each mission phase is estimated, i.e. the fuel weight fractions. For most of the fractions, statistical relationships are used obtained from the book of Roskam [4]. However, for phases 5, 8 and 9 Equation 9.1 and Equation 9.2 are used.

$$R_{cr} = \frac{V_{cr}}{c_{j_{cr}} \cdot g} \cdot \left(\frac{L}{D}\right)_{cr} \cdot ln\left(\frac{W_4}{W_5}\right) \tag{9.1}$$

$$E_{ltr} = \frac{1}{c_{j_{ltr}} \cdot g} \cdot \left(\frac{L}{D}\right)_{ltr} \cdot ln\left(\frac{W_8}{W_9}\right) \tag{9.2}$$

For those equations, the cruise speed and cruise L/D ratio are obtained by iterating with the values for lift and drag coefficient from AVL as well as recommended altitude and cruise speed for minimum SAR. Furthermore, the specific fuel consumption for the different mission phases is taken from engine specifications [1].

However, it is not the case that the aircraft will loiter and cruise to an alternate destination each time it performs a mission. Therefore, for both missions, a minimal fuel weight is computed, which will be the fuel weight required for

[1] GENX™ high bypass turbofan engines. Accessed January 2020. https://www.geaviation.com/sites/default/files/datasheet-genx.pdf

the mission itself without reserves. Both mission profiles can be seen at Figure 9.2 and Figure 9.3. The results for each mission are described in Subsection 9.1.1 and Subsection 9.1.2.

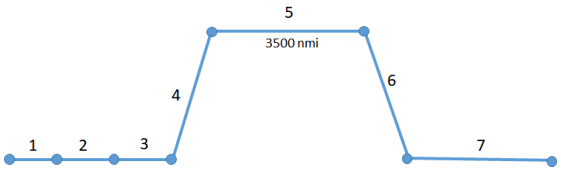

Figure 9.2: Design mission profile

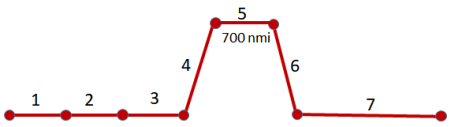

Figure 9.3: Reference mission profile

9.1.1. Design Mission - 3500 nmi

For the design mission, the aircraft has to be able to fly 3500 nmi, which means that it can spend more time climbing to a higher altitude for cruise in order to achieve maximum performance. The fuel weight fractions for this mission are presented in Table 9.1, while the performance parameters are listed in Table 9.2.

Table 9.1: Design mission fuel weight fractions

Mission phase	**Fuel weight fraction**
1 - Start of engines	0.990
2 - Taxi	0.990
3 - Take off	0.995
4 - Climb	0.980
5 - Cruise	0.818
6 - Descent 1	0.990
7 - Climb 2	1.000
8 - Cruise 2	0.970
9 - Loiter	0.971
10 - Descent 2	1.000
11 - Landing, taxi, shut down	0.992
Total fuel weight fraction	**0.723**
Total fuel weight fraction without reserves	**0.768**

Table 9.2: Performance parameters for design mission range 3500 nmi

Parameter	**Value**	**Unit**
Altitude	11.5	[km]
V_{cr}	222.4	[m/s]
M_{cr}	0.75	[-]
$c_{j_{cr}}$	$1.47 \cdot 10^{-5}$	[kg/Ns]
L/D_{cr}	20.3	[-]
L/D_{max}	23.3	[-]
$C_{L_{cr}}$	0.19	[-]
$C_{L_{max}}$	1.05	[-]
Span efficiency	0.97	[-]
$M \cdot L/D$	15.2	[-]

With this information it can be concluded that the fuel weight required for the design mission is 410 kN (42 t) resulting in a MTOW of 1480 kN (151 t). However, for a nominal mission, with no reserve fuel, fractions 6 to 9 are omitted, which means that the total fuel fraction becomes 0.768 and the aircraft should consume 35 t of fuel for each mission of 3500 nmi. The fuel weight and the operating empty are plotted versus the maximum take of weight in Figure 9.4 and Figure 9.5, in order to validate the results.

It can be seen that in both graphs the red dot is almost on the straight line, which means that the fuel weight and the operating empty weight have the same fraction of the MTOW as the reference aircraft. However, the MTOW and OEW seem lower that reference aircraft. This is due to the method used for estimation of the component weights, as explained in Subsection 8.10.1. The component weights are underestimated with this method, thus the OEW is underestimated which leads to lower MTOW. If a more accurate method for finding component weights is used, the results could be improved.

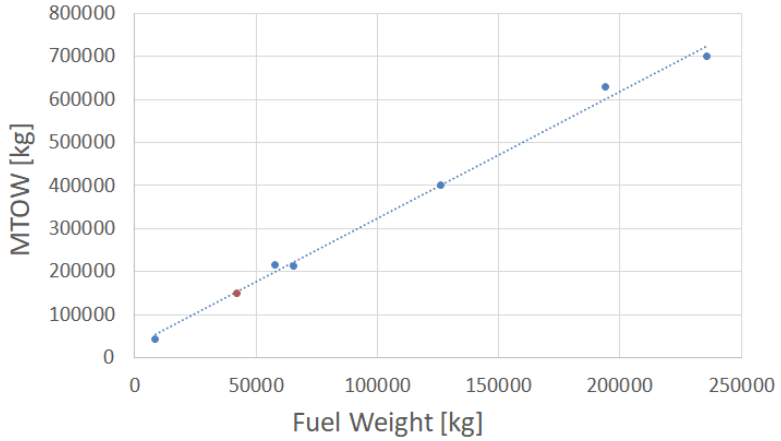

Figure 9.4: Fuel weight vs MTOW for reference BWB aircraft (blue dots) and the FB400 (red dot)

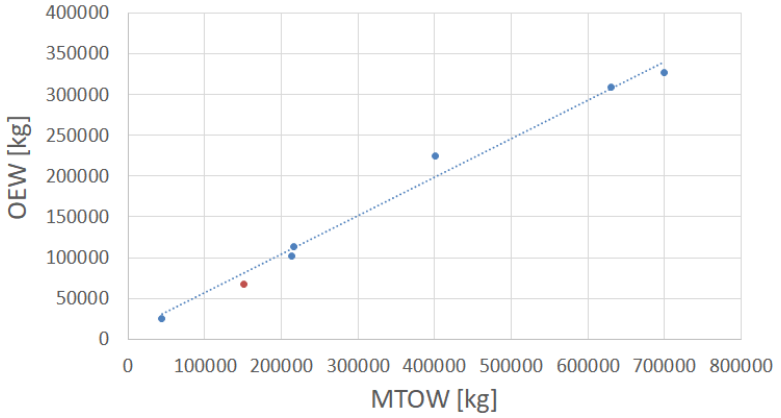

Figure 9.5: OEW vs MTOW for reference BWB aircraft (blue dots) and the FB400 (red dot)

9.1.2. Reference Mission - 700 nmi

The reference mission is assessed in a slightly different way, since the aircraft is sized to fly 3500 nmi. However, 700 nmi is a short range, which means that the fuel required for this mission is way less than for the design mission. Furthermore, the aircraft has to fly lower due to waste of energy for the climb phase of the flight. This is why it burns more of its fuel during climb compared to the range of 3500 nmi. This results in different cruise speed and L/D ratio, thus different fuel weight fractions and different fuel weight. Additionally, the cruise Mach number is driven not only by sustainability and aerodynamic analysis but also from requirement HCSR-PER-006, implying that the flight time shall be no longer than 2 hours 15 minutes, in order for the aircraft to be competitive on the market. The chosen altitude and Mach number result in a flight time of 2 hours 14 minutes. The fuel weight fractions for this mission are presented in Table 9.3, while the performance parameters are listed in Table 9.4.

Table 9.3: Reference mission fuel weight fractions

Mission phase	**Fuel weight fraction**
1 - Start of engines	0.990
2 - Taxi	0.990
3 - Take off	0.995
4 - Climb	0.980
5 - Cruise	0.964
6 - Descent 1	0.990
7 - Climb 2	1.000
8 - Cruise 2	0.970
9 - Loiter	0.971
10 - Descent 2	1.000
11 - Landing, taxi, shut down	0.992
Total fuel weight fraction	**0.852**
Total fuel weight fraction without reserves	**0.905**

Table 9.4: Performance parameters for reference mission range 700 nmi

Parameter	Value	Unit
Altitude	10.9	[km]
V_{cr}	220	[m/s]
M_{cr}	0.75	[-]
$c_{j_{cr}}$	$1.47 \cdot 10^{-5}$	[kg/Ns]
L/D_{cr}	20.3	[-]
L/D_{max}	23.3	[-]
$C_{L_{cr}}$	0.19	[-]
$C_{L_{max}}$	1.05	[-]
Span efficiency	0.97	[-]
$M \cdot L/D$	15.2	[-]

This results in fuel weight of 182 kN (18.6 t), which is 56 % less than the design missions and take off weight of 1238 kN (126.3 t), which is 16 % less than the design mission and would decrease operational cost. If the reserve mission is not performed, which is usually the case during nominal operational conditions, the aircraft would have to use 11.9 t of fuel for a range of 700 nmi.

9.1.3. Design Flexibility

The 700 and 3500 nmi missions are only two of the ranges the aircraft can fly. In Figure 9.6 all the useful combinations of payload and fuel that can be carried on board are presented, in order to show the flexibility of the design. The range is computed by extending the cruise mission phase. With this method and a total fuel capacity of 66 L and a fuel density of 800 kg/L the maximum range is 9355 km. The maximum payload is restricted by the number of seats and the volume in the cargo compartment. There is no extra space for more cargo containers, which makes the design mission payload equal to the maximum payload.

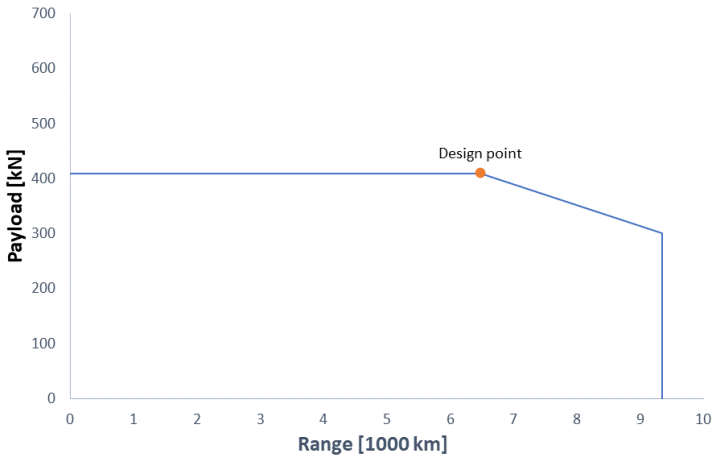

Figure 9.6: Payload-Range Diagram

9.2. Aerodynamic Performance

In the aircraft performance analysis, the aerodynamics is an important aspect to consider. In the aerodynamic analysis, the lift curve and drag polar are plotted. Both plots are presented in this section.

9.2.1. Lift Curve

In Figure 9.7, the lift curve of the aircraft is presented. It has been obtained by performing aerodynamic simulations in AVL. Note that at an angle of attack of just above 16°, the continuous line becomes a dotted line. This is because AVL is a potential flow solver and does not predict viscous effects and therefore also does not predict flow separation. For this reason, near stall conditions are indicated with the dotted line. As a rough estimation, the angle of attack at which the flow starts to separate is estimated by performing several simulations in AVL to find the angle of attack at which local airfoil sections on the wing start to reach their maximum lift coefficient. The corresponding lift coefficient to this angle of attack is 0.9 (without high lift devices). Note that the slope of the lift curve is relatively low compared to conventional aircraft. This low slope can be explained by the fact that the wings have high sweep angles and a relatively low aspect ratio.

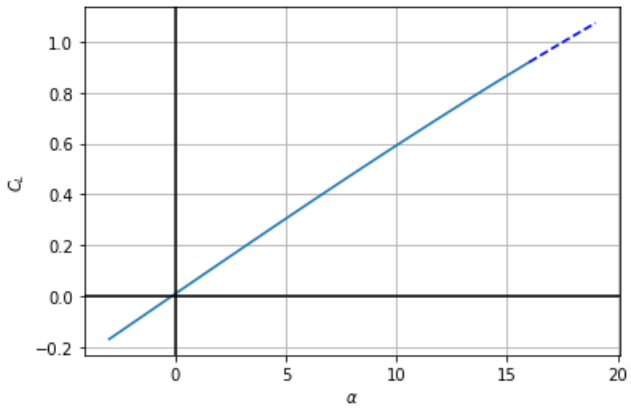

Figure 9.7: Lift Curve

9.2.2. Drag Polar

In Figure 9.8, the drag polar is presented. Similar to the lift curve, data for high angles of attack is indicated with dotted lines. The drag polar is obtained by calculating the induced drag with AVL for different values of the lift coefficient. The viscous drag (C_{D_0}) is added by estimating by using the wetted area obtained from CATIA and a friction coefficient of 0.003. By adding induced drag and viscous drag contributions, the drag polar graph is constructed.

The two term drag polar is given in Equation 9.3 By interpolating the data in Figure 9.8, the Oswald efficiency factor (e) is found to be 0.89.

$$C_D = C_{D_0} + \frac{C_L^2}{\pi A e} \tag{9.3}$$

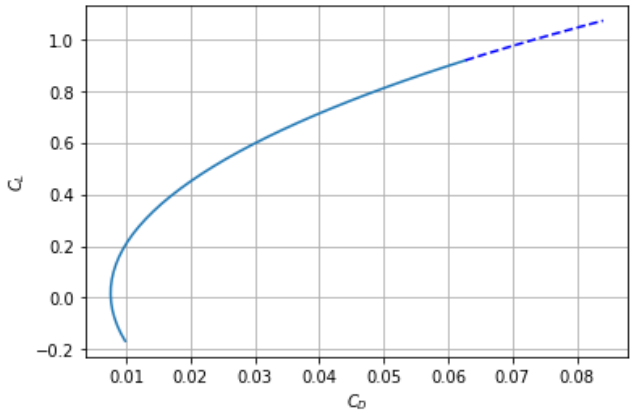

Figure 9.8: Drag Polar

9.3. Flight Performance

In order to check the compliance with the take off and landing requirements (HCSR-PER-001, HCSR-PER-002 and HCSR-PER-003) and to optimise the cruise performance of the aircraft, the flight performance is analysed.

9.3.1. TAKE OFF PERFORMANCE

The take off performance is analysed in order to check if the aircraft can take off from a balance field length of 9000 ft with the angle of attack and the lift off speed it is designed for. Firstly, the ground run distance is estimated via Equation 9.4

$$x_{\text{ground}} = \frac{{V_{\text{LOF}}}^2}{2 \cdot \overline{a}} = 1,493m \tag{9.4}$$

where $\overline{a}$ is the average acceleration during ground run and is equal to:

$$\overline{a} = \frac{g}{W} \cdot (\overline{T} - \overline{D} - \overline{D_g}) \tag{9.5}$$

The lift off speed is computed with Equation 9.6

$$V_{\text{LOF}} = 1.05 \cdot V_{\text{min}} \tag{9.6}$$

With a minimum speed of 145 kts, the ground run distance is 1493 m. The second part of the take off is the transition phase, where the transition horizontal distance is calculated using Equation 9.7.

$$x_{\text{trans}} = \frac{V_{\text{LOF}}^2}{0.15 \cdot g} \cdot sin\gamma_{\text{climb}} = 370m \tag{9.7}$$

With a climb angle of 3.4°, the transition distance of the FB400 is 370 m. Finally, the horizontal distance covered during the climb phase is computed via Equation 9.8 with a screen height of 15.2 m.

$$x_{\text{climb}} = \frac{h_{\text{scr}} - (1 - cos\gamma) \cdot \frac{V_{\text{LOF}}^2}{0.15 \cdot g}}{tan\gamma} = 133m \tag{9.8}$$

To find the total take off distance, the ground distance is summed with the airborne distance resulting in:

$$x_{\text{take-off}} = x_{\text{ground}} + x_{\text{trans}} + x_{\text{climb}} = 1,996m = 6,549ft \tag{9.9}$$

This means that the aircraft would usually need less than 9,000 ft in order to take off because of the large amount of lift it is producing.

9.3.2. LANDING PERFORMANCE

The landing performance analysis is similar to the take off but in the opposite order. Starting with the airborne phase, which includes the flare and descent distances, calculated with Equation 9.10 and Equation 9.11 with the required approach speed of 145 kts, approach angle of 3° and assumed difference in load factor $\Delta n = 0.1$

$$x_{\text{flare}} = \frac{V_{\text{app}}^2}{\Delta n \cdot g} \cdot sin\gamma_{\text{app}} = 297m \tag{9.10}$$

$$x_{\text{descent}} = \frac{h_{\text{scr}} - (1 - cos\gamma_{\text{app}}) \cdot \frac{V_{\text{app}}^2}{\Delta n \cdot g}}{tan\gamma_{\text{app}}} = 142m \tag{9.11}$$

The transition phase is estimated to be around two seconds and is computed via Equation 9.12.

$$x_{\text{trans}} = 2 \cdot V_{\text{app}} = 149m \tag{9.12}$$

Finally, the braking distance using thrust reversers is computed using Equation 9.13 and the total landing distance is the sum of the flare, descent, transition and braking distances, as shown in Equation 9.14.

$$x_{\text{brake}} = \frac{W^2}{2gS} \cdot \frac{1.3^2}{C_{L_{\max}}} \cdot \frac{1}{\overline{T}_{\text{rev}} + \overline{D} + \mu \cdot (W - \overline{L})} = 1,863m \tag{9.13}$$

$$x_{\text{landing}} = x_{\text{flare}} + x_{\text{descent}} + x_{\text{trans}} + x_{\text{brake}} = 2,451m = 8,041ft \tag{9.14}$$

This means that the landing distance is also smaller than the required distance of 9,000 ft.

9.4. Cruise Performance

In order to optimise the cruise performance of the aircraft, the range parameter, i.e. $M \cdot L/D$ is plotted versus the cruise altitude, as shown in Figure 9.9.

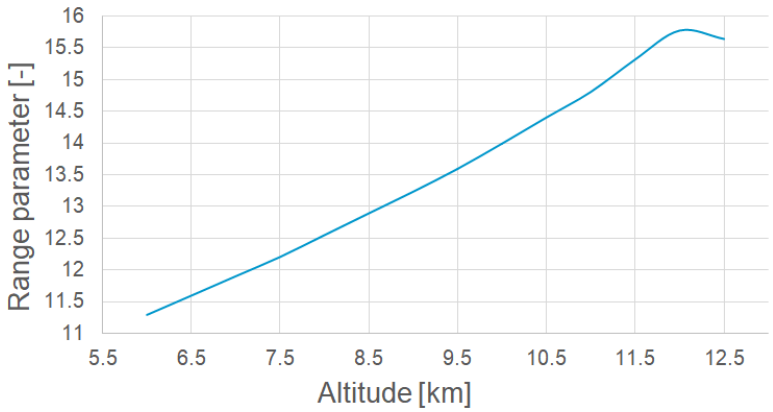

Figure 9.9: Range parameter vs altitude

It can be seen that for increasing the altitude, the range parameter increases linearly, up to the point of 12 km and then drops because the higher speeds cause more wave drag and also due to the low density, which decreases the lift force created by the aircraft.

Therefore, it can be concluded that in terms of performance, the optimal cruise altitude is 12 km. This is achieved at a Mach number of 0.78 and L/D of 20.1. However, it is chosen to design for an altitude of 11.5 km in order to reduce the radiative forcing and to save energy for climb, since the mission ranges of the aircraft are not long. If the aircraft is to perform a mission larger than 3500 nmi, it is advisable to fly at 12 km.

9.5. Comparison with Current Aircraft

In order to see how this aircraft differs from current aircraft on the market, it is compared to the performance of Boeing 777-200 [2].

It can be seen that the Boeing 777 flies a a bit lower than the FB 400, although it is designed for larger ranges. This and the fact that conventional aircraft have more wetted area in general leads to a lower L/D ratio for the Boeing 777. The lift maximum lift coefficient of FB 400 is lower because it has a large area that can help it take off and land more easily. Furthermore, it has a lower drag coefficient because of its specific geometry. In general, the FB 400 is better than current aircraft in terms of aeropropulsive performance and efficiency, since flying at higher altitude with a higher glide ratio leads to less fuel burnt. Moreover, flying higher and slower is beneficial for the specific air range values, as described in Chapter 12.

[2] Modern Airliners. Accessed January 2020. http://www.modernairliners.com/boeing-777/boeing-777-specs/

Table 9.5: Comparison of performance parameters of FB 400 and Boeing 777

Parameter	**Boeing 777**	**FB 400**	**Unit**
Altitude	11	11.5	[km]
V_{cr}	251.4	222.4	[m/s]
M_{cr}	0.84	0.75	[-]
L/D_{cr}	19.3	20.3	[-]
$C_{L_{max}}$	2.5	1.05	[-]
$M \cdot L/D$	16.2	15.2	[-]
Take off distance	8300	6,550	[ft]

10

Stability and Control Analysis

10.1. Longitudinal Stability and Equilibrium

According to the requirements and regulations, the aircraft must possess positive longitudinal stability, meaning that the aircraft will return to its equilibrium longitudinal flight condition after a change in oncoming airflow. Technically, this means that C_m has to decrease with an increasing angle of attack or:

$$C_{m_\alpha} = \frac{\partial C_m}{\partial \alpha} < 0 \tag{10.1}$$

For aircraft without horizontal tail, C_{m_α} is given by the following equation:

$$C_{m_\alpha} = C_{N_\alpha} \cdot \left(\frac{x_{cg} - x_{ac}}{MAC} \right) \tag{10.2}$$

Since the normal force on the aircraft will increase with angle of attack ($C_{N_\alpha} > 0$), the only way for C_{m_α} to be negative is if the other term on the right hand side of Equation 10.2 is negative. Note that the position of the aerodynamic centre used in the equation refers to the aerodynamic centre of the wing-fuselage combination.

One of the challenges in designing a FB400 is the absence of a horizontal stabiliser. In conventional aircraft, the horizontal tail is used to make sure that the neutral point of the aircraft is located behind the aft most centre of gravity. The FB400, however, does not have a horizontal tail. In this case, the neutral point of the aircraft is the aerodynamic centre. Equation 10.2 can therefor be written as:

$$C_{m_\alpha} = C_{N_\alpha} \cdot \left(\frac{x_{cg} - x_{np}}{MAC} \right) \tag{10.3}$$

Vortex Lattice Method

From Equation 10.3 it is apparent that the neutral point, or aircraft aerodynamic centre must be located behind the centre of gravity. In order to obtain the location of the neutral point of the FB400, a vortex lattice method is used. For this purpose, MIT's Athena Vortex Lattice (AVL) is chosen. The aircraft geometry as defined in the Class I and Class II design is defined in AVL. The discretisation of the geometry into vortex lattice panels is done using 20 chord-wise and 36 span-wise distributed panels. Both chord-wise and span-wise panelling is done in a cosine like distribution, meaning that more dense panelling is done near the leading and trailing edges and near the aircraft centre line and the wing tips. Simulations with different panelling have been performed as well, showing the same results. The geometry of the aircraft in AVL is shown in Figure 10.1.

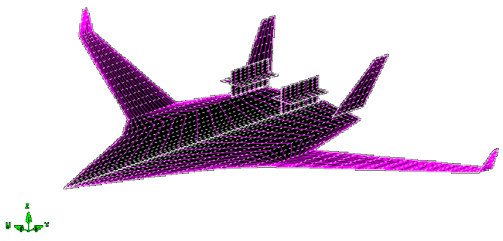

Figure 10.1: Aircraft geometry in AVL.

Once the aircraft geometry and the panelling has been set, the neutral point can be calculated. The static longitudinal stability can then be expressed by giving the static margin:

$$SM = \frac{x_{np} - x_{cg}}{MAC} \tag{10.4}$$

In particular the minimum static margin is of interest, in which the aft centre of gravity is used to calculate static margin. The estimation of the centre of gravity position has already been described in Section 8.11. In order to obtain a neutrally stable aircraft, the outer wing position and sweep angle are varied in the design iterations, as well as the longitudinal position of the engines which changes the centre of gravity location. In this way, the neutral point and aft centre of gravity can be placed very close to one another.

Equilibrium in Steady Flight

Equation 10.1 describes the condition required for longitudinal stability in flight. In order to maintain equilibrium during flight, however, it is also required to balance out the moments about the aircraft centre of gravity by trimming the aircraft. For aircraft without horizontal tails like the FB400, longitudinal equilibrium is given by:

$$C_m = C_{m_{ac}} + C_N \cdot \left(\frac{x_{cg} - x_{ac}}{MAC} \right) = 0 \tag{10.5}$$

Where again x_{ac} is equal to x_{np}. Note that the second term on the right hand side is negative for an aircraft with positive static margin. In the above discussion it was described that the aft most centre of gravity is most important in considering stability and static margins. For trimming the aircraft, however, the forward centre of gravity is more constraining. With forward centre of gravity, the lift generated by the aircraft creates the largest pitch down moment. Therefor, for both good stability and trimmed flight performance, it is important that the centre of gravity range is as small as possible. Determination of the centre of gravity range has been described in Section 8.11.
To trim the aircraft, $C_{m_{ac}}$ has to be changed by deflecting the elevators (or elevons in this case as they are also used as ailerons). In sizing the elevators, it is important to consider the effect on aerodynamic efficiency in cruise flight of elevator deflections. Preferably, the deflection of the elevators is limited such that aerodynamic efficiency is maintained and elevator hinge moments are limited. However, the moment arm of elevator surfaces is small for the FB400 which means that a larger deflection will be required as compared to conventional aircraft. For designing the elevators, however, it must be noted that take-off rotation is a constraining condition as the moment arm about the main landing gear is even smaller and larger pitching moments must be generated. Elevator sizing and deflections for take-off rotation have been described in Section 8.7. The elevator trim deflection has been estimated by using AVL for the most forward centre of gravity resulting in an elevator deflection in normal cruise of $-4.8\,\text{deg}$, with the minus sign indicating upwards deflection. The presented elevator deflection also accounts for the pitch down moment created by the engine thrust. Note that for different velocities, different pitching moment (and required engine thrust) arise. In Figure 10.2, the required elevator deflection is plotted as a function of flight speed.

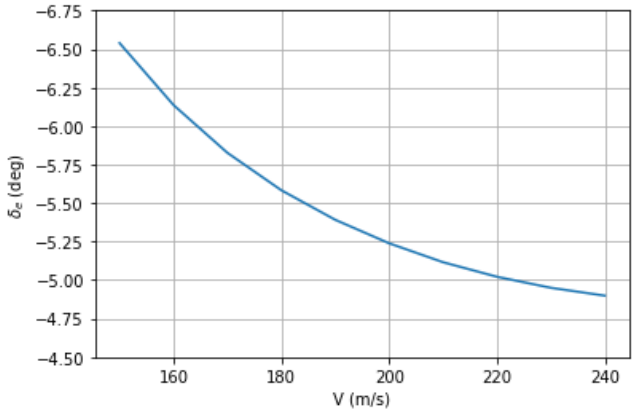

Figure 10.2: Elevator trim curve

10.2. Lateral and Directional Stability

In the previous section, longitudinal stability has been considered. In this section lateral and directional stability are analysed. In analysing the asymmetric aircraft characteristics, the side force, rolling moment and yawing moment on the aircraft are to be considered. In this section, the stability characteristics of the aircraft without control deflections are analysed by considering the non-dimensional coefficients C_{Y_β},C_{l_β} and C_{n_β}.

Side Force

The side force that is induced on the aircraft in side slipping flight is described by the non-dimensional coefficient C_{Y_β}. The aircraft vertical tails have a dominant contribution to this force coefficient. Furthermore, since the engines are placed on the rear of the fuselage and have a significant diameter, they may have a non-negligible contribution as well. Since the winglets on the wings are relatively high, they will contribute to C_{Y_β} as well. For static stability it is required that the side force opposes the side-slipping motion. This implies that:

$$C_{Y_\beta} = \frac{\partial C_Y}{\partial \beta} < 0 \tag{10.6}$$

For the FB400, the winglets, vertical tails and engines are located behind the centre of gravity allowing for a negative side-force coefficient.

Effective Dihedral

The derivative C_{l_β}, or effective dihedral, is mainly influenced by the wing dihedral or the wing sweep. An increasing wing dihedral causes a different geometric angle of attack between the left and right wing in side-slipping flight causing C_{l_β} to be more negative. Swept wings also experience a difference in lift between the left and right half's of the wing causing C_{l_β} to be more negative. It is desirable to have a negative effective dihedral or:

$$C_{l_\beta} = \frac{\partial C_l}{\partial \beta} < 0 \tag{10.7}$$

However, if the effective dihedral gets to low it might affect dutch roll characteristics. For the FB400 the dihedral angle is mostly constrained by tip clearance in banked landing. The sweep angle is constrained by the requirement to fly at high mach numbers. This might impose the need to design a yaw-damper system later on.

Directional Stability

The aircraft directional stability C_{n_β} is mostly determined by the vertical tail planes (and winglets). For stability it is desirable to have a yawing moment that opposes the side-slip angle. This implies:

$$C_{n_\beta} = \frac{\partial C_n}{\partial \beta} > 0 \tag{10.8}$$

Since the vertical tails are located behind the centre of gravity, making the tails larger would increase C_{n_β}. However, in the design, the tails were sized based on the requirement to be able to fly in a one engine inoperative condition. The desired positive directional stability was checked later on. The values for the described coefficients as obtained using AVL for the FB400 can be found in Table 10.1.

Table 10.1: Lateral and directional stability characteristics.

	C_{Y_β}	C_{l_β}	C_{n_β}
Requirement	<0	<0	>0
Value	-0.19	-0.079	0.035

10.3. Dynamic Stability

Mass Moment of Inertia

In order to analyse the dynamic stability characteristics of the FB400, the mass moments of inertia have to be determined. At this stage of the design, only empirical estimates of component weights and locations have been made which presents a large difficulty in obtaining accurate moment of inertia estimates.
In order to get a rough estimate of the aircraft moment of inertia, a method provided by [38] is applied. In the structural analysis discussed before, estimations for aircraft spar weight and skin weight have been made. Furthermore, the location of the fuel tanks in the wings has been determined. The moment of inertia contribution of the structural weight of the wing and fuselage is determined by dividing the body into several span-wise stations and five chord-wise sections. The contribution of each section is then represented by a lumped mass. The distribution of lumped masses can be seen in figure Figure 10.3.

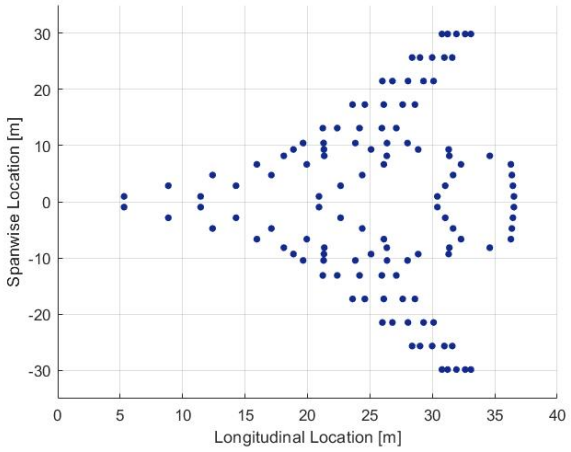

Figure 10.3: Distribution of lumped masses

The mass of each section is based on the fraction of skin and spar weight relative to total wing section mass as estimated in the aircraft structural analysis. In the method provided by [38], the structural weight varies along the span to account for the required thicker structures near the wing root. After the airframe weight components are estimated, the fuel mass is estimated at each section based on the (span-wise) location of the fuel tanks and the relative volume of the chord-wise sections. After determining the masses, the moments of inertia are calculated and added. The contributions of other components of the aircraft is estimated by modelling them as point masses. For the current analysis, components such as the engines, vertical tails, main landing gear and nose landing gear are added. Because of time constraints and the difficulty in determining accurate mass moment of inertia distribution of the passengers and cargo, the moment of inertia of the plane in 'ferry flight' condition is only used here. If further analysis is to be conducted, the contribution of passengers and cargo, as well as smaller operational items is to be added to obtain better estimates.
The total mass moments of inertia estimates are presented in Table 10.2.

Table 10.2: Estimated mass moments of inertia.

Parameter	**Value**	**Unit**
I_{xx}	$9.60 \cdot 10^6$	$kg \cdot m^2$
I_{yy}	$35.8 \cdot 10^6$	$kg \cdot m^2$
I_{zz}	$45.1 \cdot 10^6$	$kg \cdot m^2$
I_{xz}	$0.65 \cdot 10^6$	$kg \cdot m^2$

Symmetric Motions

After evaluating the static longitudinal stability of the aircraft, the dynamic stability can be analysed. Since the aircraft is symmetric about the longitudinal axis, the symmetric and asymmetric equations of motion can be decoupled and analysed separately.
The general linearized equation of motion for symmetric motion are derived in [39], for example, and are presented below in Equation 10.9. The coefficients presented are obtained by simulating the aerodynamics in AVL. AVL can then provide the coefficients in the form presented below. However, for further analysis, the matrix with it's coefficients in state-space form is used in order to directly analyse the eigenmotions in MATLAB.

$$\begin{bmatrix} C_{X_u} - 2\mu_c D_c & C_{x_\alpha} & C_{Z_0} & 0 \\ C_{Z_u} & C_{Z_\alpha} + (C_{Z_{\dot{\alpha}}} - 2\mu_c) D_c & -C_{X_0} & C_{Z_q} + 2\mu_c \\ 0 & 0 & -D_c & 1 \\ C_{m_u} & C_{m_\alpha} + C_{m_{\dot{\alpha}}} D_c & 0 & C_{m_q} - 2\mu_c K_{yy}^2 D_c \end{bmatrix} * \begin{bmatrix} \hat{u} \\ \alpha \\ \theta \\ \frac{q\bar{c}}{V} \end{bmatrix} = \begin{bmatrix} -C_{X_\delta} \\ -C_{Z_\delta} \\ 0 \\ -C_{m_\delta} \end{bmatrix} * \delta_e \tag{10.9}$$

For the aircraft to operate safely and be controllable by the pilots, it is important to define certain limits constraining the dynamic motions of the aircraft. The limits on the dynamic motions of the aircraft in this project follow the guidelines set by US Military specification MIL-F-8785C [40]. For the symmetric motions, this particularly constraints the

damping of the short period to be within certain limits (Table 10.4). When analysing the obtained state space matrices, it becomes apparent that the short period damping of the aircraft already lies within required limits. The Phugoid motions, which are also often referred to as long period motions, are normally oscillatory in nature. For the FB400, however, they become aperiodic. A possible explanation for the result might be the fact that the centre of gravity of the aircraft is so close to the neutral point, that C_{m_α} becomes very small. This might reduce the aircraft's tendency to produce a restoring pitching moment causing the oscillatory nature of the motion to reduce.

Table 10.3: PI controller gains.

Parameter	Value
K_P	-0.97
K_I	-0.98

In Figure 10.4, the Pole-Zero map of the symmetric motions is shown. As can be seen, one of the phugoid eigenvalues is to the right of the imaginary axis. To have a stable system with enough short period damping, a PI controller is introduced. The PI controller is used to reduce the pitch rate error, making the aircraft easier to control. The gains are tuned using MATLAB and presented in Table 10.3. Corresponding damping and natural frequencies of the short period motion are presented in Table 10.4.

Table 10.4: Short period damping characteristics.

Parameter	Open-loop system	Closed-loop system	Level 1 handling qualities
ζ_{sp}	0.69	0.6	$0.35 < \zeta_{sp} < 1.8$
$\omega_{n_{sp}}$	0.17	1.1	-

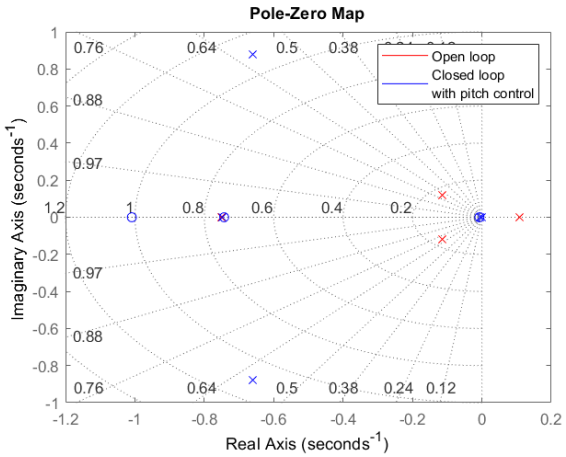

Figure 10.4: Pole zero map of symmetric eigenmotions.

Asymmetric Motions

As has been explained in the previous section, the asymmetric motions can be analysed separately from the symmetric motions. The general form of the equations of motion for the asymmetric motions where derived in [39], and are presented in Equation 10.10.

$$\begin{bmatrix} C_{Y_\beta} + (C_{Y_{\dot\beta}} - 2\mu_b)D_b & C_L & C_{Y_P} & C_{Y_r} - 4\mu_b \\ 0 & \frac{-D_b}{2} & 1 & 0 \\ C_{\ell_\beta} & 0 & C_{\ell_p} - 4\mu_b K_X^2 D_b & C_{\ell_r} + 4\mu_b K_{XZ} D_b \\ C_{n_\beta} + C_{n_{\dot\beta}} D_b & 0 & C_{n_P} + 4\mu_b K_{XZ} D_b & C_{n_r} - 4\mu_b K_Z^2 D_b \end{bmatrix} * \begin{bmatrix} \beta \\ \phi \\ \frac{pb}{2V} \\ \frac{rb}{2V} \end{bmatrix} = \begin{bmatrix} -C_{Y_{\delta_a}} & -C_{Y_{\delta_r}} \\ 0 & 0 \\ -C_{\ell_{\delta_a}} & -C_{\ell_{\delta_r}} \\ -C_{n_{\delta_a}} & -C_{n_{\delta_r}} \end{bmatrix} * \begin{bmatrix} \delta_a \\ \delta_r \end{bmatrix} \tag{10.10}$$

For the asymmetric motions, the dutch roll damping imposes the largest challenge in obtaining the required level 1 handling qualities. The required damping and natural frequencies for the dutch roll are stated in Table 10.5.

Just as for the symmetric motions, the stability derivatives for the asymmetric motions where calculated using AVL and analysed in MATLAB. As can be seen in the Table 10.5, the damping of the short period has to be increased. To do

Table 10.5: Dutch roll damping characteristics.

Parameter	Open-loop system	Closed-loop system	Level 1 handling qualities
ζ_{dr}	0.05	0.3	0.08
$\omega_{n_{dr}}$	0.67 rad/s	0.612 rad/s	0.4 rad/s
$\zeta_{dr} \cdot \omega_{dr}$	0.03 rad/s	0.18 rad/s	0.15 rad/s

so, a simple proportional controller has been tuned using MATLAB. However, with only a proportional gain, the spiral mode becomes over-stabilised. In practice this would mean that the pilots would have to constantly apply a side force on the control stick in order to maintain a constant bank angle. This is usually not a comfortable way to fly the aircraft and it is not as pilots are used to fly. To improve the control characteristics, a washout filter is applied. This allows the dutch roll damping to be improved without over stabilising the spiral mode. The resulting gain for the closed loop system is $K = -2.23$ (with a time constant for the washout filter of 5 seconds). In Figure 10.5, the pole-zero map for the open-loop and closed-loop systems are compared. Note the effect of the washout filter on the closed-loop system by a added zero at the origin.

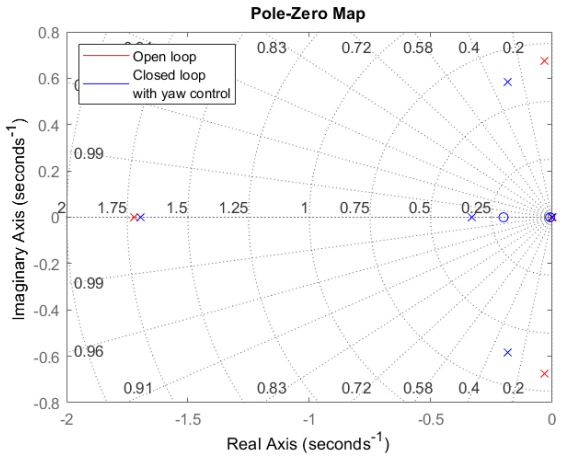

Figure 10.5: Pole zero map of asymmetric eigenmotions.

11

Operations and Logistics

In this chapter, the operations and logistics of the FB400 are discussed. Starting off with the flight and ground operations in Section 11.1 and Section 11.2 respectively. Finally, the logistics flow diagram is shown in Section 11.3 and the design logistics is explored in Section 11.4.

11.1. Flight Operation

The main problem to be solved with this project is to alleviate airport congestion that is happening in major airport hubs. Therefore, the main route the FB400 will operate at is across two major hubs that are already congested and proven to have a high demand of daily passengers.

According to the report by OAG [41], the busiest aircraft routes in the world in 2019 can be found in Asia. For domestic routes, the busiest route is from CJU-GMP (Jeju - Seoul Gimpo) with 80,000 annual flights and an average of 200 flights per day. For the international routes, KUL-SIN (Kuala Lumpur - Singapore) is the busiest with 30,000 annual flights and an average of 82 flights per day. Both of these routes are categorised as a short range route, however due to the high demand, even a high capacity long haul aircraft is used by several operators.

FB400 is designed to have the capacity of a long haul aircraft with the efficiency of a short haul aircraft. Complying with the requirement HCSR-OPR-006, 2 pilots and 8 cabin attendants will operate the aircraft. The 400 seat capacity is comparable to a wide-body aircraft that is double the capacity of the current average of narrow-body aircraft. Since the busiest domestic and international flight route is considered to be a short range, the FB400 will be able to outperform the current narrow-body aircraft in terms of capacity and the current wide-body in terms of efficiency. So the operator will be able to meet the demand while reducing its flight frequency. Thus, reducing the possibility of airport congestion because fewer flights will take place each day.

11.2. Ground Operation

Aside from its flights, another key factor for the aircraft operation is how well it operates on the ground. For the customers, it is more profitable when their aircraft is flying and not on the ground. So a shorter ground operation is preferable. The key performance indicators to be analysed of aircraft ground operations are the airport compatibility and turnaround time.

11.2.1. Airport Compatibility

It is important for the aircraft design to be compatible with the current airport facilities. The requirement of the design is constrained by gate type V airport. Not only does it constrain the dimensions of the design, but it is also restricted to the availability and layout of the ground servicing equipment. By being able to utilise the available facilities, significant cost is cut from the operation cost.

At this point of the design phase, the accessibility of the airports used by the ground servicing equipment is not yet known. To be able to analyse whether it is compatible with the current airport facilities, only the dimensions and layout of the aircraft are taken into account. By comparing it to the current layout and dimensions of a similar gate type V compatible aircraft, the span is already constrained to the gate specifications. The estimation of the ground operation layout is shown in Figure 11.1.

As shown in Figure 11.1, all of the necessary ground service equipment to carryout the entire turnaround process is compatible to the dimensions of the Blended Wing Body. It is to be noted however, that only the passenger doors and the cargo doors are designed and implemented. The other access ports such as fuel inlet, water inlet and toilet sewage are only estimated based on feasible locations as they are not yet designed. The fuel tank position is located near the root of the wing, but the fuel inlet may have to be shifted further to the tip to fit the long chain of cargo

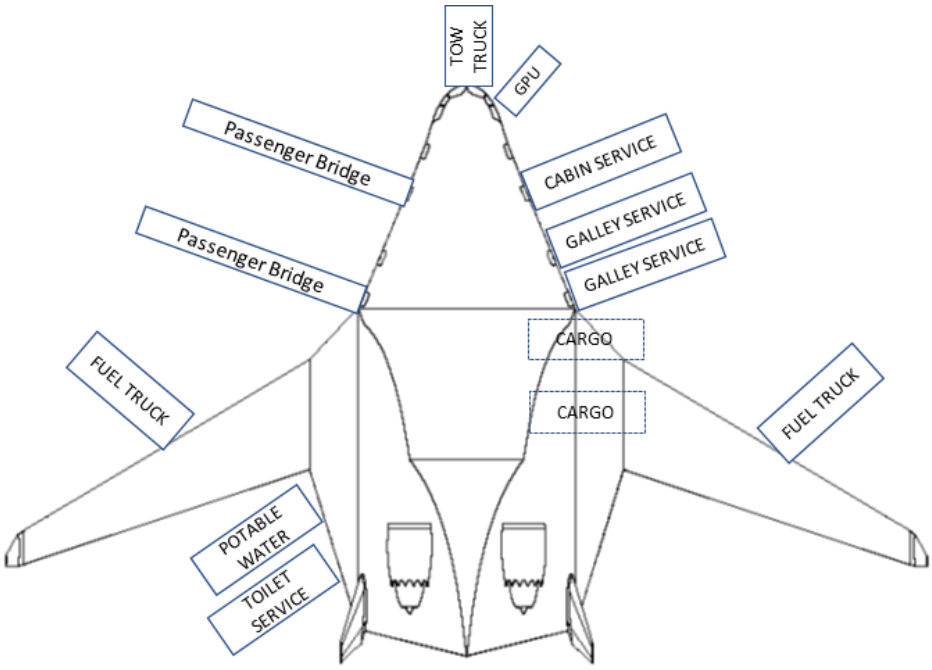

Figure 11.1: Airport ground operation layout of the Blended Wing Body

trucks. Therefore, the requirement HCSR-OPR-014 regarding the compatibility of the design to gate V ground service equipment is proven to be feasible.

According to Mike Sinnet, Boeing's VP of Product Development and Future Airplane Development, one of the reasons the Blended Wing Body is not in operation is due to the design being incompatible with the current airport facilities[1]. Therefore it is important to constrain the design from the start to be compatible with the current airport facilities. Thus, the implementation of the subsystems on later stages will take into account the accessibility of the equipment. It is already analysed that based on the dimensions, it is feasible to utilise the available ground servicing equipment.

11.2.2. Turnaround Time

The time taken for an aircraft to be on the ground in between flights is driven by the turnaround time. It is the time measured from when the aircraft is parked and the chock is set, until the chock is removed and the aircraft is pushed back. Throughout the turnaround time, several operations need to take place in coherency to prepare the aircraft for its next flight. This process includes (de)boarding of passengers, servicing of galleys and cabin, refuelling, (un)loading of cargo, and servicing of toilets and water. The turnaround time of the FB400 aircraft can be seen from Figure 11.2.

Based on Figure 11.2, the turnaround operation starts with the positioning of the passengers bridge or stairs and ends with the push back of the aircraft. To estimate the turnaround time, the reference aircraft used are the Boeing 777-300[42], the Boeing 737-900[43], and the Airbus A330-300[44]. Then, the following operations take place:

- **Deboard Passengers**: The time taken for the passengers to deboard the aircraft. Based on the reference aircraft the deboarding time is found to be approximately 40% shorter compared to the boarding time. Because it is assumed that the flow for deboarding is more organised compared to boarding.
- **Service Cabin**: The time taken to clean and prepare the cabin for the next flight. It is estimated by linearising the capacity of reference aircraft to their cabin service time, as it is assumed that the time is proportional to the number of seats.
- **Service Galley**: The time taken to service the galley with the required food/drinks and amenities. It is estimated by comparing the amount of galley and passengers to the reference aircraft, so the proportionality can be estimated.
- **Board Passengers**: The time taken to board the passengers. It is measured by developing a boarding simulator based on the simulation tool developed by Timothy Tamm [2]. The tool is calibrated by verifying the simulation to the real boarding time of the reference aircraft to compare the cabin layout of the Blended Wing Body.

[1] Don't look for commercial BWB airplane any time soon, says Boeing's future airplanes head. Accessed January 2019. https://leehamnews.com/2018/04/03/

[2] Boarding-simulator by Timothy Tamm. Accessed December 2019. https://github.com/thctamm/Boarding-simulator

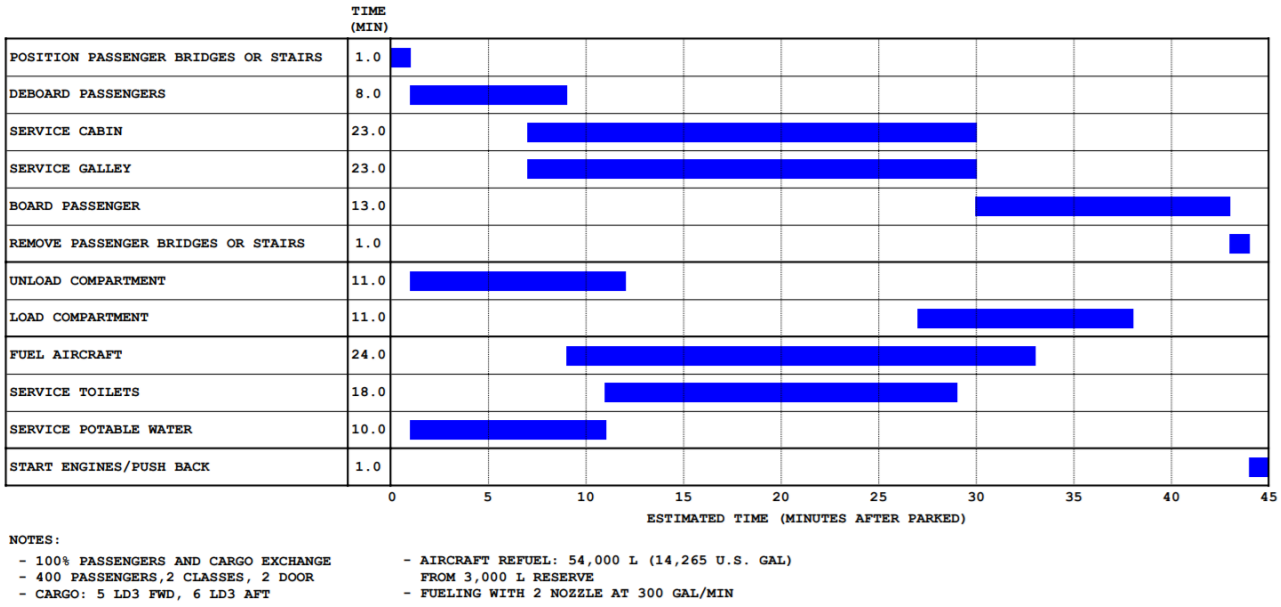

Figure 11.2: Turnaround time Gantt chart of the Blended Wing Body aircraft 3,500 nmi range mission.

- **Unload Compartment**: The time taken to unload the cargo compartments. Since LD3 compartments are used, the time taken to load or unload the compartment is assumed to be one minute for each similar to the estimation of the 777.
- **Load Compartment**: Time taken to load the cargo compartments. It is estimated to be equal to the unloading time, as the amount of cargo is assumed to be the same, which is 11 LD3-45.
- **Fuel Aircraft**: The time taken to (re)fuel the aircraft. To see the maximum fuelling time it is assumed to be filled for the maximum 3500 nmi range from empty tank with 2 nozzles operating at 300 U.S. Gal per minute each.
- **Service Toilets**: Time taken to service the toilet sewage of the aircraft. It is linearised from the reference aircraft data based on the total amount of toilet in the aircraft.
- **Service Potable Water**: Time taken to refill the potable water. It is found to be constant among reference aircraft despite the varying capacity and size.

Some of the operations are restricted to take place together and everything needs to be in the logical order. For passenger comfort, the cabin and galley services can only start when 75% of the passengers have left the cabin and it has to end before the next passengers board. With the available time, it is possible to service the toilets and potable water separately as this increases the hygiene factor of the operation, even though the ports are separate from each other. For the fuelling, it was not allowed by regulations to refuel together with (de)boarding. However, with the increase in reliability of the fuel system, the old regulation is neglected so the time can be optimised further.

Comparing the turnaround time of the FB400 to the reference aircraft with similar capacity or range, it is estimated that the turnaround time of the FB400 is in between the current narrow-body and wide-body aircraft used for similar range. Narrow-body aircraft, such as the 737, took an average of 40 minutes and wide-body aircraft, such as the 777, took 60 minutes. Meanwhile, the Blended Wing Body able to complete the turnaround process in 45 minutes. The driving factor of the turnaround time of the FB400 is the time it takes to service the cabin. Due to its high capacity, it takes a significant amount of time to clean up the cabin based on the total number of seats available. The boarding time of the FB400 is estimated to be approximately 28% faster than the current Boeing 777-300, due to the amount of four aisles compared to the typical two aisle of the Boeing 777-300.

With the 45 minutes turnaround time, the FB400 aircraft has completed requirement HCSR-OPR-005. In which it is required for the design to have a turnaround time of less than 1 hour and 45 minutes.

11.3. Logistic Flow Diagrams

To outline the logistic flow of the FB400, the logistic flow diagram is given in Figure 11.3. However, it is to be noted that the duration of each action is of different length.

In accordance to Figure 11.3, the entirety of the final report is a part of the design phase. Manufacturing comes after the completion of the design and before the first prototype. Because before mass manufacturing and delivery to the

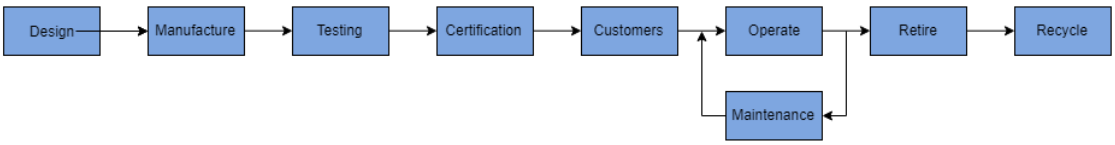

Figure 11.3: Logistic flow diagram of the concept design.

customers, testing and certification needs to be done to ensure the safety and reliability of the design. Then, the aircraft is sold and delivered to the customers, which are the airlines or aircraft leaser. In the hands of the customers, the FB400 can operates along with the occasional maintenance, so the performance stays at its optimum level for an extended period of time. Until the end of its lifespan, the FB400 is expected to be retired and recycled.

With the logistic flow diagram, the whole lifetime of the design can be anticipated and optimised accordingly. So to have an optimal performance with recycleability in mind for the end.

11.4. Design Logistics

In order to operate the aircraft all over the world, the aircraft needs to be certified by both the European Aviation Safety Agency (EASA) and the Federal Aviation Regulations (FAA). To certify the type of aircraft, the designers have to demonstrate the compliance of the aircraft to the regulatory requirements by use of ground and flight testing.

According to Airbus[3], the A380 and A350 XWB, took five and two years respectively to undergo the full extent of flight testing and certification. This process includes the static structural test, flight test, and certification. The static structural test has the purpose of pushing the aircraft structure to its limit by using a simulation rig on the ground. The flight test is designed to validate the simulation data of the actual design to undergo the limit of its flight operation, such as flying in the extreme cold of the Antarctica to the extreme heat of the Persian gulf, operational performance in failure scenarios or extreme conditions, etc. Then certification is done by the governing bodies such as the EASA and the FAA, which includes the detailed design review, test review in the lab and test review in flight.

Structural testing consists of many different tests, most importantly flight test Installation calibration test, maximum wing bending at limit load, ailerons and spoilers functioning test during maximum wing bending and a fuselage pressure test. However, most hours spend in static testing is on fatigue tests. Fatigue testing of specimen and of complete aircraft take a total duration of approximately 26 months [45]. The lifetime of the FB400 is 20 years and it is estimated that it will depart 3 times a day. During testing, 54,750 flight cycles will be simulated, 2.5 times the amount of cycles expected in its lifetime.

For the flight testing phase, 4 aircraft will be used, which is based on recommendations from Roskam [4]. Two of these will be 'heavy flight test aircraft' with instrumentation, and will be used for basic technical development and certification. These two together will test fly for 600hrs in 21 months. Additionally there will be 2 test aircraft with cabin and lighter test instrumentation, which will fly for about 900hrs in 20 months. To demonstrate the guaranteed performances in quasi-operational circumstances, the aircraft is subjected to a number of route proving tests [46] after flight testing is completed. Certification is obtained after 21 months from the first test flight. In total, the total flight testing and the commercial tour will take 2,500 flight hours over a time span of 32 months.

Looking at this process it is estimated for the FB400 to undergo 58 months of testing and certification. Even though it is a new design, it is still close to the time taken to certify the A380. Looking at new ways of testing such as climate laboratory and more capable computer simulations, the FB400 design may require shorter time than the estimated 58 months.

[3]Airbus Test Programme and Certification. Accessed January 2020. https://www.airbus.com/aircraft/how-is-an-aircraft-built/test-programme-and-certification

12

SUSTAINABILITY ANALYSIS

As far as this sustainability is concerned, an in-depth analysis will be conducted for each of the three main aspects as described in Chapter 5. The SAR methodology will be described in Section 12.1. Subsequently, a detailed analysis in the field of climate change will be conducted through Section 12.4. At last, a qualitative noise analysis will be carried out in Section 12.5.

12.1. SPECIFIC AIR RANGE

From the perspective of sustainability, there is a necessity to reduce fuel consumption as much as possible. In order to come up with the best possible fuel consumption estimation for the FB400 design, it is of importance to make use of the specific air range (SAR) methodology [47]. SAR denotes the total distance (for the entire mission or for a specific phase) that can be covered by a given aircraft per 1 kg of burned fuel. In the field of aviation, the SAR is usually expressed as 1/SAR in terms of fuel consumption per 100 km flown distance per passenger. As mentioned before, the main objective is to keep the fuel consumption (per passenger) as low as possible or the other way around to maximise the SAR. The formula that describes the SAR analytically is shown in Equation 12.1.

$$SAR = \frac{V_{cr}}{c_T \cdot T} \tag{12.1}$$

As the cruise phase is mostly dominant during flight in terms of fuel (especially in the case that 3,500nmi design mission range is considered) needed and total distance needed to be covered, steady level flight conditions should be applied. To be more specific, the drag generated by the aircraft during cruise is equal to the thrust produced by engines. At the same time, the lift should equal the weight of the aircraft during cruise. By making use of these facts and by substituting and rearranging the terms, Equation 12.1 can be rewritten in the following manner, as shown in Equation 12.2.

$$SAR = \frac{V_{cr}}{c_T \cdot 0.5 \cdot \rho V_{cr}^2 S \left(C_{D_0} + \left(\frac{W_{cr}}{0.5 \cdot \rho V_{cr}^2 S} \right)^2 \cdot \frac{1}{\pi A e} \right)} \tag{12.2}$$

Often, however, the fuel economy is represented as 1/SAR and is often also divided by the number of passengers. That will also be done in this analysis.

For this analysis a Python script was written which, first, allowed the cruise speed and altitude to vary. Later, specific design points were chosen, based on maximum attainable altitude and speed due to limits in surface area and the optimum design point in terms of SAR. For this analysis, the cruise weight has been taken as the average of the weight at the end and at the beginning of cruise. The figure below, Figure 12.1 shows a plot of the specific air range versus the Mach number. The different graphs correspond to different altitudes. From this graph, it can be seen that it is still more optimal to fly higher and faster in terms of specific air range. However, as mentioned in Section 12.6, the design point chosen is at an altitude of 11.5 km with a Mach number of 0.75 and this design point is also shown in the figure below. The fuel economy that corresponds to this design point is 1.05 kg of fuel per 100km per passenger.

However, as the reference mission is 700 nmi, an analysis for this range should also be performed and a different recommended altitude and Mach number can be chosen. The recommended altitude is again obtained by an iterative process between optimum aerodynamic performance and specific air range. This results in an altitude of 10.9 km and a Mach number of 0.75 with a specific air range of 1.06 kg fuel per 100 kilometres per passengers.

In order to find the sensitivity of this analysis towards certain parameters, a sensitivity analysis has been done. The impact of changing the lift-to-drag ratio, surface area and average cruise weight can be seen in Table 12.1 below.

Furthermore, it is quite easy noticeable from Figure 12.1 that after a certain point in terms of Mach number M_{dd}, the 1/SAR curve drastically increases.It is very important to reflect on the phenomenon that causes this. A refined examination has proved that wave drag arises at subsonic speeds in the case that the flow accelerates locally to supersonic speeds, and then eventually returns to subsonic speed through a shock wave [48]. This leads to the presence of wave

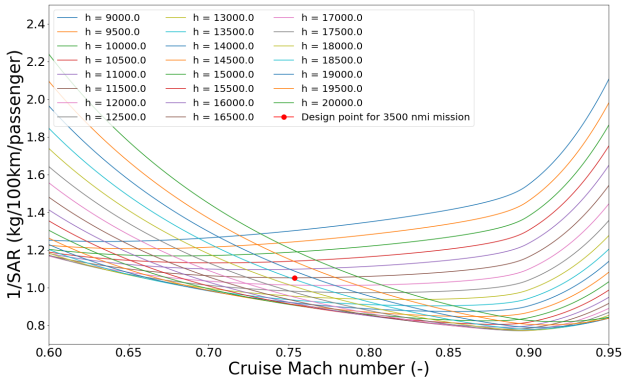

Figure 12.1: Specific Air Range for varying Mach numbers at varying altitudes, including the design point

drag at transonic freestream speeds. The total zero lift drag coefficient will increase rapidly as result of the wave drag, known as drag rise. [48] This analysis definitely needs to be taken into consideration in the design of wings and airfoils. From Equation 12.3, it becomes clear that the so-called ' drag divergence mach number (M_{dd})' depends on the sweep (leading edge) and thickness over chord ratio of the wing and a certain factor for the type of airfoil, which is chosen (supercritical or not). This factor is denoted by k_a.

$$M_{dd} = \frac{k_a}{cos\Lambda} - \frac{t/c}{(cos\Lambda)^2} - \frac{C_L}{(cos\Lambda)^3} \tag{12.3}$$

In addition, it is essential to indicate that given the complexity of the designed wing's geometry, it was not easy to calculate or deduce an effective drag-divergence mach number. Based on this, it was decided to split the wing into parts, with the principle that the same airfoil should be integrated into span width direction.

Table 12.1: Sensitivity analysis for SAR

Changing parameter	Difference in 1/SAR (%)
L/D	
10% lower	0.708 %
10% higher	0.567 %
S	
10% lower	6.886 %
10% higher	6.442 %
Average cruise weight	
10% lower	6.280 %
10% higher	6.510 %

From this table it can be concluded that the specific air range is most sensitive to surface area but the difference is still lower than 10%.

12.2. Verification and Validation

In this section the Python script and the design will be verified and validated in terms of specific air range.

For the verification of the script, unit tests were performed and comparisons were made with hand-calculations and excel sheets. Several mistakes were found this way and sequentially corrected. Examples of such mistakes are forgetting to convert degrees into radians, a typo in the standard atmosphere calculations and wrong importation of values from another document. For validation of the script, the same script was used to calculate the specific air range of an Airbus A320. The fuel economy of an A320 is 2.392 kg/100km/passenger. The result from the script was 2.333 kg/100km/passenger, which is a difference of 2.5%.

Comparing the SAR of the FB400 to the SAR of the A320 shows a large difference. This is due to the fact that they are designed for different missions. When using the FB400 for the same mission as the A320, which is 2,700 nmi with 150 passengers at an altitude of 37,000 ft and Mach number of 0.78, the SAR of the FB400 is equal to 2.67 kg fuel per 100 km

per passenger. The difference with the A320 is then 10.3% and the specific air range is now worse than for the A320. This difference can be attributed to the fact that the aircraft is designed for more passengers and a longer range and therefore has a larger operating empty weight and to the assumptions made in the process of calculating the specific air range.

12.2.1. CONTOUR PLOT

The ultimate goal of this analysis is to display the optimum fuel consumption in a comprehensive 'Altitude vs Velocity ' plot. This point will be reached in the event that the aircraft, based on its design characteristics and geometry, flies with a certain speed at a correlating altitude. The contour plots are depicting all the obtained SAR values from the in detail conducted analysis as explained in Section 12.1. It must be remarked that each contour represents a 5% negative change in the SAR plot (altitude versus speed correlation) with respect to the optimum fuel consumption. As can be seen from Figure 12.2, the design point deviates 37% from the optimum. The reason for not flying at the optimum is mentioned in Section 12.6.

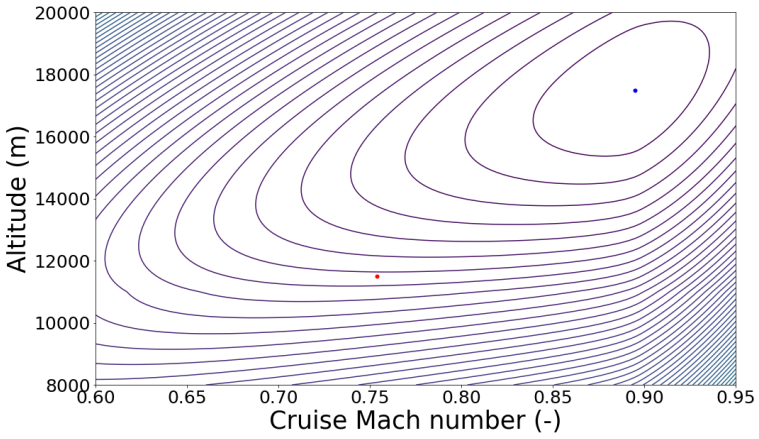

Figure 12.2: SAR contour plot for the FB400

12.3. THE COMBUSTION PROCESS

As can be seen in Figure 12.3, the production of emissions takes place by burning kerosine. As far as aviation is concerned where the most used sort of fuel is Jet A -1. Jet A-1 is a fuel type, which is composed of a complex mixture of hydrocarbons [49]. Due to the complexity of the aforementioned mixture, it is not possible to dissect the composition of jet fuel. for the full 100%. However, we know from literature study that the most common chemical notation of kerosene is $C_{12}H_{24}$ [50]. In the most ideal situation, a complete combustion of kerosene will take place. After the fuel gets mixed with air (consists of nitrogen and oxygen as active substances) in the combustion chamber, the combustion process will take place that will result in the forming of CO_2, H_2O, N_2 and O_2 Figure 12.3.

In reality, as a result of incomplete combustion and contamination (and also inpurities) of kerosene, the engine will form the so-called "by-products" [50]:

- CO
- UHC (unburned HydroCarbon)
- BC
- Soot
- NO_x
- SO_x

A specific flight stage has a direct influence on the rate of the various emissions, because of the air-to-fuel ratio, temperature and pressure differences at those stages [50]. In case of low temperatures and an incomplete combustion, UHC and CO emissions are high at high temperatures.The emissions of soot and NO_x become high in case of enlarged fuel mixtures. In accordance to [50], emissions that directly result from kerosene combustion depend on the following flight phases and the corresponding thrust setting of the enginesFigure 12.4:

- CO_2 in proportion to the amount of kerosene
- H_2O in proportion to the amount of kerosene
- SO_x in proportion to the amount of S in kerosene
- CO high with low thrust settings: taxi and idle
- UHC high with low thrust settings: taxi and idle

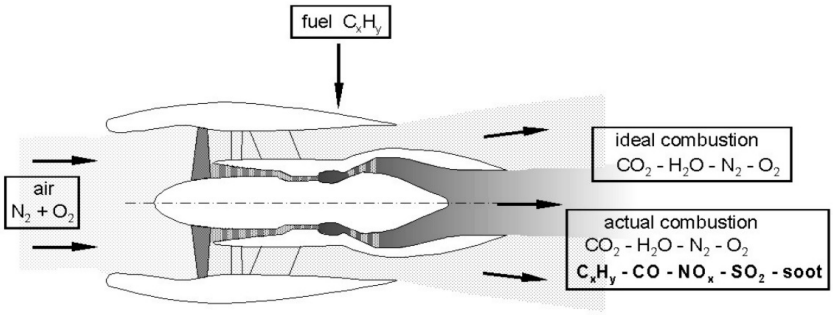

Figure 12.3: The combustion process in a turbofan engine[50]

- NO_x high at high thrust settings: take off and climb
- Soot high with high thrust settings: take off and climb

.

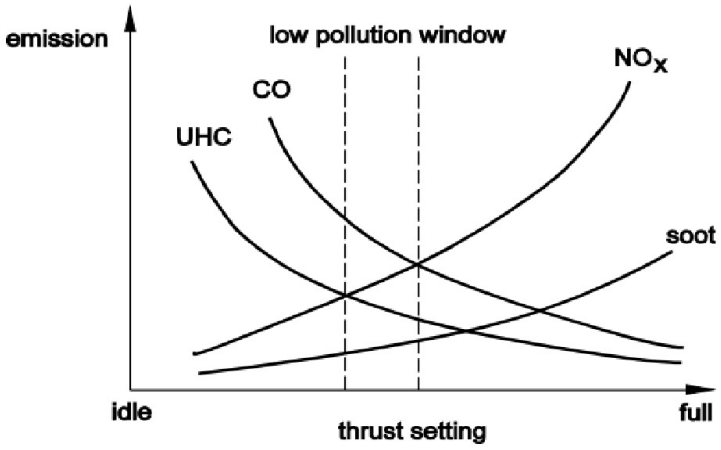

Figure 12.4: Emission level versus thrust setting[50]

As can be seen and concluded from Table 12.2, the quantities of CO_2,NO_x and H_2O (that are formed as a result of the combustion of 1 kg of kerosene) are many times larger compared to the other substances. From this point of view and Figure 12.4, only the emissions of CO_2,NO_x and H_2O are included in follow-up analyses.

Table 12.2: Various relevant substances with their corresponding emission index

Substances	Emission Values [g/kg combusted fuel]
CO_2	3,155
H_2O	1,240
NO_x	4.32-23.11
SO_x	0.6-1.17
CO	0.7-4.87
BC	0.025-0.032
Soot	0.01-0.2
UHC	0.1-0.6

12.4. Global Warming Impact

The Global Warming Potential(GWP) is a number that represents the relative contribution of gas toward global warming. It is now generally known that the contribution of aircraft to global warming is more than could have been initially expected from their carbon dioxide(CO_2) emissions alone. The foregoing has been scientifically proven [51], however, there is a lack of appropriate GWP factors for relevant emissions. As a direct consequence of this, the calculation of the CO_2 footprint (CF) or life cycle assessment (LCA) can not be carried out comprehensively. To approach this problem from a different angle, the relevant effects of aircraft emissions is discussed and elaborated in detail[52][1]. The foregoing approach is based on calculating the global warming potential that is directly related to aircraft services, by multiplying a specific radiative-forcing-index (RFI) factor with the direct CO_2 emissions of a specific aircraft. The RFI (equal to the total aviation RF divided by the aviation CO_2 RF) can range from 1 up to 2.7 [51]. In cases that emissions are exclusively considered in the higher atmosphere, then RFI factors ranging from 1 to 8.5 are recommended to use. It is highly recommended to consider an RFI factor that is equal to 2 on total aircraft CO_2 emissions, as this value is based on detailed analysed interpretations of recent scientific publications [53].

It is a fact that aviation emissions contribute to the RF of climate. In this regard, the important emissions to consider are CO_2, nitrogen oxides (NO_x), H_2O aerosols and their "forerunners" (soot and sulphate), magnified cloudiness in the shape of continued linear contrails and induced-cirrus cloudiness. It is worth mentioning that the aforementioned GWP is in most cases expressed in the unit of a kilogram of carbon dioxide equivalents per functional unit (kg CO_2-eq). GWP factors are directly taken from the Intergovernmental Panel on Climate Change (IPCC). These so-called characterisation factors enable the assessment of the relative impact of the foregoing greenhouse gases in regard to the climate change problem. By the implementation of these characterisation factors, the calculation of the GWP for each relevant (greenhouse) gas with a 100-year time horizon can be made in terms of equivalent emissions of CO_2 as mentioned before. From this given fact, it can be deduced that the value of the CO_2 GWP factor is equal to 1. However, the application of GWP is not that easy as it contains sorts of flaws that make its use difficult regarding aircraft emissions. To set an example, impacts such as contrails could be not directly related to emissions of specific greenhouse gas. In addition, indirect RF from ozone produced by NO_x emissions can not be automatically derived from a given amount of NO_x; there is no linear relationship, due to the fact that conditions as season and location (due to the nonlinear chemistry) are of influential as well [51]. Profound analysing of relevant literature studies [51] has shown that is of more pragmatic use to have a close look at the most recent historical display of RF [W/m^2] in order to compute changes in the atmosphere as a direct result of greenhouse emissions and aerosols. This historical display of RF is depicted in figure Figure 12.5 below.

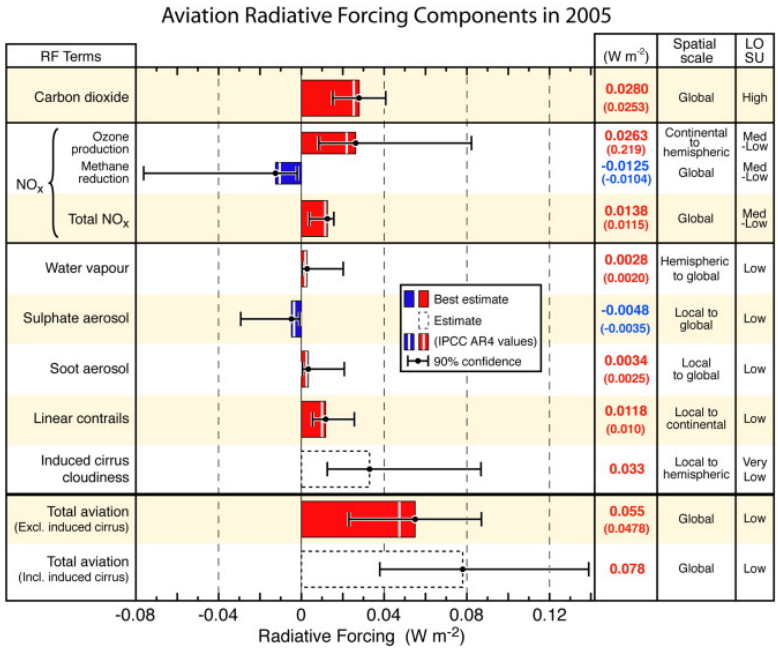

Figure 12.5: Radiative forcing components from global aviation as evaluated from preindustrial times until 2005[51]

The RF components, directly caused by aviation and as can be analysed from Figure 12.5, are as follows:

- Emission of CO_2,(positive RF).

[1]Aviation and Climate Change: A Scientific Perspective. Accessed December 2019. http://e-space.mmu.ac.uk/618290/1/Fahey$%$20and$%$20Lee$%$20CCLR$%$202016.pdf

- Emission of NO_x (positive RF). This term is the sum of three component terms: production of troposphere O_3 (positive RF);a longer-term reduction in ambient methane (CH_4) (negative RF), and a further longer-term small decrease in O_3(negative RF).
- Emissions of H_2O (positive RF).
- Formation of persistent linear contrails (positive RF).
- Aviation-induced cloudiness (AIC; potentially a positive RF).
- Emission of sulphate particles (negative RF).
- Emission of soot particles (positive RF).

12.4.1. Impact of Contrails and Nitrogen Oxides on Climate

The potential of anthropogenic activities directly caused by the use of an aircraft can not be accurately calculated or estimated. But it is essential to look at relevant conditions with major impact on global warming that can be influenced to reduce the impact on global warming by an aircraft. As can be concluded from [53], the biggest fraction of aviation's emissions is injected in the atmosphere at cruise altitudes ranging from 8 to 12 km. In studies performed by [53], the impact of change in cruise altitudes on the coverage of contrail and the corresponding RF is explored. It is found that reduction of cruise altitude by 2,000 feet at a time, the global contrail coverage (on annual basis) can be linearly decreased with respect to the cruise altitude. A maximum decrease of approximately 45% is realised based on a cruise altitude that is 6,000 ft lower compared to standard flight cruise altitudes. On the other hand [53], it is concluded that the global contrail coverage (on annual basis) by flying at higher altitudes (2,000 ft), compared to the standard flight cruise altitude, results in a relative increase of about 6%. The effects that changes in cruise altitude have on total concentration and distribution of other relevant aircraft emissions, such as NO_x (and its impact on O_3 and CH_4) and CO_2 are explored within a certain trade-off project [54]. Paramount to know is that cruising at a relatively higher altitude of 2,000 feet increases [55] the total RF due to aircraft NO_x emissions by 2 ± 1 mW/m^2, while cruising at a relatively lower altitude of 2,000 feet reduces RF by 2 ± 1 mW/m^2. As one can immediately notice, it is very difficult to come up with optimum fuel consumption and at the same time the most ideal cruising altitude. Nowadays, global mean radiative forcing of short-lived species (such as O_3) and CH_4 is reduced in case the cruise altitude decreases, whereas that of CO_2 increases as explained before (due to the fact that the fuel consumption rate increases in case the altitude decreases). In short, the RF value drops in the case that the cruising height is relatively lower and vice versa.

12.4.2. GWP Relative to Carbon Dioxide

As described in detail Section 12.4, there is a lack of accurate GWP factors for aviation-related emissions. However, it is still highly recommended to quantify the impact of all greenhouse gases (as a result of the combustion process of fuel burning) on the climate change. In this regard, it is legitimate to make use of GWP factors from IPCC, considering a 100 year time horizon, in order to express GWP in terms of equivalent emissions of carbon dioxide CO_2 [56]. From this point of view, the quantities of all greenhouse gases (GHG) that will be emitted in the atmosphere, as a direct result of the amount of fuel that will be burned by the FB400 considering its design characteristics , must be multiplied by their assigned GWP factor to obtain the equivalent of carbon dioxide [56]. The aforementioned quantities can be deduced from the chemical reaction that takes place when 1 kg of kerosene is burned Section 12.3. For a clear overview, all the relevant GHG's and their corresponding GWP factors are shown in Table 12.3.

Table 12.3: The equivalent weight in CO_2-eq per 1 kg emission at each altitude

h[m]	GWP factor [kg eq-CO_2/kg emission]	CO_2	H_2O	NO_x
8,000	-	1	0.2	77
9,000	-	1	0.2	77
10,000	-	1	0.2	77
11,000	-	1	0.2	77
12,000	-	1	0.2	77
13,000	-	1	0.2	77
14,000	-	1	0.2	77

In Table 12.4, the emission weight of each different gas is expressed per kg CO_2.

As can be drawn from Table 12.5, the impact of the FB400 on climate change is analysed at each specific alitude by converting the weight of the specific emissions in eq-CO_2 kg per netto CO_2 kg.As can be immediately noticed, it seems that the impact on climate change is the lowest (and thus the best) at higher altitude. This decision is very wrong as it is widely known that the lower an aircraft flies, the more beneficial it is from a global warming perspective. The method of GWP is not appropriate as this methodology is based on a global warming average of the greenhouse gases

Table 12.4: Emissions relative to CO_2 at each altitude

h(m)	Emissions relative to CO_2 [kg emission/kg CO_2]	CO_2	H_2O	NO_x
8,000	-	1	0.393	0.00605
9,000	-	1	0.393	0.00589
10,000	-	1	0.393	0.00572
11,000	-	1	0.393	0.00556
12,000	-	1	0.393	0.00513
13,000	-	1	0.393	0.00474
14,000	-	1	0.393	0.00437

over a timespan of 100 years and not the netto effect that the emissions of each greenhosue gas respectively have at a specific altitude.

Table 12.5: Emissions weight expressed in eq-CO_2 relative to CO_2 at each altitude

h(m)	CO_2 weight in [eq-CO_2 kg/kg CO_2]	H_2O weight in [CO_2 kg/kg CO_2]	NO_x weight in [eq-CO_2 kg/kg CO_2]	Total weight fraction in [eq-CO_2 kg/kg CO_2]
8,000	1	0.0786	0.4658	1.5444
9,000	1	0.0786	0.4537	1.5322
10,000	1	0.0786	0.4408	1.5194
11,000	1	0.0786	0.4280	1.5066
12,000	1	0.0786	0.3953	1.4739
13,000	1	0.0786	0.3648	1.4434
14,000	1	0.0786	0.3366	1.4153

12.4.3. EINO$_x$

As can be concluded from taking a proper look at Figure 12.5, it becomes quite straightforward that the impact of NO_x on the total radiative forcing due to aviation is significantly large.The emission of NO_x is per definition not the direct result of the chemical reaction that takes place as kerosene gets burned. Actually, NO_x is a by-product of complete combustion and a product of fuel purities. From thorough studies, it is known that the higher the altitude the lower the NO_x emissions become [57]. Digging a bit deeper in literature studies, it is found out that the emission index of oxides of nitrogen (EINO$_x$) depends on the engine characteristics [58]. To be more specific, the thrust settings of the engine, the pressure and temperature at the inlet and outlet of the combustor. Of course, the atmospheric layers that become thinner as the altitude increases, play a pivotal role. In [2], there are certain methodologies described in order to compute the EINO$_x$ at certain altitudes taking the design characteristics of the chosen engines into account. Engine emission information can be retrieved from the ICAO emission databank [3]. For this particular analysis, it is chosen to look at the performance of the engines for a 3,500 nm flight mission. In this regard, the cruise stage is by far the most demanding throughout the entire flight. As an aircraft usually flies during cruise with a thrust setting that is approximately 80% of its maximum thrust, it is chosen to take the reference (at sea level) EINO$_x$ equal to the EINO$_x$ corresponding to the climb-out phase. The formula, which is used to calculate the emissions of NO_x at different altitudes is given by Equation 12.4.

$$EINO_x = REINO_x \cdot e^{h} \cdot \left(\frac{\delta_{amb}^{1.02}}{\theta_{amb}^{3.3}}\right)^{1/2}; \theta_{amb} = \frac{T_{amb}}{288.15}; \delta_{amb} = \frac{P_{amb}}{1.01325} \tag{12.4}$$

In order to compute the humidity level ắt a given altitude,Equation 12.5 should be considered: Equation 12.4.

$$H = -19.0 \cdot (\omega - 0.006341) \tag{12.5}$$

In order to take a deep look at how the different parameters that Equation 12.4 is composed of should be calculated, Equation 12.6 can be assessed:

$$P_v = 0.0689475728 \cdot 0.014504 \cdot 10^{\beta} \tag{12.6}$$

[2] Scheduled Civil Aircraft Emission Inventories for 1992. Accessed on april 1996. https://ntrs.nasa.gov/search.jsp?R=19960038445

[3] ICAO Aircraft Engine Emissions Databank. Accessed on september 2019. https://www.easa.europa.eu/easa-and-you/environment/icao-aircraft-engine-emissions-databank

In order to compute the specific humidity level at a given altitude,Equation 12.7 should be considered:

$$\omega = \frac{0.62198 \cdot (\phi) P_{\mathrm{v}}}{P_{\mathrm{amb}} - (\phi) P_{\mathrm{v}}} \tag{12.7}$$

In order to take a deep look at how the different parameters that Equation 12.7 is composed of should be calculated, Equation 12.8 can be assessed:

$$P_{\upsilon} = 0.0689475728 \cdot 0.014504 \cdot 10^{\beta} \tag{12.8}$$

$$\beta = 7.90298(1 - \frac{373.16}{T_{\mathrm{amb}}}) + 3.00571 + (5.02808)\log(1 + \frac{373.16}{T_{\mathrm{amb}}}) + (1.3816 \cdot 10^{-7})[1 - 10^{11.344 \cdot (1 - \frac{T_{\mathrm{amb}}}{373.16})}] + (8.1328 \cdot 10^{-3})[10^{3.49149 \cdot (1 - \frac{373.16}{T_{\mathrm{amb}}})} - 1] \tag{12.9}$$

The computed values, by making use of the method described above, for the EINO_x are depicted in Table 12.6.

Table 12.6: $EINO_{\mathrm{x}}$ at different altitudes

h(m)	$EINO_{\mathrm{x}}$ g/kgmethod 1	$EINO_{\mathrm{x}}$ g/kgmethod 2	discrepancy %
8,000	19.09	19.20	0.59
9,000	18.59	18.71	0.65
10,000	18.06	18.21	0.83
11,000	17.54	17.70	0.90
12,000	16.20	17.69	9.18
13,000	14.95	17.68	18.29
14,000	13.79	17.68	28.16

12.4.4. VERIFICATION OF THE METHOD

In order to verify the method (been referred to in Table 12.6 as method 2) that has been worked out in Subsection 12.4.3, the NO_x emissions (corresponding to the different analysed altitudes) have been re-calculated and displayed in Table 12.6. The final results in terms of the deviation between the applied methods are as well displayed in Table 12.6. On average, the deviation is 8.37%. The alternative proposed method (or method 2 to be consistent) [4] is described in Equation 12.10

$$\mathrm{EINO}_x = \mathrm{REINO}_x \cdot \theta_{\mathrm{amb}} \cdot \exp^{h} \tag{12.10}$$

12.4.5. RADIATIVE FORCING

The metric radiative forcing is the most appropriate metric for global warming impact at a certain altitude based on a given flight mission. In order to come up with the best possible assessment, parameters such as wind, altitude and longitude should be taken into consideration. One of the well-known and best assessment tools is AirClim. However, it is not easy to implement this given software tool in the case no proper training program is followed. From this perspective, thorough literature studies have been done in order to find proper, reliable and representative radiative forcing values. As far as water vapour and CO_2 are concerned, these are two direct chemical reaction substances that get produced as a result of fuel combustion[59]. The effect of CO_2 on global climate in terms of radiative forcing is at each altitude exactly the same. However, this principle is not valid with respect to water vapour. The principle is to calculate the required amount of fuel based on the fuel consumption-analysis that has been conducted through Section 12.1 Figure 12.6. By interpolating and making simple straightforward calculations, the radiative forcing for each relevant substance can be computed at any given altitude [59]. By quantifying the contribution of each separate gas in terms of radiative forcing and summing up, the total radiative forcing at a given altitude can be estimated for the designed FB400.

Based on the extensive analysis data in Subsection 12.4.3 and the required fuel weight to complete a mission Section 12.1, the amount of NO_x emitted can be calculated. By making simple calculations, the radiative forcing can be calculated separately for all NO_x - correlating substances Figure 12.7.

[4] Scheduled Civil Aircraft Emission Inventories for 1992. Accessed on april 1996. https://ntrs.nasa.gov/search.jsp?R=19960038445

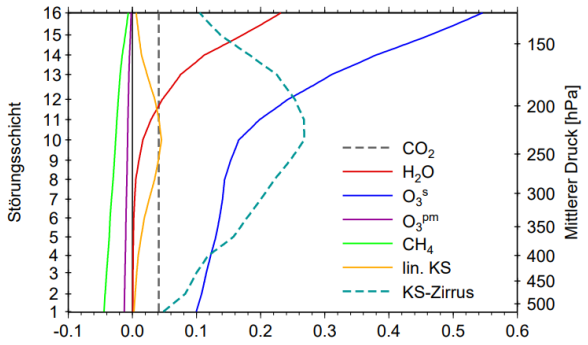

Figure 12.6: Radiative forcing in [mW/m^2 Tg burned fuel] to compute for water vapour and CO_2

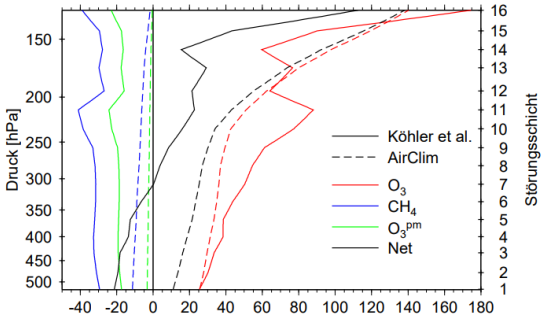

Figure 12.7: Radiative forcing in [mW/m^2 per Tg emitted NO_x] to compute for ozone and methane in terms of NO_x emissions

In Figure 12.8, the various perturbation layers with their corresponding altitude and ambient pressure are displayed. These perturbatation layers are of undisputed importance in order to perform the interpolation correctly in Figure 12.7 and Figure 12.6.

PL	Höhe[km]	Druck [hPa]
16	14.2-14.8	125-137
15	13.6-14.2	137-151
14	13.0-13.6	151-165
13	12.4-13.0	165-182
12	11.7-12.4	182-203
11	11.1-11.7	203-223
10	10.5-11.1	223-245
9	9.9-10.5	245-269
8	9.3-9.9	269-295
7	8.7-9.3	295-321
6	8.1-8.7	321-351
5	7.5-8.1	351-383
4	6.9-7.5	383-417
3	6.3-6.9	417-453
2	5.6-6.3	453-498
1	5.0-5.6	498-540

Figure 12.8: Perturbation layers related to their corresponding ambient pressure at different altitudes

In Figure 12.9, the plot of the total radiative force at a certain altitude can be observed, which is obtained from Table 12.7. In the plot, there are two coordinate-points depicted, which correspond to the 700 and the 3,500 nm missions. Compared to the lowest (and thus the best) total radiative forcing impact at 8,000 m altitude, the impact of a 700 nm flight mission of the FB400 will be 289.3% worse. In the case that a 3,500 nm flight mission is carried out, the impact of the greenhouse emissions will be 319.6% worse compared to a flight mission at an altitude of 8,000 m.

Table 12.7: Radiative forcing in [mW/m^2] at varying altitudes

h [m]	Fuel consumption [kg]	RF NO_x [mW/m^2]	RF H_2O [mW/m^2]	RF CO_2 [mW/m^2]	Total RF [mW/m^2]
8,000	$3.71 \cdot 10^4$	$-6.66 \cdot 10^{-6}$	$9.28 \cdot 10^{-8}$	$1.58 \cdot 10^{-6}$	$-4.92 \cdot 10^{-6}$
9,000	$3.41 \cdot 10^4$	0	$1.70 \cdot 10^{-7}$	$1.45 \cdot 10^{-6}$	$1.62 \cdot 10^{-6}$
10,000	$3.16 \cdot 10^4$	$4.28 \cdot 10^{-6}$	$3.16 \cdot 10^{-7}$	$1.34 \cdot 10^{-6}$	$5.94 \cdot 10^{-6}$
11,000	$2.98 \cdot 10^4$	$7.83 \cdot 10^{-6}$	$5.95 \cdot 10^{-7}$	$1.26 \cdot 10^{-6}$	$9.69 \cdot 10^{-6}$
12,000	$2.81 \cdot 10^4$	$9.56 \cdot 10^{-6}$	$1.15 \cdot 10^{-6}$	$1.19 \cdot 10^{-6}$	$1.19 \cdot 10^{-5}$
13,000	$2.72 \cdot 10^4$	$1.10 \cdot 10^{-5}$	$1.96 \cdot 10^{-6}$	$1.16 \cdot 10^{-6}$	$1.41 \cdot 10^{-5}$
14,000	$2.69 \cdot 10^4$	$1.41 \cdot 10^{-5}$	$4.44 \cdot 10^{-6}$	$1.14 \cdot 10^{-6}$	$1.97 \cdot 10^{-5}$

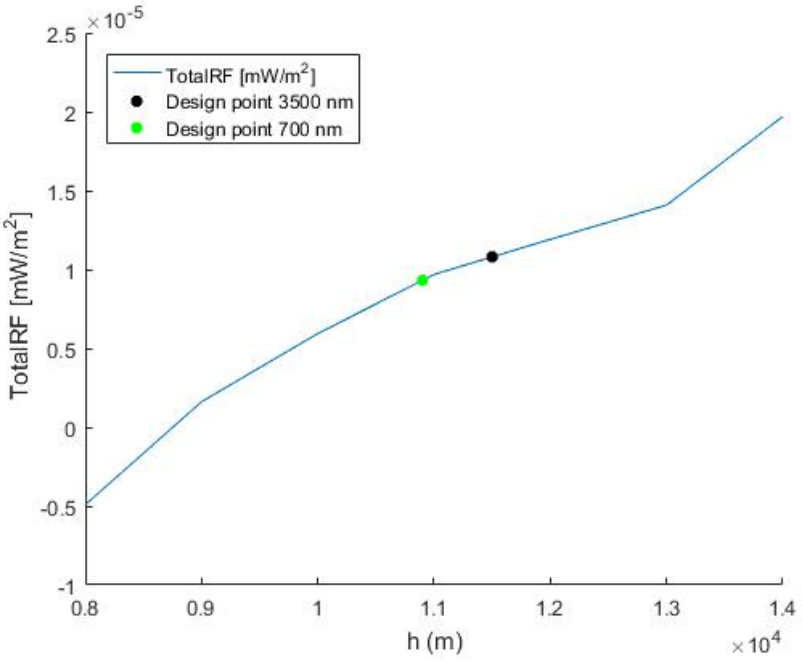

Figure 12.9: The Total RF in [mW/m^2] at various altitudes

12.4.6. Comparison between FB400 and the B777-300ER

In order to assess the performance of the FB400 regarding its own design- and flight mission characteristics, a comparison with the B777-300ER has been made. The purpose of this assessment is to determine how the FB400 performs in terms of NO_x and CO_2 compared to a reference aircraft that can be regarded as state of the art. The data required to make this comparison were obtained from [60] and are based on the CX289 Hong Kong - Frankfurt flight (9,166 km). This straightforward analysis has shown that the CO_2 per passenger and per 100 km of the FB400 is almost 70% better than the B777-300ER. In terms of NO_x per passenger and per 100 km, the FB400 performs approximately 83% better than the B777-300ER Table 12.8.

Table 12.8: Comparison between the FB400 and the B777-300ER

	Total burned fuel [kg]	Fuel per Pax and per 100 km	CO_2 per Pax and per 100 km	NO_x per Pax and per 100 km	Total covered distance [km]	Amount of seats
FB400	28843	1.1124	3.51	0.0186	6482	400
B777-300ER	113750	3.65	11.52	0.110	9,166	340

12.5. Noise Analysis

According to requirement HCSR-NF-SUS-002, the external noise level of the aircraft shall comply with the ICAO chapter 4 standards. Since at this early stage of the design it is very hard to assess noise into details, the noise analysis is performed in a qualitative manner, by comparing the geometry of the Boeing 787 and the FB400, since the Boeing 787 has the same engines and the engines are one of the components that contributes the most to the noise emissions of

an aircraft.

The requirement for noise of new aircraft states that the noise level of the aircraft shall be stage 3 or higher. The Boeing 787-8 has a stage 4 noise level, which means it complies to the noise requirement for new aircraft. However, its geometry is different from the geometry of the FB400, which would change the noise levels. Table 12.9 compares the geometry causing noise emissions and gives an evaluation if the noise level of FB400 is lower, higher or the same as the noise level of Boeing 787.

Table 12.9: Comparative noise analysis

Parameter	Boeing 787	BWB	Noise Level
Engines	Placed under the wings, GEnx-1B70 with chevrons on the fan gondel	Placed on top of fuselage between vertical tails, GEnx-1B70 with chevrons on the fan gondel and gas generator gondel	Lower
Flaps	Inboard and outboard flap increasing drag	No flaps	Lower
Slats	Along the entire wing span (54.2 m)	Along the entire wing span (40.9 m)	Lower
Landing gears	2 nose wheels, 8 main wheels retracting sideways	2 nose wheels, 8 main wheels retracting to the front and then upwards	Higher
Horizontal tail	270.4 m^2 horizontal tail	No horizontal tail	Lower
Vertical tail	1 vertical tail with area 97.6 m^2	2 vertical tails with total area 33.8 m^2	Lower
Winglets	Small winglets reducing drag	Winglets with total area 7.9 m^2	Higher
Approach speed	145 kts	145 kts	Same

Components such as high lift devices, engines and landing gears are taken into account due to most interference with free stream flow, which causes more drag and thus more external noise. As can be seen in Table 12.9, most of the components of the geometry of the FB 400 are better in terms of noise. For example the engines placed on top of the fuselage are beneficial for noise because the fuselage acts as a shield from the engine noise and reflects the noise upwards. This affects positively the take-off noise levels. Furthermore, the engines are placed between the two vertical tails which further shields the noise and reflects it upwards. The aircraft does not have flaps, therefore no noise is produced due to flap extension in take off and landing. However, slats are going to increase the noise produced by the aircraft. Compared to the slats of a Boeing 787-8, the FB 400 has a smaller wing span, thus less slat area, which results in lower noise. The vertical tails are two in this aircraft but they are a lot smaller than the vertical tail of the Boeing 787-8 and they also shield the noise from the engines. The winglets of the FB400 are larger and at a larger angle and although they reduce the total drag of the wing, their area is larger compared to the small winglets of Boeing 787-8. The approach speed for both aircraft is the same, thus no difference in the noise level due to approach speed is present.

From the comparison it can be concluded that the airframe and engines produce less noise than the Boeing 787-8, which means that the FB 400 has a noise stage 4 or higher and complies with the requirement set by ICAO. However, note that this is a very initial estimate of the noise characteristics and until the first flying model is produced and analysed, noise analysis cannot be calculated because statistical relations for noise of Blended Wing Bodies are not common in literature.

12.6. Design Altitude and Mach number

In order to design an aircraft, it should be known for what altitude and Mach number the aircraft shall be designed. As it is an objective to lower the direct operating cost, it is required to fly at an altitude and Mach number with the lowest fuel economy. This fuel economy is calculated by using the method of the Specific Air Range, as described in Section 12.1. The SAR is optimum at an altitude of 17.5 km and a Mach number 0.90. However, at higher altitudes, radiative forcing gets a lot worse. Furthermore, when decompression occurs at such high altitudes, it takes longer to reach a safe altitude for passengers to breathe. On top of this, the performance parameter is optimum at an altitude of 12 km, as mentioned in Section 9.4. After several iterations were performed, it was chosen to fly at an altitude of 11.5 km. The accompanying optimum airspeed, according to the optimum SAR at that altitude, is Mach 0.75. As airspeed does not influence the radiative forcing, it is chosen to stick to this optimum Mach number. At this altitude and Mach number, the SAR is 37% higher than the optimum and radiative forcing is 320% worse than it would be if it was flying at an altitude of 8 km. For the 700 nmi mission it is chosen to cruise at a little lower altitude as it takes a relative large part of the flight time to climb to higher altitudes. The chosen cruise altitude is 10.9 km with an optimum Mach number of 0.75.

13

AIRCRAFT SYSTEM CHARACTERISTICS

In this chapter, the characteristics of the FB400's most important systems are described. Furthermore, the systems interfaces are presented, supported by block diagrams of the different systems, including hardware and software interfaces.

13.1. FLIGHT CONTROL SYSTEM

The aircraft shall be controllable around all axes, which is regulated by the primary control of the aircraft. For pitch control, this aircraft has elevators mounted to the trailing edge of the fuselage section and to the trailing edge of the wings, as already mentioned in Subsection 8.7.2. The most outboard part of the elevators on the wings is elevons. These are ailerons and elevators combined in one to also control roll, as discussed in Subsection 8.7.1. The yaw control is performed by rudders, located on the vertical tails, as sized in Subsection 8.7.3.

Secondary control systems improve performance characteristics. In order to increase take-off, landing and stall speed performance, the aircraft slats are designed on the leading edge of the wings. Slats increase the surface area of the wing and therefore increase the lift-curve slope. They also lower the leading edge of the wing, thus increasing the curvature, which gives a combined maximum lift coefficient of 1.05, as seen in Section 8.8. They are located at 15% of the chord of the wing section and run along the entire span of that same section.

The lay-out of the control surfaces can be seen in Figure 13.1.

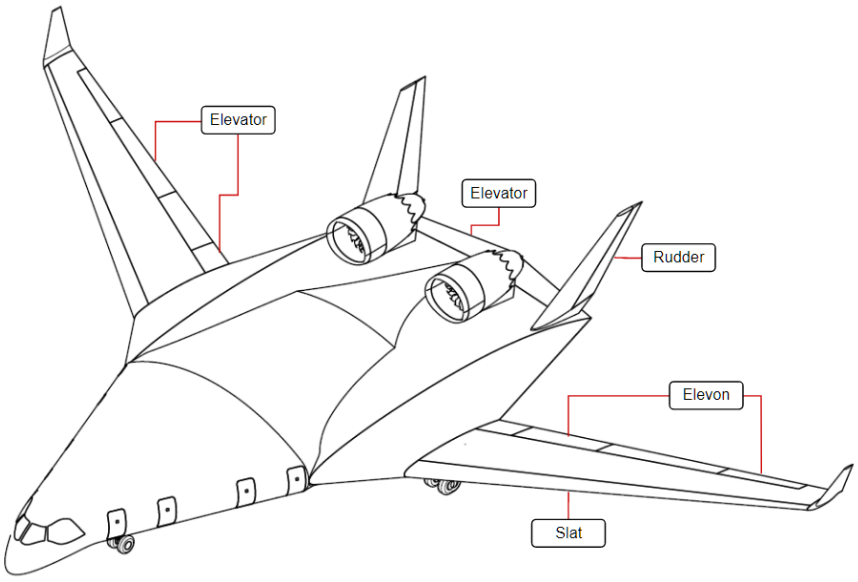

Figure 13.1: Control surface lay-out

Furthermore, as mentioned in the previous report, [2], the control system is a fly-by-light control system. Input command signals are sent to the actuators as electric signals and are converted into optical signals. Then, they are sent through a medium of optical-fibre lines and received by optical sensors. The feedback from the control surfaces and other systems is routed similarly. The flight computer then provides data for the movement of the aircraft control surfaces through these cables.

The actuation of the control surfaces is done by hydraulically pressurised actuators. The primary control surfaces also have counterbalancing hydraulic actuators which ensures that the control surface goes back to its trimmed position after a disturbance torque.

Finally, the aircraft is equipped with an autopilot system. The interaction between the pilots or autopilot and the control system and control surfaces is shown in Subsection 13.11.4 in Subsection 13.11.4.

13.2. Fuel System

The fuel system of the aircraft consists of the following parts: a fuel pump, fuel control, fuel nozzles, a fuel filter, heat exchangers, drains, fuel valves and fuel tanks [61]. To deliver the fuel, the fuel pump has two stages, a low pressure and a high-pressure stage. During the low-pressure stage, the fuel pressure is increased, after which it passes through the fuel filters. Then it continues to the high-pressure stage. Here the fuel is pressurised until above the combustion pressure. The fuel control measures the amount of fuel required by the engine and regulates that only that amount is let through to the fuel nozzle. The fuel flow to the fuel nozzle is measured by a fuel flow meter and is controlled electronically. Fuel nozzles are located in the combustion section of the engine. Additionally, fuel filters clean debris out of the fuel. In the heat exchangers, fuel is being heated and oil is being cooled. The drain should be able to remove all fuel from the aircraft. It has to be easily accessible and have a closed locking position [62]. Fuel valves allow for closing off the fuel supply to one of the engines. The fuel is held by two fuel tanks, located in section two on each side of the wing. They each have a volume of 33.0 m^3. A schematic lay-out of the fuel system of the FB400 can be seen in Figure 13.2.

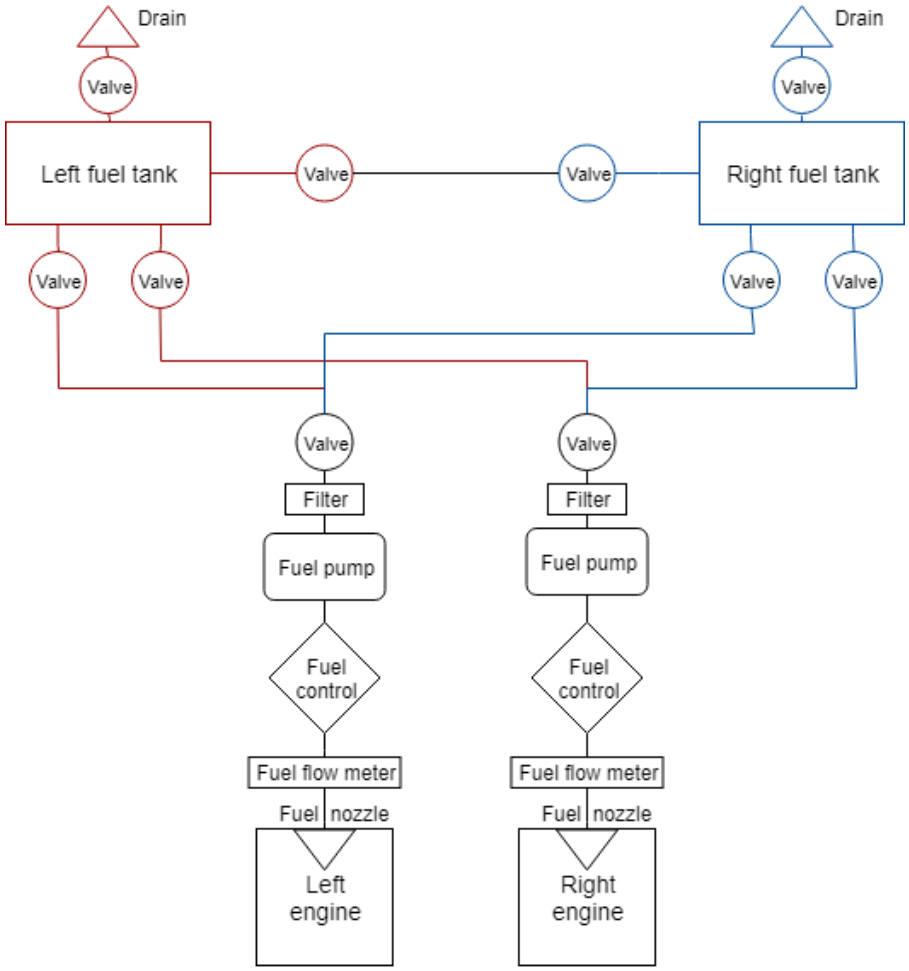

Figure 13.2: Fuel system lay-out

13.3. Power Plant

As discussed in the previous report, [2], the aircraft shall be a more electric aircraft. This means that most of the power generated by the aircraft engines is electrical power. As the aircraft has an entry into service by 2029, thus it is not possible within that time frame to design a new engine. Therefore, an existing engine has been chosen. At the moment, the GEnx is the most electric engine. This engine is being used by the Boeing 787 and 747-8. There are several different models. By comparing the existing models with the thrust required, as also done in Section 8.4, the

GEnx-1B70 is chosen. Below, a table is shown in Table 13.1 with some specifications of this engine[1].

Table 13.1: GEnx specifications

Take-off thrust [kN]	156.9
Bypass ratio at take-off [-]	9.3
Bypass ratio at top-of-climb [-]	8.8
Overall pressure ratio at take-off [-]	43.8
Overall pressure ratio at top-of-climb [-]	53.3
Air mass flow [kg/s]	1160.7
Fan diameter [m]	2.822
Base engine length [m]	4.691
Number of fan compressor stages	1
Number of booster compressor stages	4
Number of high pressure compressor stages	10
Number of high pressure turbine stages	2
Number of low pressure turbine stages	7
Combustor type	SAC/TAPS
Type of control	FADEC III
Type of bearings	2B+4R

This engine contains 18 carbon-fibre composite fan blades and a carbon-fibre composite fan case. The 6^{th} and 7^{th} low-pressure turbine stages have titanium aluminide blades. The engine nacelles also have chevrons in to further reduce engine drag and noise. All this ensures a lighter, quieter, more durable and more efficient engine. Moreover, the removal of the engines pneumatic bleed system reduces the number of parts and thus greatly simplifies assembly and maintenance. To compare, a figure showing both the no-bleed engine and the traditional bleed engine is displayed in Figure 13.3.

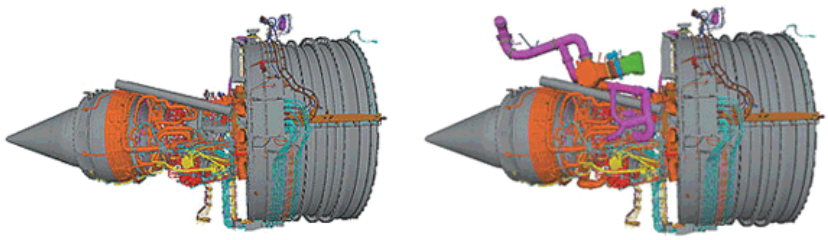

Figure 13.3: No-bleed engine (left) and bleed engine (right) [63]

Furthermore, the engines are provided with thrust reversers which are hydraulically actuated and the thrust is controllable by the autopilot system.

The engines are located on the back of the fuselage with enough clearance between each other and other significant parts, in case a turbine disc bursts. To account for fan discs bursting, the lining of the engine is covered with Kevlar. Due to the fact that the engines are located on top of the fuselage, maintenance involving removal of an engine requires a crane.

13.4. Auxiliary Power Unit

The all electric auxiliary power unit that corresponds to the GEnx engine is the APS5000 APU by Pratt & Whitney. It is a single shaft, variable speed gas turbine and can deliver 450 kVA at sea level. A battery or GPU is used to start the APU, which in turn can be used to start the engines. Furthermore, it provides electricity to the aircraft when the engines are shut off. For redundancy and optimum performance, there are two generators on both the APU and the engines. The aircraft also has a ground power unit receptor.

[1]The GEnx Commercial Aircraft Engine. Accessed January 2020. https://www.geaviation.com/commercial/engines/genx-engine

13.5. Electrical System

The electrical power is generated by the engine gearbox and the APU. There are two generators per engine and two per APU. As it has the same engines and APU as the Boeing 787, this aircraft is taken as a reference. This electrical system can run at variable frequencies which allows for optimisation of the electricity use. The electrical system can provide 235 and 115 volts alternating current and 28 and 270 volts direct current. The latter is obtained by converting 235 VAC to 270 VDC, which is done by four auto-transformer-rectifier-units. This 270 VDC is used for cabin pressurisation, fuel-tank inserting and large hydraulic pumps. Furthermore, the electrical system has two electrical/electronics bays that condition the power and distribute it to other systems. One bay supplies the 235 VAC and the other supplies the 115 VAC or 28 VDC. The cockpit contains multi-functional LCD displays. There are four Control Display Units horizontally mounted on the flight deck and one on the flight stand. The CDU keeps track of navigation, control motions and thrust commands. Furthermore, it contains an integrated surveillance system which helps with weather and traffic alerts and also contains a collision avoidance system. It also contains two Dual head-up displays which allow for the pilots to look outside while simultaneously being able to see the most important flight instruments on their glass window. The aircraft administration is done by dual electronic flight bags. An overview of the electrical system is given in Subsection 13.11.3.

13.6. Hydraulic System

The hydraulic system is used for operating actuators. A conventional hydraulic system is used for the primary flight controls, landing gear, thrust reversers and slats actuation and it is used for nose gear steering. This hydraulic system is split up into two separate parts, one connected to the left engine and one connected to the right engine. The hydraulic fluid is pressurised by hydraulic pumps, which are in turn powered by the engines. For other actuators that require less hydraulic pressure, electric motors are used to pressurise the hydraulic fluid. These can deliver 113.6 L per minute at a pressure of 34.5 MPa [63] and get their electricity from the electronics bays. A schematic overview of the hydraulic system is shown in Figure 13.4.

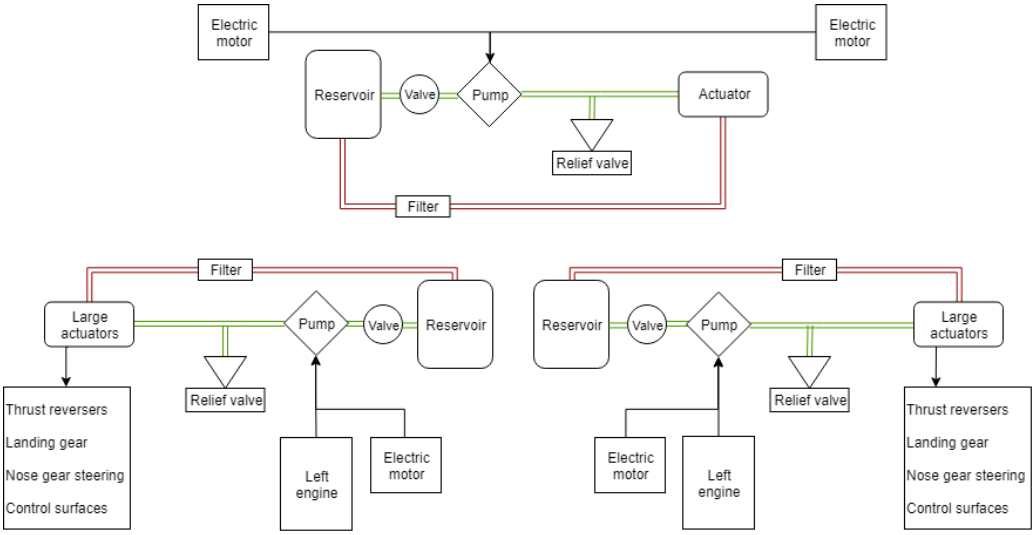

Figure 13.4: Hydraulic system lay-out

13.7. Environmental Control System

Cabin pressurisation is obtained by electric driven compressors. As mentioned before, the electrical system can run on variable frequencies and therefore, the pressurisation compressor can run at its optimum speed. The temperature of the air is regulated by low-pressure air-conditioning packs. The air runs into the cabin through special cabin air inlets. These inlets are located on the leading edge of section two. The way that the ECS is powered is also displayed in Subsection 13.11.3.

13.8. Water and Sewage System

The water and sewage system use similar system to the 787, which are the vacuum waste system and unpressurised potable water tank. Even though the capacity of the 787 is not comparable to the FB400, the tank volume required for both subsystems are comparable to the 777 which has relatively similar capacity to the FB400 [64]. Therefore, a tank volume of 2,600 L for waste and 1,000 L for potable water are implemented to the Blended Wing Body aircraft. Both fuel

tanks are located behind the cargo hold. This is chosen due to the fact that this system is relatively heavy and should therefore be placed close to the centre of gravity to minimise the shift during a flight. Since the 787 is currently already operating, that means compatible trucks are available for service in airports worldwide. With the specification of the sewage system, it can be confirmed that the waste stowage on board is segregated. Thus, it complies with requirement HCSR-NF-SUS-001.

13.9. Anti-Ice Wing

Engine inlet de-icing is still done with bleed air but the anti-icing of the wing is now also electrically regulated. The leading edge slats contain electro-thermal heating blankets. Their temperature can be regulated precisely, which is more efficient than using bleed air.

13.10. Fire Protection System

Of course, a fire on an aircraft could be a serious situation. Therefore, the FB400 has a fire protection system. Both cargo holds are fitted with smoke detectors that can alert the crew in case of fire. Furthermore, as the cargo holds are not easily accessible, there are Halon extinguishers present that can be operated from the cockpit to suppress the fire. In order to ensure that the fire will not spread to other parts of the aircraft, the walls and linings are air tight and fire resistant. Other parts of the aircraft that have a relatively large risk of catching fire are the APU and the engines. Thus, they are separated from the rest of the aircraft by fire resistant materials. Furthermore, there are both overheat and fire detectors present on multiple locations that send a warning to the cockpit. From there, pilots can shut down the fuel and air supply to the engine(s) or APU and drain all flammable fluids. There are also Halon fire extinguishers present to kill the fire if necessary. As for the cabin, there are smoke detectors, located in the lavatories, gallies and work and rest stations. These are locations that are not always occupied by passengers or crew and so a fire can start there without being noticed right away. Furthermore, multiple Halon extinguishers are present on board. As can be seen from Subsection 8.2.1, the most crucial part of the cabin is the part between the most rear exits. If there were to be a fire in that area, there are no exits left for all 350 passengers sitting behind it. Therefore, there are extra handheld extinguishers in that area, plus built in extinguishers that can be operated electronically.

13.11. System Interface

It is important for the entire system of the Blended Wing Body aircraft to work coherently. Therefore, it is needed to design the interfaces between systems and show how they are connected to each other, which will be shown in this section.

13.11.1. Interface N^2 Chart

This subsection shows the N^2 Chart of the systems interfaces.

Table 13.2: Interface N^2

Environment

Ground					Connect APU		Communication Navigation						Weather conditions Runway conditions Traffic conditions
Length C.G. limits	Fuselage	Mounting Wing position Disturbed airflow		Mounting (BWB)		Drag Disturbed airflow		Mounting	Disturbed airflow	Mounting	Disturbed airflow	Mounting Stowage	
Span	Lift Wing box Bending moment	Wing	Mounting	Mounting Fuel storage		Lift Drag	Amount of fuel					Mounting Stowage	Mounting Feedback
	Lift Braking	Lift	High lift devices			Lift Drag							Feedback
	Thrust	Thrust Airspeed Bending moment	Airspeed	Propulsion system		Drag Airspeed	Airspeed Fuel consumption	Airspeed	Airspeed	Airspeed	Airpeed		Feedback
	Power Pressurization Air conditioning		Power	Power	Power system		Power	Power	Power	Power	Power	Power	Power
	Lift Drag Aerodynamic moment	Lift Drag Aerodynamic moment			Drag	Aerodynamic characteristics	Aerodynamic moments						Feedback
Communication		Monitoring Fuel management		Fuel monitoring Fuel management		Control forces Control moments	Avionics	Control forces Control moments	Control forces Control moments	Control forces Control moments	Control forces Control moments		Navigation Communication Weather conditions
	Stability					Lift Drag	Feedback	Horizontal stabiliser	Mounting				Feedback
	Pitch control	Attitude Flow control				Pitch moment Roll moment	Feedback	Bending moment	Horizontal control surfaces				Feedback
	Stability						Feedback			Vertical stabiliser	Mounting		Feedback
	Yaw control					Yaw moment	Feedback			Bending moment	Vertical control surfaces		Feedback
	Ground support Steering Braking					Drag						Landing gear	Feedback
Communication Update flight status	Monitor	Monitor	Control	Monitor		Monitor	Monitor	Control	Control	Control	Control	Control	Cockpit

13.11.2. Systems Lay-Out

Figure 13.5 shows a schematic overview of the lay-out of the most important systems. Note that it is not drawn to scale.

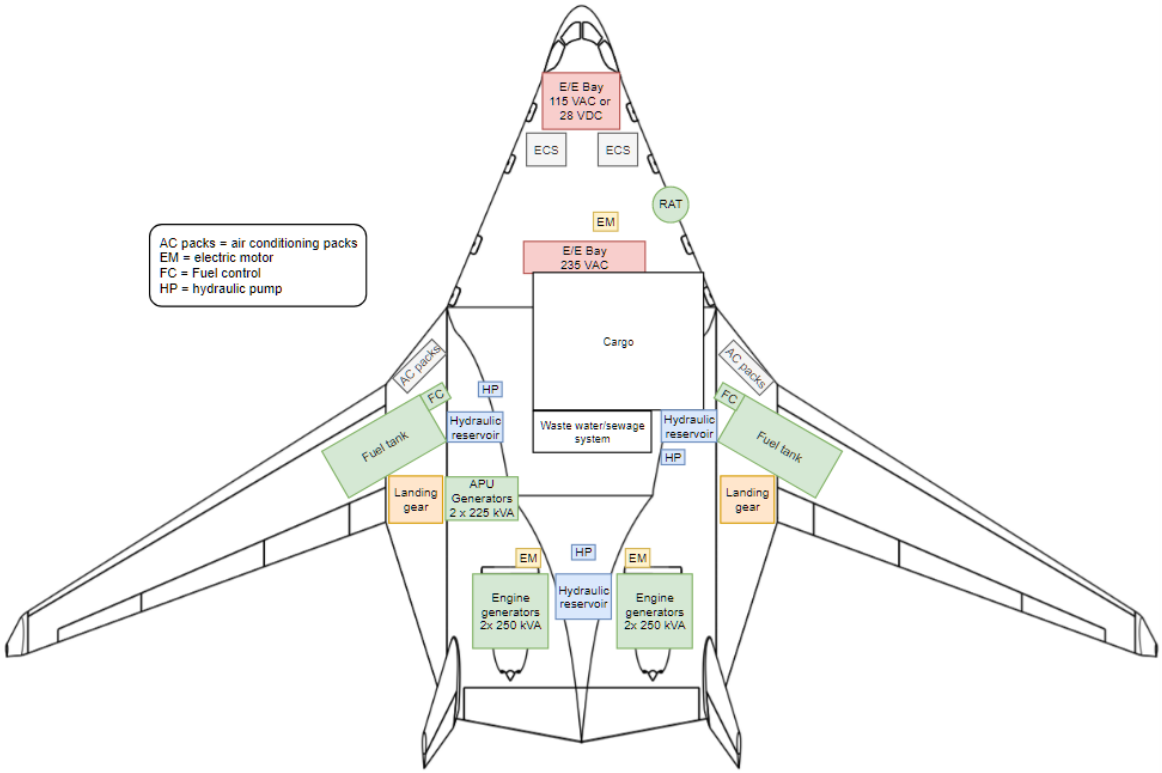

Figure 13.5: Overview of main systems

13.11.3. Electrical Block Diagrams

Figure 13.6 shows the electrical block diagram of the FB400's electrical system. The electricity is generated by the engines, APU or RAM Air Turbine, in case of emergency. It is then distributed to the electronic bays from where it is redistributed to the rest of the aircraft systems that need electrical power.

13.11.4. Data Handling Block Diagrams

Figure 13.7 shows the data handling block diagram of the control system of the FB400, starting with inputs from the cockpit until the movement of control surfaces.

13.11.5. Hardware Interface

The hardware of the aircraft is separated into four different System: engine, cabin, hydraulics and input. Since the FB400 implements a More Electric Aircraft concept, the main power distributed through the entire hardware is electricity. The main source of electricity is the engine and is distributed by using the Power Distribution hardware. Therefore the four systems are connected into one main hardware which is the power distribution.

In Figure 13.8, it is shown how each of the hardware is connected to each other through the power distribution hardware.

- **Engine System**: Aside from producing thrust, the engine also produced electricity to be stored in the battery. The electricity is utilised by the entire hardware system.
- **Cabin System**: The power distributed is used to power the cabin system such as the pressurisation and air condition of the cabin. For passenger's experience, the electrical appliances (lighting, in flight entertainment and galley equipment) also operates.
- **Hydraulics System**: To move the hydraulics, the actuators require a power source. Thus, power is also distributed to move the hydraulics of the high lift devices, control surfaces and landing gear.
- **Input System**: The pilot has the freedom to manually input the controls or to use autopilot. However, the flight

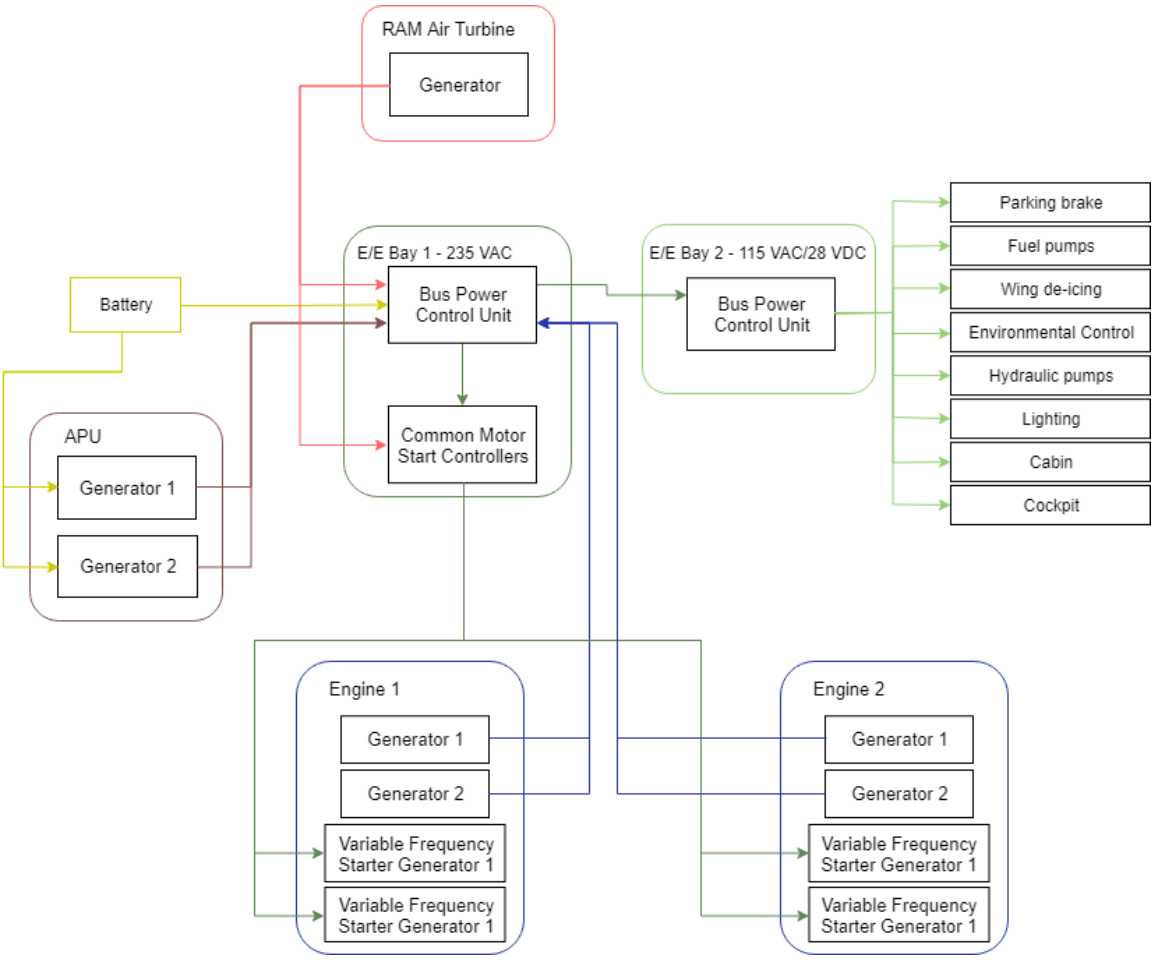

Figure 13.6: Electrical block diagram

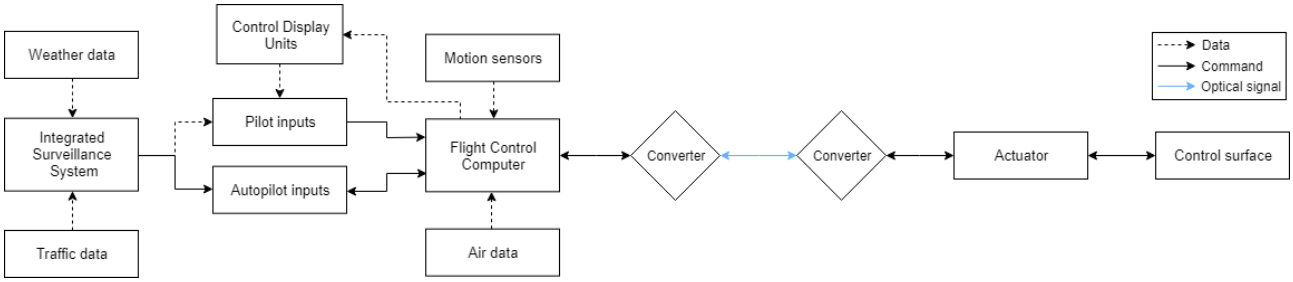

Figure 13.7: Data handling block diagram

computer requires power to operate the control and to enable the autopilot. Together with the sensor that is monitoring the hydraulics system, the flight computer can operate and alter the hydraulics system and the engine system.

The power distribution hardware act as a crucial key in the hardware interface. Especially as the entire system relies on electricity that is distributed.

13.11.6. Software Interface

Since the fly-by-optics is implemented, the aircraft requires a tremendous computing power to operate. To simplify the mapping of the software interface, only the main software system is analysed. In Figure 13.9, it is shown how the software (diamonds) interact with the systems (rectangles).

The main flow of Figure 13.9 starts with the pilot that usually acts based on a two-way communication with the Air Traffic Controller. Afterwards, the entire aircraft system and the flight computer starts. However, if a component is not started, the pilot's display shows error. If the startup sequence is successful, the input can be given. It can be in the

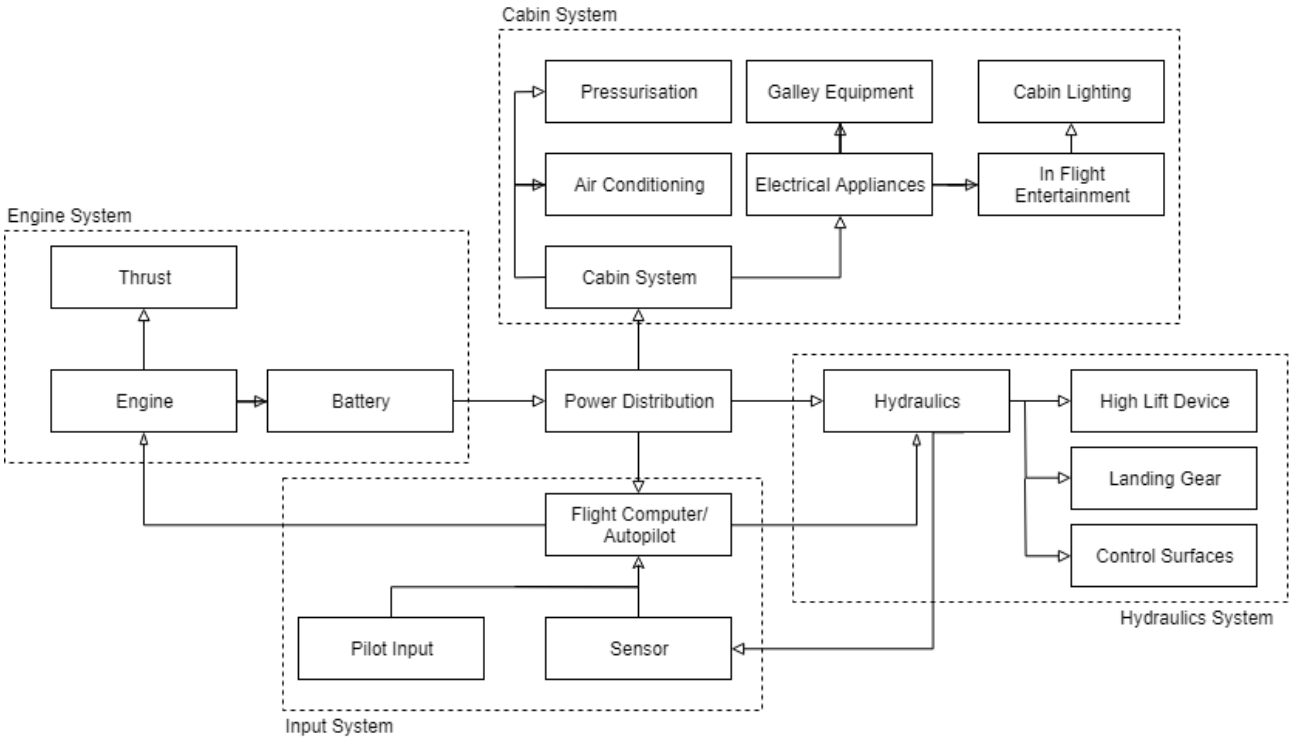

Figure 13.8: Blended Wing Body System Hardware Diagram

form of autopilot or manual input. The input is driven by two different sources, the current flight conditions (latitude, longitude, altitude, speed, etc.) and the GPS and radar system. The input then alters the engine's thrust and the flight controls (high lift devices and/or control surfaces). Moreover, the sensor monitors then changes and returns it to the flight computer so another input can be given or the autopilot can react accordingly. The pilots also have the options to deploy the landing gear or shut down the system. A warning system is present if hazard is detected by any of the software so the pilot is aware of it.

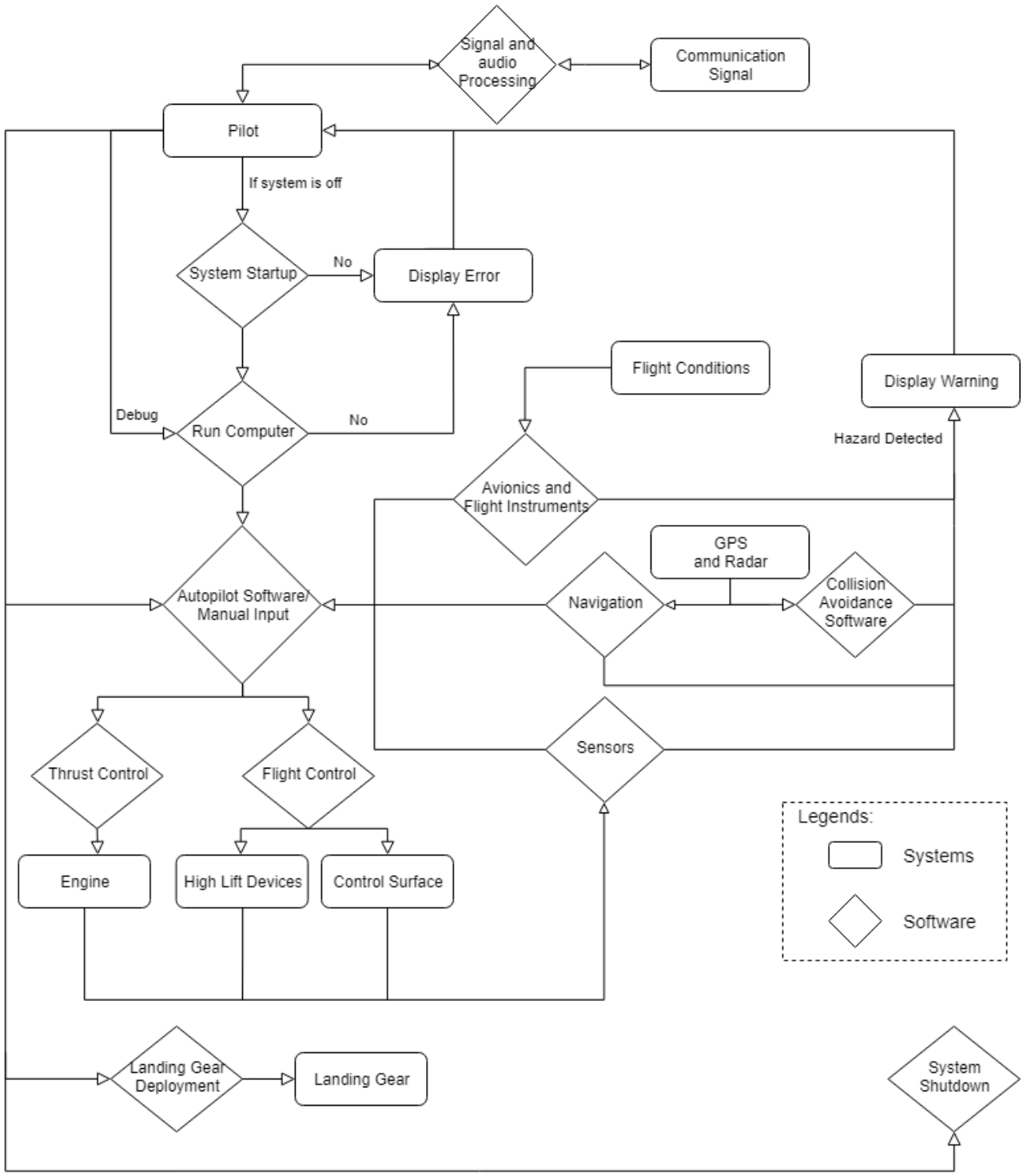

Figure 13.9: FB400 Software Diagram

14

FUTURE PLANNING

This chapter shows the future planning of the project. Firstly, a production plan is given and explained in Section 14.1. Afterwards, a flow diagram visualises the project design and development in Section 14.2. Finally, the Gantt chart is shown in Section 14.3, following from the flow diagram to show the time assigned per task.

14.1. PRODUCTION PLAN

As mentioned in Section 5.2, the concept of lean manufacturing will be implemented during the manufacturing process. The main idea here is to minimise waste during the process. An example would be to limit milling and drilling and try to see where the possibilities are for lay-up and casting processes, or even 3D printing. Furthermore, certain parts of the main assembly should be manufactured at the same site to minimise the transport needed for the parts. The production plan is shown in Figure 14.2.

However, the assembly for the FB400 is not the same as for conventional aircraft. It is more difficult to treat the wing and fuselage separately, since they are part of a whole. Figure 14.1, which has been presented before in Subsection 8.9.7, shows how the wing and fuselage interact. The assembly of the cabin includes the lateral spars and stringers running through. So the wing that is attached is the outer wing section. First the floor and ceiling will be constructed, after which the spars will be formed around and cuts in the spars will be made to allow for the presence of the floor and ceiling. The stringers will have to be connected to each other, either at the start of the outer wing section, or in the centre of wing section 2.

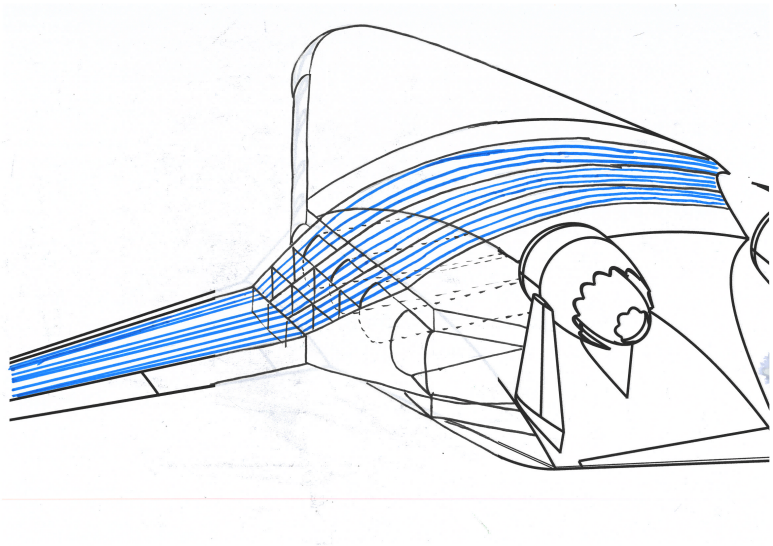

Figure 14.1: Wing fuselage interaction with stringers in blue

14.2. PROJECT DESIGN AND DEVELOPMENT LOGIC

The project design and development logic is shown in Figure 14.3. It contains the activities that will take place after the conceptual design as presented in this report. It will start with a detailed design of all the parts mentioned under "A". Afterwards, the manufacturing will start and prototypes will be built and tested. Later, the parts will be mass produced and sub-assemblies will be created. Finally the assembly will obtain its interior and the aircraft will be ready for delivery after successfully passing the last tests.

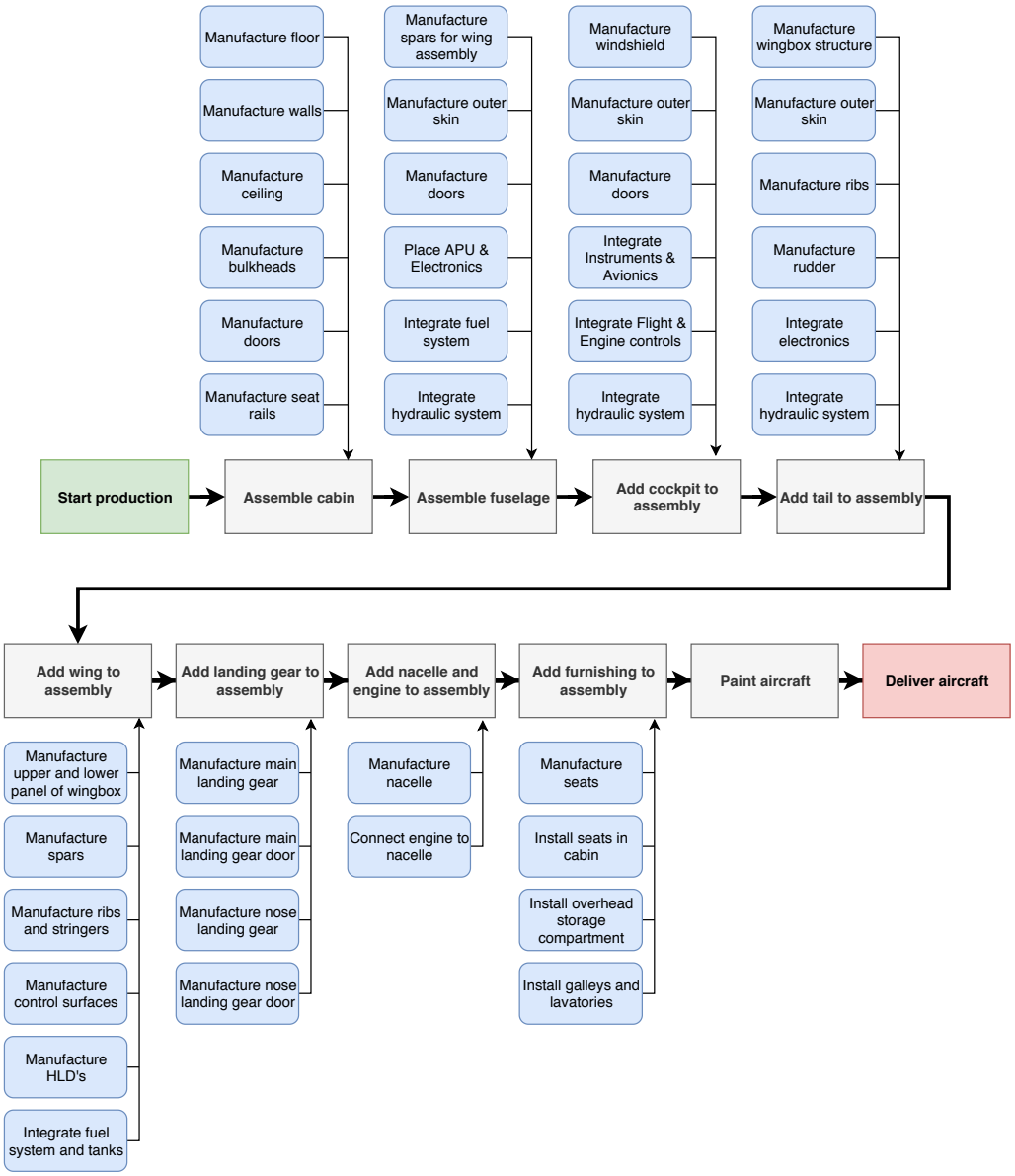

Figure 14.2: Production plan FB400

14.3. Project Gantt Chart

The project Gantt chart is created to assign a certain time period per task. This will create a clearer overview of what is expected to happen in the next few years. Figure 14.4 shows the time period from the first quarter of 2020 until the fourth quarter of 2023. Figure 14.5 shows the time period from the first quarter of 2024 until the fourth quarter 2029, where the first delivery is expected.

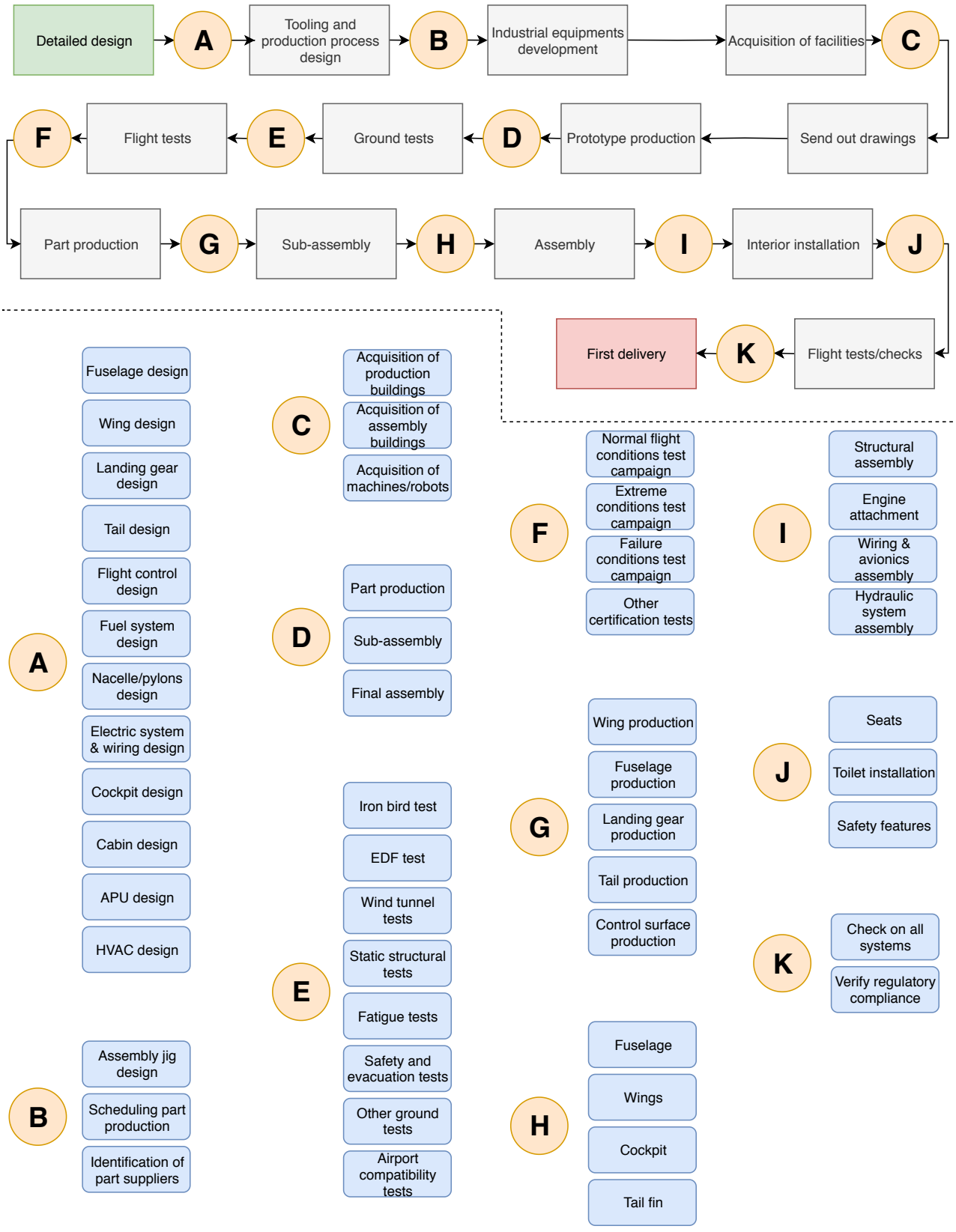

Figure 14.3: Project design and development logic FB400

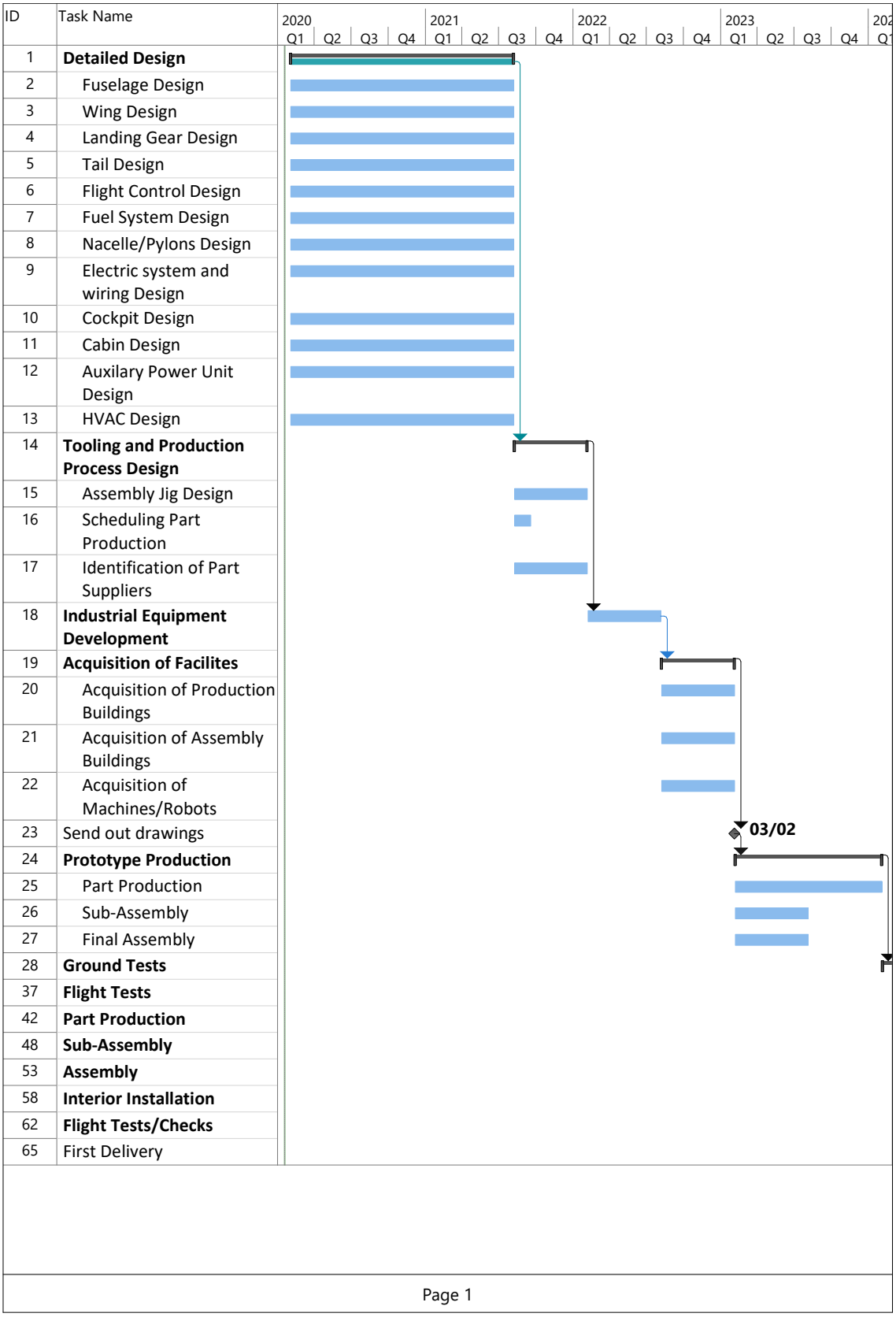

Figure 14.4: FB400 Gannt chart part 1

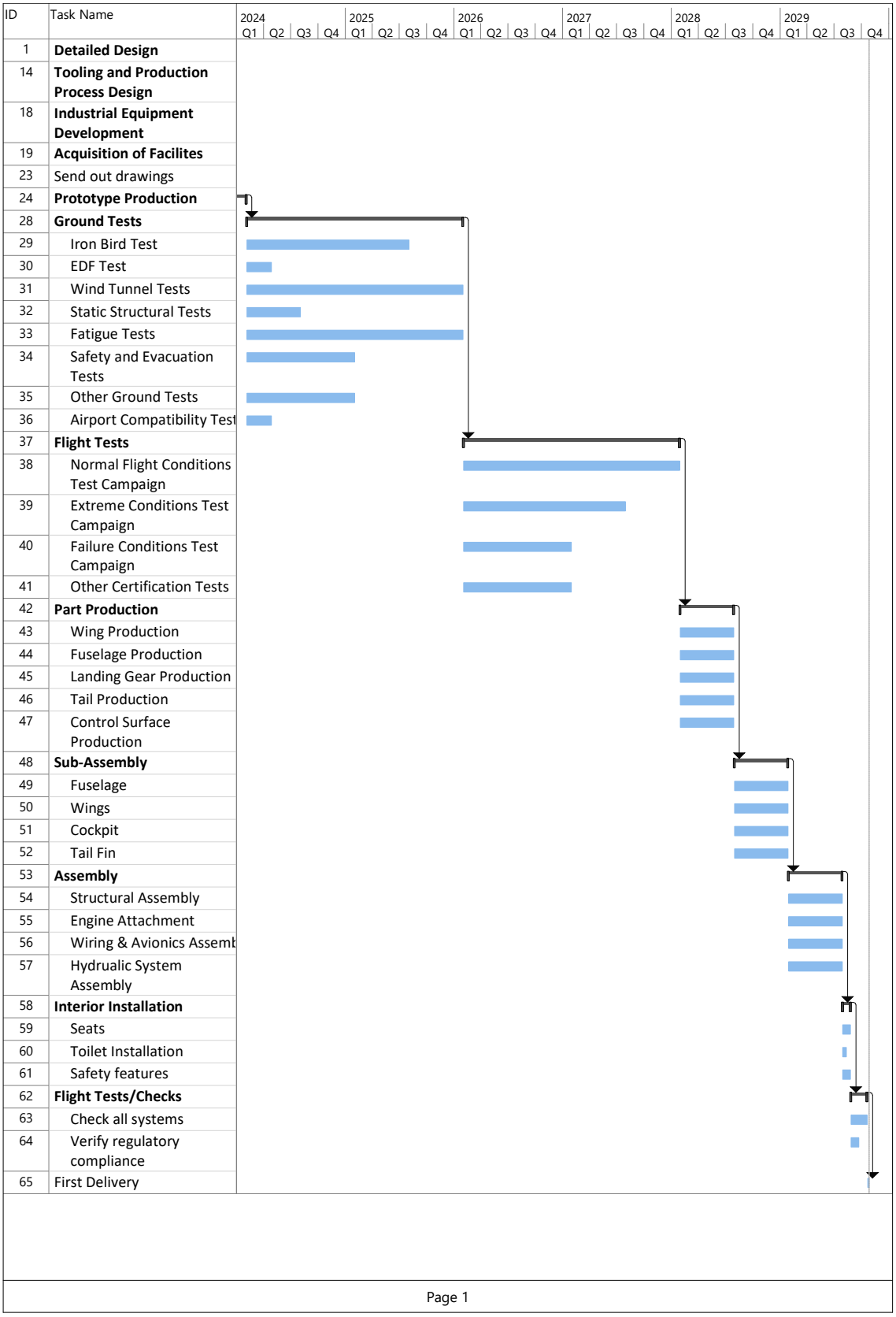

Figure 14.5: FB400 Gantt chart part 2

15

FINANCIAL ANALYSIS

This chapter gives an overview of the estimated costs of the aircraft. In Section 15.2 and Section 15.3, the development and production cost and the operational cost results are given and elaborated, respectively. Then, in Section 15.4 the return on investment is given. This chapter concludes with an overview of the costs the blended wing body is expected to have and its resulting position in the future market.

15.1. COST BREAKDOWN STRUCTURE

The lifetime cost of the FB400 is calculated using the method given in Roskam's VIII book[4] on cost estimation. First, this section provides the cost break down structure of the aircraft lifetime cost. Than, a brief explanation of Roskam's method and the assumptions taken is given.

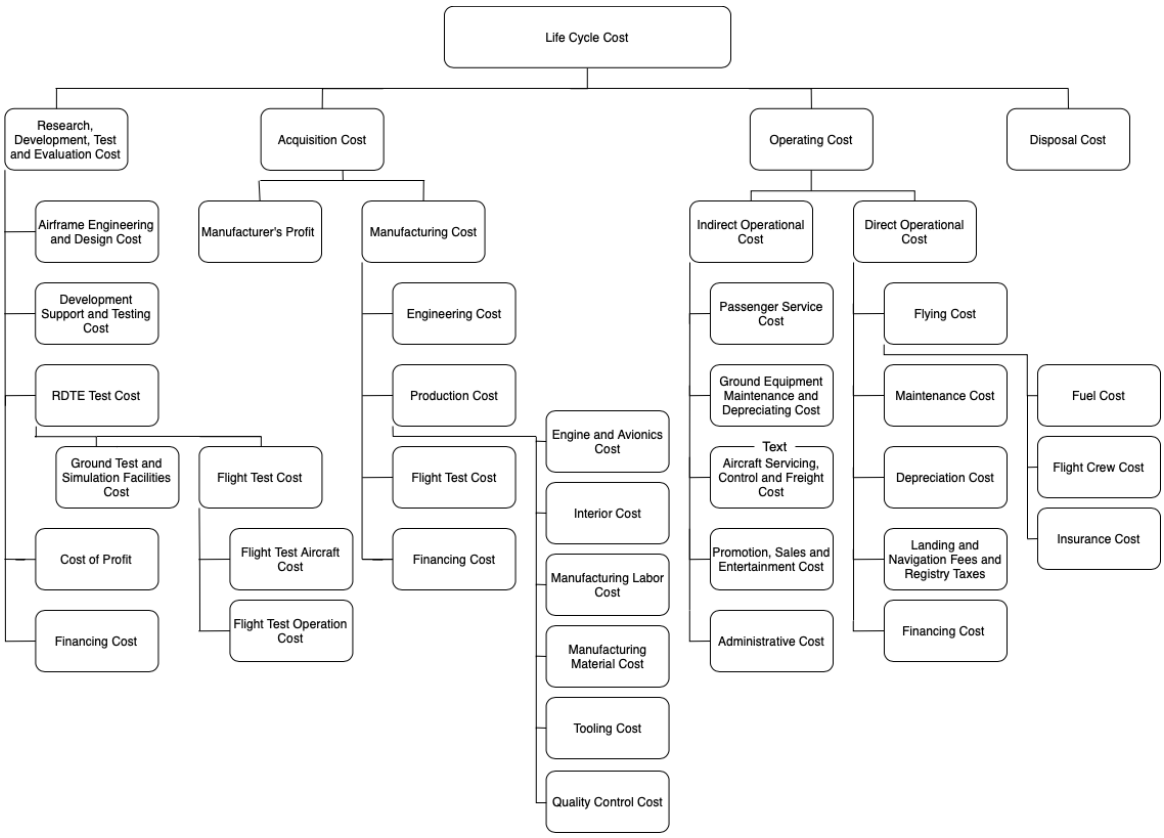

Figure 15.1: Cost Breakdown Structure

To account for inflation a Cost Escalation Factor(CEF) is used. Roskam uses a CEF with base year 1970. For years later than 2017, a formula is given. For the FB400 project, this formula is slightly updated to years later than 2019 by use of the inflation calculator[1]. For the development and manufacturing phase, the 2025 CEF value is used. For the operational phase, 2030 is used.

[1] CPI Inflation Calculator. Accessed January 2019. http://www.bls.gov/data/inflation_calculator.htm

15.2. Development and Production Phase Cost

The unit cost of the FB400 consists of the development and production cost per aircraft, calculated on the basis of a total production (and total order) of 1353 aircraft over a time span of 15 years. As mentioned before, Roskam's method is used and it is assumed that the average CEF factor for the development and production phase is 2025. In Subsection 15.2.1, the main contributions to the research, development, test and evaluation(RDTE) cost are described and the manufacturing cost in Subsection 15.2.2. In subsection Subsection 15.2.3, the results of this section is validated by recalculating the costs with a simplified method that was developed in 2012 and therefore, possible errors due to the outdated relations in the book could come forward.

15.2.1. Development Phase

The contributions to RDTE cost are shown in Table 15.2. For the flight testing phase, 4 aircraft will be used, which is based on recommendations from Roskam[4]. Two of these will be 'heavy flight test aircraft' with instrumentation, and will be used for basic technical development and certification. These two together will test fly for 600hrs in 21 months. Additionally there will be 2 test aircraft with cabin and lighter test instrumentation, which will fly for about 900hrs in 20 months.The cost of the flight test aircraft are high, mainly due to the test equipment and the extra tooling cost for the amount being build.

Flight test aircraft 3 and 4 will be made available for the market, meaning some changes in the test aircraft cost. In all four test aircraft cost, the avionic system and the engines are incorporated. The list price of the GEnx-1B is $28.7 million in 2017[2]. For this cost analysis, it is estimated that the price in 2022 will be the same as in 2017. Cost information on the avionics systems is difficult to obtain at this stage of the design. From Raymer [19], it is assumed that avionics cost 5-25% of the flyaway cost or $4516 per pound mass. Using the cost per mass, the cost of the avionics are assumed to be $5.9m. For the total of 2500 flight test hours, a value of $3 per gallon is assumed, half of the $6 during the operational phase of the aircraft in 2030. The 'difficulty level' as mentioned in Roskam, of the FB400 is higher than average. A factor 3.5 to 4 has been chosen in order to take into account the unconventional design and the challenges the designers are facing, for example regarding the pressurisation and stabilisation of the aircraft. As shown in Table 15.2, the total development cost is around $17.8 billion in 2025. This is comparable to the A350, which had an estimated development cost of $12 to $15 billion dollars in 2013.[3]

Table 15.1: Development Cost Program in 2025 b$

Program Cost	**Value b$**
Airframe Engineering and Design Cost	10.4
Development Support and Testing Cost	0.50
Test and Simulation Facilities Cost	6.50
Flight Test Aircraft Cost	4.95
Flight Test Operating Cost	0.41
Total Testing Cost	11.9
Profit Cost	3.2
Financing Cost	6.50
Total RDTE Cost	**32.5**

15.2.2. Manufacturing Phase

The design choices that have strong influence on the the manufacturing time and cost are described in this subsection. Table 15.2 shows the results obtained by Roskam's method with some modifications in order to make it more applicable to modern day manufacturing. First of all, the airframe engineering and design cost for the FB400 is assumed to be higher than conventional aircraft as the pressurisation of a Blended Wing Body is more complex. Because of the new design, more tooling cost are accounted for by increasing the 'difficulty level' of the aircraft design. The relatively high manufacturing cost is due to both high material cost and the larger amount of man-hours required for composite aircraft manufacturing. The production of composites for the aerospace industry is for a relatively large part done manually, with highly skilled employees required. Manually manufacturing composites still gives better quality than any automatic process could do and due to regulations in the aerospace industry the process of automating production requires high re-certification cost. It is therefore that still in 2028, during the manufacturing phase, it

[2]GEnx Engine to Power Its Boeing 787 Dreamliners.Accessed January 2019. https://www.geaviation.com/press-release/genx-engine-family/china-eastern-selects-genx-engine-power-its-boeing-787-dreamliners

[3]A350: The aircraft that Airbus did not want to build https://www.bbc.com/news/business-22803218

is assumed to have high cost[4].

Table 15.2: Production Cost Program in 2028 b$

	Value b$ per program	**Value B$ per unit**
Airframe Engineering and Design Cost	7.03	5.19
Aircraft Production Cost		
Manufacturing Material Cost	31.0	22.9
Tooling Cost	15.4	11.4
Manufacturing Cost	63.4	46.8
Avionics and Engine Cost	85.1	62.9
Interior Cost	6.26	4.62
Quality Control Cost	9.51	7.03
Flight Test Cost	0.47	0.35
Financing Cost	4.7	40.4
Total Manufacturing Cost	273	201
Acquisition Cost	300	222

15.2.3. Result Validation

At first, the values of the RDTE and the manufacturing phase were unrealistically low. Roskam's equations are based on existing aircraft in the market. It is common for high capacity aircraft to have a large range and vice versa. The FB400, being a high capacity short range aircraft, is unique in itself and has a low weight for a 400 passenger aircraft. In the majority of Roskam's equations, weight plays a role. This means that the values calculated, are underestimating the aircraft size and capacity. This is confirmed by equation Equation 15.1[65] which is based on reference aircraft and gives an Aircraft List Price(ALP) of only $127m in 2014.

$$\text{ALP}_{\text{WB}}[\$\text{M}] = 205.88 \cdot ln(\text{MTOW}) - 876.62 \tag{15.1}$$

To take into account the range and the amount of seats of the FB400, another equation is used. From reference aircraft list prices, the weight of the seats is estimated to be 85% and the remaining 15% is for range. This results in Equation 15.2, which gives values of $305m and $312m for a range 700nm and 3500nm respectively.

$$\text{ALP}_{\text{WB}}[\$\text{M}] = 0.85 \cdot [255.29 \cdot ln(\text{Seats}) - 1178.1] + 0.15 \cdot [32.7 \cdot e^{1.53 \times 10^{-4} \cdot \text{Range}}] \tag{15.2}$$

In order to validate the estimated unit cost, a different method is used. This method is an slightly updated version of Raymer[19], which is based on the Dapca-IV[66] method. This modified version[67] is based on 2012 cost relations and therefore considered to be better applicable. It is a short and simplified method that is used to validate the results obtained from the Roskam method. This method gives a difference of 15% and is given in Table 15.3.

In Table 9.5, the unit, recurring and non-recurring cost are given. For the statistical calculations, the list price is changed to the unit price by assuming a 10% profit of the company. Compared to the statistical data, Roskam is estimated to be too low. Therefore, a unit price of $283 is taken as an estimate as well as the non-recurring cost and recurring cost from the Raymer method.

15.3. Operational Cost

One of the objectives of this project is to have low operational cost. For aircraft that will be operational in 2030 and that are fuelled by conventional jet A fuel, the future operating cost are dominated by the fuel cost. As can be seen in Table 15.5, the weight of the fuel cost on the operational cost is to such extent that 'inconvenient' design options, like the high location of the engines, are considered minor compared to the fuel cost reduction it gives. In order to be consistent with Roskam's method, this chapter divides the operational cost in direct operating and indirect operating cost. Since the formulas used in Roskam's book can be outdated, the results obtained are compared to values from data collection on operational cost of 52 airlines by IATA In case of large differences that can not be motivated, are calculated again with methods[68] and [65].

[4]Why conversion costs of composites in Aerospace are still way too high https://www.airborne.com/why-conversion-costs-of-composites-in-aerospace-are-still-way-too-high/

Table 15.3: RDTE and manufacturing phase using the updated version of Raymer.

	Man-hours	Rate, $/hr	Total Cost b/$	Cost per Unit m/$	
Engineering	72.7m	113	17.1	38.0	
Development Support			1.00	2.21	
Flight test operations			0.36	0.80	
Tooling	40.5m	77.8	6.62	14.7	
Certification Cost			**24.3**	**55.7**	
Manufacturing Labor	23.4m	67.6	33.2	64.5	
Quality Control			9.39	20.8	
Materials/Equipment			15.1	33.4	
Units produced in 5 years					451
Quantity Discount Factor					0.586518
				Without QDF	With QDF
Engines				57.4	33.7
Avioncis				5.87	3.44
Total Cost to Produce				**246.9**	220.7
Manufacturer's liability insurance				36	32.0
Minimum selling price				**283**	253

Table 15.4: Comparison of cost between different methods

	Roskam	Raymer	Statistics
Unit Cost M$	246	283	275-280
Non-Recurring Cost B$	26.6	24.3	
Recurring Cost B$	300	334	

Table 15.5: Estimated DOC for the FB400 for a 700nm mission in 2030 US$

Component of DOC	**$/nm**	**ASM $cents**
Total Cost	89.6	19.5
Fuel Cost	35	7.61
Crew Cost	1.53	0.333
Insurance Cost	4.64	1.00
Maintenance Cost	7.48.	1.62
Depreciation Cost	9.78	1.99
Landing Fees	8.39	1.82
Navigation Fees	2.19	0.476
Taxes	0	0
Financing Cost	6.27	1.36

The largest influence on the DOC is the fuel cost. In Table 15.6, the $ per aircraft seat-mile is given(ASM). The values for the B737-MAX and A319NEO were obtained from an analysis on fuel cost, in which the mission range is 600nm. For the comparison with the FB400, a mission of 600nm was taken and a fuel price of $3 per US Gallon[5]. As shown, the fuel cost per seat-mile is lowest for the FB400.

The landing fees calculation in Roskam's book is outdated and a relations based on reference data is used to recalculate it. Since one of the objections of FB400 project is to reduce airport congestion, reference data from busy aircraft has been chosen. Equation 15.3 give the formala [65] used for both North America and Europe, which depend on maximum gross landing weight and maximum take of weight respectively, in kg-tons. The new values for landing fees are $7661 and $4080 per landing, of which the average is added to Table 15.5 per nm and ASM.

[5]Embraer continues and refines its strategy at the low-end of 100-149 seat sector. https://leehamnews.com/2014/01/13/embraer-continues-and-refines-its-strategy-at-the-low-end-of-100-149-seat-sector/

Table 15.6: Fuel cost comparison at 600nm mission at a fuel price of $3 per US Gallon and a 100% load factor

Aircraft	ASM $cents
737-7MAX	0.0430
A319NEO	0.0425
FB400	0.0392

$$\begin{aligned} \text{LandingFees}_{\text{NorthAmerica}}[\$] &= 15.66 \cdot (MGLW) \\ \text{LandingFees}_{\text{Europe}}[\$] &= 8.34 \cdot (MTOW) \end{aligned} \tag{15.3}$$

The formulas to calculate the navigation fees are given in Equation 15.4[65] for both the North America and Europe and give $0.569 and $3.82 per nm. Again, there is a significant difference between the two and the average is taken and added to Table 15.5.

$$\begin{aligned} \text{NavigationFees}_{\text{NorthAmerica}}[\$] &= 0.3070 \cdot (distance) \\ \text{NavigationFees}_{\text{Europe}}[\$] &= 0.113 \cdot \text{distance} \cdot \sqrt{\text{MTOW}} \end{aligned} \tag{15.4}$$

15.3.1. Maintenance Cost

Because of the composite material used, the maintenance cost are lower. As can be seen in Table 15.5 the maintenance cost are comparable to conventional aircraft currently flying, therefore worth mentioning. Maintenance cost can be influenced by different factors and will be discussed in this subsection. High diversion of an fleet increases the operational cost. Especially for maintenance cost, segmenting the fleet per airport or area is a solution to lower the maintenance cost. The FB400 is aimed at high demand routes and the target markets are concentrated areas of which most operate via hub and spoke networks. This means that more equipment is available which partly solves the extra cost of the inconvenient location of the engines.

15.3.2. Indirect Operational Cost

In this subsection no quantitative values are given. It is assumed, based on Roskam and statistical data that the indirect operating cost is given as a 55% of the direct operating cost. In Table 15.7, the final values of the indirect operational cost are given as well as the final total operational cost per nautical mile and aircraft-seat-mile.

Table 15.7: Final results of operating cost given in $2030

	$/nm	ASM $cents
DOC	89.6	19.5
IOC	49.3	10.7
TOC	138.9	30.2

Generally, the designer has little influence on the indirect operational costs(IOC) and Roskam does not give a quantitative method for it in his book. So in this subsection, the parts on which the designer has some leverage, a distribution will be given. The IOC consists of the sum of the indirect operational cost of passenger services(pax), cost of maintaining and depreciating ground equipment and ground facilities(sta), cost of aircraft and traffic servicing, control and for freight(ascf), cost of promotion, sales and entertainment(pse) and lastly the cost of general administrative expenses(gaa).

$$IOC = IOC_{\text{pax}} + IOC_{\text{sta}} + IOC_{\text{ascf}} + IOC_{\text{pse}} + IOC_{\text{gaa}} \tag{15.5}$$

With the expected rise in fuel prices, airlines have to find another way to reduce their operational cost. One of the ways designers have leverage is in designing for low turn around time and fast ground handling operational times. This section describes the actions taken and their cost results both on operational cost but also on possible increases in unit price or extra fuel cost due to weight increase.

The extra cost of the foldable passengers seats described in section8.2 will have an increase in interior cost of the FB400 of $2.2 million. For the Airbus A320-like baseline aircraft used in the ALOHA project, the annually utilisation of the aircraft increases, but so does the DOC per seat-nm. However, for the FB400, the gain in productivity results in more profit. There is no quantifiable value of the reduction in cost, however, in the ALOHA project it is concluded that there is a 45% reduction in deboarding time, a 16.6% reduction in boarding time and the cleaning time is reduced with 33%. Additionally, there is will be two passenger bridges and more aisles than conventional wide-body aircraft, making it more convenient. This is already incorporated in the Gantt chart on operational time.

Turnaround time is also directly related to the accessibility of the aircraft when servicing, i.e. if service vehicles can simultaneously access the aircraft. The designer has influence on this and as described in chapter 11, the FB400 is accessible to service the aircraft in a shorter amount of time. Design of the freight compartment is related to the way freight must be handled(people, containers and handling equipment). The FB400 body is designed such that there is only cargo in containers. With two cargo departments which can be used simultaneously, ground handling costs are reduced. For short-range aircraft this is beneficial and therefore cost reducing[69].

15.4. Return on Investment

The route New York-LaGuardia-Chicago was used as an reference for the cost prices. By taking inflation into account, the average ticket prices were $248 and and $372 for economical and business seats respectively. By using the a fuel price comparable to today's, the FB400 has a return on investment of 92%. This means that the FB400 is very compatible in the market. Unfortunately, with just inflation, it is not possible to get a representative estimation as the fuel prices will rise to such extent that it difficult to estimate the future ticket prices.

16

TECHNICAL RISK ANALYSIS

This chapter elaborates upon the technical risk analysis of the high capacity short range transport aircraft. After the technical risks have been identified and analysed in the previous design stages, mitigation plans have been applied during this design stage [1] [2]. Consequently, those risks that are not applicable at this stage are removed or relocated and new risks are identified which will be valid for future stages of the design and life-cycle of the aircraft. Section 16.1 shows the identified risks and their categorisation, whereas the mitigation techniques for these risks and their position in the risk map are shown in Section 16.2.

16.1. TECHNICAL RISK IDENTIFICATION AND CLASSIFICATION

While developing a new product, different risks might occur during different stages of its life cycle. Therefore, the technical risks that are analysed for this aircraft are divided into four main categories - design, manufacturing and maintenance, operations and end-of-life. Each of the categories has its own specific risks that need to be closely managed. The risks that occurred in previous design stages have been mitigated by performing sensitivity analysis, verification and validation, which is why they are no longer a threat for the design and are not mentioned in this report. However, they can still be found in the risk map before mitigation (Table 16.2).

16.1.1. DESIGN RISKS

DR-09 Stability requirements not met: Static and dynamic stability is very sensible to changes in the design, therefore if a design change is made and the stability is not updated, the requirements could not be met eventually.
DR-1.01 Non-flexible design: The design is highly sensitive to changes which might lead to large design constraints and therefore small space for optimisation.
DR-1.09 Design does not allow for family concept: If the aircraft is designed and optimised only in a certain configuration, it might not allow for creation of aircraft family based on it.
DR-1.10 Difficulties in certification: The aircraft might require more time to be certified or even new certification requirements from aviation authorities.
DR-2.01 High development and unit cost: The design might require new parts and components which will significantly increase the cost of the final product.

16.1.2. MANUFACTURING AND MAINTENANCE RISKS

MMR-01 Manufacturing resource limitations: There is a possibility that the manufacturing process is limited by resource availability, This might include people, materials, machines, production methods, etc.
MMR-02 Insufficient production quality: During manufacturing of a product, there is always the risk that some flaws will occur and not be detected. This could be due to transport or production damages and could lead to unsatisfied clients or even inability to perform operations.
MMR-03 Extended manufacturing time: The unconventional design could lead to more manufacturing time compared to conventional aircraft, which will affect the cost and schedule of the project.
MMR-05 Limited availability of spare parts: Spare parts of new aircraft are usually sparse, which could lead to maintenance time extension.
MMR-06 Incorrect/incoherent manufacturing tolerances: The tolerances that have been designed might not be possible to achieve during manufacturing.
MMR-07 System integration errors: While production and manufacturing, there is a possibility that the systems are not correctly integrated into each other. This could include wiring of electronics or improperly integrating the propulsion system.
MMR-08 Extended maintenance time: New aircraft may have longer maintenance time in the beginning due to untrained workers.
MMR-1.01 Limited opportunities for service: For new aircraft the service opportunities are going to be smaller and there is a possibility that the aircraft could not be maintained everywhere.

MMR-1.02 High manufacturing cost: The new aircraft might require new materials and manufacturing methods which are more expensive.
MMR-1.03 Low maintenance flexibility: Since the aircraft is new, spare parts and components of other aircraft might not be compatible with it.

16.1.3. Operational Risks

OR-01 Major structural failure: This includes failure of major structural components such as wing, tail or fuselage.
OR-02 Structural failure due to impact: Impact with foreign objects (ex. birds) during flight could lead to severe structural damage.
OR-03 Structural degradation due to operational conditions: Specific operational conditions such as moisture, salt, extremely low or extremely high temperatures could lead to material and structural damages.
OR-04 Structural degradation due to fatigue: If the loading cycles of the structure or its components are exceeded, fatigue stress could be potential threat for the structure.
OR-06 Wing failure due to heavy dynamic loads and fluttering: If during the mission operation the aircraft encounters unstable flight region in terms of aeroelasticity, fluttering and buffering could occur, which would then cause severe structural damage to the wing.
OR-09 Engine failure: This could happen either due to material failure, structural failure or propulsion system failure.
OR-10 Failure of combustion system: This risk could occur due to excessive fuel injection and could lead to inability to provide thrust to the aircraft.
OR-11 Damages to fuel tank: Punctures in the fuel tank could lead to functional flaws of the fuel tanks.
OR-12 Fuel leakage: Fuel leakage could appear due to fuel pipe or fuel tank damages and could lead to damages to other systems.
OR-14 Power system failure: Short circuit or sparks in the electronics might lead to failure of the whole power system of the aircraft.
OR-15 On-board computer failure: Failure of the electronics or power system could lead to failure of the on-board computer.
OR-16 Unreliable autopilot: The autopilot might be mislead by failure of instruments or bad weather and fail to perform its functions.
OR-17 Critical centre of gravity (c.g.) shift: This risk could occur both during ground operations and mid-flight. Ground c.g. shift could happen due to wrong loading of the aircraft, while mid-flight c.g. shift might be caused by movements of the fuel and payload.
OR-18 Control system malfunction: Control system failure or malfunction could be caused by failure in the control surfaces, linkages or operating mechanisms.
OR-19 Sensors and avionics failure: Due to bad weather conditions, there is a possibility that the Pitot tubes freeze and the instruments are not showing correct data.
OR-20 Unrecoverable stall during flight: Increasing the angle of attack while decreasing the velocity might lead to unrecoverable stall of the aircraft.
OR-21 HLD failure: Failure of the high lift devices could be structural (broken flap or slat) and functional (jammed flap or slat)
OR-22 Landing gear failure: Mostly during take off and landing, the landing gear damper or the tires could fail.
OR-23 Aircraft unable to steer: This risk is related to the ground operations and would follow from failures in the nose landing gear.
OR-24 Payload exceeds design margins: The risk could occur if the aircraft is loaded with excessive amount of fuel and heavy payload.
OR-26 Crash due to low visibility during flight at low altitudes: Clouds could restrict the visibility of the pilot. This, combined with instrumentation failure could lead to a severe ground impact.
OR-27 Extensive crew training: The aircraft to be designed is unconventional and new on the market, the pilots and crew would need more time to be trained.
OR-1.02 Flight display failure: During flight, there is a possibility that the displays providing flight data to the pilots fail.
OR-1.03 Increased global warming impact: Although reducing the global warming impact is part of the mission objectives of the aircraft, it is possible that competitive aircraft become better in terms of global warming impact. This would mean that the project objective is not met.
OR-1.05 Clients and users do not trust the aircraft: Passengers might not be confident enough to fly in a new aircraft and potential clients might not trust in its qualities.
OR-1.07 Aircraft produces high external noise: Due to aerodynamic configuration and engine selection the noise produced by the aircraft might be at unacceptable level.

16.1.4. End-of-Life Risks

EOLR-01 Usage of non-recyclable materials: One of the end-of-life solutions for the aircraft is to recycle some of its parts and materials. However, if non-recyclable materials are used, this would not be possible.
EOLR-03 Regulations for recycling changing: Regulations for the recycling process of aircraft can change in the future and the current design selection for recyclability would not be applicable in the future.
EOLR-05 Fuel residue: If fuel is not properly drained from the tank, it may become a fire hazard during the recycling process.
EOLR-06 Improper storage leading to non-recyclable materials: Rust may develop with improper storage in between retirement and recycle process, preventing the material to be fully recycled.
EOLR-07 Batteries still connected during recycling process: During the recycling process the batteries might get punctured and become a fire hazard.

16.2. Technical Risk Management

This section analyses the likelihood and impact of the technical risks, as shown in Table 16.1. However, only the risks with changed likelihood and impact are shown, since the severity of the other risks remains the same as before and has already been analysed [1] [2]. A risk map before mitigation is shown in Table 16.2. Mitigation plan for the most severe risks has been created, which leads to the risk map after the mitigation, as shown in Table 16.3.

Table 16.1: Technical risks (likelihood and impact classification)

Risk ID	Likelihood	Impact
DR-09	Rare - The stability derivatives have been calculated and it is confirmed that at this design stage the aircraft meets its requirements.	Serious - The requirements are not going to be met, which leads to unreliability and lack of verification of the design.
DR-2.01	Possible - The aircraft is unconventional, thus more resources have to be spent on the design and certification process.	Moderate - This does not affect the quality of the design, only the cost of the product.
OR-23	Rare - The landing gear has been designed to sustain extreme loads, thus the possibility of this risk occurring could be if the tire is flat or the strut fails structurally.	Minor - The risk does not affect performance of other systems and does not hinder the safety of the aircraft performance.
OR-27	Likely - The aircraft is new on the market and previous experience might not be enough to operate it. Pilots and crews need to undergo extensive training first before operating the aircraft.	Trivial - This would not affect the performance of the system but could cause a delay of the product on the market.
EOLR-01	Rare - For most of the aircraft carbon fibre will be used, which is proved to be recyclable [70].	Moderate - The risk will not affect the aircraft performance but will interfere with the sustainability strategy.

Table 16.2: Technical Risk map before mitigation - most severe risks are at the top right (red region), least severe risks are at the bottom left (green region)

Impact\Likelihood	Remote (1)	Rare (2)	Unlikely (3)	Possible (4)	Likely (5)
Extreme (5)	MMR-04 OR-01 OR-03 OR-15 DR-14 DR-12	OR-02 OR-05 OR-26 OR-20 OR-1.05			
Serious (4)	OR-04 OR-07 OR-10 OR-24 DR-03 DR-06	DR-04 DR-10 MMR-07 OR-09 OR-21 DR-1.02 DR-1.05 DR-05 DR-11 DR-13 DR-1.04	MMR-02 OR-12 OR-14 OR-18 DR-09 OR-06 OR-1.03 OR-1.04		
Moderate (3)	DR-07 EOLR-07 OR-1.02 DR-01	OR-11 OR-13 EOLR-05 DR-1.07 DR-1.08	OR-17 OR-22 DR-02	OR-19 EOLR-01 OR-25 DR-15 DR-1.03 DR-1.10 MMR-1.01 MMR-1.03 DR-2.01	
Minor (2)	EOLR-03 OR-1.01 DR-08	MMR-01 EOLR-06 OR-1.06	MMR-03 MMR-08 OR-23 DR-1.06 OR-1.07	EOLR-04 MMR-1.02	OR-08 DR-1.01
Trivial (1)	OR-28	MMR-09	MMR-06	MMR-05 OR-27 DR-1.09	

It can be seen that no risks are present in the red area. However, there are a lot of risks in the orange area. This means that those risks are potential threats to the project and should be managed closely. Therefore, mitigation plans have been created for some of them. The design risks that are not present anymore are mitigated by performing sensitivity analysis, verification and validation of the design.

DR-09: Mitigated by analysing the stability of the aircraft and designing a controller so that the system meets the

stability requirements.
OR-05: Mitigated by analysis of the extreme load factors and design of the structure accordingly.
OR-08: Mitigated by selection of anti-icing and de-icing systems.
OR-25: Mitigated by designing the landing gears and tires such that they can operate on iced runways.
OR-1.04: Mitigated by selecting a design with short boarding time.
EOLR-01: Mitigated by selection of materials that are recyclable.

After mitigation of the risks is performed, it can be seen on Table 16.3 that less risks are present and most of the design risks are no longer a threat for the aircraft. However, the majority of the manufacturing and maintenance and operational risks cannot be mitigated because this is a very early stage of the design.

Table 16.3: Technical Risk map after mitigation - most severe risks are at the top right (red region), least severe risks are at the bottom left (green region), mitigated risks are in bold

Impact\Likelihood	Remote (1)	Rare (2)	Unlikely (3)	Possible (4)	Likely (5)
Extreme (5)	OR-01 OR-03 OR-15	OR-02 OR-26 OR-20 OR-1.05			
Serious (4)	OR-04 OR-10 OR-24	MMR-07 OR-09 OR-21 DR-09	MMR-02 OR-12 OR-14 OR-18 OR-06 OR-1.03		
Moderate (3)	EOLR-07 OR-1.02	OR-11 EOLR-05 EOLR-01	OR-17 OR-22	OR-19 DR-1.10 MMR-1.01 MMR-1.03 DR-2.01	
Minor (2)	EOLR-03	MMR-01 EOLR-06 OR-23	MMR-03 MMR-08 OR-1.07	MMR-1.02	DR-1.01
Trivial (1)			MMR-06	MMR-05 DR-1.09	OR-27

17

RAMS ANALYSIS

This chapter provides preliminary analysis of the Reliability, Availability, Maintainability and Safety (RAMS) characteristics of the aircraft. RAMS characteristics are crucial for the aircraft, since they determine its operative cost, compatibility with airport and maintenance equipment. These four terms are defined as follows [71]:
Reliability: the probability that a system can perform its function under given conditions for a given time interval.
Availability: the probability that the system is operating satisfactorily under given conditions for a given time interval.
Maintainability: the probability that a given maintenance action, for a system under given conditions of use can be carried out within a stated time interval.
Safety: the degree to which a system is free from unacceptable risk of causing harmful effects.

The four points are analysed respectively in Section 17.1,17.2, 17.3 and 17.4.

17.1. RELIABILITY

Reliability can be considered as the degree to which the system meets its performance standards throughout its lifetime. Therefore, the reliability of the aircraft should be as close to 100% as possible, in order to satisfy the potential customers and stakeholders. The total reliability of a system can be expressed as a product of the reliability of its components, i.e. Equation 17.1.

$$R_{\text{system}} = \prod_{\text{i}=1}^{\text{n}} R_{\text{i}} \tag{17.1}$$

Reliability can also be expressed as a probability function. It is the probability that a certain failure will not occur and could be expressed with Equation 17.2.

$$R = 1 - P_{\text{f}} \tag{17.2}$$

Here, P_f is the probability of failure, which can also be presented as a cumulative distribution function, as shown in Equation 17.3.

$$P_{\text{f}} = F(t) = \int_{-\infty}^{t} f(t)\,dt \tag{17.3}$$

Weibull distribution is used because of the possibility of fine tuning the parameters to best fit the data. This implies that the reliability function becomes Equation 17.4

$$R = 1 - \int_{-\infty}^{t} f(t)\,dt = 1 - (1 - e^{-\frac{\text{t}}{\eta}\cdot\beta}) = e^{-\frac{\text{t}}{\eta}\cdot\beta} \tag{17.4}$$

where x is the time interval and η and β are the Weibull parameters. Since those parameters are usually obtained from statistics, it is impossible to estimate them at this stage of the design because there are no commercial blended wing bodies flying. However, statistical data for the separate components of the aircraft can be taken from existing aircraft in order to come up with an initial guess for the reliability of the whole aircraft. The data is taken for small aircraft and scaled in terms of MTOW and complexity of each system [72]. A fault tree as shown in Figure 17.1 and Figure 17.2 are used to determine the components that could possibly fail and the most critical failure modes. The main failures which have the worst effect on the aircraft performance are coloured in red, the ones with lower effect are in yellow and the ones with least effect on the performance are in green.

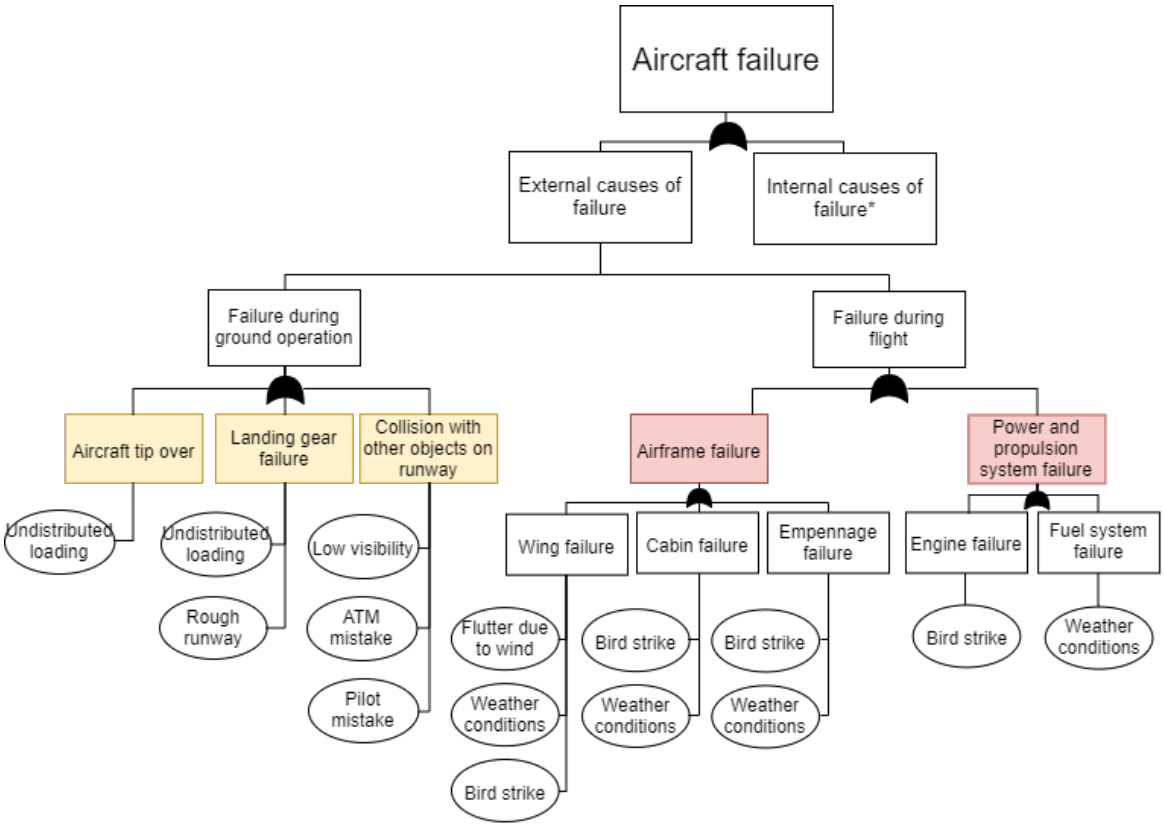

Figure 17.1: Aircraft Fault Tree (External causes to failure)

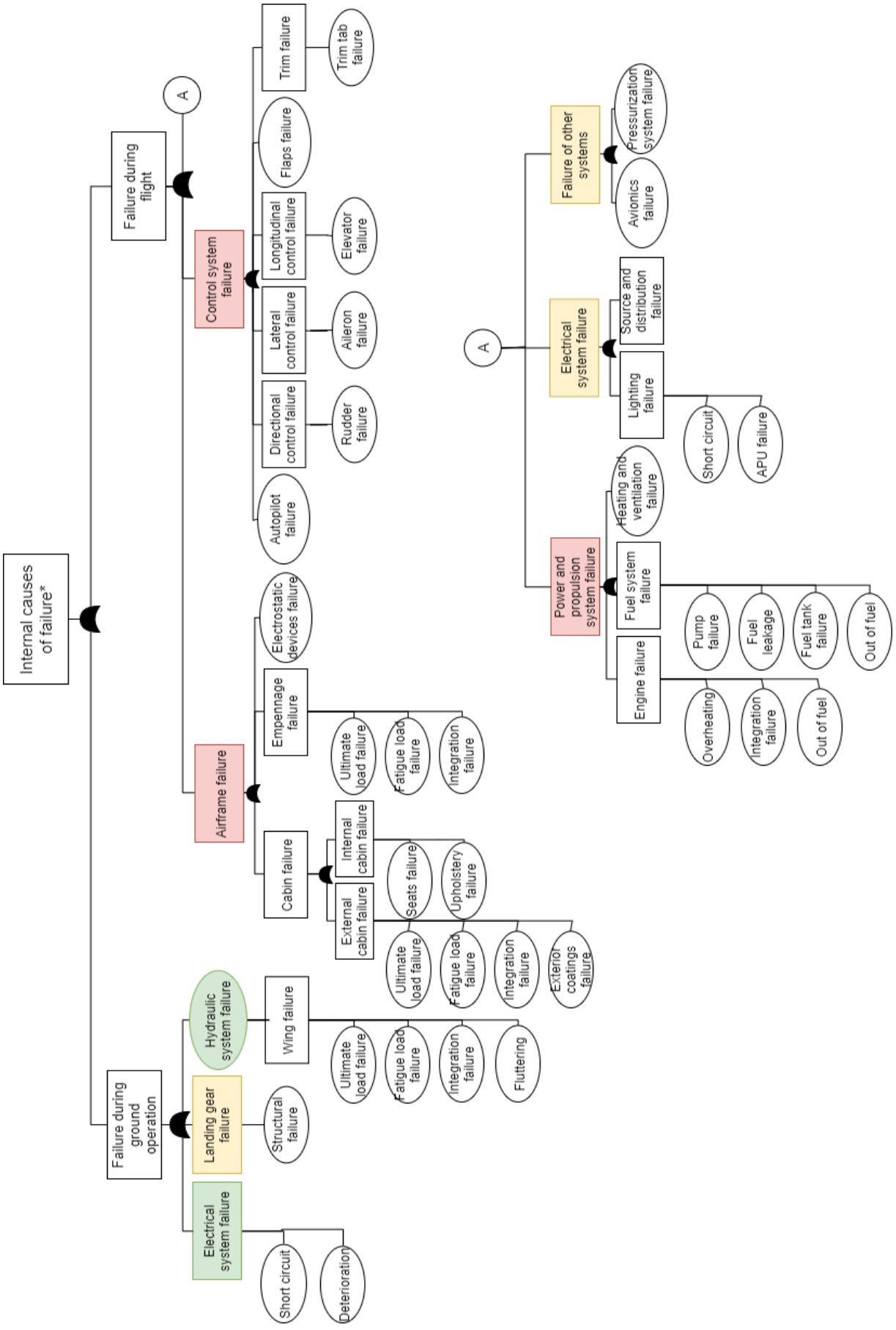

Figure 17.2: Aircraft Fault Tree (Internal causes to failure)

It can be seen that the aircraft could fail due to external or internal reasons. External failure rates could not be predicted but it can be seen that the most critical external causes of failure are bad weather conditions and bird strike, while the most critical external failure modes are airframe failure and propulsion system failure. In terms of internal failure causes, the most critical systems are airframe, propulsion and control. This is because of the specific integration of the wing and fuselage of the blended wing body. Furthermore, the engines are installed on top of the fuselage and in case of engine failure, they could cause damages to the fuselage. Finally, failure of the control system is critical because the aircraft could become unstable due to its shape, engines installed in the back and CG shift.

Table 17.1 shows the Weibull parameter estimation of the components of the aircraft that could fail and the corresponding hazard rate and reliability, with the hazard rate computed using Equation 17.5 and reliability computed per flight hour using Equation 17.2.

$$\lambda = \left(\frac{\beta}{\eta}\right) \cdot \left(\frac{t}{\eta}\right)^{\beta-1} \tag{17.5}$$

Table 17.1: Reliability of aircraft components

Type of failure	**Eta (η)**	**Beta (β)**	**t**	**Reliability**	**Hazard rate**
Airframe					
Electrostatic devices	1917.0	0.86	1	0.9996	1.29E-03
Empennage	1637.1	0.39	1	0.9998	2.18E-02
Cabin	1265.3	0.29	1	0.9998	3.65E-02
Exterior coatings	602.4	0.37	1	0.9994	3.46E-02
Seats	1470.1	0.66	1	0.9996	5.36E-03
Upholstery	864.3	0.36	1	0.9996	3.16E-02
Wing	1383.2	0.61	1	0.9996	7.40E-03
Aircraft Control System					
Autopilot	N.A.	N.A.	N.A.	N.A.	N.A.
Directional	4729.0	1.85	1	0.9996	2.94E-07
Longitudinal	1535.6	0.41	1	0.9997	2.02E-02
Lateral	1901.9	0.59	1	0.9997	6.86E-03
Slats	1287.6	0.25	1	0.9998	4.17E-02
Trim	869.7	0.19	1	0.9998	5.25E-02
Hydraulic	3977.4	1.14	1	0.9997	8.98E-05
Landing gear	2405.1	0.92	1	0.9996	7.13E-04
Steering	5763.2	1.65	1	0.9997	1.03E-06
Lighting	1130.3	0.33	1	0.9997	3.24E-02
Source and distribution	997.3	0.33	1	0.9997	3.38E-02
Powerplant					
Engines	6968.2	1.58	1	0.9998	1.34E-06
Fuel	1033.6	0.29	1	0.9997	3.87E-02
Heating and ventilation	844.2	0.32	1	0.9996	3.7E-02
Other systems					
Avionics	N.A.	N.A.	N.A.	N.A.	N.A.
Pressurisation	N.A.	N.A.	N.A.	N.A.	N.A.
Total				**≈ 0.9933**	**≈ 4.03E-01**

Most of the systems are similar to existing aircraft systems and would therefore be with similar reliability. However, due to the complex wing-fuselage integration, the reliability of the airframe would be lower. Moreover, the blended wing body concept has never been used in commercial aviation before, which means that the airframe would be more prone to begin-of-life failures, if not designed and manufactured properly. Values for pressurisation system, autopilot and avionics have not been found but since the total reliability is a product of all single reliability values, the failure of other systems would only decrease the reliability. Furthermore, the reliability also depends on maintenance policies applied by the airlines, i.e. if the aircraft is monitored and maintained often and correctly, less failures would occur, thus reducing the probability of failure and increasing the reliability. It should be noted that the reliability of the aircraft is less for longer flights because of the large effect of the flight time (see Equation 17.4).

17.2. AVAILABILITY

Availability is essentially the time for which the aircraft is available to perform its mission. It can be quantified using Equation 17.6, where MTTF is the mean time to failure or up-time and MTTR is the mean time to repair or downtime.

$$\text{Availability} = \frac{\text{MTTF}}{\text{MTTR} + \text{MTTF}} \tag{17.6}$$

In order to increase availability, the MTTF has to be increased and the MTTR has to be increased. This can be achieved by optimising the preventive maintenance, which is especially important for this aircraft, since availability of spare parts, especially structural parts, is going to be low, at least in the beginning. Moreover, replacement of engines is harder than for conventional aircraft with engines below the wings. This is why it is recommended that regular checks and preventive maintenance is performed more often than in tube and wing aircraft.

17.3. MAINTAINABILITY

Maintenance of an aircraft includes all the actions required to maintain the aircraft in serviceable condition. These actions might include monitoring, scheduled maintenance and repair. They can be split into 3 main categories - line maintenance, base maintenance and component maintenance.

Line maintenance prepares the aircraft for daily flights and includes daily checks, pre-flight checks and small scheduled maintenance tasks. It is used for trouble shooting, component replacement and minor repairs. Line maintenance for the Blended Wing Body would differ from conventional tube and wing aircraft mainly because of the engine placement. The wing has panel doors on the bottom surface of section 2 (3.5 m from ground) and section 3 (4.7 m from ground), such that both internal and external structural inspection can be performed. The APU is placed in section 2 of the left wing, next to the landing gear bay and can be accessed through the landing gear bay. Moreover, the avionics bay is in section 1, to the right of the cargo bay, such that the line replacement unit can be accessed and replaced through a panel door on the bottom of the fuselage. There are two electronic bays, one on each side of the cargo compartment, also accessed through panel doors. However, there are systems that could cause maintenance complications and delays such as propulsion system and pitch damping system. The aircraft has a pitch damping system which means that there are additional actuators that have to be maintained. This could cause slower maintenance and thus increase the maintenance cost. Furthermore, the engines are placed on top of the fuselage between the two vertical tails, which makes them less accessible compared to tube and wing aircraft. If an engine is to be inspected, one has to climb on top of the fuselage using a ladder and walk towards the engine. If it has to be replaced, however, cranes are required in order to lift it. This means that if an engine has to be replaced and a crane is not available, the maintenance cost and downtime would increase, which would affect availability of the aircraft, according to Equation 17.6.

The logistic delay that could occur due to limited resources is dependent on spare part unavailability, mobilisation time, transport unavailability, maintenance crew unavailability and maintenance equipment unavailability. As can be seen in Equation 17.7, it is the sum of all the delay times due to the each unavailability, multiplied by the probability of the delay happening [71].

$$\begin{aligned} D_{\text{logistic}} = T_{\text{spare..part}} \cdot P_{\text{delay}} + T_{\text{mobilisation..time}} \cdot P_{\text{delay}} + T_{\text{transport..availability}} \cdot P_{\text{delay}} + \\ T_{\text{crew..availability}} \cdot P_{\text{delay}} + T_{\text{equipment..availability}} \cdot P_{\text{delay}} \end{aligned} \tag{17.7}$$

Therefore, the higher the probability of equipment availability to replace or repair a part, the longer the logistic delay and therefore longer downtime for the whole aircraft. This means that if the aircraft needs an engine replacement at airport where no cranes are available, the logistic delay is going to increase, which will then cause lost of revenue due to unavailable aircraft.

Base maintenance is more extensive and is performed less frequently. It includes airframe, engines and systems deterioration checks, removal of defects, implementation of new technology, repainting and cabin reconfiguration. Airframe is easily accessible on bottom of the planform and on the inside of the wing section because it has panel doors. However, the top part of the planform has to be inspected by walking on top of the aircraft. The landing gears could be easily removed and replaced, the tails are also accessible. As mentioned before, engines should be inspected by walking on top of the fuselage and opening the cowling.

Component maintenance is maintenance of the components after they are removed from the aircraft. This includes engines, APU, seats, etc. The aircraft does not have any specific unconventional systems that have to be treated dif-

ferently than those of tube and wing aircraft. Therefore, all components are compatible with maintenance equipment and component maintenance is not the most critical for this aircraft.

17.4. SAFETY

Safety is one of the most important features of an aircraft. The aircraft has to provide safety to all the crew, passengers and maintenance workers during its operations, therefore safety standards and requirements as set by CS25 have to be complied to. The aircraft has to be safe in multiple categories. According to accidents and incidents reports [1], most safety issues occur due to air ground communications, airspace infringement, wildlife strike, controlled flight into terrain, fire, ground operations, airworthiness, level bust, loss of control, loss of separation, runway excursion and incursion, wake vortex turbulence, weather conditions, emergency evacuations and human factor. The aircraft does not differ much from tube and wing aircraft for most of the causes of safety issues. However, it has specific design features which could affect the safety during the following scenarios:

- Wildlife strike: The aircraft has no windows in the cabin, except for cockpit windows, which will improve the safety due to wildlife strikes because the skin panels are stronger than windows.
- Fire: Due to the engine location, a potential engine fire could spread along the fuselage and cause damage to the cabin. Moreover, if an engine fire occurs on ground, it would be harder for firefighters to reach the engines, because they are not close to the ground. However, the engine location decreases the probability of wing fire. Furthermore, a fire in the cargo compartment could cause electronics or avionics failure. This can be assessed with fire proof walls of the cargo compartment.
- Emergency evacuations: The aircraft has four aisles and eight emergency exits in the front of the cabin, which will make the emergency evacuation faster than in conventional aircraft. However, the emergency exits are all placed in the front of the aircraft which will cause the evacuation to be more chaotic. Therefore, a recommendation for operation is to train the crew members such that they organise equal flow of people to each door in case of an emergency situation.

[1] Accident and Serious Incident Reports: WX, Acessed January 2020, https://www.skybrary.aero/index.php/Accident_and_Serious_Incident_Reports:_WX

18

Final Concept Design

In this chapter the final concept design is presented. The requirement's compliance matrix is analysed in Section 18.1 and the final configuration is summed up in Section 18.2.

18.1. Compliance Matrix

After the final concept is completed, the requirements need to be checked again whether they are achieved. The list of requirements are compiled in Table 18.1 to show the compliance matrix and in respective section the subject is discussed.

18.2. Final Concept Configuration

After 10 weeks of designing process, the concept configuration is finalised. Not only does the design needs to be functional, but it has to be feasible as well.

18.2.1. Feasibility

Since the start of the blended wing body concept, multiple disadvantages have been exposed. The FB400 has faced and overcome these challenges. In the next sections, the individual feasibility problems are stated and answered by the FB400.

In order to fit in the current air transport structure, the design has to be compatible with airports. The FB400 has a wing span of 65 m which allows for compatibility with a type V gate. Moreover, the passenger doors allow for quick boarding and the cargo doors are accessible for the ground handling. Numerous foldable chairs are included in the cabin which results in a faster time for cleaning the aircraft.

It is difficult to place a landing gear on a blended wing body which allows for take-off and landing rotation, yet also for the weight distribution over the nose and main landing gear. Furthermore, the wing tip clearance had to be taken into account. However, the FB400 has a landing gear that fulfils all the requirements. The loads on the nose gear are high enough to allow for steering, but low enough to withstand the forces introduced into the structure.

The main reason for the expected increase in structural weight is because the pressurised section is not circular anymore. The fuselage is more oval shaped, which will introduce higher stresses because of the larger radii of the circles. The FB400 limited this weight by keeping a relatively low radii, meaning the fuselage will get more round. The influence on aerodynamic performance is minor since the lift over drag ratio barely changes.

There is no room on the side of the cabin for emergency exits since this is where the wing is located. Some creativity was needed to locate the exits. Since the economy class has 4 aisles, there is enough room for everyone to move forward to the front of the aircraft, where 8 emergency exits are located. Furthermore, there are multiple exit possibilities for the same seat. Therefore, it is expected that the evacuation time is comparable to conventional aircraft.

Since a blended wing body does not have a tail, it is difficult to trim during flight. Large deflection angles of the elevator might be required for cruise flight [14]. However, the centre of gravity of the FB400 is located as close as possible to the neutral point to limit the elevator deflections. Also the travel of the centre of gravity during flight is limited, to minimise the elevator deflection and thus drag.

In his thesis, Brown assumes a constant centre of gravity when making minor changes to the wing during the iterations. During the iterations of the FB400, the centre of gravity is updated constantly to the millimetre. This resulted in accurate results for stability and control.

Regarding passenger comfort, there are two main concerns - limited numbers of windows and high roll rates on

Table 18.1: Requirement compliance matrix

Identifier	Requirement	Compliance	Ref. Section
Structural			
HCSR-STR-001	The cabin shall be pressurised to 8,000 ft pressure altitude at maximum flight altitude	Fuselage strength	Subsection 8.9.4
HCSR-STR-002	Wing span shall be smaller than 65 m to conform to type V gate dimensions	64.8m	Subsection 8.3.2
HCSR-STR-003	Tail height shall be smaller than 20.1 m to conform to type V gate dimensions.	12.1m	Section 18.2
HCSR-STR-004	Business class seats shall have a 36" pitch	Implemented	Section 8.2
HCSR-STR-005	Business class seats shall have a 21" width	Implemented	Section 8.2
HCSR-STR-006	Economy class seats shall have a 32" pitch	Implemented	Section 8.2
HCSR-STR-007	Economy class seats shall have a 18" width	Implemented	Section 8.2
HCSR-STR-008	The aircraft shall fit in a A380 hangar of 180m x 140m x 27.5 m	64.8m x 42.9m x 12.1m	Section 18.2
HCSR-STR-009	Aircraft cargo compartments shall allow storage of at least 5 cubic feet of luggage per passenger	>5	Section 8.2
HCSR-STR-010	The pilot overnose angle shall be at least 11 degrees	22 deg	Subsection 8.2.7
HCSR-STR-011	The pilot overside angle shall be at least 35 degrees	20 deg	Subsection 8.2.7
HCSR-STR-012	The aircraft systems shall fit into the aircraft	Designs fit	Chapter 13
HCSR-STR-013	All passengers and crew shall fit and be seated in the aircraft	Seats placed	Section 8.2
HCSR-STR-014	The required volume of fuel shall fit inside the tanks	Done	Subsection 8.9.1
HCSR-STR-015	The passenger cargo shall fit inside the cargo hold	Done	Section 8.2
Performance			
HCSR-PER-001	The aircraft shall be able to take-off from a runway with dry pavement (sea level ISA+15 degrees C) with a balanced field length of 9000 feet at maximum take-off weight accoriding to FAA 14 CFR part 25	Done	Section 8.3
HCSR-PER-002	The aircraft shall be able to land on a runway with dry pavement (sea level ISA +15 degrees C) at the end of the design range mission	Done	Section 8.3
HCSR-PER-003	The maximum approach speed shall be 145 kts at the end of the design range mission	Done	Section 8.8
HCSR-PER-004	The aircraft shall have a parking brake	Done	Chapter 13
HCSR-PER-006	For a mission range of 700 nmi the aircraft shall have a flight time of under 2 hours 15 minutes under no wind conditions	Done	Chapter 9
HCSR-PER-007	The engines shall have a specific fuel consumption (SFC) lower than 0.6	Done	Chapter 13
HCSR-PER-008	In the landing configuration, the steady gradient of climb may not be less than 3.2 percent	Done	Section 8.3
HCSR-PER-009	With one engine inoperative take off and landing gear retracted, The steady gradient of climb may not be less than 2.4 percent for two-engine aircraft	Done	Chapter 8
HCSR-PER-010	Take-off distance shall be the distance greater between the OEI take off length, the accelerate-stop distance and 115 % of the take off distance when all engines operatives	Done	Chapter 8
HCSR-PER-011	The positive limit manoeuvring load factor n for any speed up to Vn shall not be less than 2.1 + 24,000/ (W + 10,000) except that n may not be less than 2.5 and need not be greater than 3.8 - where W is the design maximum takeoff weight	Done	Section 8.9
HCSR-PER-012	The negative limit manoeuvring load factor shall not be less than -1.0 at speeds up to VC	Done	Section 8.9
HCSR-PER-013	If wing flaps are to be used during takeoff, approach, or landing the resulting limit load factor shall not exceed +2.0	Not applicable	No flaps
HCSR-PER-014	Reference stall speed, VSR shall not be less than than 1-g stall speed	Done	Section 8.3
Operation			
HCSR-OPR-001	The aircraft shall fit 400 passengers	Done	Section 8.2
HCSR-OPR-002	Business class shall fit 50 passengers	Done	Section 8.2
HCSR-OPR-003	Economy shall fit 350 passengers	Done	Section 8.2
HCSR-OPR-004	The aircraft's Entry into Service shall be 2029	Done	Section 14.1
HCSR-OPR-005	The aircraft shall have a turnaround time of less than 1h45m	Done	Chapter 11
HCSR-OPR-006	The aircraft crew shall consist of 2 pilots and 8 cabin attendants	Done	Chapter 11
HCSR-OPR-007	Aircraft fuselage shall have at least two type A doors available for standard boarding operations.	Done	Chapter 11
HCSR-OPR-008	If a Type A, Type B, or Type C exit is installed, there shall be at least two Type C or larger exits in each side of the fuselage.	Done	Section 8.2
HCSR-OPR-009	Emergency exits at each side of the aircraft shall include at least two Type I exits or larger	Done	Section 8.2
HCSR-OPR-010	For the maximum number of passengers in the aircraft, the amount and type of emergency exits shall be installed complying with part 25.807 of 14 CFR part 25	Done	Section 8.2
HCSR-OPR-011	At any point between seats, the passenger aisle width more than 63.5 cm above floor shall be at least 50.8 cm and the passenger aisle with less than 63.5 cm above floor shall be at least 38.1 cm	Done	Section 8.2
HCSR-OPR-012	For any passenger seat in the cabin, their shall be no more than two adjacent seats between seat and a cabin aisle	Done	Section 8.2
HCSR-OPR-013	In case of emergency, all passengers (in full capacity) and number crew members shall be evacuated from the aircraft to the ground within 90 seconds	Done	Section 8.2
HCSR-OPR-014	Aircraft's dimension and layout shall be compatible with the gate V ground servicing equipment with sufficient clearance and distance for ground operation	Done	Subsection 18.2.2
HCSR-OPR-015	The aircraft shall have at least one accessible lavatory	Done	Section 8.2
Stability and Control			
HCSR-SCR-001	The aircraft shall have level 1 handling qualities when all systems are in their normal operating state; level 2 flying qualities after failures occurring approximately once during the aircraft's lifetime; level 3 flying qualities after rare failures	Done	Chapter 10
HCSR-SCR-002	The time to achieve 30 deg bank angle shall be less than 1.5 sec	Done	Subsection 8.7.1
HCSR-SCR-003	Longitudinal control force for prolonged application shall be less than 10 lbs	Done	Subsection 8.7.2
HCSR-SCR-004	The aircraft shall have stable longitudinal eigenmotions	Done	Chapter 10
HCSR-SCR-005	The aircraft shall have stable dutch roll mode characteristics	Done	Chapter 10
Sustainability			
HCSR-NF-SUS-001	The aircraft shall allow for segregated waste stowage on board	Done	Chapter 13
HCSR-NF-SUS-003	Noise level shall comply with the ICAO chapter 4 standards	Done	Section 12.5

blended wing bodies. The latter is a bigger concern for the passengers seated far away form the centre line. The lack of windows has been solved by projecting the outside views on the walls of the cabin. Furthermore, the emergency exits will have small windows, so the possibility to look outside still exists during cruise. The roll rates have been tackled with the use of inboard ailerons. The ailerons have been designed for a roll rate of 30 degrees in 1.5 seconds, however this is only used in emergency situations. During nominal flight, the FB400's roll rates are limited to give the passengers the same experience as they would have in a conventional aircraft.

One of the reasons why a large company like Boeing or Airbus has not switched its production line to blended wing

bodies is because the current solution of aircraft works. It is expensive to change the whole production line for a totally new design. However, if a new company is started, it is worth the risk because there is simply no plan B of the old conventional design. All the development and manufacturing processes have to be set up anyways, so there is less negative impact of setting it up for a different type of aircraft.

The fuel prices are expected to rise over the next years. This is not a feasibility problem for the blended wing body, but it is an extra reason why the FB400 will fit in the market. The aerospace industry is searching for fuel efficient designs. The FB400 shows a low fuel weight for a reference mission of 700 nmi, meaning the direct operational costs are low.

18.2.2. DESIGN

After the design has been finished, the most important and driving dimensions of the aircraft are determined and a three-view drawing is created.

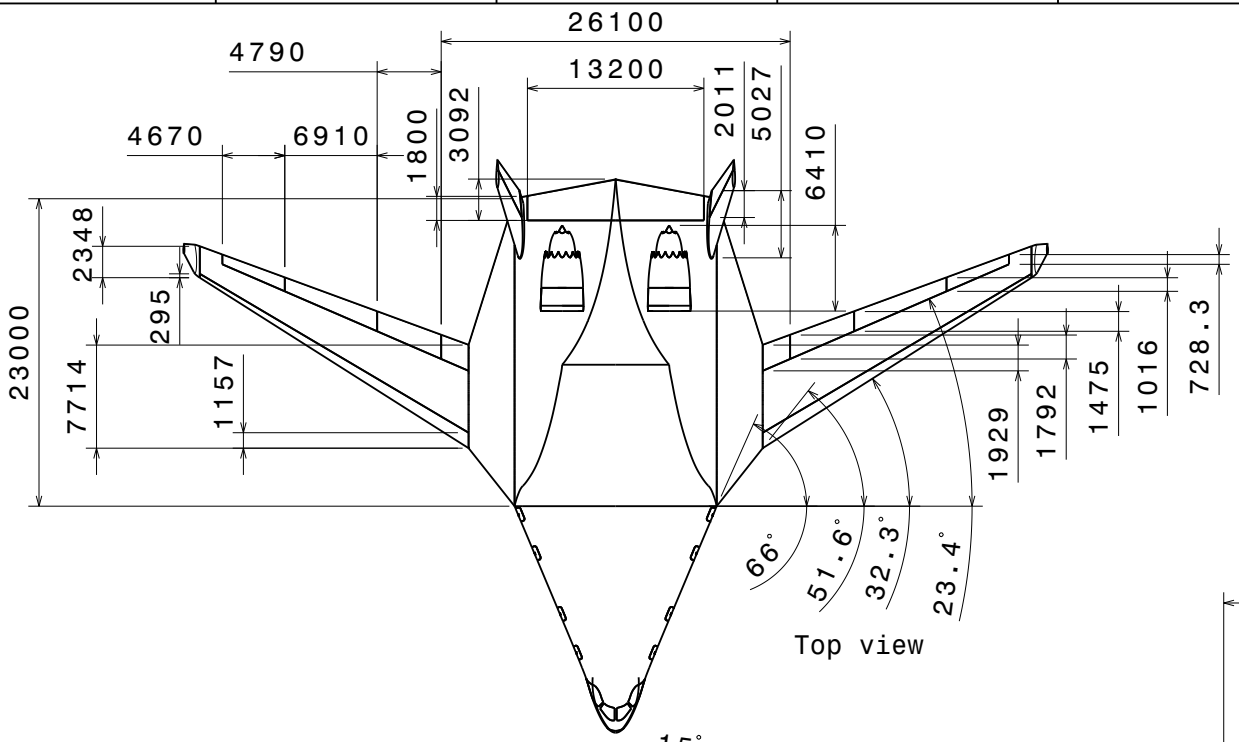

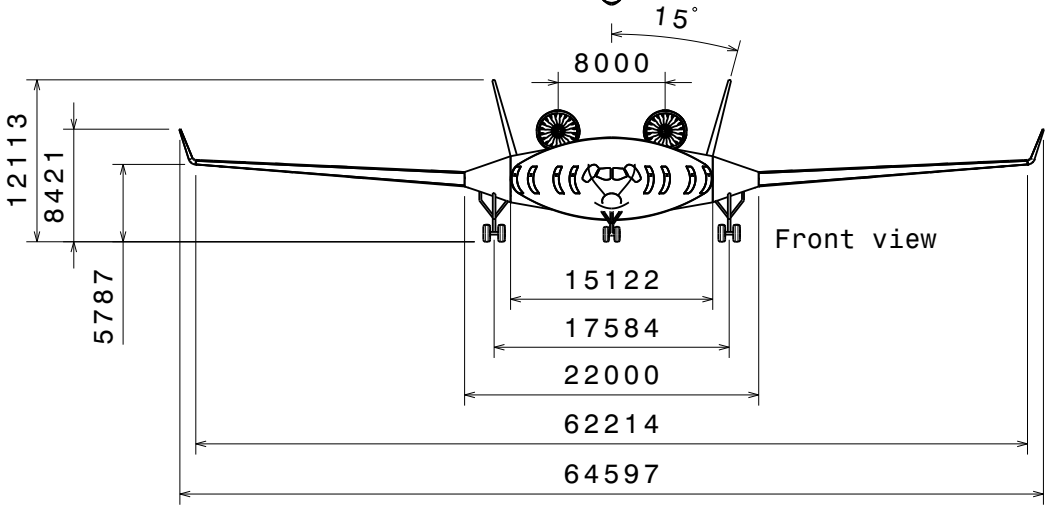

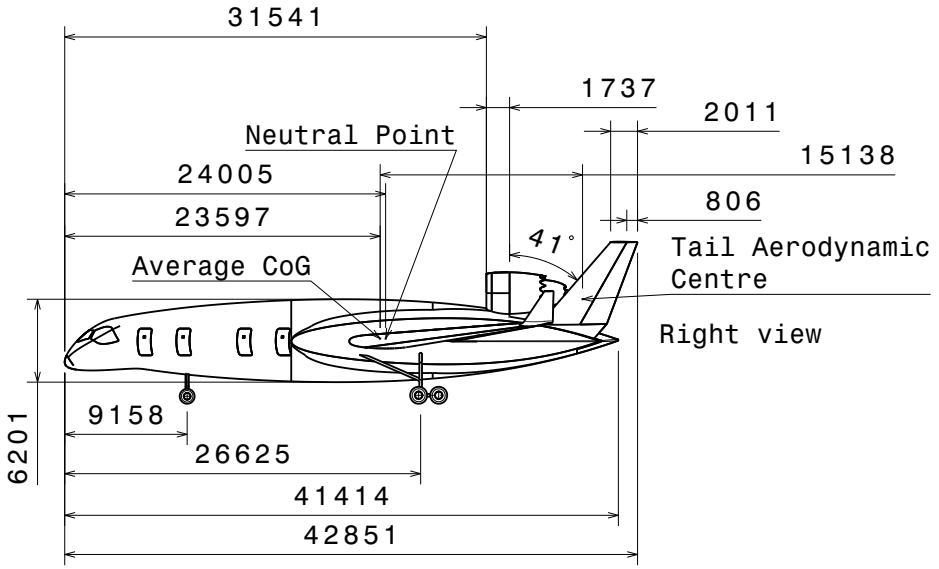

DASSAULT SYSTEMES

DRAWN BY	J Holtermann	DATE	28.01.2020	DRAWING TITLE	FB 400 Overview
CHECKED BY	R Vos	DATE	28.01.2020	SIZE: A3	DRAWING NUMBER: HCSRTA-BWB-MainAssembly
DESIGNED BY	Group 4	DATE	28.01.2020	REV: A	
SCALE 1:400				SHEET 1/1	

19

Conclusion and Recommendations

In this chapter the report is concluded in Section 19.1 and further design recommendations are stated in Section 19.2.

19.1. Conclusion

The project objective was to design an aircraft that is able to carry 400 passengers over a 3,500 nmi range. Furthermore, the design should minimise global warming impact, the operating cost and the recurring cost on a reference mission of 700 nmi. This resulted in the FB400, a Blended Wing Body aircraft with two GEnx-1b70 engines mounted on top of the fuselage and a large open cabin area with a 2-class configuration.

In order to reach the design objectives while still complying with regulations some key design features were implemented. The emergency exits are all located in the front of the cabin to allow direct access to the outside and easy coordination in case of evacuation. The cabin was structurally designed based on the method of Hoogreef [34], resulting in a large open section to allow for freedom in passenger configurations. The mobile services of the FB400 consist of slats on the leading edge to increase the maximum lift coefficient and multiple elevons on the trailing edge for control of the aircraft. It also has two vertical fins with rudders next to the engines for directional stability and control.

The FB400 design shows that it can perform the reference mission of 700 nmi with a 56% better specific air range than an Airbus a320, which is an aircraft that is typically used on a mission 700 nmi mission. Compared to an aircraft with the same passenger capacity like the Airbus a330 it shows a 51% better specific air range. This efficiency is reached by having a much lower operating empty weight and better aerodynamic performance than conventional tube and wing aircraft. Having a low specific air range also has a positive effect on the global warming impact of the aircraft. To further reduce the global warming impact some manufacturing methods and end of life solutions have been analysed. Although not being a top level design objective the FB400 also shows improvements in noise levels compared to conventional aircraft. This is a result of positioning of the engines on top of the fuselage and in between the vertical tails. Furthermore, the lack of flaps and horizontal tail surfaces can be shown to reduce noise levels as well.

From the financial analysis the direct operating cost, the recurring cost and the unit cost have been estimated to be 89.6 dollar/nautical mile, 334 million dollar and 283 million dollar respectively based on a 700 nmi mission. Furthermore it has been shown that there is a gap in the market with the capacity of 400 passengers and a design range of 3,500 nmi.

To conclude, the FB400 design has shown to be able to compete with the current commercial aircraft by reducing fuel consumption, while still being compatible with existing airports and comply with regulations. It has shown to be a good choice to alleviate airport congestion with a fast turn-around time. Moreover, reflecting on the requirements that have been set at the start of the design, it can be concluded that all requirements have been met.

The next steps in the design process would consist of doing a more detailed aerodynamic analysis based on CFD and using finite element methods to design the individual structural components. To test the aerodynamic performance and to check the controllability of the aircraft, small scale models should be made. This is followed by the detailed design phase, in which all the parts should be able to be manufactured and tested. This is followed by assembly and full scale testing of the aircraft. Finally, in 2029 the first aircraft should go into service.

19.2. Recommendations

As this is just a preliminary design, certain improvements have to be made for a final design. Below are listed the proposed recommendations.

- A detailed estimation of the fuel weight shall be made.
- A more sophisticated stability and control analysis should be done using CFD modelling and wind tunnel test-

ing as AVL is not accurate enough for a detailed design.

- A more detailed estimation of the aircraft moments of inertia should be made.
- The aircraft high lift devices and control surfaces are over designed at the moment and should be optimised.
- The analysis is lacking an analysis on the loads on the nose gear due to the deployment of thrust reversers upon landing.
- A detailed analysis on the accessibility points for ground handling should be performed for operations.
- A more accurate lay-out of the aircraft should be drawn including the positioning of all the systems.
- A more extensive analysis on the actual rudder surface required should be performed.
- The structure is over-designed because the ribs are not optimised. For future development of the design, analyse the buckling conditions and optimise the structure.
- Landing gear struts and retraction mechanisms should be designed in the future development of the design.
- The actual noise that the FB400 produces should be measured using an actual model.
- Emergency exits are not optimally positioned in the current design. An improvement could be a smart solution to put emergency exits on the rear part of the cabin. This will improve evacuation time and safety characteristics.
- Estimation of the evacuation time would be beneficial for certification procedures. This could be done by creating a simulation of the flow during evacuation procedure and estimating the evacuation time.
- The cockpit needs to be redesigned such that it becomes longer and the over-nose angle is increased, the cockpit windows should also be increased. Packaging with radar should be considered.
- In the stability analysis of the trim conditions, the thrust force should be considered in order to account for the pitch down moment created by the engines.
- The fuel economy of the aircraft should be measured.
- More detailed analysis of wing structure could be done as the current analysis underestimates the wingbox weight as in reality the wingbox structure follows the contour of the airfoil.
- Global warming impact could be reduced even more if the aircraft is designed to fly at lower altitude. However, note that this will negatively affect the aeropropulsive performance of the aircraft.

BIBLIOGRAPHY

[1] DSE Group 4. *High Capacity Short Range Transport Aircraft - Baseline Report Fall DSE 2019*. Tech. rep. TU Delft, 2019.

[2] DSE Group 4. *High Capacity Short Range Transport Aircraft - Mid-Term Report Fall DSE 2019*. Tech. rep. TU Delft, 2019.

[3] Moshe Givoni and Piet Rietveld. *Choice of Aircraft Size - Explanations and Implications*. Discussion Paper. 2006.

[4] Jan Roskam. *Airplane Design: Part I-VIII*. Roskam Aviation and Engineering Corporation, 1990.

[5] R.J. Hamann and M.J.L. van Tooren. *Systems Engineering & Technical Management Techniques*. AE3-S01 Lecture Notes. 2019.

[6] J. Sinke. *Lean Manufacturing*. Lecture Slides. Delft University of Technology, 2019.

[7] et al Asselman B. *Final Report - Bigger is Better*. Tech. rep. Delft University of Technology, 2019.

[8] Rick LeBlanc. "Airplane Recycling and Value Extraction". In: *URL: https://www. thebalance. com/airplane-recycling-and-value-extraction-2877922* (2016).

[9] Alma van Oudheusden. "Recycling of composite materials". In: (2019).

[10] Ankit Kumar Pandey et al. "Sustainable manufacturing process for recycling of aluminum alloy waste into direct product by high-pressure torsion process". In: *Materials Today: Proceedings* 18 (2019), pp. 3099–3108.

[11] M. Damen. *Introduction to Airplane Certification*. 2014.

[12] *X-48 Hybrid/Blended Wing Body*. National Aeronautics and Space Administration, 2012.

[13] Roelof Vos and Joris Melkert. *Wing and Propulsion System Design*. Lecture Slides. Delft University of Technology, Delft, 2016.

[14] M.T.H. Brown. "Conceptual Design of Blended Wing Body Airliners". MA thesis. Delft University of Technology, 2017.

[15] R. Vos, Francois Geuskens, and Maurice Hoogreef. "A New Structural Design Concept for Blended Wing Body Cabins". In: Apr. 2012. DOI: 10.2514/6.2012-1998.

[16] Roelof Vos and Joris Melkert. *The Design of the Fuselage*. Lecture Slides. Delft University of Technology, Delft, 2018.

[17] American Institute of Aeronautics and Astronautics. *Undergraduate Team Aircraft Design Competition*. Accessed November 2019. URL: https://www.aiaa.org/get-involved/students-educators/Design-Competitions.

[18] R Vos and J.A Melkert. *The Design of the Fuselage*. Lecture Slides. Delft University of Technology, Delft, 2018.

[19] Daniel P. Raymer. *Aircraft Design: A Conceptual Approach*. American Institute of Aeronautics and Astronautics, Inc., Washington, DC, 1992.

[20] P.Krammer D. Scholtz O. Junker. *AIRCRAFT DESIGN FOR LOW COST GROUND HANDLING - THE FINAL RESULTS OF THE ALOHA PROJECT*. Tech. rep. Aero - Aircraft Design and Systems Group, Hamburg University of Applied Sciences, Hamburg, Germany, 2010.

[21] D. William Conner and Ira D. Jacobson. "Passenger Ride Comfort Technology For Transport Aircraft Situations". In: *NASA TECHNICAL MEMORANDUM* (1976).

[22] Egbert Torenbeek. *Synthesis of Subsonic Airplane Design*. Delft University Press, Delft, The Netherlands., 1982.

[23] B.R. Pascual. "Engine-Airframe Integration for the Flying V". MA thesis. Delft University of Technology, 2018.

[24] R Vos and J.A Melkert. *Landing gear and Empennage design*. Lecture Slides. Delft University of Technology, Delft, 2016.

[25] O. Fabrizio. *Aircraft aerodynamic analysis – Mobile surfaces of the wing*. Lecture Slides. Delft University of Technology, 2016.

[26] Fabrizio Oliviero. *Aircraft Aerodynamics Analysis - Fundamentals*. Lecture slides. 2017.

[27] Malcom Brown and Roelof Vos. "Conceptual Design and Evaluation of Blended-Wing Body Aircraft". In: *2018 AIAA Aerospace Sciences Meeting*. DOI: 10.2514/6.2018-0522.

[28] Joris Melkert and Calvin Rans. *AE2135-I Structural Analysis & Design*. Lecture Slides. 2017.

[29] K.n. Arunkumar, N. Lohith, and B.b. Ganesha. "Effect of Ribs and Stringer Spacings on the Weight of Aircraft Structure for Aluminum Material". In: *Journal of Applied Sciences* 12.10 (2012), pp. 1006–1012. DOI: 10.3923/jas.2012.1006.1012.

[30] A. Elham and M. J. van Tooren. "Tool for preliminary structural sizing, weight estimation, and aeroelastic optimization of lifting surfaces*". In: *Proceedings of the Institution of Mechanical Engineers, Part G: Journal of Aerospace Engineering, 230(2), 280–295* (2016).

[31] Markus Kaufmann, Dan Zenkert, and Per Wennhage. "Integrated cost/weight optimization of aircraft structures". In: *Structural and Multidisciplinary Optimization* 41.2 (2010), pp. 325–334.

[32] X Tan et al. "Cost-efficient materials in aerospace: Composite vs aluminium". In: *Collaborative Product and Service Life Cycle Management for a Sustainable World*. Springer, 2008, pp. 259–266.

[33] K. Stanford Bret and K. Dunning Peter. *Optimal Topology of Aircraft Rib and Spar Structures under Aeroelastic Loads*. URL: https://ntrs.nasa.gov/archive/nasa/casi.ntrs.nasa.gov/20140007307.pdf.

[34] M.F.M. et al Hoogreef. *A New Structural Design Concept for Blended Wing Body Cabins*. Tech. rep. Kluyverweg 1, 2629HS Delft, the Netherlands: Delft University of Technology, 2012.

[35] Inc. Desktop Aeronautics. *Aircraft Design: Synthesis and Analysis*. Accessed January 2020. 2001. URL: http://rahauav.com/Library/Design-performance/Aircraft%5C%20Design,%5C%20synthesis%5C%20and%5C%20analysis.pdf.

[36] D. Howe. *Blended wing body airframe mass prediction*. Tech. rep. Cranfield, Bedfordshire, UK: College of Aeronautics, Cranfield University, 2001.

[37] R. Vos, J.A. Melkert, and B.T.C. Zandbergen. *Analysis of aircraft configurations*. AE1222-II Lecture slides, Delft University of Technology. 2016.

[38] Tilbe Mutluay. "The Development of an Inertia Estimation Method to Support Handling Quality Assessment". MA thesis. Delft University of Technology, 2015.

[39] J.A. Mulder et al. *Flight Dynamics, Lecture Notes AE3202*. TU Delft, 2013.

[40] David J. Moorhouse and Robert J. Woodcock. *Background Information and User Guide for MIL-F-8785C, Military Specification - Flying Qualities of Piloted Airplanes*. Air Force Wright Aeronautical Labs, 1982.

[41] OAG. *Busiest Routes 2019*. 2019.

[42] *Boeing 777-200/300 Airplane Characteristics for Airport Planning*. 2011.

[43] *Boeing 737 Airplane Characteristics for Airport Planning*. 2013.

[44] *A330 Aircraft Characteristics Airport and Maintenance Planning*. 2019.

[45] Airbus. *Test programme and certification*. Accessed January 2020. URL: https://www.airbus.com/aircraft/how-is-an-aircraft-built/test-programme-and-certification.html#structural.

[46] H. Altfield. *Commercial Aircraft Projects*. Ashgate Publishing Limited, 2010.

[47] Jonathan Lovegren and R John Hansman. *Estimation of potential aircraft fuel burn reduction in cruise via speed and altitude optimization strategies*. Tech. rep. 2011.

[48] R Hendrickson and Dario Rajkovic. "5.1 The Importance of Drag". In: (1997).

[49] Rick Rosenkrantz. "Finding the climate optimal cruise altitude for a selection of aircraft types and mission combinations". In: (2019).

[50] Gerrit JJ Ruijgrok and DM Van Paassen. *Elements of aircraft pollution*. Delft University Press The Netherlands, 2005.

[51] Niels Jungbluth and Christoph Meili. "Recommendations for calculation of the global warming potential of aviation including the radiative forcing index". In: *The International Journal of Life Cycle Assessment* (2018).

[52] C. Azar and J. A Johansson. "Valuing the non-CO2 climate impacts of aviation". In: *Climatic Change* (2012), pp. 559–579. DOI: 10.1007/s10584-011-0168-82.

[53] David S Lee et al. "Aviation and global climate change in the 21st century". In: *Atmospheric Environment* 43.22-23 (2009), pp. 3520–3537.

[54] M. Gauss et al. "Impact of aircraft NOx emissions on the atmosphere – tradeoffs to reduce the impact". In: *atmospheric chemistry and physics* (2006), pp. 1529–1548. DOI: 10.5194/acp-6-1529-2006.

[55] Ole Amund Søvde et al. "Aircraft emission mitigation by changing route altitude: A multi-model estimate of aircraft NOx emission impact on O3 photochemistry". In: *Atmospheric Environment* 95 (2014), pp. 468–479.

[56] Brian Cox and Hans-Jörg Althaus. "How to include non-CO2 climate change contributions of air travel at ETH Zurich". In: (2019).

[57] Jasper Faber et al. "Lower NOx at higher altitudes policies to reduce the climate impact of aviation NOx emission". In: *CE Delft Solutions for environment, economy and technology* (2008).

[58] Martin Plohr. "Anwendungsorientierte Methoden zur Analyse und Modellierung des Emissionsverhaltens moderner Triebwerke mit gestuften, mageren Brennkammersystemen auf Basis thermodynamischer Triebwerksmodelle". In: (2016).

[59] Katrin Dahlmann. "Eine Methode zur effizienten Bewertung von Maßnahmen zur Klimaoptimierung des Luftverkehrs". PhD thesis. lmu, 2012.

[60] Marcus Burzlaff. *Aircraft Fuel Consumption–Estimation and Visualization*. Hamburg: Aircraft Design and Systems Group (AERO), Department of Automotive . . ., 2017.

[61] Federal Aviation Administration. *Airplane Turbofan Engine Operation and Malfunctions Basic Familiarization for Flight Crews*. www.faa.gov, 2015.

[62] "Aircraft Fuel System". In: Federal Aviation Administration. Chap. 14.

[63] Boeing. "787 No-bleed systems". In: *Aero* (2010).

[64] J. Fossen. *Preparing Ramp Operations for the 787-8*. 2008.

[65] José Miguel Vasconcelos Oliveira. *Development of Operating Cost Models for the Preliminary Design Optimization of an Aircraft*. Tech. rep. Tecnico Lisboa, 2015.

[66] R. W. Hess and H. P. Romanoff. *Aircraft Airframe Cost Estimating Rela- tionships*. Rand Corp., 1987.

[67] Gudmundsson. *General aviation Aircraft Design*. Elsevier, 2014.

[68] Sylvia MEYER. *Ein Vergleich von DOC-Methoden hinsichtlich der Kosten für Gebühren*. 2004.

[69] Paul Clark. *Buying the Big Jets*. Ashgate, 2007.

[70] SR Naqvi et al. "A critical review on recycling of end-of-life carbon fibre/glass fibre reinforced composites waste using pyrolysis towards a circular economy". In: *Resources, conservation and recycling* 136 (2018), pp. 118–129.

[71] A.C. Marquez. *The Maintenance Management Framework*. Springer-Verlag London Limited, 2007.

[72] D. Pettit and A. Turnbull. *General Aviation Aircraft Reliability Study*. Tech. rep. NASA, 2001.

A

APPENDIX

A.1. REFERENCE AIRCRAFT

Table A.1: Reference aircraft from Airbus and Boeing.

Aircraft	Pax	Class	Range (km)	Price (USD)	OEW (kg)	MTOW (N)	Max Payload (kg)
Boeing 747-8	410	3 class	14310	418.4	220128	4391937	76067
Boeing 777-9X	426	2 class	13500	442,2	181400	3448549	73500
A330-900 NEO	280	3 class	13400	296.4	137000	2462310	44000
A330-800 NEO	240	3 class	15100	259.9	132000	2462310	44000
A330-300	270	3 class	11750	264.2	129400	2374020	45600
A330-200	230	2-class	13450	238,5	120600	2374020	49400
A330-300	270	3 class	11750	264.2	129400	2374020	45600
Boeing 777-300	396	2 class	11136	279	160530	2936819	66770
Boeing 787-9	296	2 class	13950	292,5	128850	2491740	52587
Boeing 787-8	248	2 class	13530	248,3	119950	2236680	43318
A321 NEO	200	2 class	7400	129,5	50100	951570	25500
Boeing 737 MAX 7	143	2 class	7130	99,7	45070	787606	20882
A320 NEO	165	2-class	6300	110,6	44300	774990	20000
A319 NEO	135	2-class	6850	101,5	42600	740655	17700
Boeing 777-200LR	317	2 class	15843	346,9	145150	3408485	61600
Boeing 777-200ER	313	2 class	13080	306,6	138100	2918966	59422
VELA3	750	N.A.	N.A.	N.A.	327000	700000	137000
NACRE	750	N.A.	N.A.	N.A.	309000	630000	127000
OREIO	162	N.A.	6500	N.A.	112850	215820	45360
N2A-EXTE	262	N.A.	11112	N.A.	101820	214000	46720
ACFA	450	N.A.	13334	N.A.	225000	401000	50000
Regional jet	98	N.A.	926	N.A.	24820	43890	10600